AXIAL GROUND MOVEMENT EFFECTS ON BURIED SMALL-DIAMETER MDPE PIPES

by

© Thirojan Jayabalasingham

A Thesis Submitted to the

School of Graduate Studies

In partial fulfillment of the requirements for the degree of

Master of Engineering

Faculty of Engineering and Applied Science

Memorial University of Newfoundland

May 2025

St. John's Newfoundland and Labrador Canada

Abstract

The widespread use of medium-density polyethylene (MDPE) pipelines for natural gas distribution across North America necessitates a robust understanding of soil-pipeline interaction mechanisms, particularly under conditions of ground movement caused by geohazards like landslides. This thesis investigates the axial soil-pipeline interactions in MDPE pipelines using full-scale testing and three-dimensional finite element modelling (FEM). The research addresses critical knowledge gaps in how varying backfill compaction methods, soil densities, and displacement rates affect axial forces and pipe strains, offering insights for enhancing pipeline resilience in geohazard-prone environments. Fifteen full-scale tests were conducted on 42.2 mm and 60.3 mm diameter MDPE pipes embedded at two depths and subjected to controlled axial displacements of soil. These tests were performed at varying soil displacement rates and using different backfill compaction techniques (vibratory plate compactor, hand tamper and no compaction). The influence of compaction on pipe forces was significant with the highest forces for vibratory compaction, while the displacement rate showed only minor effects. The findings underscore a gradual mobilization of axial strain from the anchored end toward the free end of the pipe as soil displaces axially, indicating the progressive mobilization of shearing resistance along the pipe length. Existing ALA (2005) and PRCI (2017) guidelines underpredicted peak force for pipes in dense sands. Three-dimensional FEM simulations were used to explore the mechanism of soil-pipe interaction involved during axial ground movements. While the FEM models captured peak forces effectively, limitations were observed in pre-peak and post-peak behaviour, suggesting the need for further refinement. The study emphasizes the significant role of compaction methods and soil parameters in governing pipeline response to ground movement. The findings contribute essential data for refining pipeline design guidelines and improving infrastructure resilience against geohazard-induced soil movements.

Dedication

This thesis is dedicated to the loving memory of my father, Jayabalasingham Selliah, whose unwavering belief in me continues to guide my every step. Though he is no longer with me in this world, his spirit remains my greatest source of strength and inspiration. His love, wisdom, and sacrifices have shaped the person I am today, and every achievement of mine is a tribute to his legacy. The loss of my father is a wound that time cannot heal, but his presence lives on in my heart, lighting the way forward. This work is my humble way of honouring his life and keeping his dreams alive.

Acknowledgement

First and foremost, I would like to express my sincere gratitude to my supervisor, Dr. Ashutosh Sutra Dhar, for his invaluable knowledge, experience, and unwavering encouragement throughout the research program. His mentorship has not only enhanced my technical knowledge but also strengthened my critical thinking abilities, which greatly boosted my confidence in the field. My appreciation also extends to Dr. Bipul Hawlader for sharing his expertise in geotechnical engineering, which was crucial to the success of this research. I would like to gratefully acknowledge the financial and in-kind support provided by the Alliance Grants program of the National Science and Engineering Research Council of Canada, FortisBC Energy Inc., SaskEnergy Canada Inc., and WSP Canada Inc. Their generous contributions were instrumental in conducting this research.

A special thanks goes to Parththeeban Murugathasan, whose recommendation allowed me to study at Memorial University of Newfoundland. I will be forever grateful for his support and belief in my potential. I would also like to express my heartfelt gratitude to my wife, Sutharsika, whose encouragement and unwavering support were constant sources of strength throughout this journey. Her belief in me helped me navigate the challenges of this program.

The dedication and assistance of my research team over the past two years have been essential to this project's success. I would like to acknowledge Dr. Auchib Reza, Saifa Prioty, Darren Andersen, Sudipta Chakraborty, Sudipto Nath Priyom, and Mahmud Hassan for their hard work and contributions. Additionally, I want to thank Billy Bidgood, John Stamp, the entire technical services team, and laboratory staff Jamal Tinkov, Shawn Oregan, and Matt Curtis for their guidance and expertise in the lab.

Finally, I am deeply grateful to my parents and friends, whose unconditional support and constant encouragement sustained me through the challenges of this journey. Their belief in me made this achievement possible.

Table of Contents

List of Figures

List of Table

List of Symbols

The following symbols are used in this thesis.

α	Soil adhesion factor
γ	Unit weight of the soil
γ'	Effective unit weight of soil
$\gamma_{d,max}$	Maximum dry unit weight of soil
$\gamma_{d,max,proctor}$	Maximum dry unit weight of soil from Proctor test
$\gamma_{d,min}$	Minimum dry unit weight of soil
$\Delta\gamma$	Difference in unit weight between the pipe and backfill soil
δ	Pipe-soil interface friction angle
δ_{ps-r}	Residual plane strain interface friction angle
ε	Axial strain
ε_{peak}	Peak axial strain
$\dot{\varepsilon}$	Strain rate
η	Fitting parameter, hyperbolic constant, empirical coefficient
ξ	Normal stress adjustment factor
σ	Stress
σ'_c	Confining pressure
σ_h	Total horizontal stress
σ'_{mp}	Mean effective stress
σ_v	Total vertical stress
$\Delta\sigma_{com}$	Compaction-induced lateral stress

φ	Internal friction angle of soil
$\emptyset'_{crit}$	Critical state friction angle of soil
$\emptyset'_p$	Peak friction angle of soil
ψ_p , ψ_{max}	Peak dilation angle of soil
$c_e(e, \dot{\varepsilon})$	Hvorslev cohesion as a function of void ratio (e) and strain rate ($\dot{\varepsilon}$)
$f(A)_{unsat}$	Mobilized axial skin friction for unsaturated conditions
Δt	Thickness of the shear zone
$(u_a - u_w)_{av}$	Average matric suction around the pipe
A	Pipe's cross-sectional area
a , b , c , d	Constant obtained from uniaxial tension or compression tests
c	Cohesion of soil
c_u	Undrained shear strength of soil
C_c	Coefficient of curvature
C_u	Coefficient of uniformity
D	External diameter of the pipe
D_{50}	Mean particle size
E_{ini}	Initial modulus of elasticity of MDPE
E_p	Modulus of elasticity of pipe material
E_s	Modulus of elasticity of soil
e	Void ratio
e_{max}	Maximum void ratio
e_{min}	Minimum void ratio

f	Interface friction factor
f_R	Roughness-dependent soil-pipe interface friction factor
G	Shear modulus of soil
H	Burial depth to the springline of the pipe
I	Moment of inertia of the pipe wall
I_D	Relative density
I_R	Relative dilatancy index
K_0	At-rest lateral earth pressure coefficient
K	Effective lateral earth pressure coefficient
K^*	Modified earth pressure coefficient
k	Material constant
L	Mobilized frictional length, Length of pipe
l	Mobilized frictional length
M_W	Moment Magnitude scale of earthquake
N_a	Normalized axial pullout force
n	Power law exponent
P	Axial pullout force
P_a	Atmospheric pressure, reference pressure
P_u	Peak axial pullout force
p'	Mean effective confining pressure
Q , R	Fitting parameters
S	Degree of saturation

S_f	Relative flexural stiffness
T_u	Maximum axial force per unit length of the pipe
u_a	Pore air pressure
u_c	Critical axial displacement where the mobilized dilation angle reaches its peak
u_w	Pore water pressure
v	Poisson's ratio
W_p	Weight of the pipe
x	Distance from the leading end of the pipe

List of Abbreviations

The following abbreviations are used in this thesis.

3D	Three-dimensional
2D	Two-dimensional
AC	Alternating Current
AGA	American Gas Association
ALA	American Lifelines Alliance
ALLAE	Artificial Strain Energy for whole model from ABAQUS analysis
ALLFD	Frictional Dissipation for whole model from ABAQUS analysis
ALLIE	Internal Energy for whole model from ABAQUS analysis
ALLKE	Kinetic Energy for whole model from ABAQUS analysis
ALLVD	Viscous Dissipation for whole model from ABAQUS analysis
ALLWK	External Work for whole model from ABAQUS analysis
ASCE	American Society of Civil Engineers
ASTM	American Society for Testing and Materials
CER	Canada Energy Regulator
CEPA	Canadian Energy Pipeline Association
CGA	Canadian Gas Association
CNL	Constant Normal Load
CNS	Constant Normal Stiffness
CSA	Canadian Standards Association
DC	Direct Current
DE	Discrete Element

DEM	Discrete Element Method
DFOS	Distributed Fiber Optic Sensing
FE	Finite Element
FEM	Finite Element Modelling
FE-DE	Finite-Element Discrete-Element
FOS	Fibre Optic Sensor
FSR	Force Sensing Resistor
GPS	Global Positioning System
HDPE	High Density Polyethylene
HWI	Hybrid-Winkler Interface
InSAR	Interferometric Synthetic Aperture Radar
LiDAR	Light Detection and Ranging
LVDT	Linear Variable Displacement Transducer
MC	Mohr-Coulomb
MDPE	Medium-Density Polyethylene
MMC	Modified Mohr-Coulomb
ODiSI	Optical Distributed Sensor Interrogator
OFDR	Optical Frequency Domain Reflectometry
PE	Polyethylene
PGD	Permanent Ground Deformations
PHMSA	Pipeline and Hazardous Materials Safety Administration
PRCI	Pipeline Research Council International
PSI	Pipe-Soil Interaction

PVC	Polyvinyl Chloride
SDR	Standard Dimension Ratio
UAV	Unmanned Aerial Vehicle
UMAT	User Material
USCS	Unified Soil Classification System

CHAPTER 1: Introduction

1.1 Background

Energy pipelines are critical infrastructures, typically buried underground, that transport oil and gas from production sites to end-users in a safe, efficient, and reliable manner. In Canada, a substantial portion of the gas distribution network relies on MDPE and HDPE pipes, particularly for low-pressure applications. MDPE pipes have become the preferred material choice for gas distribution due to their favorable properties such as flexibility, corrosion resistance, and ease of installation ((PHMSA, 2018). According to the Canadian Gas Association (CGA, 2021), a significant share of Canada's 840,000 km pipeline network (Figure 1-1) is composed of MDPE and HDPE distribution pipelines, with over 450,000 km dedicated to distribution systems (Natural Resources Canada, 2020). According to (CEPA, 2016), more than 90% of Canada's energy production is transported through pipelines. Although pipelines are generally safer compared to other modes of energy transport, they are still susceptible to both natural and man-made hazards, such as corrosion, material fatigue, accidental external damage (e.g., from digging), and ground movements (Allegro Energy Consulting, 2005; Williams and Glasmeier, 2023). Among these, ground deformation hazards including landslides, soil liquefaction, uplift, subsidence, and tectonic fault movement, pose significant risks to the structural integrity of pipelines and the safety of surrounding geoenvironments (Kishawy and Gabbar, 2010; Feng et al., 2015; Lee et al., 2016; Psyrras and Sextos, 2018; Weerasekara and Rahman, 2019; Vesseghi et al., 2021).

Since pipeline networks traverse wide geographical areas, they often pass through regions prone to ground movements. During the route planning phase, engineers aim to avoid areas of high geohazard susceptibility, but this is not always feasible. In some cases, trenchless technologies such as pipe jacking, micro-tunneling, and horizontal directional drilling can be employed for pipeline installation (Marinos et al., 2019). However, in regions experiencing slow ground displacements over a long time, land development and the installation of buried service networks may occur before the ongoing permanent ground deformation is recognized. Despite the inherent advantages of MDPE pipes for energy distribution, they are particularly susceptible to damage from these persistent ground movements. Ground deformation can excessively strain pipelines, potentially leading to leaks or ruptures, posing a significant threat to buried infrastructure. Moreover, unlike transmission pipelines—which benefit from deeper burial depths and greater wall thickness—distribution pipelines are typically installed at shallower depths, making them more vulnerable to surface-induced ground deformations. As a result, evaluating the performance of buried MDPE distribution pipelines under varying ground movement conditions has emerged as a critical aspect of pipeline integrity management (Weerasekara, 2007, 2011; Weerasekara and Wijewickreme, 2008; Wijewickreme and Weerasekara, 2015; Reza and Dhar, 2021a, 2021b). This process demands continuous assessment and the implementation of effective mitigation strategies to address geohazards proactively (Weerasekara & Rahman, 2019).

Failure incidents involving energy pipelines, which can lead to leaks and the release of hazardous substances such as gas or oil, often result in significant economic and social consequences. In the United States, between 2010 and 2019, numerous incidents related to gas transmission and gathering pipelines, hazardous liquid pipelines, and gas distribution networks were reported (PHMSA, 2024). Specifically, 1,226 incidents were recorded for gas transmission and gathering pipelines, resulting in 25 fatalities, 108 injuries, and property damage exceeding $1.3 billion. Similarly, 3,978 incidents involving hazardous liquid pipelines were reported, leading to 10 fatalities, 26 injuries, and over $2.8 billion in property damage. Gas distribution pipelines experienced 1,094 incidents, causing 105 fatalities, 522 injuries, and more than $1.2 billion in property damage. These statistics highlight the critical need for robust pipeline safety and integrity management strategies to mitigate the risks associated with pipeline failures.

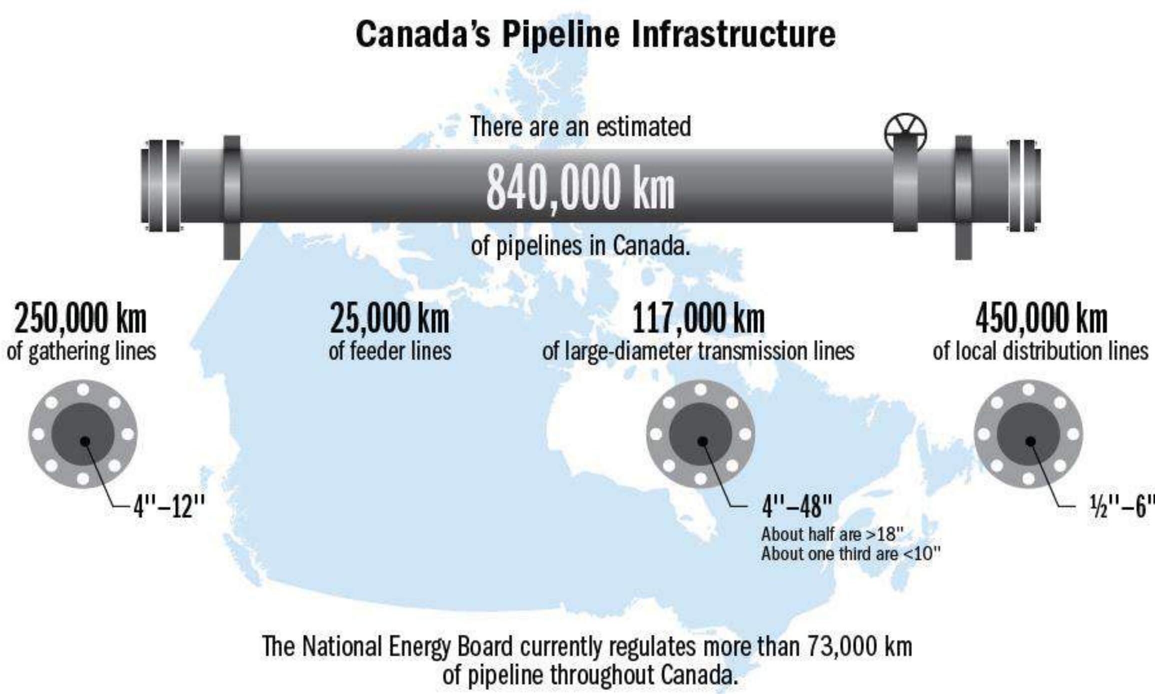

Figure 1-1: Canada's pipeline infrastructure (after Natural Resources Canada, 2020)

Figures 1-2 illustrate a few disasters that resulted from energy pipeline incidents due to earthquake ground movements. Although the Loma Prieta ($M_W = 6.9$), Northridge ($M_W = 6.7$), and Hyogoken-Nanbu ($M_W = 6.9$) earthquakes were of moderate magnitude; their proximity to densely populated urban centers with energy pipeline infrastructure significantly amplified the consequences. These earthquake-induced ground movements caused extensive damage to gas and liquid fuel pipelines, leading to leaks and, in some cases, explosions (O'Rourke, 1996). Given the potential for severe damage and hazardous outcomes, it is critical to evaluate the structural integrity of pipelines exposed to ground movements to ensure their safe operation. Robust assessments and proactive mitigation strategies are essential for managing the risks associated with such geohazards and preventing future incidents.


(a)


(b)


(c)

Figure 1-2: (a) Fire consumes homes in the Marina District after the Loma Prieta earthquake in San Francisco 1989 (NBC News, 2014). (b) Explosions due to the Northridge earthquake in 1994 (Los Angeles Daily News, 2024). (c) Kobe City was on fire due to the Hyogoken-Nanbu earthquake 1995 (Tokyo Weekender, 2023).

Aside from earthquake-induced ground movement effects, pipelines impacted by slow-moving landslides have been the focus of studies for assessing pipeline performance and integrity (Rizkalla et al., 1993; Bruschi et al., 1996; Bughi et al., 1996; Lee et al., 2009; Marinos et al., 2019; Cheng et al., 2021; Vasseghi et al., 2021; Wong et al., 2021; Bonasera et al., 2024). Weerasekara et al. (2023) conducted a monitoring study of the gas distribution system in the Marble Hill subdivision in Chilliwack, British Columbia, which predominantly utilizes MDPE pipes. Similarly, Ferreira and Blatz (2021) investigated the stresses on gas pipelines located in landslide-prone areas of Manitoba, while Wong et al. (2021) examined the effects of landslide-induced ground movements on buried pipelines in Alberta. These studies demonstrate the growing awareness of the need for specific integrity assessment strategies tailored to the characteristics of MDPE pipes.

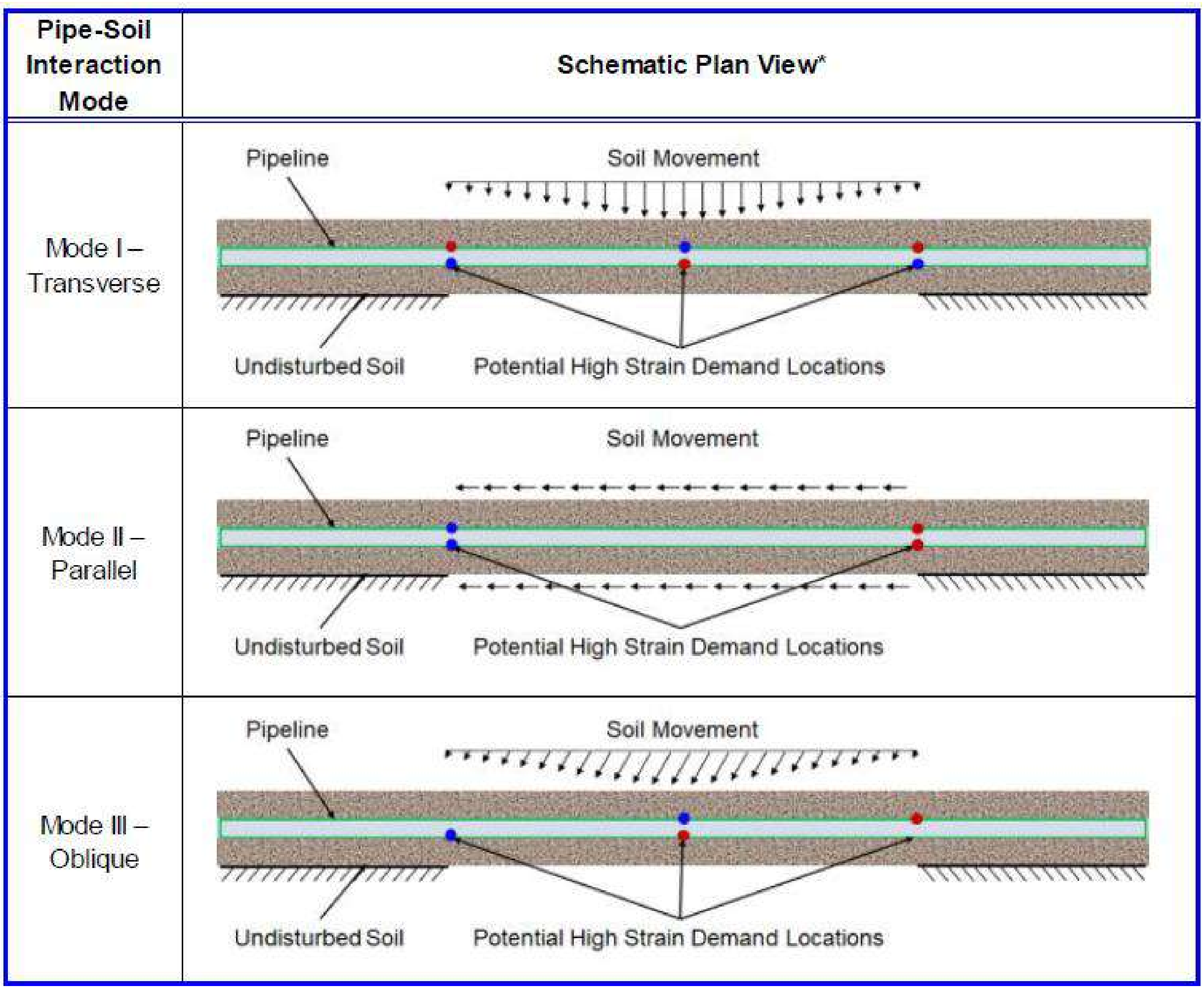

Figure 1-3: Three modes of pipe-soil interaction (after Yu et al., 2020)

The behaviour of buried pipelines subjected to ground movement varies depending on the direction of the ground movement relative to the pipeline's orientation. These movements can significantly deform MDPE pipelines, leading to bending, buckling, or rupture depending on the nature and direction of the soil displacement relative to the pipe axis. A straight pipe segment can be exposed to three typical modes of ground movements, as shown in Figure 1-3 (Yu et al. 2020). Longitudinal ground movements along the pipeline's length can induce axial compression, leading to buckling or axial tension, potentially causing fractures. In contrast, transverse ground movements perpendicular to the pipeline generate bending or lateral displacement, creating misalignments and stress concentrations. Vertical ground movements, such as uplift or subsidence, may lift the pipeline, leading to breaks or causing sinking, inducing compressive forces that can result in sagging (Weerasekara, 2011; Ni, 2016). This thesis investigates the behaviour of MDPE pipes subjected to longitudinal ground movement.

Much of the existing research has focused on the axial pipe-soil interaction for rigid steel pipelines (O'Rourke et al., 1995; Wijewickreme et al., 2009; Bilgin and Stewart, 2009b; Sheil et al., 2018, 2021; Al-Khazaali and Vanapalli, 2019; Marino and Osouli, 2020; Murugathasan et al., 2021). Parameters for calculating the axial soil force in the current design guidelines, such as ALA (2005) and PRCI (2017), were primarily derived from full-scale tests on rigid steel pipes. Unlike steel pipelines, MDPE pipes exhibit low modulus of elasticity, strain-rate dependent behaviour, and large deformation capacity, which introduces additional complexities in assessing their axial soil-pipe interaction performance under geohazard conditions. However, studies focusing on the axial response of MDPE pipes are relatively limited, highlighting a gap in the understanding and design recommendations for this type of material in pipeline applications. The development of standardized, experimentally validated procedures for evaluating the axial soil-pipe interaction of MDPE pipes remains a critical need for the gas distribution industry. This thesis addresses this gap by providing a comprehensive investigation of the axial soil-pipe interaction for MDPE pipes under longitudinal ground movements. The study employs experimental and numerical approaches to assess the axial responses specific to MDPE pipelines, thereby contributing to the broader understanding required for improved design and integrity management of distribution systems.

1.2 Motivation

The increasing use of flexible pipes in gas distribution networks is driven by their favourable properties, such as durability, flexibility, lightweight nature, and resistance to corrosion. Among these, polyethylene (PE), especially MDPE, has emerged as a suitable material for pipeline construction and has been adopted widely, including in higher-pressure systems. According to CGA (2021), the majority (71%) of gas distribution pipelines in Canada consist of high-density polyethylene (HDPE) and MDPE. However, no well-validated guidelines exist for assessing MDPE pipes subjected to ground movements.

While several researchers (Anderson, 2004; Weerasekara, 2007, 2011; Weerasekara and Wijewickreme, 2008; Wijewickreme and Weerasekara, 2015; Reza and Dhar, 2021a, 2021b, 2024; Reza et al., 2023a) have experimentally investigated the axial pullout responses of smaller-diameter MDPE pipes buried in the sand under different conditions (loose, medium-dense, and dense sand; various burial depths), these studies primarily focus on the pipe-pull mechanism where the pipe is pulled through a stationary soil mass. Conversely, the soil-pull mechanism, where the soil mass moves relative to a stationary pipe, has not been studied for MDPE pipes despite its relevance in certain cases, such as landslides. Some research on soil-pull has been conducted for other materials, such as copper pipes (Rostami et al., 2023), but there remains a gap in understanding the behaviour of MDPE pipes under this mechanism.

Though researchers have examined the effects of ground movement rates on the axial pullout behaviour of buried MDPE pipes (Anderson, 2004; Weerasekara, 2011; Wijewickreme and Weerasekara, 2015; Reza and Dhar, 2021a; Reza and Dhar, 2021b; Reza et al., 2023a), the effects of ground movement rates on soil-pull mechanisms remain unexplored.

Landslide studies indicate that ground movement rates can vary significantly, from very slow to extremely rapid (Bruschi et al., 1995; Scarpelli et al., 1995; Cheaib et al., 2022). While many slow landslides exhibit relatively steady movements, detailed monitoring has shown that movement can fluctuate, slowing during dry seasons and accelerating during wet seasons (Keefer and Johnson, 1983; Kalaugher et al., 2000; Wood Environment & Infrastructure Solutions, 2021; Bonasera et al., 2024). The axial pipe-soil interaction under different ground movement rates can exhibit distinct behaviours, which are not considered in the current guidelines. Through pipe-pulling tests, Reza and Dhar (2021a, 2021b) demonstrated that the interface friction factors for MDPE pipes can be rate-dependent.

Moreover, as gas distribution pipelines often traverse urban areas, backfill soils near existing structures and road embankments are typically compacted. This compaction increases the lateral earth pressure on buried pipes due to compaction-induced locked-in stresses (Duncan and Seed, 1986; Massarsch and Fellenius, 2002; Gui et al., 2020; Ezzeldin et al., 2022). Various compaction methods are employed in industry, and compaction-induced stresses differ based on the compaction effort (Duncan et al., 1991). These increased lateral stresses can elevate the interface frictional resistance, resulting in higher axial pullout resistance. However, current guidelines do not consider the effect of compaction-induced stresses on the axial pullout behaviour of buried pipes. Reza and Dhar (2024) employed compaction-induced lateral earth pressures in numerically simulating the axial pullout responses of MDPE pipes.

In summary, while the use of MDPE pipes in gas distribution networks has grown due to their favourable properties, such as flexibility and corrosion resistance, current design guidelines are inadequate for assessing the behaviour of the pipes when subjected to ground movements. Previous studies have predominantly focused on the pipe-pull mechanism, leaving a critical gap in understanding the soil-pull scenario, which is relevant for conditions like landslides. Moreover, the influence of compaction-induced stresses and ground movement rates on axial pullout behaviour remains underexplored, with no comprehensive guidelines currently available. This research seeks to bridge these gaps by studying the axial pipe-soil interaction of MDPE pipes under diverse conditions, including varying ground movement rates and compaction-induced stresses, to develop a more robust understanding of MDPE pipe behaviour in gas distribution systems.

1.3 Objectives

The primary objective of this thesis is to develop a comprehensive understanding of the behaviour of smaller-diameter MDPE pipes subjected to axial ground movement, with a particular focus on the scenario where the pipe is fixed at one end, and the surrounding soil mass moves relative to the pipe. Given that the performance of flexible MDPE pipelines is heavily influenced by the pipe–

soil interaction, this research aims to enhance the understanding of this interaction through both experimental investigations and numerical simulations. The specific objectives of the research are as follows:

1) Investigating the effects of backfill compaction methods on the axial pulling of MDPE pipes. This objective aims to assess how different compaction techniques influence the axial pullout resistance of buried MDPE pipes, with particular attention to the impact of compaction-induced stresses.
2) Examining the effects of pipe-pulling versus soil-pulling on the soil-pipe interaction. A comparative study will be conducted to evaluate the differences between the traditional pipe-pull mechanism (where the pipe is pulled through stationary soil) and the soil-pull mechanism (where the soil moves around a fixed pipe), which has not been extensively studied for MDPE pipes.
3) Examining the effects of pulling rates during soil-pulling. This objective focuses on understanding how varying rates of ground movement (i.e., pulling rates) influence the axial pipe-soil interaction, which is particularly relevant in landslide-prone areas where ground movement rates can fluctuate.
4) Investigating the loading-unloading-reloading responses of buried MDPE pipes. This objective explores the mechanical behaviour of MDPE pipes subjected to cyclic loading conditions, such as those that occur in dynamic soil environments where ground movements may periodically accelerate or decelerate.
5) Investigating the development of strains along the pipe length during axial soil movement. The study will analyze the distribution and evolution of strains along the length of the

MDPE pipe when subjected to axial soil movements, which is critical for understanding localized stress concentrations that could lead to failures.

6) Investigating the axial pipe-soil interaction through three-dimensional (3D) continuum finite element modelling. This objective aims to develop and validate a 3D finite element (FE) model to simulate the axial pipe-soil interaction, providing a more detailed and nuanced understanding of the mechanics involved, including the influence of soil properties, pipe material behaviour, and boundary conditions.

These objectives collectively aim to advance the understanding of MDPE pipe behaviour in response to ground movements, particularly in the context of soil-pulling mechanisms and varying ground conditions, thereby contributing to the development of more robust design guidelines for gas distribution systems.

1.4 Framework of Thesis

This thesis is structured in a traditional format, with the study's outcomes presented across five chapters and additional material provided in the appendices.

Chapter 1: Introduction

This chapter provides an introduction to the research topic, focusing on the axial pipe-soil interaction and the motivations behind the study. It outlines the research objectives and highlights the major contributions of this work.

Chapter 2: Literature Review

In this chapter, an extensive review of the literature on buried MDPE pipes subjected to axial ground movement is presented. It also explores the effects of compaction-induced stresses on buried structures. Additionally, various proposals made by researchers for estimating axial resistance are reviewed, along with an overview of FEM for the axial pullout behaviour of pipes.

Chapter 3: Laboratory Investigation of Buried Small-Diameter Medium-Density Polyethylene Pipes Subjected to Relative Axial Ground Movement

This chapter details the setup of a full-scale soil-pull testing facility. It describes the use of distributed fibre optic sensors to measure strain distribution along the pipe's length. The effects of compaction methods on the axial pipe-soil responses are explored. The behaviour of the pipes during loading-unloading-reloading cycles is thoroughly investigated. A version of this chapter will be submitted as a technical paper in a peer-reviewed journal. A part of this work has been published in a conference paper at the 77th Canadian Geotechnical Conference, GeoMontreal 2024, Montreal, Canada.

Chapter 4: Finite Element Modelling of Buried Medium-Density Polyethylene Pipes in Sand Subjected to Axial Pullout Loads

This chapter presents the results of 3D FEM of the interactions between MDPE pipes and surrounding sand under axial ground movement conditions. Numerical techniques were developed to account for the compaction-induced load during analysis.

Chapter 5: Conclusions and Recommendations

The final chapter summarizes the conclusions drawn from the research presented in previous chapters and offers recommendations for future research. In addition, problem-specific conclusions are provided at the end of Chapters 3 and 4, as well as the appendices (Appendices A–C).

Appendix A: Effects of Backfill Compaction Method on the Axial Pipe-Soil Interaction for Buried Small-Diameter MDPE Pipes

This appendix includes a technical paper published at the GeoMontreal 2024 conference, presenting findings on the impact of backfill compaction methods on axial pipe-soil interaction.

Appendix B: Earth Pressure Measurements with Low-Pressure Transducers

As the earth pressures significantly contribute to the axial pullout resistance of pipe, earth pressure development during backfilling and compaction was examined in an independent study. This appendix discusses the results of earth pressure measurements, aiming to understand how lateral earth pressure varies during the backfilling and compaction processes.

Appendix C: Soil Index Property Tests

Index properties (i.e., grain-size distribution and minimum and maximum densities) of the sand used in the test facilities were examined. The results of the index property tests are discussed in Appendix C.

1.5 Key Contributions

Conference paper

Jayabalasingham, T., Reza, A., Dhar, A. (2024). *Effects of Backfill Compaction Method on the Axial Pipe-Soil Interaction for Buried Small-Diameter MDPE Pipes*, 77th Canadian Geotechnical Conference, GeoMontreal 2024, Montreal, Canada, October 15th-18th.

Journal paper

Jayabalasingham, T., Dhar, A. (2024). *Laboratory Investigation of Buried Small-Diameter Medium-Density Polyethylene Pipes Subjected to Axial Ground Movement* (to be submitted).

Co-authorship Statement

All research work presented in this thesis, including relevant conference and journal publications, was carried out by the author of this thesis, Thirojan Jayabalasingham, under the supervision of Dr. Ashutosh Sutra Dhar. The first draft of the manuscript was prepared by Thirojan Jayabalasingham and subsequently revised based on feedback from the co-authors and the peer-review process. As a co-author, Dr. Ashutosh Sutra Dhar provided support in developing the research idea, offered guidance on areas requiring further elaboration, and reviewed the manuscript. Dr. Auchib Reza contributed to the organization of the manuscripts, assisted with numerical modelling, and reviewed the documents.

CHAPTER 2: Literature Review

2.1 Introduction

Pipelines are essential infrastructure for various engineering applications and serve mainly for fluid transport, including liquid petroleum, gas, water, and sewage. Depending on the usage and environmental conditions, different materials are used for the pipelines. Steel is preferable for high-pressure applications due to its strength and durability. For water and gas distribution systems, polyethylene, particularly MDPE, is used due to its flexibility and corrosion resistance. PVC is commonly used in water supply and sewage systems due to its cost-effectiveness and ease of installation. Concrete is preferred for large-diameter water and sewer pipelines because of its robustness and longevity (Ozanne, 2011).

CER (2021) categorizes gas pipelines in Canada into four major groupings: gathering, feeder, transmission, and distribution. Gathering pipelines transport produced gas from the production sites to processing facilities. This will normally be a smaller-sized pipeline with extensive line networks in the production field. A feeder pipeline is used to transfer processed gas to main transmission pipelines that convey large volumes of gas over long distances to gas markets. Lastly, distribution pipelines transport the processed gas from the distribution centres to the end-users, which are the residential, commercial, and industrial customers. These pipelines are characterized by smaller diameters and are commonly found within urban and suburban areas, ensuring the final delivery of utilities directly to homes and businesses.

Given their extensive range, distribution pipelines are susceptible to both natural and man-made hazards that can compromise their integrity and functionality (Allegro Energy Consulting, 2005). Natural disasters such as earthquakes, landslides, floods, and extreme weather conditions can induce ground movements, erosion, and physical damage to pipelines. More importantly, earthquakes and landslides may lead to permanent ground displacement and exert an imposed stress on the pipelines, which may eventually cause them to rupture or leak. It is, therefore, of fundamental importance to understand the interaction between the soil and the pipeline in these conditions and how these conditions interact in a resilient pipeline. Over the last several decades, extensive research has been conducted to understand the mechanisms of pipe-soil interaction for buried pipelines subjected to relative ground movements. This chapter provides a comprehensive overview of previous experimental and numerical studies on the relative axial pipe-soil interaction of flexible MDPE pipes. Specific literature reviews relevant to the discussions in Chapters 3 and 4 are presented within those respective chapters.

2.2 Directions of Ground Movements

Ground movements can be in different directions with respect to the pipeline orientations, and their impact on the pipeline structure can be different. Longitudinal ground movements occur along the pipeline's length and can induce axial compression or tension. Axial compression applies compressive forces to the pipeline, potentially leading to buckling or deformation. Conversely, axial tension introduces tensile forces that may cause stretching or fractures. Transverse ground movements happen perpendicular to the pipeline's axis, generating shear forces that can result in bending or lateral displacement. Such movements may push the pipeline sideways, causing misalignment or localized stress concentrations. Vertical ground movements include uplift and subsidence. Uplift involves the ground lifting the pipeline vertically, inducing tensile stress that may cause breaks or expose the pipeline. Subsidence, the sinking or settling of the ground, generates forces that can lead to bending or sagging of the pipeline. Understanding these directional ground movements and their effects is essential for designing pipelines that can withstand various geotechnical challenges (Weerasekara, 2011; Ni, 2016).

2.3 Laboratory and Field Tests

Several research studies investigated the axial pullout response of buried polyethylene pipes through full-scale laboratory experiments and field tests (Anderson, 2004; Weerasekara, 2007; Weerasekara and Wijewickreme, 2008; Bilgin and Stewart, 2009a; Weerasekara, 2011; Wijewickreme and Weerasekara, 2015; Reza and Dhar, 2021a; Reza and Dhar, 2021b; Reza et al., 2023a). In all the tests, the pipes were pulled at specific pulling rates in a stationary soil mass.

Anderson (2004) conducted an extensive study on the behaviour of MDPE pipes subjected to axial ground movement in medium to loose and dense sands. The medium-to-loose sand used in the experiments was not compacted during placing and had an average density of 14.6 kN/m^3, corresponding to a relative density of approximately 60%. In contrast, the dense sand, which was compacted using a vibratory plate tamper (gasoline-powered Bartell model B1318), exhibited an average density of 15.7 kN/m^3 and a relative density of approximately 97%. The experimental setup involved pulling a 5-meter-long MDPE pipe at a constant rate of 10 mm/h. Two different pipe diameters, 60 mm and 115 mm, were evaluated for the medium-to-loose sand. The 60 mm diameter pipe achieved a peak pullout force of 1.87 kN. For two 115 mm diameter pipes, peak pullout forces of 4.45 kN and 3.76 kN were recorded. These peak forces were observed within a displacement range of 7 to 12 mm. The burial depths for these pipes were 720 mm and 750 mm for 60.3 mm and 115 mm pipes, respectively. In parallel tests conducted in dense sand, pipes with diameters of 15 mm, 60 mm, and 115 mm were assessed. The 15 mm diameter pipe achieved a peak pullout force of 1.2 kN, while the 60 mm and 115 mm diameter pipes exhibited peak pullout forces of 4.7 kN and 11.9 kN, respectively. These peak forces were observed at a higher displacement of 84 mm, 44 mm, and 399 mm for 115 mm, 60 mm, and 15 mm diameter pipes, respectively. The burial depths for the 15 mm and 60 mm diameter pipes were 480 mm, and the 115 mm diameter pipe was buried at a depth of 520 mm.

Weerasekara and Wijewickreme (2008) conducted full-scale axial pullout tests on MDPE pipes to examine their performance under axial loading conditions in dense sand. The tests were carried out using 3.8 m long MDPE pipes with nominal diameters of 60.3 mm and 114.3 mm. These pipes were embedded into Fraser River sand, with a density equal to 15.8 kN/m^3, representing a relative density of about 75%. The burial depth to the springline of the pipes was 600 mm. The sand was compacted using a 0.5-ton static roller. The roller made four passes in each of the lateral and longitudinal directions to ensure that the desired level of compaction was achieved. The pipes were subjected to axial pullout at a constant rate of 36 mm/h. It was found from the experiments that the peak pullout resistances for 60.3 mm and 114.3 mm diameter pipes are 4.1 and 6.9 kN, respectively. These peak resistances were observed at a relative pipe displacement of approximately 20 mm. They derived a closed-form solution to address the nonlinear material behaviour in MDPE pipes under axial loading to establish strain, force, and mobilized frictional length along the pipe for a known relative axial ground displacement, with due consideration given to shear-induced dilation and frictional degradation. Instead of the at-rest lateral earth pressure coefficient (K_0), they used coefficients of lateral earth pressure (K) of 2.4

and 1.4 for 60.3 mm and 114.3 mm diameter MDPE pipes to match the peak axial resistance during pullout tests.

Weerasekara (2007) conducted additional tests on MDPE pipes with three strain gauges attached to the soil-pipe interaction surface. Other than that, all other conditions remained the same as described in the previous paragraph. They reported peak pullout forces of 5.9 kN and 10.2 kN for MDPE pipes of 60.3 mm and 114.3 mm diameters, respectively. These peak forces were observed at a higher relative pipe displacement of approximately 45 mm. Pipe surface roughness was significantly affected by the placement of the strain gauges, resulting in higher peak forces and corresponding displacements.

Weerasekara (2011) and Wijewickreme and Weerasekara (2015) conducted field tests to examine the axial pullout response of MDPE pipes with a diameter of 60.3 mm and a length of 8.5 m. The pipes were buried in dense sand with a density of 16 kN/m^3 at a depth of 560 mm. The sand around the pipes was compacted using a vibratory plate tamper with four passes, and the area adjacent to the pipe's springline was compacted with a hand tamper. The study recorded various peak axial forces under different conditions. For pipes buried at 560 mm, peak forces were 5.4 kN at a pulling rate of 0.6 mm/min and 6.9 kN at 2.1 mm/min. At a burial depth of 980 mm, a peak force of 5.9 kN was observed at a pulling rate of 2.1 mm/min. A test with pipes buried at a depth of 560 mm and subjected to intermittent pulling rates of 0.6 mm/min, 0.15 mm/min, and 2.1 mm/min recorded peak forces of 3.6 kN, 4.3 kN, and 5.2 kN, respectively. In another test with a pipe buried at a depth of 560 mm, a pulling rate of 0.73 mm/min with a ten-day relaxation period before reloading at the same rate resulted in a peak force of 5.2 kN. They considered a nonlinear, strain rate–dependent stress–strain response of the MDPE pipe material to analyze the pipe responses under axial soil loading to account for the pulling rate effects.

Reza and Dhar (2021a) conducted axial pullout tests on 60.3 mm diameter MDPE pipes, each 4 m in length. The effect of pulling rates of 0.5 mm/min, 1 mm/min, and 2 mm/min was investigated. The pipes were buried to a depth of 480 mm in medium-dense sand compacted to a density of 14.5 ± 0.5 kN/m³ through kneading and levelling. Peak pullout forces of 1.78 kN, 2.5 kN, and 2.84 kN were reported for the respective pulling rates, with corresponding pipe displacements ranging from 9 mm to 12 mm. Another set of tests was conducted with strain gauges attached at one-fourth, half, and three-fourths of the pipe's length under the same conditions. These tests showed increased peak axial pullout forces of 2 kN, 2.6 kN, and 3.2 kN for the respective pulling rate at pipe displacements between 10 mm and 15 mm. The observed increase in pullout forces was attributed to the additional frictional resistance provided by the strain gauges during the pulling process.

Reza and Dhar (2021b) investigated the impact of axial relative ground movement on MDPE pipes with a diameter of 42.2 mm and a length of 4 m. These pipes were buried at a depth of 340 mm in loosely packed sand with a density ranging from 12 kN/m³ to 13 kN/m³, without compaction. The tests were conducted at pulling rates of 0.5 mm/min, 1 mm/min, and 2 mm/min. Strain gauges were installed at one-fourth, half, and three-fourths along the length of the pipe within the soil container. The peak axial pullout forces recorded were 0.77 kN, 0.87 kN, and 1.3 kN for the respective pulling rates, with corresponding pipe displacements between 6 mm and 13 mm. In a subsequent experiment, the burial depth was increased to 560 mm while maintaining all other conditions constant. This deeper burial resulted in a peak pullout force of 1.14 kN at a pulling rate of 0.5 mm/min. Throughout all the tests, the moisture content of the backfill sand ranged from 0.5% to 2%. The displacements for peak ranged from 6 mm to 14 mm.

Reza et al. (2023a) conducted an extensive investigation into the axial behaviour of buried MDPE pipes with a length of 4 meters in dense sand conditions. Their study proposed simplified methods for calculating the pullout resistance, mobilized frictional length, and axial strains on the pipe walls. In total, eleven full-scale tests were performed—six of which involved the use of strain gauges, while the remaining five with bare pipes. The burial depths varied according to pipe diameter to keep a constant depth-to-diameter ratio (i.e., 8): pipes with a diameter of 42.2 mm were buried at a depth of 340 mm, whereas those with a diameter of 60.3 mm were buried at a depth of 480 mm. For all tests, the backfill soil was compacted using a hand tamper with six passes, resulting in sand densities ranging from 18 kN/m^3 to 19.2 kN/m^3. For the bare pipe tests, the peak pullout forces for the 42.2 mm diameter pipes were 2.58 kN, 3.51 kN, and 3.7 kN at pulling rates of 0.5 mm/min, 1 mm/min and 2 mm/min, respectively. Similarly, for the 60.3 mm diameter pipes, peak pullout forces of 3.72 kN and 4.76 kN were recorded at pulling rates of 0.5 mm/min and 1 mm/min, respectively. In the tests involving strain gauges, the axial pullout forces were significantly higher. For the 42.2 mm diameter pipes, the peak forces were 3.24 kN, 3.66 kN, and 4.06 kN for pulling rates of 0.5 mm/min, 1 mm/min, and 2 mm/min, respectively. For the 60.3 mm diameter pipes, the peak forces increased to 4.99 kN, 5.62 kN, and 5.79 kN for the same pulling rates. These results demonstrated an approximate 35% increase in axial pullout forces due to the presence of strain gauges. The displacements for peak ranged from 45 mm to 55 mm for 42.2 mm diameter pipes and 16 mm to 40 mm for 60.3 mm diameter pipes. To further enhance their analysis, Reza et al. (2023a) introduced a normal stress adjustment factor derived from cavity expansion theory, which accounts for the dilation-induced increase in normal stress on the pipe surfaces.

Bilgin and Stewart (2009a) investigated the thermal effects on high-density polyethylene (HDPE) pipes with a diameter of 168.3 mm and a length of 1.22 meters under temperature-induced cyclic loading. Their study revealed a decrease of 60% in axial pullout forces corresponding to reductions in pipe diameter due to temperature variations from 21°C to 2°C. The pipes were buried at a depth of 760 mm in sand with a density of 17 kN/m^3, which was compacted using a hand tamper. During the tests, the pipes were pulled at a rate of 24 mm/min, with the moisture content of the sand ranging from 3% to 5%. The recorded peak pullout forces were 8.5 kN at 21°C, 6.8 kN at 10°C, 4.9 kN at 7°C, and 4.6 kN at 6°C. These findings indicate that lower temperatures significantly reduce the pullout forces, which is associated with the reduction of pipe diameter.

2.4 Pulling Rate Effect

Researchers have studied the impact of ground movement rates on the behaviour of buried MDPE pipes (Anderson, 2004; Weerasekara, 2011; Wijewickreme and Weerasekara, 2015; Reza and Dhar, 2021a; Reza and Dhar, 2021b; Reza et al., 2023a).

Anderson (2004) conducted a seminal investigation into the effect of displacement rate on the axial pullout behaviour of MDPE pipes. This study involved axial pullout tests with incremental increases in displacement rates, starting at an initial rate of 10 mm/h. The findings indicated that the effect of displacement rate on axial pullout force is negligible at slower rates. However, when the displacement rate was increased to 300 mm/h, there was a slight upward trend

(8%) in the axial pullout force with further displacement. This increase was attributed to the collapse of the arched soil zone above the pipe crown, which likely contributed to the increased resistance.

Further research by Weerasekara (2011) and Wijewickreme and Weerasekara (2015) reported a significant increment of approximately 28% in the axial pullout force of buried MDPE pipes with a diameter of 60.3 mm in dense sand when the pulling rate was increased from 0.6 mm/min to 2.1 mm/min while maintaining other conditions constant. In their analysis, Wijewickreme and Weerasekara (2015) incorporated a nonlinear, strain rate-dependent stress-strain response of the MDPE pipe material to better understand the effects of varying pulling rates under axial soil loading conditions.

Reza and Dhar (2021a, 2021b) expanded on prior research by investigating the effects of pulling rates on MDPE pipes with diameters of 42.2 mm and 60.3 mm. Their studies demonstrated a positive correlation between peak pullout force and ground movement rates. Specifically, they proposed friction factor values for different pulling rates: 0.75 for 0.5 mm/min, 0.86 for 1 mm/min, and 0.9 for 2 mm/min, which simulated the test results using finite element analysis. Reza and Dhar (2021a) observed a 60% increase in axial pullout forces when the pulling rate was raised from 0.5 mm/min to 2 mm/min for 60.3 mm diameter MDPE pipes buried in medium-dense sand. Similarly, Reza and Dhar (2021b) reported a 69% increase in axial pullout forces for the same rate increase in 42.2 mm diameter MDPE pipes in loose sand.

Reza et al. (2023a) also examined the effects of varying pulling rates on the pullout resistance of MDPE pipes buried in dense sand. For 42.2 mm diameter pipes, the pullout resistance increased by 25% for pipes with strain gauges and by 43% for bare pipes when the pulling rate was increased from 0.5 mm/min to 2 mm/min. Similarly, for the 60.3 mm diameter pipes, the pullout resistance increased by 16% for pipes with strain gauges over the same pulling rate range (0.5 mm/min to 2 mm/min). For bare 60.3 mm pipes, the pullout resistance showed a 28% increase when the pulling rate was increased from 0.5 mm/min to 1 mm/min. These results highlight the significant influence of the pulling rate on the mechanical behaviour of MDPE pipes in dense sand conditions. Note that all studies presented above examined the pullout responses of pipes where a pipe was pulled through static soil. The responses of static pipes exposed to moving ground were not examined, which is the focus of the current study.

2.5 Cyclic loading

Weerasekara (2007) performed a series of pull-push (loading-reversal loading) tests on MDPE pipes of 114-mm diameter. The measured mobilized frictional force was found to be significantly greater during the pushing than during the pulling. The reason for this difference is that under pushing, the diametric expansion of the pipe increases the normal stress and consequently enhances the pullout resistance.

A number of cyclic tests were carried out by Bilgin and Stewart (2009a) to assess the pullout resistance of buried HDPE pipes under repeated cyclic loading conditions, specifically simulating the influence of thermal contraction and expansion caused by seasonal temperature fluctuations. These tests were conducted at 21°C, 10°C, 7°C, and 6°C. The results showed that a significant reduction of the resistance to shearing would happen under cyclic loading. It was reported that at 21°C, after just 10 cycles, the shearing resistance was reduced by 72%.

Reza et al. (2023b) conducted shaking table tests to examine the influence of tensile and compressive loadings on HDPE pipes with a diameter of 89.5 mm. The pulling rate was set at 3000 mm/min. Their results indicated that the frictional resistance during compression was significantly higher than during tension. Moreover, the study found that a large degradation in frictional force occurred during the initial cycles, with the rate of degradation diminishing in subsequent loading cycles.

2.6 Relaxation Test

Several researchers have examined the long-term relaxation behaviour of buried MDPE pipes (Weerasekara, 2011; Wijewickreme and Weerasekara, 2015; Reza, 2024). Weerasekara (2011) and Wijewickreme and Weerasekara (2015) conducted a ten-day relaxation experiment on MDPE pipes with a diameter of 60.3 mm, which were subjected to axial loading. The pipes were buried at a depth of 560 mm, and the axial loading was applied at a rate of 0.73 mm/min. Over the ten-day period, they observed a reduction of 2.4 kN in the axial force due to relaxation. Similarly, Reza (2024) carried out a nine-day relaxation test on MDPE pipes with a diameter of 42.2 mm buried at a depth of 600 mm in dense sand, with the pulling rate set at 0.5 mm/min. Reza (2024) reported a 20% reduction in axial pullout forces during the relaxation period. This reduction in axial forces was attributed to the stress-relaxation properties inherent to polyethylene materials. Both studies also noted a redistribution of axial strain throughout the relaxation phase.

2.7 Design Guidelines

The beam-on-spring analysis has been the industry practice for assessing and designing pipelines subjected to ground movements (ASCE, 1984; ALA, 2005; PRCI, 2017). A series of independent bilinear elastic-perfectly-plastic springs is employed around the pipeline to represent the resistances/forces from the surrounding soil. The soil springs are defined in the axial, horizontal, and vertical directions relative to the pipeline. Figure 2-1 shows the spring analogy for analyzing pipeline-soil interaction. As the soil springs in X, Y, and Z directions are independent and perpendicular to each other, the force in one direction will not affect the other two directions. When considering the axial loading of buried pipes, the primary source of loading is the friction between the pipe and the surrounding soil. For pipes buried in cohesionless soil conditions, ASCE (1984) and ALA (2005) recommended Equation 2-1 to estimate the maximum axial force per unit length acting on the surface of the buried pipes, where T_u is the maximum axial force per unit length of the pipe; D is the external diameter of the pipe; H is the burial depth (depth to the springline of the pipe); γ is the unit weight of the soil; K_0 is the lateral earth pressure at-rest; and δ is the pipe-soil interface friction angle.

$$T_u = \pi D \gamma H \left(\frac{1 + K_0}{2}\right) \tan\delta \qquad \text{Equation 2-1}$$

Based on the average normal stress around the pipe, Equation 2-1 determines the maximum axial force per unit length of the pipe. The average normal stress is the mean value of the overburden pressure and the at-rest lateral earth pressure at the pipe springline. Equation 2-1 assumes an idealized soil pressure distribution around the pipe. Newmark and Hall (1975) and Kennedy et al. (1977) calculated the axial soil loads on pipes subjected to strike-slip fault movement using this equation. PRCI (2009) introduced the effective coefficient of lateral earth pressure that varies from the value of at-rest conditions for loose sand and up to a value of 2 for the dilative dense sand conditions, based on the recommendations provided by Wijewickreme et al. (2009). It is worth noting that the Equation 2-1 proposed is based on the outcome of the full-scale tests on the larger-diameter rigid steel pipes. Hence, determining the maximum axial force on the flexible pipes can lead to conservative analysis, and often, a reduction factor is suggested to soften the soil springs (Xie et al., 2013; Saiyar et al., 2016).

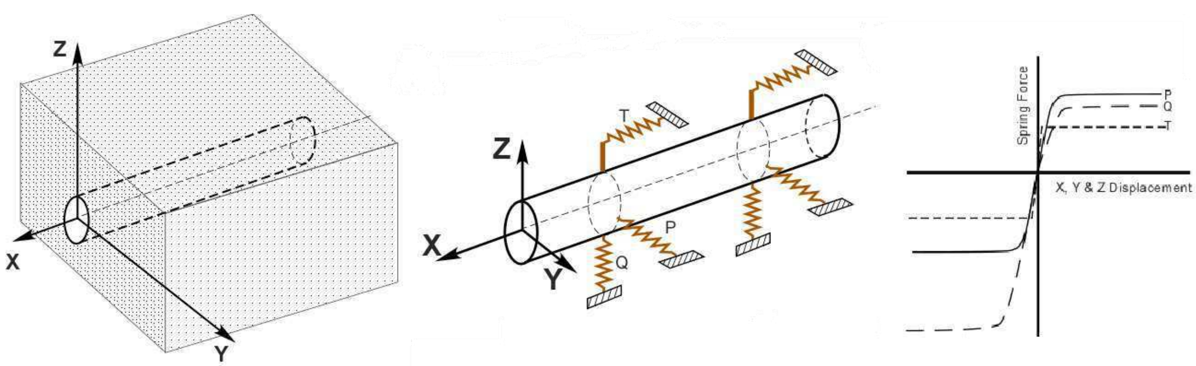

Figure 2-1: Spring analog for analyzing pipeline-soil interaction (after PRCI, 2009)

Several researchers have noted discrepancies in the design equations recommended by ASCE (1984), ALA (2005), and PRCI (2017) for determining the peak axial pullout force of buried pipelines. Though the design equation accurately predicts the maximum axial forces for the steel pipes buried in loose sand, it underpredicts the maximum axial forces for the steel pipes buried in dense sand (Paulin et al., 1998; Karimian, 2006; Wijewickreme et al., 2009; Sarvanis et al., 2017; Meidani et al., 2017; Sheil et al., 2018; Al-Khazaali and Vanapalli, 2019; Murugathasan et al., 2021). However, for the flexible pipes, the predicted axial pullout force is often higher than the experimental results for loose sand, and the predicted axial pullout force is significantly lower than what the experimental results indicate for dense sand (Anderson, 2004; Weerasekara and Wijewickreme, 2008; Wijewickreme and Weerasekara, 2015; Reza and Dhar, 2021a, 2021b; Reza et al., 2023a).

The interface characteristics between the soil and pipeline significantly influence the axial pullout behaviour of buried pipes. Key factors such as surface roughness and coating hardness of the pipeline have a direct impact on the soil-pipe interaction and, consequently, on the interface shear strength, which determines the axial pullout resistance (Dove and Frost, 1999; Han et al., 2018; Ghanadizadeh et al., 2022). The shear strength at the interface is governed by the interface friction angle, which is influenced by both the internal friction angle of the soil and the friction factor of the pipe coating. The interface friction angle typically ranges between 50% and 100% of the peak friction angle of the surrounding soil (Yimsiri et al., 2004).

Early studies by O'Rourke et al. (1990) on sand-polymer interfaces demonstrated that the interface friction strength increased with soil density and decreased with the hardness of the polymer coating. Based on direct shear tests, they proposed a friction factor for polymer materials in the range of 0.55 to 0.65. Later, ALA (2005) and PRCI (2017) recommended a friction factor of 0.6 for polyethylene-coated pipelines. Table 2-1 provides a summary of interface friction angle factors for various pipe coating materials based on the recommendations of ALA (2005) and PRCI (2017). More recently, Reza and Dhar (2021a, 2021b) used finite element analysis to propose friction factors for polyethylene under varying ground movement rates. They suggested values of 0.75 for 0.5 mm/min, 0.86 for 1 mm/min, and 0.9 for 2 mm/min.

Guo and Zhou (2024) conducted large-scale axial pullout tests to study the effects of surface roughness and coating hardness on buried pipes. They proposed a roughness-dependent soil-pipe interface friction factor, with values ranging from 0.35 for smooth surfaces to 0.99 for rough interfaces. Their findings indicated that 72-79% of the increase in axial resistance due to surface roughness could be attributed to an increase in the interface friction coefficient. Additionally, shear-induced dilation of the surrounding soil was found to influence the interface friction (Karimian, 2006; Wijewickreme et al., 2009). Moreover, the dilatancy behaviour at the soil-pipe interface is closely correlated with the roughness of the interface (Lings and Dietz, 2005; Zhang et al., 2011; Farhadi and Lashkari, 2017).

Table 2-1: Interface friction angle factor for different external pipe coating materials ALA (2005) and PRCI (2017)

Pipe Coating	f
Concrete	1.0
Coal Tar	0.9
Rough Steel	0.8
Smooth Steel	0.7
Fusion Bonded Epoxy	0.6
Polyethylene	0.6

Although Equation 2-1 accounts for the effects of roughness and hardness on the interface friction angle, it neglects their influence on the contact pressure between the pipe and the surrounding soil during ground movements (Lings and Dietz, 2005; Abuel-Naga et al., 2018; Guo and Zhou, 2024). During the pullout process, the contact pressure exerted on the pipe surface is likely influenced by soil arching effects and constrained dilation at the soil-pipe interface (Guo and Zhou, 2024). Karimian (2006) and Wijewickreme et al. (2009) noted that the contact pressure on the surface of rough steel pipes increases due to constrained dilation of the surrounding soil, which in turn leads to greater axial pullout resistance. Sheil et al. (2018) also observed that soil arching affects the contact pressure around fusion-bonded epoxy-coated steel pipes, consequently influencing their pullout behaviour. Following the initial soil dilation, the contact pressure decreases with increased displacement due to frictional degradation, which is primarily driven by particle crushing and rearrangement (Anderson, 2004; Weerasekara, 2011). Prior to pullout, the roughness of the soil-pipe interface does not significantly impact the initial contact pressure distribution on the pipe surface. However, studies by Karimian (2006), Wong et al. (2021), and Guo and Zhou (2024) show that the average contact pressure on the pipe surface increases during the axial pullout process. As lateral strains develop in the soil due to relative movement between the pipe and the surrounding soil, the normal stress acting on the pipe increases compared to at-rest conditions. This increase in radial pressure, which occurs during the pullout process, causes the surrounding soil to stiffen, and this increased soil stiffness generally results in greater pressure on the pipe (Meidani et al., 2018).

Several researchers have proposed alternative equations for estimating axial soil loads beyond Equation 2-1, as found in various studies (Danish Submarine Pipeline Guidelines, 1985; McAllister, 2001; Meidani et al., 2018; Al-Khazaali and Vanapalli, 2019; Wong et al., 2021; Reza and Dhar, 2021a; Reza et al., 2023a; Guo and Zhou, 2024; Reza and Dhar, 2024).

The Danish Submarine Pipeline Guidelines (1985) introduced Equation 2-2, derived by integrating shear stresses around the pipe to estimate the frictional force per unit length of the pipeline. In this equation, φ represents the soil's internal friction angle, while W_p denotes the weight of the pipe. The guidelines accounted for the weight of the pipeline in their estimation.

$$T_u = \left[\frac{\gamma D}{2} \tan\varphi \left(H + \frac{D}{2}\right) \pi(1 + K_0) + \frac{4W_p}{3\pi}(2 + K_0) - \frac{\gamma D}{3}(2 + K_0)\right] \tan\delta \qquad \text{Equation 2-2}$$

McAllister (2001) proposed Equation 2-3 to determine the axial resistance of buried pipelines for burial depths up to three times the pipe diameter, incorporating the pipe's weight in the formulation.

$$T_u = \left[2D\gamma \left(H - \frac{D}{2}\right) + W_p\right] \tan\delta \qquad \text{Equation 2-3}$$

Meidani et al. (2018) developed Equation 2-4, which introduced a modified earth pressure coefficient, K^*, instead of the conventional at-rest earth pressure coefficient. This equation was derived from a 3D discrete-element (DE) analysis of steel pipes buried in dense sand. The modified coefficient, K^*, is given in Equation 2-5, where E_s is the soil's Young's modulus and Δt represents the thickness of the shear zone.

$$T_u = \pi D\gamma H \left(\frac{1 + K^*}{2}\right) \tan\delta \qquad \text{Equation 2-4}$$

$$K^* = 2.75K_0\left(\frac{E_s}{\gamma H}\right)^{0.38}\left(\frac{\varphi}{45}\right)^{1.39}\left(\frac{\Delta t}{D}\right)^{0.42}$$ Equation 2-5

Al-Khazaali and Vanapalli (2019) proposed Equation 2-6, which is based on experimental investigations of the axial force-displacement behaviour of buried pipelines in saturated and unsaturated sand. In this formulation, $f(A)_{unsat}$ represents the mobilized axial skin friction for unsaturated conditions, γ' is the effective unit weight of soil, $(u_a - u_w)_{av}$ is the average matric suction around the pipe, S is the degree of saturation, η is a fitting parameter, δ_{ps-r} is the residual plane strain interface friction angle, and ψ_p is the peak dilation angle. The equation accounts for the influence of matric suction on interface shear strength and the dilatancy at the soil-pipe interface.

$$f(A)_{unsat} = \left[\gamma' H\left(\frac{1+K_0}{2}\right) + (u_a - u_w)_{av}S^{\eta}\right]\tan\left(\delta_{ps-r} + \psi_p\right)$$ Equation 2-6

Wong et al. (2021) introduced Equation 2-7, incorporating rate-dependent soil strength and variations in effective stress. In their formulation, α represents a soil adhesion factor dependent on the normalized shear strength of the soil, $c_e(e, \dot{\varepsilon})$ is the Hvorslev cohesion as a function of void ratio (e) and strain rate ($\dot{\varepsilon}$), σ_v and σ_h are the total vertical and horizontal stresses, respectively, and u_w is the pore water pressure. For simplicity, they took stresses and pore water pressure at the pipe embedment depth; however, for more accurate results, these should be integrated around the pipe's periphery.

$$\frac{T_u}{\pi D} = \alpha c_e(e, \dot{\varepsilon}) + \left[\frac{(\sigma_v - u_w) + (\sigma_h - u_w)}{2}\right] \tan\delta \qquad \text{Equation 2-7}$$

Reza and Dhar (2021a) proposed Equation 2-8, which calculates the non-dimensional maximum axial pullout force for MDPE pipes buried in loose to medium-dense sand. In this equation, P_u is the peak axial pullout force and L is the mobilized frictional length. They also considered the effect of ground movement rates.

$$\frac{P_u}{\pi D L \gamma H} = 0.183 \ln(pulling\ rate\ in\ mm/min) + 0.46 \qquad \text{Equation 2-8}$$

Reza et al. (2023a) formulated Equation 2-9, incorporating a normal stress adjustment factor (ξ) to account for dilation-induced increases in normal stress on buried pipes.

$$T_u = \xi \pi D \gamma H \left(\frac{1 + K_0}{2}\right) \tan\delta \qquad \text{Equation 2-9}$$

Guo and Zhou (2024) developed Equation 2-10, which takes into account the average contact pressure increment due to constrained dilation, pipe weight, and a roughness-dependent soil-pipe interface friction factor. In their formulation, G represents the soil shear modulus, ψ_{max} is the peak dilation angle of the soil, u_c is the critical axial displacement where the mobilized dilation angle reaches its peak, $\Delta\gamma$ is the difference in unit weight between the pipe and backfill soil, and f_R is the roughness-dependent soil-pipe interface friction factor.

$$T_{max} = \pi D \left[\gamma H \frac{1 + K_0}{2} + 2G \frac{u_c}{D} \tan \psi_{max} + \frac{D}{4} \Delta\gamma \right] \tan(f_R \varphi) \qquad \text{Equation 2-10}$$

Reza and Dhar (2024) proposed Equation 2-11, which is based on finite-element analysis for estimating the maximum axial pullout force of buried pipes observed in laboratory tests. This equation incorporates the compaction-induced lateral stress ($\Delta\sigma_{com}$) and considers the variations in contact pressure resulting from shear-induced dilation or changes in pipe diameter.

$$T_u = \xi \pi D \left(\frac{\gamma H + K_0 \gamma H + \Delta\sigma_{com}}{2} \right) \tan \delta \qquad \text{Equation 2-11}$$

These proposed equations reflect the continuous advancement in the understanding and modelling of axial soil loads on buried pipelines, incorporating various factors such as soil conditions, pipeline materials, dilation effects, and ground movement rates.

2.8 Compaction-Induced Stresses

Several authors explored the compaction-induced lateral pressures experimentally (Rehman and Broms, 1972; Carder et al., 1977; Carder et al., 1980; Duncan and Seed, 1986; Duncan et al., 1991; Clayton et al., 1991; Clayton and Symons, 1992; Massarsch and Fellenius, 2002; Chen and Fang, 2008; Gui et al., 2020; Ezzeldin et al., 2022) and using finite element analysis (Katona et al., 1976; Taleb and Moore, 1999; Elshimi and Moore, 2013; Dezfooli et al., 2015; Ezzeldin and El Naggar, 2021, 2022; Saleh et al., 2021; Vilca et al., 2024; Reza and Dhar, 2024). Table 2-2 summarizes the horizontal stresses on the buried structure caused by backfill compaction reported by different authors. More recently, Reza and Dhar (2024) employed compaction-induced lateral earth pressure similar to Duncan and Seed (1986) in the three-dimensional finite-element (FE) analysis that successfully simulated the measured pipe response obtained during the axial movements of pipes in dense sand.

Table 2-2: Summary of compaction-induced horizontal stresses on the buried structures

Source	Compaction Method	Soil Type	Maximum Induced-Stress (kPa)	Depth (m)	Remarks
Rehman and Broms (1972)	Loose	Gravelly Sand	21	0.75	Due to the wheel loads of 7.5 tons
	Vibratory Plate	Gravelly Sand	7.6	0.75	
	Loose	Silty Fine Sand	12.8	0.75	
	Vibratory Plate	Silty Fine Sand	6	0.75	
Carder et al. (1977)	Twin–roll Vibratory Roller	Clean Medium Sand	11.3	0.83	
Carder et al. (1980)	Static Roller	Silty Clay	14.5	0.83	
Duncan and Seed (1986)	Single Drum Roller	Sand	25.7	0.22	Roller 0.3 m away from wall
		Sand	54.6	0.17	Roller 0.15 m away from wall
Clayton et al. (1991)		Medium to high plasticity clay	0.2 to 0.4 times C_u		
Clayton and Symons (1992)		Clay	0.8 times C_u		
Chen and Fang (2008)	Vibratory Plate	Air-dry Ottawa Sand	7.6	0.25	
Gui et al. (2020)	Vibratory Plate		28.6		
	Vibratory Roller		30.6		
Ezzeldin et al. (2022)	Vibratory Plate	Air-dry Ottawa Sand	5.9	0.45	
Katona et al. (1976)			34.5		Applied vertical pressure to simulate compaction

Taleb and Moore (1999)		Granular	Rankine Passive Earth Pressure	Upper limit for induced-stress
Elshimi and Moore (2013)			Kneading coefficient times Rankine Passive Earth Pressure	Upper limit for induced stress
Dezfooli et al. (2015)		Cohesive Soil	0.5 times C_u	
Ezzeldin and El Naggar (2021)			15 to 30	Applied surface loading to simulate compaction
Ezzeldin and El Naggar (2022)			10 to 40	Applied surface loading to simulate compaction
Vilca et al. (2024)		Cohesive Soil	0.8 times C_u	
Saleh et al. (2021)	Jumper Jack		Distributed strip load	
	Embedment Wheel		Distributed line load	

2.9 Numerical Studies

Several researchers have conducted numerical investigations on axial pipe-soil interaction, contributing significantly to the understanding of this complex phenomenon (Wijewickreme et al., 2009; Meidani et al., 2017, 2018, 2020: Al-Khazaali et al., 2019; Murugathasan et al., 2021; Muntakim and Dhar, 2021; Reza and Dhar, 2021a; Reza and Dhar, 2021b; Saberi et al., 2022; Reza and Dhar, 2024).

Wijewickreme et al. (2009) developed a two-dimensional (2D) continuum-based finite difference model to investigate the axial pullout behaviour of buried steel pipes using FLAC 2D software. In their study, the pipes were radially expanded by 0.7 mm to 1 mm to capture the shear-induced dilation effect. They compared the simulated normal stresses on the pipe with the experimental data during backfilling and pipe pullout tests in order to validate the model. The soil elements were modelled using the Duncan-Chang model (Duncan and Chang, 1970; Byrne et al., 1987), which is based on a hyperbolic relationship between stresses and strains and incorporates the Mohr-Coulomb failure criterion. This model is basically a nonlinear elastic model with loading and unloading/reloading elastic moduli that are stress-dependent and formulated using power law functions. The interface between the pipe and soil during radial expansion of the pipe was modelled using unbonded interface elements with the Coulomb shear strength criterion.

Meidani et al. (2017) conducted the analysis of a buried steel pipe in axial loading embedded in dense granular material using the 3D discrete-element method (DEM) by using the open-source code YADE. In DEM, interactions between soil particles are treated as dynamic processes in which equilibrium is attained when internal and external forces are balanced. The model has been validated against experimental test results from Wijewickreme et al. (2009). The backfill soil was modelled by discrete spherical particles of different sizes, for which the radius expansion method was applied to achieve a porosity of 0.41. Calibration of the soil properties was done by simulation of triaxial tests on the sand used in the studies of Wijewickreme et al. (2009) and from the results of Karimian (2006). The pipe was modelled using triangular facet elements (flat discrete elements) that do not allow for the development of axial or radial deformation in the pipe structure. Cundall's linear elastic-plastic law, which is capable of transmitting moments between particles, was used as the contact law between particles. During pipe pullout, they noticed that most of the soil movement occurred around the pipe within a zone of approximately 1.5 times the pipe diameter, resulting in volume change and an increase in normal stress acting on the pipe.

Meidani et al. (2018) also employed the 3D DEM as described in the previous paragraph. The model was validated by comparing the results of the radial earth pressure acting on the pipe with the existing analytical solution of Hoeg (1968) and with the axial pullout experimental test results of Karimian (2006).

Al-Khazaali et al. (2019) developed a plain strain 2D FE analysis using SIGMA/W software to investigate the behaviours of buried rigid and flexible pipelines in saturated and unsaturated conditions. The soil was modelled using the elastic-perfectly plastic Mohr-Coulomb constitutive model for both saturated and unsaturated conditions. The semi-empirical model proposed by Vanapalli et al. (1996) was used to predict the effective shear strength of unsaturated soil and to derive the apparent cohesion of soil for modelling the unsaturated sand. The depth-dependent modulus of elasticity of unsaturated sand was estimated using the semi-empirical method proposed by Vanapalli and Oh (2010). Using line area, the soil-pipe interface was generated around the external surface of the pipe.

Meidani et al. (2020) developed a coupled finite-discrete element (FE-DE) approach to investigate the response of buried MDPE pipes in dense sand subjected to axial soil movements using a modified version of the open-source code YADE. The axial pullout test results of Weerasekara (2007) were used to validate the model. The MDPE pipe was modelled using eight-noded hexahedral finite elements, and the soil was modelled using spherical discrete elements. They used interface elements to transfer the forces between the discrete and finite element domains. They found that the pipe experienced significant elongation combined with a slight distortion in the pipe cross-section during the axial pullout of MDPE pipes.

Murugathasan et al. (2021) modelled the axial pullout behaviour of ductile iron pipes buried in loose and dense sand by using 3D FE analysis in ABAQUS. The model was validated with the experimental results. The soil and pipe are modelled as deformable bodies using eight-node linear brick elements with reduced integration (C3D8R). The stress-strain behaviour of sand was modelled with the Mohr-Coulomb plasticity model. The surface-to-surface contact approach was used to simulate the contact between the pipe and the soil. From the finite-element analysis, they found that the dilation of the surrounding soil increases the normal stresses on the pipe.

Muntakim and Dhar (2021) developed a 3D FE analysis using ABAQUS to explore the axial response of buried MDPE pipes. The model was validated with the experimental results reported in Weerasekara and Wijewickreme (2008). The soil and the pipe domains were modelled using C3D8R elements. General contact algorithm was used for the contact between the pipe and the soil. The Mohr-Coulomb model was used to model the stress-strain behaviour of sand. Based on finite-element analysis, they introduced a normal stress factor ζ for rationally calculating the normal stress and, hence, the pullout force for buried MDPE pipes.

Reza and Dhar (2021a, 2021b) developed a 3D FE analysis to model the axial soil-pipe interaction of MDPE pipes using ABAQUS. The model was validated with the results of full-scale axial pullout tests. The pipe and soil domains were modelled using C3D8R solid elements. The general contact algorithm was used to model the contact behaviour between soil and MDPE pipe. The MDPE pipe was idealized as a linear elastic material. For the soil, the elastic-perfectly plastic model with Mohr-Coulomb plasticity was employed to model the stress-strain behaviour and shear failure of the sand. From the FE analysis, they proposed pulling-rate-dependent interface friction reduction factors for MDPE pipes. They suggested a normal stress adjustment factor ζ to account for the reduction of normal stress due to the reduction in pipe diameter.

Saberi et al. (2022) proposed a hybrid-Winkler interface (HWI) approach for simulating soil-pipe interaction behaviour under cyclic loading using ABAQUS with a user subroutine UMAT. The model was validated with the experimental test results from the studies of Sheil et al. (2018) for steel pipes, Weidlich and Achmus (2008) and Bilgin and Stewart (2009a) for HDPE pipes. This approach consisted of beam elements to represent the pipe structure, Winkler springs to represent soil mass, and a solid thin-layer interface element to represent the soil-pipe interface. A bounding surface plasticity constitutive model was used to model the interface element (Saberi et al., 2016). The thickness of the interface element was assumed to be between 5 and 22 times the mean particle size of the surrounding soil. The Winkler springs are defined using the bi-linear elastic-perfectly plastic, as recommended in ALA (2005). Eleven parameters were required for the HWI interface constitutive model, which were determined using constant normal load (CNL) and constant normal stiffness (CNS) interface shear tests.

Reza and Dhar (2024) developed a 3D continuum-based FE model similar to the Reza and Dhar (2021a, 2021b). In addition, they applied compaction-induced stresses as thermal expansion stresses based on Saleh et al. (2021) to simulate the real-life compaction-induced stresses on buried pipes. They also performed beam-on-spring analysis using ABAQUS. The pipeline was modelled as a Timoshenko beam using PIPE21 elements, and the pipe-soil interaction (PSI) was modelled using the pipe-soil interaction element (PSI24).

2.10 Summary

The literature review highlights the studies on the behaviour of buried MDPE pipes subjected to axial ground movements, with a focus on experimental and numerical studies. Axial pullout tests have been extensively used to examine how MDPE pipes respond to varying soil conditions, pipe diameters, and pulling rates. These tests demonstrate that peak pullout resistance increases with larger pipe diameters, deeper burial, and denser soils. Higher pulling rates generally lead to greater pullout resistance, emphasizing the significance of understanding soil-pipe interaction for pipeline integrity subjected to ground movement conditions.

Numerical models, including FE and DE methods, have been developed to simulate soil-pipe interactions. These models help analyze the impact of axial loading on both MDPE and steel pipes, accounting for factors like soil compaction, shear-induced dilation, and variations in contact pressure. Validated by experimental data, these models provide deeper insights into the complex behaviours of buried pipes, helping refine design equations and predictions.

The review also discusses the effects of surface roughness, coating hardness, and soil arching on the axial pullout behaviour of buried pipes. Rougher surfaces and denser soils tend to increase friction at the soil-pipe interface, enhancing pullout resistance. Additionally, temperature fluctuations and cyclic loading have been found to reduce the pullout resistance of pipes, especially in colder conditions. Current design guidelines often tend to underpredict or overestimate axial forces for flexible MDPE pipes, prompting the need for the development of more accurate models and equations for various soil conditions.

While several researchers (e.g., Anderson, 2004; Weerasekara, 2007, 2011; Weerasekara and Wijewickreme, 2008; Wijewickreme and Weerasekara, 2015; Reza and Dhar, 2021a, 2021b, 2024; Reza et al., 2023a) have experimentally investigated the axial pullout responses of small-diameter MDPE pipes buried in sand under varying conditions (loose, medium-dense, and dense sand; different burial depths), their work has predominantly focused on the pipe-pull mechanism, where the pipe moves relative to stationary soil. However, the soil-pull mechanism where the soil mass moves relative to a stationary pipe, has not been systematically studied for MDPE pipes, despite its critical relevance in practical ground movement scenarios such as landslides.

Furthermore, although prior studies have examined the effects of pulling rates on axial pullout behaviour under pipe-pull conditions, the influence of displacement rates under the soil-pull mechanism remains largely unexplored. Similarly, the impact of compaction-induced stresses on axial soil-pipe interaction, particularly under active ground movement, has not been comprehensively addressed in previous research.

Addressing these notable research gaps, this thesis presents full-scale experimental studies specifically designed to examine the soil-pull mechanism, systematically varying ground movement rates and compaction methods. In addition, three-dimensional finite element modelling was employed to simulate the observed behaviours, providing a refined understanding of the mechanics governing axial soil-pipe interaction for MDPE pipes. The outcomes of this work contribute critical insights necessary for the development of more robust and reliable design methodologies for buried flexible pipelines subjected to geohazard-induced ground movements.

CHAPTER 3: Laboratory Investigation of Buried Small-Diameter Medium-Density Polyethylene Pipes Subjected to Axial Ground Movement

3.1 Introduction

Natural gas transmission and distribution pipelines are the major energy infrastructure in North America. According to PHMSA (2018), there are ~2.54 million miles of natural gas pipelines in the United States, of which distribution lines account for ~87%, and transmission lines account for ~12% of total pipe. Distribution pipelines are typically smaller diameter lines with lower pressures that deliver natural gas directly to local homes and businesses (American Gas Association, 2022). Plastic pipes are the most common type of pipe used in the gas distribution network. Among them, medium-density polyethylene (MDPE) is widely used for making distribution networks because of its favourable properties like flexibility, strength, lightweight, resistance to corrosion, and aging (PHMSA, 2018) The MDPE pipes have the added advantage over high-density polyethylene (HDPE), as they exhibit higher ductility and fracture toughness, although having a long-term strength and stiffness similar to HDPE (Stewart et al., 1999). In some European countries, such as the UK, Denmark, and France, more than 90% of the gas pipelines in urban areas are currently made up of MDPE (Li et al., 2022).

Over two decades, from 1999 to 2019, there were 1,438 reported incidents related to natural gas distribution pipelines (Williams and Glasmeier, 2023). These incidents consisted of corrosion, material fatigue, and external damage from activities like accidental digging and ground movements (Allegro Energy Consulting, 2005). Ground deformation hazards such as landslides, soil liquefaction, uplift, subsidence, and tectonic fault movements often threaten the structural integrity of the pipelines and the safety of the surrounding environment and infrastructure

(Kishawy and Gabbar, 2010; Feng et al., 2015; Lee et al., 2016; Psyrras and Sextos, 2018; Weerasekara and Rahman, 2019; Vesseghi et al., 2021). In Peru, for instance, the individual sections of the Camisea pipeline system exploded on multiple occasions between 2004 and 2007 after landslide motions were initiated by heavy rainfall (Lee et al., 2009). Marinos et al. (2019) analyzed the landslide hazards affecting the Trans Adriatic Pipeline in Albania and reported that permanent ground deformation (PGD) compromised the pipeline integrity. In 2018, the China-Myanmar gas pipeline exploded due to a combined effect of long-term rainfall and engineering activities-triggered landslides in Guizhou, China (Cheng et al., 2021). Vasseghi et al. (2021) studied the failure of an underground natural gas pipeline that occurred in Iran in 2019; a landslide initiated by very intense rainfall caused the pipeline to rupture.

Slope inclinometers and vibrating wire piezometers are typically used to measure ground movements and pore water pressures in landslide-prone areas (Mines et al., 2022) as a part of the integrity assessment of pipeline networks. Survey-based technologies such as GPS units and survey prisms (Groves and Wijewickreme, 2013; Ferreira and Blatz, 2021) and remote sensing technology such as LiDAR, InSAR, UAV photogrammetry, and laser scanning (Macciotta and Hendry, 2021) also accompanied the monitoring of ground movements. However, estimating the pipe conditions utilizing the measured ground movements from different methods is still very challenging. Rajani et al. (1995) proposed limit equilibrium and force-displacement approaches to determine the axial loads on the pipe due to longitudinal ground movements. Currently, pipe responses (e.g., pipe wall strain, peak axial force) to ground movements are generally calculated using beam-on-spring analysis for a known (measured) ground displacement (ALA, 2005; PRCI, 2017). The design guidelines proposed elastic-perfectly plastic soil parameters for axial, lateral, and vertical springs. These springs are developed based on small-scale laboratory tests of rigid pipes. However, cross-sectional and longitudinal deformations along the pipe length are expected for flexible pipes during ground displacement. Therefore, the soil parameters developed based on rigid pipes may not apply to flexible MDPE pipes.

Although some experimental studies were conducted to investigate the response of flexible (HDPE and MDPE) pipes under axial loading (Anderson, 2004; Weerasekara and Wijewickreme, 2008; Bilgin and Stewart, 2009a; Wijewickreme and Weerasekara, 2015; Reza and Dhar, 2021a, 2021b; Reza et al., 2023a; 2023b), more field and laboratory test data for flexible pipes are required for improvement of the understanding the behaviour and then, the design guidelines for the pipes. Bilgin and Stewart (2009a) measured the reductions in pipe diameter that affect the interface shear resistance between the pipe and soil. Weerasekara and Wijewickreme (2008) and Reza et al. (2023a) used cavity expansion theory to account for soil dilation in dense sand to simulate the pipe response during ground movements. Wijewickreme and Weerasekara (2015) introduced the concept of frictional degradation in their analytical formulations, hypothesizing that individual pipe sections would be subjected to distinct levels of interface shear displacements. Reza and Dhar (2021a and 2021b) suggested pulling rate-dependent interface friction coefficients to account for the time-dependent response of the pipe material.

Furthermore, all the studies on the axial loading of pipelines were conducted by pulling a pipe through a static soil mass, referred to as "Pipe-Pull". However, axial force on the static pipe against moving soil, referred to as "Soil-Pull", which is often a realistic scenario of ground movement against pipelines, was not examined. During analysis, the mechanism behind pipe-pull and soil-pull is assumed to be the same for the same relative movement. The assumption of this equality implies that the soil's shearing resistance encountered due to the moving pipe is equivalent to the shearing resistance during the soil movement against static pipes. While this assumption of equal forces might be useful for conceptual analysis, real-world conditions (where soil particles move against fixed pipes versus a pipe pulled through static soil) may involve complexities that lead to differences in measured forces. For instance, as soil displaces, finer particles could occupy the spaces between larger particles, thereby increasing the contact area with the interface structure (Yang et al., 2010). Particles near the interface may also exhibit rolling and overriding of neighbouring particles during shearing, which could result in non-uniform particle displacement around the pipe. On the other hand, soil particles at the interface may not move at all during pipe-pull, particularly for a smooth pipe like MDPE. Therefore, the contact pressure between the soil and the pipe could differ in each scenario (i.e., pipe pullout and soil box displacement). In order to examine the possible distinctions between the two methods, the current study compares the behaviour of MDPE pipes subjected to pipe pullout and soil box displacement against a static pipe.

Gas pipelines are typically buried just below the ground surface at depths of less than one meter (Ferreira and Blatz, 2021). When these pipelines are situated near existing structures or beneath road embankments, the backfill soils are often compacted. The compaction of soil adjacent to structures is particularly significant for pipes and culverts that are buried at shallow depths (Taleb and Moore, 1999; Elshimi and Moore, 2013). Various compaction methods are utilized according to industry practices. The type of compaction equipment employed, such as manual tampers, static rollers, vibrating plate tampers, rammers, etc., influences the depth and degree of compaction (Duncan and Seed, 1986). The compaction efforts for transmission and distribution pipelines differ substantially due to variations in size, depth, operating pressure, soil conditions, and environmental and regulatory requirements. Transmission pipelines may necessitate more rigorous compaction to ensure structural integrity and stability due to their larger scale and higher operational stresses. During compaction, vertical and horizontal earth pressures in the soil mass increase due to the force or energy transferred by compaction equipment. While post-compaction earth pressures generally decrease, the horizontal pressures remain significantly higher than precompaction levels, while vertical pressures revert to overburden pressure values (Duncan et al., 1991).

Over a four-year observation period, Ferreira and Blatz (2021) noted that compaction-induced stresses either remained at their initial levels, slightly diminished, or completely dissipated. Near the surface, residual lateral pressures can exceed typical at-rest pressures and may approach passive pressure values (Duncan et al., 1991; Chen and Fang, 2008). Residual earth pressures, accounting for 40% to 90% of the peak lateral pressure increment due to compaction, may persist as locked-in stresses (Duncan and Seed, 1986). Ferreira and Blatz (2021) specifically reported locked-in stresses on pipelines caused by backfill compaction using the back of an excavator bucket. The force exerted by a vibratory roller is estimated to be approximately two to four times its static weight (Duncan and Seed, 1986). Numerous researchers have investigated compaction-induced lateral earth pressures through experimental studies (Rehman and Broms, 1972; Carder et al., 1977; Carder et al., 1980; Duncan and Seed, 1986; Duncan et al., 1991; Clayton et al., 1991; Clayton and Symons, 1992; Massarsch and Fellenius, 2002; Chen and Fang, 2008; Gui et al., 2020; Ezzeldin et al., 2022) and finite element analysis (Katona et al., 1976; Taleb and Moore, 1999; Elshimi and Moore, 2013; Dezfooli et al., 2015; Ezzeldin and El Naggar, 2021, 2022; Saleh et al., 2021; Vilca et al., 2024). More recently, Reza and Dhar (2024) employed compaction-induced lateral earth pressure in the 3D FE analysis that successfully simulated the measured pipe response obtained during the axial movements of pipes in dense sand. However, the current design guidelines (ALA, 2005; PRCI, 2017) do not account for the effect of backfill compaction method in estimating the maximum axial soil resistance of pipes subjected to axial ground movement.

Landslides are complex geological phenomena with considerable variability in characteristics such as speed, volume, and movement type (Cheaib et al., 2022). The effects of the rate of ground movements and the pipe-soil relaxation mechanisms are the two crucial factors for understanding the interaction between soil and buried pipelines, especially for MDPE pipes, as they show nonlinear time-dependent stress-strain behaviour (Bilgin et al., 2007; Das and Dhar, 2021). Ferreira and Blatz (2021) investigated the stresses on gas pipelines in the landslide-prone zones of Manitoba, where average downslope ground movements are 25 mm/year at Harrowby site and 40 mm/year at St. Lazare site. In another study, Groves and Wijewickreme (2013) analyzed the response of MDPE pipes in a slow-moving landslide in Chilliwack, British Columbia, documenting the total ground movement as 450 mm over seven years at an average rate of 5 mm/month. In this regard, the study by Bruschi et al. (1996) and Bughi et al. (1996) describes a case with extensive details on the field monitoring practices undertaken for the pipeline installed in the mountainous regions of Italy, which are historically associated with slow but very widespread ground movement. Rizkalla et al. (1993) investigated landslide conditions in northern Alberta, highlighting the risks posed by sensitive river valley slopes to buried pipelines. Their findings indicated that the observed ground movements varied annually, ranging from slow creeping motions to a rate of 60 mm per year. Wong et al. (2021) also studied the ground movement that affected the pipelines in Grande Prairie, Alberta, Canada. They reported that the average slope movement varies about 10-20 mm per year. On the other hand, Bonasera et al. (2024) undertook a detailed study of the slow landslide at Nevissano, Piedmont, Italy. Their investigation revealed a significant ground displacement, measuring approximately 90 mm over a period of seven years, from 2017 to 2024.

The ground movements discussed above classification pertain to very slow-moving landslides, according to Cruden and Varnes (1996). However, slow landslides have the potential to gain speed rapidly as a result of occurrences like earthquakes, as documented by Cheaib et al. (2022) in their study of landslides triggered by the 2017 Sarpol Zahab earthquake in Iran. Seasonal variations also affect the rate of ground movement as it increases during periods of high precipitation or snowmelt and decreases during drier periods (Keefer and Johnson, 1983; Kalaugher et al., 2000; Bonaser et al., 2024). Ground movement can be intermittent in nature, with periods of inactivity followed by the reactivation of slow-moving landslides (Wood Environment & Infrastructure Solutions, 2021). The reactivation of the ground movements is often due to heavy rainfall or ice and snow melting. These inactive periods may cause relaxation that could reduce the stresses imposed by the ground movements (Bruschi et al., 1995; Scarpelli et al., 1995). The ground movement rate can differ from place to place and even within the same area, with stress relaxation at the pipe-soil interaction. Furthermore, it has been observed that not every ground movement in a landslide will occur in the same direction, although the overall trend of movement may be in a specific direction (Wood Environment & Infrastructure Solutions, 2021). Hence, the effect of ground movement rates and relaxation behaviour on the axial or compressive response of buried MDPE pipelines should be examined thoroughly.

Ferreira and Blatz (2021) demonstrated that pipeline responses vary between slower and sudden landslides, with a gradual increase in longitudinal stress during slower ground movements and a distinct increase during sudden ground movements. In some instances, longitudinal stress decreases during ground movements, possibly due to a soil-pipe relaxation mechanism. Reza and Dhar (2021a and 2021b) and Reza et al. (2023a) experimentally investigated the pulling rate effects (0.5 mm/min to 2 mm/min) on the axial pullout behaviour of MDPE pipes, revealing the rate-dependency of the interface frictional behaviour. Weerasekara (2011), Wijewickreme and Weerasekara (2015), and Reza (2024) investigated the impact of stress relaxation in MDPE pipes by stopping the pipe pulling for 9 to 10 days during axial pullout tests. It was found that the measured pullout resistance dropped significantly, and the pipe wall strains were redistributed along the pipe length during the relaxation period (over 9 to 10 days). However, these tests were conducted by pulling the pipe through a stationary soil mass.

Under the background discussed above, to cover up the prevailing knowledge gap, this research is conducted to understand different factors that govern the axial pullout response of buried MDPE pipes. In particular, attention is paid to the effects of different methods of backfill compaction, intermittent ground movements, ground movement rates, and the effects of soil-pipe relaxation and under loading-unloading-reloading cycles. This chapter presents findings from full-scale laboratory tests conducted at the testing facility of Memorial University of Newfoundland. The tests dealt with pipes of different diameters, rates of pulling, compaction techniques, and burial depths. The experimental setup consists of a fixed pipe (fixed at one end only) with a moving soil block. Key parameters such as the mobilization of axial soil resistance, pipe elongation, strain at the pipe's restrained end outside the soil box, and strain distribution along the pipe were monitored during the tests. Thus, through a systematic analysis of these quantities, the present study provides important knowledge on the mechanical behaviour of buried MDPE pipes and hence helps in devising better design and construction practices related to buried piping systems.

3.2 Experimental Setup

3.2.1 Test Facility

A full-scale axial soil-pipe interaction test facility developed at the Memorial University of Newfoundland was employed to conduct the experiments. This setup, previously used for axial pullout tests by pulling the pipe through a stationary soil block (Murugathasan et al., 2021; Reza and Dhar, 2021a; 2021b; 2023a; Chakraborty, 2022), has been modified to allow a soil block to move against a pipe fixed at one end (Andersen and Dhar, 2023; Andersen, 2024), thereby simulating a real-world ground movement scenario. Figure 3-1 presents the schematic layout of the test facility.

The test setup includes a base frame, hydraulic ram reaction frame, backstop frame, carriage frame, linear bearings, steel tank, hydraulic actuator system, and data acquisition system. The base and backstop frames are permanently bolted to the concrete floor and reinforced against the reaction frame of the hydraulic ram, ensuring a rigid foundation for the test setup. Six linear bearings are mounted between the base and carriage frames and provide a near-frictionless movement system. The facility contains a steel tank of internal dimensions of 4 m x 2 m x 1.5 m (length x width x height), which facilitates a range of burial depths to be achieved for the pipes. The presence of stiffeners provides a structurally reinforced soil box to resist lateral deformations by providing it with rigid boundary conditions in vertical and horizontal planes (Murugathasan et al., 2018). The boundary effect is ruled out due to the wide width of the soil box in axial pullout tests (Reza and Dhar, 2021a; Guo and Zhou, 2024). A hydraulic actuator system pulling the soil tank at different rates of pulling up to 10 mm/min simulates differential rates of ground movement. The mechanism moves a carriage frame sliding on six linear bearings between a base frame, with a travel limit of 300 mm. However, the maximum allowed movement for the tank is 150 mm due to the limitation of the built-in hydraulic ram LVDT system. Although the facility limits the maximum soil displacement to 150 mm, this does not impact the validity of the test results. Peak axial forces were consistently mobilized before soil displacements of 90 mm during both trial and full-scale tests, with typical displacements reaching 90 mm and up to 120 mm in one case. Since the study focuses on peak pullout forces and not post-peak behaviour, the available displacement capacity was sufficient to achieve the research objectives. Facility instrumentation includes load cells, LVDTs, potentiometers, pressure transducers, fibre optic sensors, and electrical strain gauges, all of which are connected to a data acquisition system through a personal computer for simultaneous data collection. A detailed description of the instrumentation system is discussed in Section 3.3.2. Additional information on the test facility may be found in Andersen and Dhar (2023) and Andersen (2024).

3.2.2 Instrumentation System

The current research mainly focuses on the behaviour of MDPE pipes subjected to axial ground movements. Hence, most of the instrumentation concentrated on measuring the loads and strains on the pipe when exposed to the movement of the soil in the test box. The instrumentations used are described in the following sections.

3.2.2.1 Load Cells

A pancake load cell (Model: Omega LCHD-5K) with a capacity of 22.5 kN (5000 lbs) is positioned between the pipe's fixed end and the backstop frame of the test facility to measure the pipe's axial forces developed during the movement of the soil box. The backstop frame includes a vertical channel section designed to accommodate the load cell installation. Vertical and horizontal alignment of the load cell is made with the pipe segment, and then the load cell is bolted to the steel channel section. A custom-made connector is then threaded into the center shaft of the load cell, its opposing end connected to the steel adapter via a clevis and shear bolt connection (Figure 3.2). It is important to note that the steel adapter is initially threaded into the MDPE pipe during the pipe preparation. In addition, the clamping ring is tightened to the end of the pipe to secure the threaded steel adapter. Figure 3-2 illustrates the connection between the load cell and the pipe segment, and Table 3-1 provides the specifications for the Omega LCHD-5K load cell.

The Omega LCHD-5K load cell is a high-performance sensor featuring high-quality strain gauges that ensure excellent linearity and stability. This leads to very accurate and repeatable measurements. The working principle of the load cell is based on the strain gauge technology; the strain gauges are bonded on a metal structure known as the load-bearing element (Omega Engineering, 2024). When a force is applied, the load-bearing element undergoes slight deformation (either elongation or compression), depending on the direction of the applied force. This deformation is transmitted to the strain gauges, which are resistive elements sensitive to strain. The deformation alters the electrical resistance of the strain gauges, a change that is subsequently captured by a Wheatstone bridge circuit. The bridge output signal is directly proportional to the changes in resistance from this characteristic and is related to applied load. The output signal of the load cell was calibrated for the measured force.

3.2.2.2 LVDTs

Linear Variable Displacement Transducers (LVDTs) (Model: Honeywell JEC-AG DC-DC Long Stroke) were employed to measure the displacement of the pipe segment's free end and the tank movement during axial pullout tests. The Honeywell JEC-AG DC-DC Long Stroke LVDT is capable of measuring linear displacements over extended distances, with a measurement capacity of 110 mm. The LVDTs positioned at the pipe's free end and the backstop frame are utilized to measure the pipe's elongation, whereas the LVDT attached to the tank wall monitors the tank's movement. The arrangement of the LVDTs is depicted in Figure 3-3, and the specifications of the Honeywell JEC-AG LVDTs are detailed in Table 3-2.

LVDT works on the principle of a moving ferromagnetic core and three coils arranged on the sensor longitudinally (Honeywell, 2024). A core is attached mechanically to an object whose position is being measured, and it is further connected to two secondary coils along with one primary coil. A magnetic field is established at the same frequency, typically in the order of kilohertz, in the region around the primary when an alternating current (AC) is passed through the primary coil. These fields induce voltages in the secondary coils. The position of the movable core corresponds linearly to the differential voltages in the secondary. In its operating principle, when the core is centrally placed at the null position of the LVDT, the magnetic flux linked between the two secondary coils is equally distributed. Consequently, balanced but opposite voltages are induced across the secondary coils, thereby ultimately producing a null output or zero differential voltage. As the core deviates from this central position, the symmetry of the magnetic flux distribution is disturbed. This, in turn, presents an imbalance of the voltages induced in the secondary coils. This imbalance thus creates a differential voltage that is proportional to the displacement of the core from the null position. The polarity of this differential voltage tells the direction in which the core is moving; therefore, the sign of the voltage changes as the core moves in the positive or negative direction with respect to the null position. DC-DC LVDTs contain additional electronic circuitry that is used to demodulate the incoming AC signal and eventually convert the differential voltage at the output into direct current (DC). The DC output is directly proportional to linear displacement.

3.2.2.3 String Potentiometers

In addition to using LVDTs, string potentiometers (Model: Kyowa DTPA-A-500) with a 500 mm capacity are attached to both the free and fixed ends of the pipe to measure its elongation. The Kyowa DTPA-A-500 is a potentiometer-type displacement transducer that translates the expansion or contraction of a sensing wire into an electrical signal to measure displacements. The arrangement of the potentiometers is depicted in Figure 3-4, while the specifications of the Kyowa DTPA-A-500 potentiometers are summarized in Table 3-3.

The operational mechanism of string potentiometers involves a flexible stainless-steel cable that is coiled onto a precision-engineered drum located within a protective casing (Kyowa Electronic Instruments Co Ltd, 2024a). As the object to which this cable is attached moves, the cable extends or retracts with respect to the sensor; the movement makes the drum rotate. This drum is mechanically coupled to a high-precision potentiometer working as a variable resistor. When the drum revolves, its wiper is moved across the resistive element, changing the value of the resistance. The variation in resistance is linear with the length of the extended cable. This, in turn, is proportional to the displacement of the object to which it is attached. The potentiometer is normally used as a part of the external electrical circuit in a voltage divider configuration. As a result, resistance variation gives a corresponding change in output voltage. This voltage can be measured with great precision and used to give a very accurate indication regarding the position or displacement of an object.

3.2.2.4 Electrical Resistivity Strain Gauges

To monitor the axial strain during testing, electrical resistivity strain gauges (Model: Kyowa KFEL-5-120-C1) were attached to the pipe's crown, invert, and springlines near the fixed end outside the soil box. These high-elongation foil-type sensors are designed for the measurement of very large strains in materials and structures, ranging from the elastic through to the plastic zones. Unlike conventional strain gauges intended for small deformations, Kyowa KFEL-5-120-C1 gauges are engineered to handle significant elongations with high accuracy and durability. In the axial pullout tests of MDPE pipes, higher axial strains are expected because of its lower modulus of elasticity and higher elongation behaviour. The KFEL series strain gauges can measure strains up to 10% to 15% under simple tension strain conditions. The surface of the MDPE pipe segments is prepared by roughening with sandpaper to create a textured finish, followed by wiping with alcohol wipes. The CC-36 strain gauge adhesive, compatible with the strain gauges, is applied to this textured surface to ensure it accommodates and transfers the larger strains without peeling off the pipe's surface. The strain gauges are then positioned on the adhesive layer and pressed down with poly sheeting by thumb for 30 to 60 seconds. The gauges were then left undisturbed in order to cure for about one hour. The time of application of finger pressure varied with temperature and humidity levels, with lower levels requiring a longer application time. The copper wires of the strain gauges are connected to an external terminal through soldering arranged in a U-shaped loop to prevent damage during pullout tests. Multi-stranded wires are used to connect the gauges to the data acquisition system. To protect the strain gauges during handling and test preparations, they are wrapped with poly sheets and secured with sheathing tape. Figure 3-5 illustrates the arrangement of the electrical resistivity strain gauges, and Table 3-4 provides the specifications for the Kyowa KFEL-5-120-C1 strain gauges.

A strain gauge functions based on the principle that the electrical resistance of a material changes in response to mechanical deformation (Kyowa Electronic Instruments Co Ltd, 2024b). Strain gauges are fabricated from a very thin conductive material arranged in a grid pattern and bonded securely on the surface of the object that is under investigation. When such an object is subjected to tensile or compressive loading, the strain gauge shall deform along with it. This strain changes the electrical resistance of the gauge in direct proportion. A Wheatstone bridge circuit normally works to measure this tiny change in resistance. The circuit translates this change in resistance to a voltage signal. This voltage signal, after calibration, provides a precise measurement of the strain in the object.

3.2.2.5 Fibre Optic Sensor System

A LUNA ODiSI 6100 Fiber Optic Sensor System is used to capture the mobilization of axial strains along the length of a pipe during pullout tests. This system represents a major innovation in monitoring technology, with accurate high spatial resolution measurements of both strain and temperature over long distances. The ODiSI 6100 system is based on Distributed Fiber Optic Sensing (DFOS) with the help of Optical Frequency Domain Reflectometry (OFDR) and a single-mode optical fibre as the primary sensing element. This system can provide measurements of strain and temperature with extraordinarily high spatial resolution (Luna Innovations Inc., 2020). It achieves this by analyzing Rayleigh backscattering, a phenomenon that occurs when a laser pulse propagates through the optical fibre and interacts with the inherent imperfections within the fibre. When the fibre undergoes changes in strain or temperature, these fluctuations induce alterations in the properties of the backscattered light. The ODiSI system precisely captures and processes these variations, enabling the accurate determination of both the location and magnitude of the changes along the entire length of the fibre. The system comprises an Optical Distributed Sensor Interrogator (ODiSI), standoff cables, remote modules, a dedicated instrument controller, and high-definition fibre-optic strain sensors. The fibre-optic strain sensor has a strain limit of 3%, though the system can only measure strain up to 1.5%. The pipe segment is initially laid on a flat surface, and its crown is abraded in multiple directions using coarse and fine sandpapers to create a hatch abrasion pattern. Afterward, the pipe is cleaned with alcohol wipes. The crown is marked, and the sensors are aligned along this path. Kapton dots are placed at 250 mm to 300 mm intervals to temporarily secure the sensors in the desired position. Polyurethane epoxy is then applied to both ends of the sensors. Once hardened, a catalyst is applied between the Kapton dots, followed by an M-bond 200 adhesive to bond the sensor to the MDPE pipe's surface. The Kapton dots are then removed, and catalyst and M-bond adhesive are applied to these spots to ensure continuous sensor contact with the pipe surface. The setup allows for cure for about 12 to 24 hours. Subsequently, a thin layer of silicone caulking is applied over the bonded sensors to protect them during handling, pipe laying, and compaction. Sheathing tape is then placed over the caulking layer as an additional protective measure and to reduce friction. Detailed instructions for the installation of fibre optic sensors can be found in Luna Innovations Inc. (2017). Figures 3-6 and 3-7 illustrate the fibre-optic sensor system and the step-by-step procedures for instrumenting the fibre-optic sensors, respectively. Table 3-5 summarizes the specifications of the high-definition fibre-optic strain sensors.

3.2.2.6 Low-Pressure Transducers

The Low-pressure transducers (Model: Kyowa PGM-02KG) are used to measure the vertical and horizontal soil pressures. The transducers of this model have been very successful in measuring very low-pressure values with good accuracy and stability. Similar transducers of this kind were used with great success by Chen and Fang (2008) to measure the vertical and horizontal soil pressures during their backfilling and compaction in their research study. The arrangement of these pressure transducers is illustrated in Figure 3-8, and their specifications are detailed in Table 3-6. These transducers are designed to measure pressure with precision using strain gauge technology. The basic working principle is based on a diaphragm that deforms under the action of applied pressure (Kyowa Electronic Instruments Co Ltd, 2024c). Such deformation results in the change of electrical resistance of strain gauges bonded to the diaphragm. These strain gauges are properly arranged in a Wheatstone bridge circuit, making it possible to transform very small changes in resistance into an electrical signal that could be measured. The signal is then amplified and processed by the internal electronics of the transducer, and this gives a standardized output, mostly in the form of analog signals to accurately reflect the applied pressure. The calibration process of the low-pressure transducers is discussed in Appendix B.

3.2.2.7 Data Acquisition System

To accurately capture the effects of a slow movement rate, all instrumentations are recorded at a frequency of 2 Hz. This ensured that the data reflected the gradual changes in the monitored parameters. Various signals from the instrumentation, with the exception of those from fibre-optic sensors, are collected and recorded using the National Instruments NI Signal Express 2015 module. This module provided a robust platform for acquiring and analyzing the data from multiple sources, ensuring comprehensive data collection. On the other hand, the signals from the fibre-optic sensors are collected and recorded through the LUNA ODiSI 6100 system. Figure 3-9 shows the arrangement of the data acquisition system. By utilizing these specialized systems for different types of sensors, the experiment ensured high-quality data collection and precise monitoring of the slow movement effects.

3.2.3 Material Characteristics

3.2.3.1 Sand Backfill

Locally available, clean, well-graded sand, that is commonly used in research on the pipe-soil interaction at Memorial University of Newfoundland (Reza and Dhar, 2021a, 2021b) has been selected in the present study as a backfill material. This sand is manufactured through the mechanical crushing of rocks (Saha, 2021). The sand comprises approximately 1.3% fines and 98.7% sand particles. It exhibits a standard proctor compaction maximum dry density of 18.8

kN/m³ with an average particle size of 0.742 mm, a coefficient of uniformity of 5.81, and void ratios ranging from a minimum of 0.33 to a maximum of 0.65 (Saha et al., 2019; Saha, 2021). However, in the current study, following ASTM D4254-16 and ASTM D4253-16e1 procedures, respectively, the maximum and minimum dry density tests yielded values of 16.58 kN/m³ and 19.62 kN/m³, respectively, with corresponding maximum and minimum void ratios of 0.55 and 0.31. The reason for this difference in the maximum void ratio is the procedure followed for the test to determine the minimum dry density of the sand. It is also worth noting that the values of maximum and minimum dry density for any particular sand very much depend on the standards used to determine them (Blaker et al., 2015; Lunne et al., 2019).

The results from the standard Proctor compaction test performed by Saha (2021) on the sand sample, as illustrated in Figure 3-10, reveal notable trends in the dry unit weight of the sand in relation to varying moisture contents. Initially, the dry unit weight is at its maximum when the moisture content is 0%. This peak dry unit weight decreases with an increase in the moisture content up to a certain limit; above 4% of moisture content, a reverse is experienced, and this dry unit weight rises further with an increase in moisture content. However, after reaching a moisture content of 10%, the compaction curve transitions to the wet side, indicating that additional moisture no longer contributes to an increase in dry unit weight.

Furthermore, particle size analysis tests in accordance with ASTM D6913-17 were performed in the current study. The resulting grain size distribution curve, as shown in Figure 3-11, closely matched those reported by Saha et al. (2019). This consistency confirms that the soil particles remain intact, not fragmenting into smaller particles despite repeated use of sand for full-scale tests involving compaction efforts with both vibratory plate and hand tampers.

Saha (2021) researched the mechanical properties of sand under direct shear and triaxial tests. The research found that the friction angle of the sand is influenced by its density, level of stress, and moisture content. Saha (2021) presented Figure 3-12, which depicts the relationship between moisture content, the angle of internal friction, and the dry unit weight of compacted sand. Based on this figure, the internal friction angles corresponding to soil densities of 18.1 kN/m³ and 17.5 kN/m³ were reasonably estimated to be 44° and 42°, respectively. Adopting Equation 3-1, as suggested by Bolton (1986), the calculated dilation angles for the indicated densities were 11°, 9°, and 2°. On the other hand, Chakraborty and Salgado (2010) provided Equation 3-2 to compute the dilation angle at very low confining pressure, Where ψ_p is the peak dilation angle of soil; $\emptyset'_p$ is the peak friction angle of soil; and $\emptyset'_{crit}$ is the critical state friction angle of soil. The application of Equation 3-2 yielded dilation angles of 15°, 12°, and 3° for the corresponding density-dependent friction angles. Bolton (1986) developed the equation based on high confining stress, whereas Chakraborty and Salgado (2010) came up with their equation based on low confining stress for both two-dimensional and three-dimensional conditions. The latter is most applicable to this present study, considering that the pipes in this present work are buried at shallow depths (i.e., H = 625 mm), where the magnitude of the confining pressure would be on the low side. As such, the dilation angles determined using the method of Chakraborty and Salgado (2010) give a better representation of the conditions of this study. A critical state friction angle of 35° has been reported by Saha (2021) for the backfill sand. Concerning the kneading effect during backfilling and levelling, it was challenging to maintain the soil layers in a pure loose condition. Considering these, a friction angle of 37° was reasonable for the uncompacted backfill with a density of 14.8 kN/m³. Table 3-7 provides a summary of the soil classification and relevant properties of the backfill sand. Further information on the backfill sand can be found in Saha (2021).

$$\psi_p = \frac{\emptyset'_p - \emptyset'_{crit}}{0.8} \qquad \text{Equation 3-1}$$

$$\psi_p = \frac{\emptyset'_p - \emptyset'_{crit}}{0.6} \qquad \text{Equation 3-2}$$

The stress-dependent modulus of elasticity of the backfill soil was determined using the power law equation of Janbu (1963), as given by Equation 3-3, where E_s is the elastic modulus of soil; k is the material constant; p' is the mean effective confining pressure; P_a is the atmospheric pressure; and n is the power law exponent.

$$E_s = kP_a \left(\frac{p'}{P_a}\right)^n \qquad \text{Equation 3-3}$$

The equation proposed by Janbu (1963) has been extensively used for estimating the modulus of elasticity of soil in numerical modelling for pipe-soil interaction analysis (Taleb and Moore, 1999; Yimsiri et al., 2004; Guo and Stolle, 2005; Daiyan et al., 2011; Jung et al., 2013). The k value of sand varies from 100 to 400 for loose sand to dense sand (Holtz et al., 2011). In the current study, values of $k = 150$ for dense sand (vibratory compaction), $k = 125$ for dense sand (hand compaction), and $k = 100$ for loose sand were used, with n value of 0.5 (Roy et al., 2016; Reza and Dhar, 2021a, 2021b, 2024; Muntakim and Dhar, 2021; Fellenius, 2023). Atmospheric pressure was considered to be 101.3 kPa. The mean effective confining pressure in Equation 3-3 was calculated based on the initial geostatic stress conditions prior to any ground movement. It is primarily derived from the vertical effective stress using the effective unit weight of the soil and the burial depth, assuming at-rest lateral earth pressure conditions (i.e., K_0 state). Stress changes due to pipe movement, shear-induced dilation, or strain-softening behaviour are not included in this estimation. Therefore, the modulus E_s represents the small-strain stiffness of the soil under undisturbed conditions. While this assumption is valid for capturing the initial stiffness relevant to mobilizing peak pullout forces, it may not fully reflect stiffness degradation or non-linear behaviour during large displacements. Using equation 3-3, the elastic modulus of soil was calculated as 5.08 MPa for vibratory plate compaction, 4.16 MPa for hand compaction, and 3.06 MPa for loose sand at a depth of 625 mm. Similarly, at a depth of 340 mm and 480 mm, the elastic modulus of soil was determined as 3.07 MPa and 3.65 MPa, respectively, for the hand compaction of backfill.

In addition, this study incorporated tests on Ottawa sand, which was specifically used for the sand replacement test. The primary objective of these supplementary tests was to verify and calibrate the parameters associated with Ottawa sand. According to the relevant standards outlined earlier, Ottawa sand's minimum and maximum dry densities were determined to be 15.24 kN/m^3 and 17.16 kN/m^3, respectively. This is consistent with the findings of Carey et al. (2020), who reported minimum and maximum dry densities of 14.62 kN/m^3 and 17.23 kN/m^3, respectively, for Ottawa sand. In further investigations within this study, various filling methods were employed to determine the minimum dry density of Ottawa sand, which was identified as 14.87 kN/m^3. When applying similar filling methods, the minimum dry density of sand was found to be 15.55 kN/m^3.

These findings highlight the variability in reported densities and underscore the necessity for a standardized approach to determining the minimum and maximum dry densities of sand on a global scale, as advocated by Blaker et al. (2015) and Lunne et al. (2019). The test for minimum and maximum dry densities of backfill sand and Ottawa sand is discussed in Appendix C.

3.2.3.2 MDPE Pipe Material

The present study focused on CSA B137.4 certified MDPE pipes. These pipes were selected in two different sizes: one with an outer diameter of 42.2 mm and a wall thickness of 4.22 mm, corresponding to a standard dimension ratio (SDR) of 10, and the other with an outer diameter of 60.3 mm and a wall thickness of 5.48 mm, corresponding to an SDR of 11. The stress-strain relationship of the material has a pronounced effect on the axial pullout behaviour of MDPE pipes. Previous works have shown that the stress-strain responses of MDPE are very nonlinear and extensively dependent on both the strain rate and temperature. (Stewart et al., 1999; Sulieman and Coore, 2004; Hamouda et al., 2007; Bilgin et al., 2007; Bilgin and Stewart, 2009a; Weerasekara, 2011; Das and Dhar, 2021). However, in the case of very small strains, MDPE shows linear stress-strain behaviour (Bilgin et al., 2007; Das and Dhar, 2021). To study the viscoelastic behaviour of MDPE, researchers conducted uniaxial tests with MDPE specimens (Anderson 2004, Weerasekara 2011, Das and Dhar 2021). Hamouda et al. (2007) conducted uniaxial tension-relaxation tests, which indicated that the relaxation behaviour of MDPE is markedly sensitive to the rate of strain. Liu et al. (2008) tested the creep behaviour of HDPE and MDPE pipe materials and identified that the molecular structure of these two different materials varies, leading to different kinds of responses under loading conditions. Das and Dhar (2021) investigated the strain rate-dependent mechanical behaviour of MDPE and revealed that for strain rates less than 10^{-6}/s, the influence of strain rate on MDPE stress-strain responses is negligible. This is validated by the findings of Sulieman and Coore (2004) that the strain rates between 10^{-1}/s and 10^{-5}/s have a pronounced effect on the stress-strain responses of MDPE: modulus of elasticity increases with an increase in strain rates. Figure 3-13 shows the rate-dependent stress-strain responses obtained from constant strain-rate tests by Das and Dhar (2021). Weerasekara and Wijewickreme (2008) also tested the initial modulus of elasticity of MDPE at 20 °C, with a value of 645 MPa obtained. Das and Dhar (2021) have further extended this and tested the initial modulus of elasticity over several strain rates of 10^{-6}/s to 10^{-2}/s, with values obtained being between 325 MPa and 1054 MPa. The MDPE material exhibits typical relaxation behaviour, where an initial sharp decrease in stress is observed that gradually steadies with time (Das and Dhar, 2021).

Stewart et al. (1999) noted that the modulus of polyethylene is significantly influenced by temperature variations; within the range of 0 to 49 °C, the modulus can vary by a factor of two, with higher values at lower temperatures. The effects of temperature and strain rate on the stress-strain behaviour of the polyethylene material tested by Stewart et al. (1999) are plotted in Figure 3-14. Bilgin and Stewart (2009a) studied the temperature-dependent stress-strain behaviour of MDPE pipes and found that lower temperatures correspond to a higher modulus of elasticity. Bilgin et al. (2007) also conducted laboratory experiments to determine the thermal and mechanical properties of polyethylene pipes and reported that, on account of the viscoelastic nature of this material, the magnitude of the temperature effect on its modulus is also relatively high. In the current study, all tests were carried out at an ambient temperature of about 20 °C to reduce the thermal effects on MDPE pipe material.

3.2.4 Test Preparation

3.2.4.1 Pipe Specimen Preparation

All axial pull-out tests were conducted on straight MDPE pipes, 4.6 m long, available by cutting original pipes that were of a length of 6 m. Tests were performed for both bare and instrumented pipes; instrumentation included strain gauges and fibre optic sensors on the pipe wall. The end walls of the soil tank were designed with 177 mm diameter holes, one each on the ends, covered with rubber gaskets and steel plates to enable the insertion of MDPE pipes in the soil tank. The holes cut in the rubber gaskets are 3 mm larger than the pipe diameter, and the holes in the steel plate are made slightly larger than the holes in the gasket so that a minimum amount of friction between the tank and pipe in the tank can be assured while performing axial pullout testing. It was found that the friction offered by the gasket was only 0.2 kN (Reza and Dhar, 2021a), which was very minimal compared to the axial pullout forces. The pipe was inserted into the tank through the rubber gasket hole near the hydraulic ram and placed on top of the prepared soil bed, as discussed in Section 3.2.4.2. The length of the pipe was parallel to the length of the soil container, with ends extending out at both ends via a rubber gasket to ensure a constant length of pipe-soil interaction of 4 m during testing. The alignment of the pipe was checked using a string run parallel to the pipe from end to end along the tank walls. After aligning the pipe, the backfilling was completed, as noted in following section.

3.2.4.2 Soil Bed Preparation and Backfilling

Soil was first placed in the tank and compacted up to the invert level of the pipe. The invert level was established with level pegs using string, and a spirit level was used to ensure that the portion between the adjacent level pegs was level. The soil bed was compacted using either a battery-operated vibratory plate tamper (Wacker Neuson APS1135e) or a hand tamper (W = 115 mm, L = 290 mm) to achieve the desired density (Figure 3-15) or left in a loose condition without compaction.

The backfilling process began once the pipe was placed and aligned, as detailed in section 3.2.4.1. A 10T overhead crane was used to lift and pour the sandbags inside the soil tank. The soil was layered in approximately 100 mm to 150 mm thick increments to achieve the desired burial depth. The top surface of each layer was levelled using a handmade spreader. Afterwards, each layer was compacted as described earlier. Sand cone tests, in accordance with ASTM D1556 (2016), and in-situ density measurement cylinders (degree of disturbance < 10%) were carried out on the surface layer to confirm that the desired density conditions were achieved. It is important to note that the density measured using the sand cone method can be influenced by the shape and depth of the excavated hole (Park, 2010). Determining the soil density of loose, uncompacted sand using sand cone replacement tests proved challenging. As a result, proctor compaction test moulds and relative density test moulds were utilized to measure the density of the loose sand. Figure 3-16 illustrates the in-situ density tests conducted on the backfill soil. Finally, the burial depth was reconfirmed, and any excess soil was trimmed away.

The average soil density for tests compacted with the vibrating plate tamper was 18.1 kN/m^3 (54% relative density, 96% relative compaction), while the hand tamper resulted in an average density of 17.5 kN/m^3 (30% relative density, 93% relative compaction), and the loose condition had an average density of 14.8 kN/m^3 (78% relative compaction). The moisture content of the sand for all tests ranged between 1% and 2%. At these moisture contents, the effect of suction was reported to be negligible (Saha 2021). It is noted that, after each test, the soil tank was emptied right up to the bottom of the invert level of the pipe instead of making a trench to install pipes for the next tests. However, Reza and Dhar (2021a) suggested that the trench effect is negligible at distances greater than 5 times the pipe diameter. Figure 3-17 provides the step-by-step for the test preparation. It is important to note that the pipe used in each test was not reused in subsequent tests to eliminate the potential effects of any residual stresses.

3.2.5 Test Programme

This chapter covers the results of fifteen comprehensive full-scale tests. These tests investigated various parameters and their effects on the behaviour of straight MDPE pipes under different conditions. The parameters included two pipe diameters (42.2 mm and 60.3 mm), three different burial depths (340 mm, 480 mm, and 625 mm), and four pulling rates (0.25 mm/min, 0.5 mm/min, 1 mm/min, and 2 mm/min). Additionally, different compaction techniques were evaluated, including the use of a vibratory plate tamper, a hand tamper, and scenarios where no compaction was applied. Instrumentation with fibre-optic sensors was employed in two tests to precisely monitor and record the strain distribution along the pipe. Table 3-8 provides a comprehensive summary of the full-scale tests conducted in this study, detailing the specific conditions and configurations for each test.

Tests 1 through 7 and Tests 9 through 12 were conducted at a burial depth of 625 mm, whereas Tests 14 and 15 were performed at a burial depth of 600 mm. Additionally, Test 8 was conducted at a burial depth of 480 mm and Test 13 at 340 mm. These varied depths were selected to facilitate direct comparison with previous pipe pull tests conducted using the same testing facility and backfill materials (Reza et al., 2023a). The burial depths were measured from the pipe springline to the top surface. The compaction methods for these tests varied: Tests 1, 2, 7, 9, and 10 utilized a vibratory plate tamper with one pass for compaction. In contrast, Tests 3, 4, 8, and 11 through 15 employed hand tampers with five passes of blows. Tests 5 and 6 were kept in a loose condition without any compaction efforts. The selected pulling rates corresponded to moderate slides (Class 4) according to the landslide velocity classification system established by Cruden and Varnes (1996). Fibre optic sensors were installed along the pipes in Tests 7 and 15 to measure axial strain mobilization during the pulling process, providing detailed strain data critical for understanding the mechanical behaviour of the buried pipes under these conditions. In addition, in Test 12, low-pressure transducers were utilized to measure the vertical and lateral earth pressure during backfilling, compaction, and pullout tests.

For Tests 1, 2, 8, 9, 10, and 13, a specific protocol was followed: after the tank was displaced by 10 mm, it was held stationary for 20 minutes to allow the pipe and the entire system to undergo a relaxation period. Subsequently, the displacement of the soil tank was resumed until a total movement of 90 mm was achieved. The total displacement was larger than that needed to cause the maximum axial force (peak force) on the pipe. The pipe responses beyond the peak force are influenced by the length of the pipe samples (Reza et al., 2023a) and, therefore, are not used for interpretation of the test results. In Tests 3 and 4, the soil tank was displaced up to 45 mm. For Test 7, the maximum tank displacement was 60 mm. The maximum tank displacement was 90 mm for Tests 5, 6, 11, and 12. Additionally, Tests 14 and 15, which are described in detail in Section 3.4.5, follow a similar methodology but are distinguished by their specific parameters and conditions. The detailed descriptions and results of all tests provide further insights and contribute to a comprehensive understanding of soil-pipe interaction under various experimental conditions.

3.3 Test Results

3.3.1 Force-Displacement Responses

The movement of the soil in the tank applies axial force to the pipe buried in it through the interface shear. The axial force increases with the tank movement until the interface shear strength is fully mobilized over the entire pipe-soil interface and then stabilizes or decreases based on the post-peak behaviour of the interface shearing resistance. Figures 3-18 and 3-19 present the force-displacement responses for Tests 1 to 7 (with a pipe diameter of 60.3 mm) and Tests 9 to 12 (with a pipe diameter of 42.2 mm). These tests were conducted on bare MDPE pipes (except Test 7, which was instrumented with fibre optic sensor) subjected to four different displacement rates, ranging from 0.25 mm/min to 2 mm/min, and employed various backfill compaction methods. As depicted in Figures 3-18 and 3-19, the load (i.e., axial soil force) increases nonlinearly with the tank displacements. This nonlinearity in the force-displacement response becomes apparent almost immediately, beginning at a tank displacement of approximately 0.5 mm. Similar observations have been reported in the literature with pipe-pulling tests by Weerasekara and Wijewickreme (2008), Reza and Dhar (2021a, 2021b), and Reza et al. (2023a). The observed nonlinearity is due to the non-uniform mobilization of the interface frictional force along the length of the pipe. It results from progressive failure (reaching the shear strength or peak shearing resistance) at the soil-pipe interface from the restrained end toward the free end of the pipes as the soil tank moves toward the free end. The progressive mobilization of interface shearing strength initiates from the restrained end within the buried portion of the pipe and propagates toward the free end. This phenomenon has been previously observed, for example, by Chakraborty et al. (2023), using fibre optic sensors attached to the pipes.

The force-displacement responses obtained from all tests exhibit a high degree of consistency at lower tank displacements, as illustrated in Figures 3-18 and 3-19. This consistency in the initial portion of the displacement responses indicates that the burial conditions of the test pipes were consistent. Specifically, the straightness and depth of burial of the pipes were maintained consistently across all tests, ensuring that the initial conditions were similar. The deviations seen at higher displacements are due to properties of the inherent soil-pipe interaction and not due to deviations in the burial conditions of the pipes. In general, the axial force is lowest for the pipes in loose backfill and highest for the pipes in backfill compacted using vibratory plate tamper. The forces for backfill compacted using the hand tamper were in between the other two. No significant difference in the load-displacement responses was observed for changing the soil pulling rate for each kind of test. Table 3-9 shows the peak axial forces developed for each test and the corresponding soil displacement. Note that the soil displacements at the peak axial forces are not the displacement at the maximum longitudinal force per unit length specified in the design guidelines (i.e., ALA 2005, PRCI 2017). These displacements correspond to the mobilization of shearing resistance over the 4 m length of the pipe samples, which can differ for different lengths of the tested pipe samples. In the current study, which focuses on the soil-pull mechanism, the peak force location for each test is defined as the soil displacement corresponding to the measured maximum axial pullout force. It is important to note that this definition differs from the pipe-pull mechanism, where the peak force is typically associated with the initiation of trailing end movement of the pipe. For Tests 1 to 6 (Figure 3-18) and 9 to 12 (Figure 3-19), a distinct reduction in axial pullout force following the peak was observed, making the peak locations easily identifiable. However, for Test 7 (Figure 3-18), where fiber optic sensors were attached to the pipe, the axial force plateaued and remained approximately constant with further increases in soil displacement. In this case, the peak force location was defined as the point where the maximum axial force was first reached before the curve stabilized.

The effects of successive pulling on axial resistance are illustrated in Figures 3-18 and 3-19 for the pipes in backfill compacted using the vibratory plate tamper (Tests 1, 2, 9 and 10). In these tests, the tank’s movement was stopped at the displacement of 10 mm for 20 minutes and then moved again. Upon stopping the tank's movement at the displacement of 10 mm, the axial force immediately decreases by approximately 1 to 1.5 kN (Tests 1 and 2) and then remains steady for the duration of the hold period. Despite this immediate reduction, no further decrease in axial force was observed during the 20-minute relaxation period. It is likely that the force could continue to diminish over a longer relaxation period due to the time-dependent properties of the pipe material. The initial drop in axial force can be attributed to the redistribution of stresses that occurs when the tank movement ceases. This redistribution is influenced by the condition of the hydraulic system, whether it is maintained in a holding position or shut down to release the tank (Andersen, 2024). In this study, the hydraulic system was kept running to maintain the soil tank's position. During the reloading phase, the axial force increased along the same path as the unloading path and continued to rise until the pipe-soil interface shear strength was fully mobilized along the entire buried length of the pipe. After the full mobilization of shear strength, the pulling forces slightly decreased, indicating a strain-softening effect. As noted earlier, the peak force and the post-peak response are dependent on the pipe sample length and do not represent a general scenario. Therefore, post-peak responses were not investigated further.

Among the pipes in backfill compacted using the vibratory plate tamper, Test 7 in Figure 3-18 demonstrates axial force comparable to that observed in Tests 1 and 2 despite being equipped with fibre optic sensors along its entire length. While the instrumentation (i.e., fibre optic sensor with silicon caulking) can increase the surface roughness, the smooth sheathing tape used to cover sensor can reduce the surface roughness (Andersen, 2024). Thus, overall effect of the instrumentation was not significant on the load-displacement response for Test 7. The sheathing tape covers about 13% of the surface area of the pipe.

As discussed earlier, the peak forces observed during the tests cannot be predicted using the equation available in the design guidelines. Researchers proposed a higher coefficient of lateral earth pressure (K) in the design equation to calculate higher peak forces observed during the tests (Wijewickreme et al. 2009, Matymish et al. 2023). The peak axial forces observed in the current study and the corresponding lateral earth pressure coefficients required to simulate the peak force using the design equation are presented in Table 3-10. The lateral earth pressure coefficients are calculated using the friction factor value of 0.6 for the loose backfill and 0.75 for the compacted backfill. Previous research has demonstrated that the friction factor for MDPE is influenced by the pulling rate. Specifically, Reza and Dhar (2021a) proposed a rate-dependent friction factor, reporting values of 0.75 for a pulling rate of 0.5 mm/min, 0.86 for 1 mm/min and 0.9 for 2 mm/min. As discussed in the following section 3.3.2, the full-scale axial pullout tests conducted in this study indicated that pulling rate variations had minimal influence on frictional resistance. On the other hand, even though ASCE (1984), PRCI (2009) and PRCI (2017) recommend a friction factor of 0.6 for MDPE pipes, experimental evidence suggests that soil particle embedment into the flexible pipe surface increases friction at the pipe-soil interface (Scarpelli et al., 2003; Reza et al., 2023a; Guo and Zhou, 2024). Visible scratches and embedded soil particles on the MDPE pipe surface were observed after the tests. Consequently, a friction factor of 0.75 for the pipes in dense sand is considered reasonable.

As illustrated in Table 3-10, the vibratory compaction method (i.e. Tests 1, 2, 9, and 10) yielded K values in the range of 1.31 to 1.38 for 60.3 mm diameter pipes and 1.40 to 1.55 for 42.2 mm diameter pipes. Since both pipe sizes were buried at the same depth (i.e. 625 mm), the compaction-induced stresses generated by vibratory compaction were similar for both cases. However, according to the elastic cavity expansion theory, the normal pressure exerted on the pipe due to soil dilation is inversely proportional to the pipe diameter (Boulon and Foray, 1986; Johnston et al., 1987). Consequently, the dilation-induced effect is more pronounced for smaller diameter pipes, leading to the observed higher K values for 42.2 mm pipes compared to 60.3 mm pipes when subjected to vibratory compaction.

A similar trend was observed for the hand tamper compaction method (i.e. Tests 3, 4, 11, and 12), where the K values ranged from 0.40 to 0.45 for 60.3 mm pipes and 0.70 to 0.89 for 42.2 mm pipes. Given that these pipes were buried at the same depth (i.e. 625 mm), the compaction-induced stress from hand tamping was comparable across both cases. However, as previously mentioned, the dilation-induced effect was more significant for the 42.2 mm pipes, which resulted in higher K values compared to their 60.3 mm counterparts under identical hand tamper compaction efforts. When comparing the effect of different compaction methods, it is evident that vibratory compaction (Tests 1, 2, 9, and 10) consistently required higher K values than hand tamper compaction method (Tests 3, 4, 11, and 12). This observation aligns with previous research indicating that vibratory compaction generates dynamic forces that induce stress waves capable of penetrating deeper into the soil (Terzaghi et al., 1996). Supporting this, Holtz et al. (2022) asserted that vibratory compaction enhances densification over a thick soil layer compared to static compaction methods. Consequently, at any given depth within the influence zone, the compaction-induced stresses from vibratory compaction tend to be greater than those from hand tamper compaction. This explains the significantly higher K values observed for vibratory compaction compared to hand tamper compaction at a burial depth of 625 mm.

At shallower burial depths (i.e. 340 mm and 480 mm), hand tamper compaction resulted in substantially higher K values, reaching 1.54 in Test 8 and 3.08 in Test 13. This can be attributed to the increased compaction-induced stresses at shallower depths, which can approach passive earth pressure values (Duncan et al., 1991; Chen and Fang, 2008). Given that Test 8 was conducted at a shallower depth than Tests 3 and 4, both of which underwent the same hand tamper compaction effort, the higher compaction-induced stresses in Test 8 led to elevated K values. Similarly, in Test 13 (42.2 mm pipe at 340 mm burial depth), the combined effect of increased compaction-induced stresses and a more pronounced dilation-induced effect resulted in significantly higher K values than those recorded in Tests 11 and 12, which were subjected to the same compaction effort but at a greater burial depth. For the tests involving loose backfill conditions, an additional 10% increase in pullout force was considered to account for the challenges associated with maintaining uniform soil density across soil layers. Under these conditions, the calculated K value was 0.25, which is comparable to the theoretical at-rest earth pressure coefficient (K_0).

The lateral earth pressure coefficient calculated based on recommendation in Meidani et al. (2018) are also included in Table 3-10. Meidani et al. (2018) proposed a modified lateral earth pressure coefficient (Equation 3-4) to account for the shear-induced dilation of the surrounding soil, where K^* is the modified lateral earth pressure coefficient; K_0 is the lateral earth pressure coefficient at-rest, which can be determined from $K_0 = 1 - \sin\varphi$, as suggested by Jaky (1944); E_s is the modulus of elasticity of soil, the stress-dependent E_s can be calculated from Equation 3-3, as proposed by Janbu (1963); γ is the unit weight of the soil; H is the burial depth of the pipe; φ is the friction angle of soil, and the selection of friction angle for the respective compaction efforts was discussed in Section 3.2.3.1; Δt is the thickness of the shear zone; and D is the external diameter of the pipe. The thickness of the shear zone can be estimated as $10D_{50}$, where D_{50} is the mean particle size (Roscoe, 1970; Bridgewater, 1980). The D_{50} of the backfill sand used in the current study was varies from 0.885 mm to 0.897 mm, which implies a shear zone thickness of 8.85 mm to 8.97 mm, and there were no evident for such higher shear zone thickness during axial pipe-soil interaction of smaller diameter pipes. Karimian (2006) observed the movement of soil particles around the pipe and determined that the active sheared annular zone ranges from 1.2 mm to 2.8 mm during axial pullout tests of steel and polyethylene pipes in various soil conditions. A shear zone thickness of 0.8 mm, which is nearly equal to D_{50} was reasonably assumed to estimate the lateral earth pressure coefficient using Equation 3-4.

$$K^* = 2.75K_0\left(\frac{E_s}{\gamma H}\right)^{0.38}\left(\frac{\varphi}{45}\right)^{1.39}\left(\frac{\Delta t}{D}\right)^{0.42} \qquad \text{Equation 3-4}$$

In Table 3-10, the K values derived from Meidani et al. (2018) (Equation 3-4) closely align with those obtained in the present study for both 42.2 mm (Tests 9 and 10) and 60.3 mm (Tests 1 and 2) MDPE pipes in sand compacted using the vibratory plate compactor. However, for the application of hand tamper compaction method, the calculated K values from Meidani et al. (2018) were consistently higher than the experimentally determined values for both 42.2 mm (Tests 11 and 12) and 60.3 mm (Tests 3 and 4) pipes. For 60.3 mm pipes subjected to different compaction efforts (Tests 1, 2, 3 and 4), the Equation 3-4 produced relatively consistent K values, as was also observed for 42.2 mm pipes under varying compaction conditions (Tests 9, 10, 11 and 12). This trend is attributed to the fact that Equation 3-4 was derived primarily based on soil dilation effects around the pipe without explicitly accounting for compaction-induced stresses. The slightly higher Meidani et al. (2018) derived K values for 42.2 mm pipes compared to 60.3 mm pipes are consistent with the dilation-induced effect, which is more pronounced for smaller diameter pipes. At shallower depths, the dilation-induced effect is intensified due to lower confining pressure, whereas the stress-dependent elastic modulus of soil is lower. The combined effect of these factors resulted in the Meidani et al. (2018) K value for Test 8 (60.3 mm pipe at 480 mm depth) being similar to those for Tests 3 and 4 (60.3 mm pipes at 625 mm depth) when subjected to identical hand compaction conditions. However, for Test 13 (42.2 mm at 340 mm depth), the dilation-induced effect became dominant, leading to a higher calculated K value compared to those for Tests 11 and 12 (42.2 mm pipes at 625 mm depth) under similar hand compaction conditions.

Although the K values estimated using Equation 3-4 provide reasonable approximations in some cases (when the vibratory compaction method was applied), these are inconsistent for the other cases. This raises concerns regarding the accuracy and reliability of the K value given by Equation 3-4. Therefore, further research is necessary to estimate the axial forces on the pipe with a proper understanding of the mechanics of soil-pipe interaction.

3.3.2 Effects of Ground Movement Rate

Figures 3-18 and 3-19 also illustrate the effect of soil displacement rates on the pipe's axial resistance to movement. Overall, the maximum forces changed slightly for changing the ground movement rates from the minimum to the maximum values considered in this study. For the 60.3 mm diameter pipes (Figure 3-18), peak forces of 6.44 kN (Test 1) and 6.63 kN (Test 2) were measured for the vibratory plate compaction of backfill for pulling rates of 0.5 mm/min and 2 mm/min, respectively. Similarly, peak forces of 3.56 kN (Test 3) and 3.68 kN (Test 4) were observed for the hand compaction of backfill at pulling rates of 0.25 mm/min and 1 mm/min, respectively. For the loose backfill, peak pullout forces of 1.31 kN (Test 5) and 1.63 kN (Test 6) were recorded at pulling rates of 0.5 mm/min and 2 mm/min, respectively. Thus, the pullout peak forces of the 60.3 mm diameter MDPE pipes have increased by 2.9%, 3.5%, and 24.2% for vibratory compaction, manual compaction, and loose backfill, respectively, when the displacement rate is increased from the lowest to the highest rates.

For the 42.2 mm diameter pipes (Figure 3-19), peak pullout forces of 4.68 kN (Test 9) and 4.96 kN (Test 10) were measured for the vibratory plate compaction of backfill for pulling rates of 0.5 mm/min and 2 mm/min, respectively. For the hand compaction of backfill, peak pullout forces of 3.03 kN (Test 11) and 3.35 kN (Test 12) were observed at pulling rates of 0.5 mm/min and 2 mm/min, respectively. Thus, the peak forces were higher by 5.9% and 10.7%, respectively, for increasing displacement rates during both vibratory and manual compaction methods for MDPE pipes with diameters of 42.2 mm.

In general, the increases of peak forces for the pipes in compacted sand are not significant (2.9% to 10.7%), considering the uncertainties involved in the placement and compaction of backfill soil. Somewhat larger difference for the pipes in loose sand can be attributed to the inherent challenges in maintaining a uniformly loose soil condition across different tests. For hand compaction, the uniform soil condition might be possible, while vibratory compaction can provide more uniform condition. The pulling rate effects were less significant (<5.9%) for the pipes in backfill compacted with a vibratory plate compactor. Anderson (2004) also found negligible effect of pulling rates below 300 mm/h (5 mm/min) for MDPE pipes buried in backfill compacted with vibratory and manual compaction methods.

The above findings contradict the conclusions of Weerasekara (2011), Wijewickreme and Weerasekara (2015), Reza and Dhar (2021a, 2021b), and Reza et al. (2023a) that the pulling rate affects the pullout force of buried MDPE pipes pulled against static soil, where higher pulling rates produced higher peak pullout forces. Wijewickreme and Weerasekara (2015) observed a 57.7% increase in peak axial resistance by increasing the pulling rate of the pipe from 0.6 mm/min to 2.15 mm/min for a 60.3 mm diameter pipe. Similarly, for increasing the pulling rate from 0.5 mm/min to 2 mm/min for a 60.3 mm diameter pipe in Reza and Dhar (2021a), the peak axial resistance increased by 59.5%. The increase for the 42.2 mm diameter pipes was 60% for the same change of pullout rate, Reza and Dhar (2021b). The discrepancy between the current observations and those reported in Wijewickreme and Weerasekara (2015) and Reza and Dhar (2021ab) can be attributed to the nonlinear, time-dependent properties of the pipe material, which become more pronounced when the pipe is pulled against static soil. Note that the soil was moved against a pipe fixed at one end in the current study, while Wijewickreme and Weerasekara (2015) and Reza and Dhar (2021ab) pulled a pipe against a static soil. Polymer materials like MDPE show sensitivity to strain rate and rate dependence, with materials showing stiffer and stronger responses at higher strain rates. Therefore, at higher pipe pulling rates, the pipe material's effective stiffness increases and gives rise to higher peak pullout forces. Also, when the pulling rate is high, the surrounding soil may not have had sufficient time to reorganize and relax, so there is a lack of soil relaxation, which may contribute to higher confining pressures on the pipe. These increased pressures contribute to higher normal and shear stresses resisting the pipe's movement. On the other hand, the load is applied to the pipe through the movements surrounding soil in tests conducted in the current study. Thus, the load transfer mechanism might be different. The findings underscore the need for further research to explore the interactions between pipe materials, soil conditions, and displacement rates, contributing to the broader field of geotechnical engineering and infrastructure development.

3.3.3 Effects of Backfill Compaction Methods

Axial soil resistances for 60.3 mm and 42.2 mm diameter pipes subjected to different compaction efforts can also be observed in Figures 3-18 and 3-19. The compaction efforts include the use of a vibratory plate tamper in Tests 1, 2, 9, and 10, a hand tamper in Tests 3, 4, 11, and 12, and no compaction in Tests 5 and 6. All other conditions were kept constant across the tests, with the pulling rate being the variable factor. As discussed in Section 3.3.2, the effect of the pulling rate was considered insignificant for both vibratory and manual compaction methods. However, higher pulling rates for the uncompacted backfill resulted in higher axial forces, potentially due to inconsistent backfill conditions that could not be ensured during free fall and spreading of soil. The results indicate that compaction with the vibratory plate tamper provided significantly higher axial force—80% more for the 60.3 mm diameter pipes and 51% more for the 42.2 mm diameter pipes—compared to the hand tamper compaction. The axial force of the 60.3 mm diameter pipes increased by 147% for using hand-tamping compaction from the uncompacted loose condition. This significant increase in axial force with compaction can be attributed to the additional soil stresses, specifically "locked-in" compaction-induced stresses on the pipe surface, resulting in higher interface frictional resistance. Based on the measurements of compaction-induced earth pressure on non-deflecting soil-structure interfaces, Duncan and Seed (1986) and Duncan et al. (1991) showed that the residual horizontal earth pressure for compacted backfill can be higher and be specific to the compactors, such as a roller, vibratory plates, and rammer plates. The different methods of compacting the backfill soil have likely influenced the normal stresses acting on the pipes differently, which in turn affected the shear resistance of the pipes during soil displacement. The vibratory plate tamper produced higher normal stresses and shear resistances on the pipe surface, increasing the axial force. The hand tamper also enhanced compaction over the loose condition but was less effective in increasing the shearing resistance than the vibratory plate tamper compaction. Understanding these variations is crucial for accurately predicting the behaviour of buried pipelines under different soil compaction conditions.

Duncan and Seed (1986) reported that the load exerted by vibratory compaction can be two to four times higher than that of static roller compaction. Thus, the axial force on pipes in the backfill compacted using a static roller can be less than the force in the backfill compacted using the vibratory plate compactor. Figure 3-20 compares the axial forces for a pipe buried in a backfill compacted using the vibratory compactor (Test 1) with the results of a similar pipe in backfill compacted using a static roller reported in Weerasekara and Wijewickreme (2008). Both tests involved 60.3 mm diameter MDPE pipes buried at nearly identical depths and subjected to similar displacement rates. Specifically, the buried pipe length was 4 meters in Test 1 and 3.8 meters in the test by Weerasekara and Wijewickreme (2008), with burial depths of 625 mm and 600 mm, respectively. The pulling rates were 0.5 mm/min for Test 1 and 0.6 mm/min for the test by Weerasekara and Wijewickreme (2008). The axial forces in Figure 3-20 have been normalized by pipe diameter, length, buried depth, and sand density to facilitate the comparison. The normalized axial pullout forces observed in Figure 3-20 indicate that the forces from the vibratory plate compaction (Test 1) are higher than those from the static roller compaction. This is perhaps due to the larger compaction load the vibratory plate tamper applied, resulting in higher normal stresses on the pipes. Note that, in the test reported by Weerasekara and Wijewickreme (2008), the pipe was pulled directly through static soil, whereas in Test 1, a soil mass moved against a restrained pipe. This difference in the test methodology might also contribute to the variations observed in the results. The comparison between the pipe-pull and soil-pull methods is critical for understanding the influence of compaction techniques on soil resistance and is discussed in the following section (Section 3.3.4).

3.3.4 Pipe-Pull Versus Soil-Pull

Axial pullout forces obtained from the soil-pull tests from the current study and pipe-pull tests from Reza et al. (2023a) are compared in Figure 3-21. In the pipe-pull test, the leading end of the pipe is directly pulled, which translates into the elongation of the pipe until the trailing end begins to move. Conversely, in the soil-pull test, the elongation of the pipe is calculated from the difference between the readings of two LVDTs, one positioned at the fixed end of the pipe and the other at the free end. This setup allows for the estimation of pipe elongation during the soil displacement. Accordingly, axial forces are plotted against the pipe elongation in Figure 3-21 for a direct comparison.

For these tests, the height-to-diameter (H/D) ratio was maintained at 8. The burial depths were 340 mm for the 42.2 mm diameter pipes and 480 mm for the 60.3 mm diameter pipes. Consistent compaction efforts using a hand tamper were applied across these tests to ensure soil conditions similar to those in Reza et al. (2023a). Additionally, the pullout rate for the pipes and the soil box displacement rate were kept constant, at 0.5 mm/min for the 60.3 mm diameter pipes and 2 mm/min for the 42.2 mm diameter pipes, to provide a corresponding comparison. As depicted in Figure 3-21, the axial resistances were higher for the soil box displacement tests than for the pipe pullout tests. This difference in peak force between the two mechanisms is more pronounced for the 60.3 mm diameter pipes. During the soil mass displacement, finer soil particles have the potential to settle into the voids among the larger soil particles, leading to an increased contact area at the pipe-soil interface (Yang et al., 2010). This settling effect enhances the soil's density and compaction around the pipe, resulting in higher shear forces at the interface. Consequently, the axial forces in the soil-pull tests can be higher than those in the pipe-pull tests.

Thus, the differences in the axial force in Figure 3-21 can be attributed to the increased contact area and shear stresses during soil displacement for the 60.3 m diameter pipe (Test 8). However, for the 42.2 mm pipe (Test 13), the overall magnitude of increase in interfacial shear resistance is less pronounced due to less surface area than the 60.3 mm diameter pipe. The jumps observed in the load-displacement responses for Test 8 and Test 13 were due to the loading-unloading and reloading cycle applied during the tests to examine the behaviour. The discrepancies observed between soil-pull and pipe-pull tests necessitate a deeper investigation into the fundamental deformation mechanisms at the soil–pipe interface, specifically the distinction between rolling and overriding behaviors. Rolling behaviour occurs when the soil mass undergoes relative rotation along the surface of the stationary or moving pipe. In this mechanism, the interface experiences reduced shear engagement, resulting in lower mobilized resistance (Ni, 2003). Rolling is typically promoted by high soil flexibility, smooth interface conditions, and boundary constraints that allow soil elements to slip and rotate around the pipe. In contrast, overriding behaviour is characterized by the progressive accumulation and displacement of soil over and around the pipe, with limited freedom for rotational motion (Ni, 2003). This mechanism involves significant shear mobilization at the contact interface, leading to higher resistance forces. Overriding is generally favored by denser soils, rougher interface conditions, and restrictive boundary conditions that inhibit free soil movement (Al-Khazaali & Vanapalli, 2019).

In the present study, these mechanisms manifest differently between the two test types. The soil-pull tests — where the soil mass was displaced relative to a stationary pipe — triggered more overriding behaviour than initially anticipated. As the soil was forced to move over and around the stationary pipe, particularly across the crown and sides, it developed substantial shearing resistance. Overcoming these stresses required higher forces, resulting in elevated pull-out resistance measurements. Conversely, in the pipe-pull tests, where the pipe moved relative to stationary soil, the interaction promoted greater rolling behavior. The motion of the pipe, influenced by specific loading rates and surface conditions, allowed the adjacent soil to locally rotate and reconfigure around the pipe. This reduced the amount of active shearing at the interface, thereby lowering the mobilized resistance and resulting in lower pull-out forces compared to the soil-pull tests. The differences in the pipe-pull and soil-pull mechanisms can be further explained by examining the pipe elongations, as presented in Section 3.3.7.

3.3.5 Loading-Unloading-Reloading Responses

To investigate the loading-unloading-reloading responses of buried MDPE pipes, Tests 14 and 15 were conducted on 42.2 mm diameter MDPE pipes buried at a depth of 600 mm with a pulling rate of 0.5 mm/min. Test 14, conducted on a bare pipe, involved pulling the soil tank to a displacement of 95 mm (beyond mobilization of interface sharing resistance over the entire pipe length), followed by a 20-hour relaxation period, then pushing back 35 mm, with a subsequent 24-hour relaxation period. In contrast, Test 15 was performed on an MDPE pipe instrumented with fibre optic sensors along its length, as detailed in Section 3.2.2. This test included two cycles of loading, unloading, and reloading. In the first cycle, the soil tank was pulled to a displacement of 120 mm, followed by a 20-hour relaxation period. The tank was then pushed back 100 mm, causing the pipe to buckle towards the fixed end, which was mitigated by slightly pulling the tank 40 mm to straighten the pipe. The second cycle involved pulling the tank 60 mm, followed by another 20-hour relaxation period, and then pushing back 70 mm.

Figures 3-22 and 3-23 illustrate the variation of axial resistance over time for Tests 14 and 15, respectively. In both tests, the axial resistance increased non-linearly, reaching peak values of 3.76 kN at a tank displacement of 38 mm for Test 14 and 6.31 kN at a displacement of 102 mm for Test 15. The higher peak load observed in Test 15 can be attributed to the additional frictional forces introduced by the soft silicone caulking layer used to protect the fibre optic sensors. The silicone caulking covers approximately 15% of the pipe's surface area. Unlike Test 7, the sheathing tape was not used on top of the caulking in Test 15, allowing soil particles to penetrate the silicone caulking and increase the frictional coefficient (Scarpelli et al., 2003). The use of sheathing tape in Test 7 has proven to reduce the frictional resistance. In a previous study, Reza et al. (2023a) reported parallel scratches on the pulled-out surface of an MDPE pipe, confirming that the sand particles penetrated inside the pipe material. Guo and Zhou (2024) also observed soil particle embedment and scratches on the surface of the epoxy-asphalt-coated steel pipes. Given that silicone caulking is softer than the pipe material, it is highly probable that sand particles could penetrate the caulking, thereby increasing the axial resistance. When the hydraulic pump was stopped following the first pull, the pulling tests exhibited an abrupt drop in axial forces of between 0.5 and 1 kN, which matches closely with the 1 to 1.5 kN drop observed in Tests 1 and 2. This drop in force is most likely due to elastic stored energy being released. The pipe and surrounding soil can store elastic energy during pulling, and upon removal of the hydraulic force, the pipe may elastically rebound, leading to a reduction in axial force. After this sudden fall, the residual force slowly attenuated by relaxation, showing non-linear behaviour for the first few hours and linear decreasing at the rate of 0.31% per hour (Chakraborty et al., 2023). This relaxation behaviour can be attributed to the time-dependent properties of the pipe material and the soil–pipe interface interactions. Similar findings have been previously reported by Weerasekara (2011), Wijewickreme and Weerasekara (2015), and Reza (2024), which show significant reductions in pullout forces during the relaxation period of 9–10 days.

The axial force generated by soil movement caused axial deformation, resulting in the movement of the pipe's free end along with the soil mass. This free-end movement corresponds to the elongation of the pipe due to the axial force. Figures 3-22 and 3-23 demonstrate that the pipe’s elongation closely follows soil movement and axial force development, with elongations of approximately 25 mm for Test 14 and 60 mm for Test 15. In both tests, elongation was slightly reduced by 1 to 2 mm following the stopping of the hydraulic pump and subsequent relaxation, mirroring the behaviour of the reaction force. This indicates that pipe deformation is associated with stress redistribution, resulting in a reduction of axial force. It is important to note that the soil mass movement (test cell) was greater than pipe elongation from the beginning, indicating the mobilization of shear stress along the entire pipe length from the beginning. In contrast, when a pipe is pulled against a static soil mass, relative ground movement is gradually mobilized from the pulling end to the trailing end (Reza and Dhar 2021a, 2021b, 2023a; Wijewickreme and Weerasekara 2015). In their tests, the trailing end did not move immediately upon load application. Therefore, the load transfer mechanisms on the pipe from the surrounding soil differ when a soil mass moves against a static pipe compared to when a pipe is pulled against a static soil mass.

During the reverse movement (pushing) of the soil box, both the axial force and pipe elongation decreased. However, due to the differing load transfer mechanisms between pulling and pushing, the unloading did not follow the same path as the loading. In both tests, the axial forces eventually reduced to zero during the pushing phase. Continued movement of the soil box beyond this point generated compressive reaction forces on the pipes. This resulted in pipe buckling during the first pushing phase of Test 15, a phenomenon not observed in Test 14, as the pushing displacement and resulting compressive forces were comparatively less. Compressive forces of 2.3 kN and 5.6 kN were recorded during the first pushing phase of Tests 14 and 15, respectively. In Test 15, the pipe's response during reloading mirrored its behaviour during the initial loading despite reduced peak axial force and overall pipe elongation. The maximum reaction force during reloading was 5.3 kN, and the maximum pipe elongation was 52.3 mm, indicating a reduction in soil resistance of approximately 10% during the second load cycle. The observed phenomenon can be attributed to the arching effect that arises after the initial cycle when the interface bonding is released. In subsequent cycles, the residual shearing resistance decreases further. This reduction in shearing resistance may be due to the breakage of the soil structure at the interface, which in turn influences the circumferential distribution of normal contact stress on the pipe (Saberi et al., 2022). The reduction of axial force (interface shearing resistance) during repeated loading was also in Bilgin and Stewart (2009a), Sheil et al. (2018), and Reza et al. (2023b). Bilgin and Stewart (2009a) noted that ten cycles of loaded HDPE pipes lead to a reduction of axial resistance by 72%. Sheil et al. (2018) indicated that changes in peak axial resistance become minimal after five loading cycles for steel pipes. Reza et al. (2023b) showed a 40% reduction in resistance for HDPE pipes and a 21% reduction for ductile iron pipes after three loading cycles. These findings suggest that the decrease in soil resistance due to repeated loading is a consistent and significant factor affecting the performance of different types of pipes under cyclic loading conditions.

3.3.6 Normalized Axial Forces

To compare the axial pullout results, axial forces are normalized according to the pipe diameter, burial depth, burial length, and soil density, as specified in Equation 3-5, where N_a is the normalized axial pullout force; P is the axial pullout force; γ' is the effective unit weight of soil; D is the external diameter of pipe; H is the burial depth to the springline; and L is the mobilized frictional length of the pipe. This normalization process standardizes the forces, facilitating the comparison of results across different studies, pipe sizes, materials, and soil conditions.

$$N_a = \frac{P}{\gamma' \pi D H L} \qquad \text{Equation 3-5}$$

Figures 3-24 and 3-25 illustrate the normalized peak forces for a burial depth of 625 mm. For pipes with a diameter of 60.3 mm, the normalized peak forces are as follows: 0.75 to 0.77 for vibratory compaction, 0.43 to 0.44 for hand compaction, and 0.19 to 0.23 for loose uncompacted soil. For pipes with a diameter of 42.2 mm, the normalized peak forces are 0.78 to 0.83 for vibratory compaction and 0.52 to 0.58 for hand compaction. Additionally, for a burial depth of 480 mm, the normalized force for a 60.3 mm pipe is 0.78, while for a burial depth of 340 mm, the normalized force for a 42.2 mm pipe is 1.25. Higher normalized forces were observed for smaller diameter pipes (42.2 mm) than for larger pipes (60.3 mm) under both vibratory and hand compaction methods. According to the elastic cavity expansion theory, the normal pressure exerted on the pipe due to soil dilation is inversely proportional to the pipe diameter (Boulon and Foray, 1986; Johnston et al., 1987). Consequently, the dilation-induced increase in frictional resistance is higher for smaller pipes. This observation aligns with the findings of Reza et al. (2023a) during experimental axial pullout tests. The effect of compaction on the normalized force is more pronounced for pipes buried at a shallow depth. Reza et al. (2023a) also reported significantly higher normalized forces for tests conducted in dense sand compared to those in loose sand, supporting the impact of compaction on normalized forces and, consequently, axial resistance. The higher normalized forces observed for compacted backfill, whether achieved through vibratory or hand compaction, are attributed to the compaction-induced locked-in stresses exerted on the pipes during the compaction process.

Figure 3-26 presents a comparative analysis of the normalized axial resistance obtained from the pullout tests conducted in the current study against those reported in the literature. Note that most tests in the literature focus on pullout tests where a pipe is pulled from a static soil mass. In contrast, the methodology of the current study involves moving a soil block while maintaining one end of the pipe fixed. Additionally, variations in soil conditions and test facilities, including differences in geometry, further distinguish the current study from previous literature. Figure 3-26 also incorporates nondimensional peak axial forces calculated using guidelines from ALA (2005) and PRCI (2017), as described by Equation 3-6. For the ALA (2005) calculations, a coefficient of lateral earth pressure at rest (K_0) of 0.5 was used, whereas the PRCI (2017) guidelines employed an effective lateral earth pressure coefficient (K) of 2, based on findings by Wijewickreme et al. (2009). Although some of the results for both the ALA (2005) and the PRCI (2017) estimations matched the predictions of these guidelines, most of the data points do not, which implies that there is inconsistency with the analysis methodologies suggested in these guidelines.

$$N_a = \frac{P}{\gamma' \pi D H L} = \frac{K_0 + 1}{2} \tan\delta \qquad \text{Equation 3-6}$$

Although a higher value of K has been suggested in PRCI (2017) to account for the effects of soil dilation in dense sand, this may apply to a particular case. For example, the effects of dilation appear to be different for different pipe diameters. In the current study, despite the similar densities for vibratory compaction and hand tamper compaction, the K values required to simulate the test results significantly differ. As discussed earlier, the K values for the tests with vibratory compaction were higher than that of hand tamper compaction. Meidani et al. (2018) showed that the normal stress increases around a pipe during pullout decreases with increasing pipe diameter, consistent with the current study and in Reza and Dhar (2023a). Besides, Equations (3-5) and (3-6) do not account for the compaction-induced stresses. Several researchers (Rehman and Broms, 1972; Carder et al., 1977; Carder et al., 1980; Duncan and Seed, 1986; Duncan et al., 1991; Clayton et al., 1991; Clayton and Symons, 1992; Massarsch and Fellenius, 2002; Chen and Fang, 2008; Gui et al., 2020; Ezzeldin et al., 2022) have indicated that compaction significantly increase lateral earth pressure, which persist as locked-in stresses post-compaction.

The present study further indicates the impact of compaction on the axial pullout behaviour of buried flexible pipes when the soil is moved against a restrained pipe. The axial resistance values normalized for vibratory compaction were much higher than those for loose and hand compactions, attesting to the role compaction in this axial pullout behaviour. These observations collectively highlight the need for a better understanding of soil-pipe interactions, particularly considering the effects of soil compaction, to develop more accurate predictive models and guidelines.

3.3.7 Elongation of Pipes

During axial pullout tests, the shear force acting on the pipe-soil interface of flexible MDPE pipes (i.e., measured axial force) leads to deformation of the pipe segment. The elongation due to deformation can be measured through measuring the displacement at both ends of the pipe segment. Figures 3-27 and 3-28 illustrate the elongation observed for 60.3 mm and 42.2 mm diameter pipes, respectively, under different compaction methods of the backfill: vibratory compaction, hand compaction, and no compaction. As shown in these figures, the elongation increases consistently with the soil tank displacement until the displacement corresponding to the peak axial force is reached. As mentioned earlier, interface shear stress is gradually mobilized from the fixed end as the tank moves, increasing the axial forces and elongation with the movements. The maximum shearing resistance is mobilized over the entire pipe length when the axial force is the maximum (the peak value). Beyond the peak axial forces, the tank movement occurs by sliding over the pipe surface with almost a constant interface shear stress equal to the peak shearing resistance, stabilizing the elongation. As the shear strength is mobilized to the free end of the pipe, some redistribution of interforce shear stress occurs, reducing the axial force and elongation for the pipes in loose backfill or hand-compacted backfill. For backfill compacted using the vibratory plate compactor, the interface shear strength mobilization is nonlinear beyond the peak axial force. This results in the nonlinear increase of elongation with soil tank movements.

The maximum elongations are higher for pipes in compacted backfill due to the higher axial forces. The 60.3 mm MDPE pipes subjected to vibratory compaction exhibit a maximum elongation of approximately 30 mm, those subjected to hand compaction show an elongation of about 20 mm, and those in a loose backfill exhibit an elongation of approximately 5 mm. Similarly, for 42.2 mm MDPE pipes, vibratory compaction results in a maximum elongation of around 60 mm, while hand compaction leads to an elongation of approximately 30 mm. Higher elongation is seen for the 42.2 mm diameter pipes because of their lesser axial stiffness.

3.3.8 Axial Strain Distribution

In two specific tests, Test 7 and Test 15, fiber optic sensors were employed to capture the mobilization of axial strain along the entire length of the pipe. In contrast, the other tests utilized discrete electrical strain gauges to measure axial strain outside the soil tank without interfering the pipe surface within the soil. Figures 3-29 and 3-30 present a comparative analysis of the axial strain mobilization at various locations along the pipe length. The development of axial strains in a pipe is fundamentally connected to the axial stress or force applied to the pipe. This axial stress results from the shear stress at the interface between the pipe and the surrounding soil. The interaction between the pipe and the soil, particularly the shear stress generated at their interface, plays a crucial role in determining the magnitude and distribution of axial stress and strain along the length of the pipe. Although axial strain was measured continuously along the pipe's length, data from specific locations (L/8, L/4, 3L/8, L/2, 5L/8, 3L/4, and 7L/8 from the fixed end of the pipe, L is length of the pipe within the box) are plotted in Figures 3-29 and 3-30. The axial strain measurements were taken at the pipe's crown.

Note that the fibre optic sensors employed in these tests are capable of measuring strains up to 3%; however, the ODiSI system used in conjunction with these sensors is limited to measuring strains up to 1.5%. During the experiments, it was observed that the maximum strain recorded by the ODiSI system was 1.3%. Beyond this threshold, the sensor arrays failed to measure the strains accurately.

As seen in Figures 3-29 and 3-30, the mobilization of axial strain in both Tests 7 and 15 commences at the fixed end of the pipe almost instantaneously after tank displacement. The axial strain at locations far from the fixed end begins only after a certain value of tank displacement. This is consistent with the behaviour of axial strain mobilization observed in previous studies conducted by Weerasekara and Wijewickreme (2008), Wijewickreme and Weerasekara (2015), Reza and Dhar (2021a, 2021b), and Reza et al. (2023a). They observed similar axial strain mobilization patterns when a pipe was pulled through static soil, with strains initiating near the leading end as it displaced. The 42.2 mm diameter pipes (Figure 3-30) exhibited comparatively higher strains than the 60.3 mm diameter pipes (Figure 3-29) at the same levels of soil movement due to lower axial stiffness of the 42.2 mm diameter pipes.

In Figure 3-29, for Test 7, axial strains at the locations L/8, L/4, 3L/8, L/2, 5L/8, 3L/4, and 7L/8 began to initiate at tank displacements of 1.4 mm, 2.4 mm, 3.7 mm, 4.8 mm, 7.2 mm, 10.4 mm, and 14.2 mm, respectively. The corresponding tank displacements for Test 15 (Figure 3-30) at the initiation of axial strains at these positions were 2.4 mm, 6.6 mm, 13.8 mm, 22.6 mm, 34.2 mm, 45.8 mm, and 57.6 mm, respectively. These observations indicate that the interface shearing resistance is progressively mobilized at increasing distances from the fixed end, i.e., 0.5 m, 1 m, 1.5 m, 2 m, 2.5 m, 3 m, and 3.5 m (i.e., L/8, L/4, 3L/8, L/2, 5L/8, 3L/4, and 7L/8 from the fixed end), corresponding to the displacements mentioned above.

Axial strain distributions along the pipe length measured using a fibre optic sensor are illustrated in Figures 3-31 and 3-32, respectively. These figures show the gradual mobilization of axial strains (hence the axial force) along the pipe length with soil movement, which are similar to those reported from pipe pulling tests in Reza and Dhar (2021ab and 2023a). Figures 3-31 and 3-32 show that the strains are constant outside the tank wall as the axial force is constant. Due to the interface frictional (shear) forces within the soil mass, the axial force decreases with the distance from the restrained end, as does the axial strain. The decrease of axial strain is linear over a distance where the frictional force is constant (i.e., peak frictional resistance is mobilized) and then nonlinear with nonlinear mobilization of the shear force. The axial strains are zero, where the interface shear stress (and axial force) is zero. Thus, from the measured strains, the length of shear strength mobilization along the pipe length could be estimated at different levels of soil displacements. Table 3-11 shows the mobilized friction length and the corresponding soil movements and axial forces.

The distribution of axial strain becomes linear in Test 7 (Figure 3-31) beyond the mobilization of shearing resistance over the entire pipe length of 4 meters, corresponding to a tank displacement of 25 mm. The peak pullout force is reached at a tank displacement of 51.6 mm in Test 7. In Test 15 (Figure 3-32), the axial strain distribution become linear over the entire pipe length of 4 meters at the soil displacement of 75 mm, and the peak axial force is achieved at 102.8 mm displacement. Beyond the peak force, the axial strain does not change. This is consistent with almost constant axial force observed after the peak pullout values (Figures 3-18 and 3-23).

Reza et al. (2023a) proposed Equation 3-7 as a simplified method to calculate axial strain at any point within the mobilized frictional length, where ε is the axial strain; P is the axial pullout force corresponding to the mobilized frictional length l; A is the pipe's cross-sectional area; E_p is the modulus of elasticity of pipe material, and x is the distance from the leading end of the pipe.

$$\varepsilon = \frac{P}{AE_p l^2}(l - x)^2 \qquad \text{Equation 3-7}$$

Figures 3-33 and 3-34 compare the measured axial strain with those calculated using Equation 3-7, as proposed by Reza et al. (2023a). Although the strains are underpredicted by Equation 3-7, the calculation is considered reasonable given the uncertainties involved in the parameters of the MDPE pipe materials. While the modulus of elasticity of MDPE varies with tank displacement, a constant initial modulus of elasticity value of 550 MPa for MDPE was employed for calculating axial strains.

3.3.9 Axial Strains at Restrained End

Axial strains were measured outside the soil box at the restrained end (shown in Figures 3-35 and 3-36). At the fixed end, the mobilized axial force is equal to the reaction force measured at the load cell. Thus, the axial force on the pipe segment extending outside the box towards the load cell is equivalent to the mobilized force. The peak axial strain on this pipe segment can be determined using Equation 3-8. During the tests, the axial strain on the pipe segment outside the soil box was measured using discrete electrical resistivity strain gauges. Figures 3-35 and 3-36 compare axial strain during pullout tests. The peak axial strain values calculated from Equation 3-8 show good agreement with the measured peak axial strain values, confirming the modulus of elasticity chosen for the pipe material (i.e., 550 MPa).

$$\varepsilon_{peak} = \frac{P}{AE_p} \qquad \text{Equation 3-8}$$

As illustrated in Figures 3-35 and 3-36, the method of compaction significantly influences the axial strains experienced by the pipe segments. For the 60.3 mm pipe, tests conducted with vibratory plate compaction achieved a maximum strain of about 11000 με, while tests with no compaction resulted in a much lower maximum strain of around 1500 με. Similarly, for the 42.2 mm pipe, vibratory plate compaction led to a peak strain of about 18000 με, in contrast to the tests with hand compaction, which reached a maximum value of around 10000 με. The increased peak axial strains are attributed to the higher axial forces mobilized during the pulling process, which are more significant in tests involving vibratory plate compaction compared to those using hand compaction or uncompacted backfills. Furthermore, in tests using vibratory plate compaction, higher axial strains were measured for the 42.2 mm pipes compared to the 60.3 mm pipes. This difference is due to the relatively greater elongation of the 42.2 mm pipes, which results from their lower stiffness compared to the 60.3 mm pipes.

Note that the test conducted at a higher pulling rate (Test 10) exhibited higher axial strains than the test at a lower pulling rate (Test 9), shown in Figure 3-36 for the 42.2, even though the axial pullout forces did not differ significantly. This discrepancy may be attributed to the alignment of the strain gauge. If the strain gauge is slightly off the crown of the pipe, it will measure the resultant strain rather than the true axial strain. Due to a potential reduction in the pipe's diameter, a compressive strain occurs radially while a tensile strain develops along the pipe's length. Consequently, if the strain gauge is misaligned and measures the resultant strain, it may record a lower value than the actual axial strain. Additionally, as seen in Figures 3-35 and 3-36, Tests 1, 2, 9, and 10 included a relaxation period after the tank was pulled by 10 mm. Observations suggest that axial strains were not significantly redistributed during this relaxation period, possibly due to the relatively short duration of the relaxation phase.

3.4 Conclusions

This chapter presents the results of fifteen full-scale axial pullout experiments conducted at the testing facility of Memorial University of Newfoundland. The experiments involved MDPE pipes of two different diameters, which were buried at three varying depths. Tests were performed under four distinct pulling rates, ranging from 0.25 mm/min to 2 mm/min. During these experiments, axial force, axial strain, pipe elongation, and earth pressures were recorded to evaluate the performance of the pipes under different conditions. The following conclusions have been derived from the study:

- While most previous studies investigated the axial pullout behaviour of a pipe by pulling a pipe through a static soil mass (pipe pull test), the current research examines the behaviour of a pipe directly exposed to axial ground movements by moving a soil mass against a restrained pipe (soil pull test).
- Axial forces on pipes subjected to soil pull tests were higher than those for pipe pull tests. The effects of soil particle movements around the pipe surface during soil pull are more significant than during pipe pull, resulting in finer particles' movements into the void space

of coarser particles. This can lead to an increased contact area at the pipe-soil interface during soil pulling.

- The mechanism of interface shear stress mobilization is similar for both soil pull and pipe pull tests. The interface shear stress is mobilized at the restrained end first and then progresses toward the free end with soil movement. The axial force maximizes when the interface shear strength is mobilized over the entire pipe length. The load transfer mechanism was well captured through distributed strain measurements using the fibre optic sensors.
- The tank displacement rate had an insignificant effect on the axial force for the range of ground movement rates considered. However, the pulling rate impacted the pulling force during pipe-pulling tests, as reported in the literature.
- The compaction method was found to affect the axial force on the pipe significantly. For the MDPE pipes with diameters of 60.3 mm and 42.2 mm, axial resistance was approximately 80% and 51% higher, respectively, for the backfill compacted using a vibratory plate tamper than for hand tamper compaction even for a similar relative compaction value for the backfill soil. The axial resistance was higher by as high as 147% for pipes in backfill compacted with hand tamping compared to the pipes in uncompacted loose conditions. The compaction is likely to induce locked-in stresses, increasing the interface shearing resistance, which is different for different compaction methods.
- The axial force on the pipe drops for stopping the ground movement. However, the effect of relaxation was insignificant for the duration of the relaxation time considered in this study. Soil resistance was found to diminish during repeated loading cycles. A reduction of approximately 10% was observed during the second load cycle.

- The normalized forces were higher for smaller-diameter pipes than the larger ones at the same burial depths. This is due to the larger effect of soil dilation for smaller-diameter pipes. While PRCI (2017) recommends using a higher coefficient of lateral earth pressure to account for the dilation effect, the effect of compaction methods and the diameter-dependent dilation were not considered.
- Although the K values estimated using Meidani et al. (2018) provide reasonable approximations for some cases, these were inconsistent for the other cases. The equation proposed by Meidani et al. primarily accounts for the effects of soil and does not account for the compaction-induced stresses.
- The simplified strain calculation proposed in Reza et al. (2023a) was successful to some extent in estimating the axial strains measured during the tests.

3.5 Acknowledgements

This research study received funding from the Alliance Grants program of the National Science and Engineering Research Council of Canada. Financial and in-kind support from FortisBC Energy Inc. and SaskEnergy Canada Inc., as well as in-kind support from WSP Canada Inc., are gratefully acknowledged. The authors would like to express their gratitude for the valuable technical and laboratory assistance provided by the research group and laboratory technicians.

Table 3-1: Specification of the Omega LCHD-5K load cell

Capacity	5000 lbs
Type	Tension and Compression loadcell
Output	2 mV/V ±0.25%
Excitation Voltage	10 Vdc (15 Vdc max.)
Bridge Resistance	350 Ω bonded foil strain gage
Accuracy	0.25% of full scale
Deflection	0.001" to 0.003" Typical
Operating Temperature Range	-65°F to 250°F
Safe Overload	150% of capacity
Ultimate Overload	300% of capacity
Material	17-4 PH stainless steel
Connector	PT06F-10-6S

Table 3-2: Specification of the Honeywell JEC-AG LVDT

Capacity	110 mm
Nonlinearity	±0.25 % full scale
Output load (min.)	2000 Ω with three-wire supply
Output impedance	2 Ω
Output sensitivity	±5 VDC or 0 VDC to 10 VDC
Operating Temperature	-50 °C to 80 °C (-58 °F to 176 °F)

Table 3-3: Specification of the Kyowa DTPA-A-500 potentiometers

Rated Capacity	500 mm
Nonlinearity	Within ±0.3% RO
Rated Output	2.5 mV/V (5000 $\times 10^{-6}$ strain) ±10%
Recommended Excitation	1 to 5 V AC or DC
Response Speed	1000 mm/s
Operating Temperature	-10 to 80ºC (Non-condensing)
Measuring Force	2 N (Max. 2.8 N)
Degree of Protection	IP40 (IEC 60529)

Table 3-4: Specification of the Kyowa KFEL-5-120-C1 electrical strain gauges

Gauge Factor	2.11 ± 1.0%
Gauge Length	5 mm
Gauge Resistance	119.8 ± 0.2Ω
Temperature Coefficient	+0.015% / °C
Applicable Gauge Cement	CC-36

Table 3-5: Specification of the high-definition fiber-optic sensors

Fiber Type	Polyimide Coated Low Bend Loss Fiber
Strain Relief	20 cm, Fiberglass
Sensor Diameter	155 µm
Termination Diameter	286 µm
Minimum Bend Radius	10 mm
Operating Temperature – Sensing Region	-40 to 300 °C

Table 3-6: Specification of the low-pressure transducers

Rated Capacity	20 kPa
Rated Output	0.75 mV/V or more
Safe Temperature	-20 to 70°C
Safe Excitation	5 V AC or DC
Recommended Excitation	1 to 3 V AC or DC
Input Resistance	350 Ω ±10%
Output Resistance	350 Ω ±10%
Safe Overloads	150%
Material	Case: Stainless steel
Degree of Protection	IP54 (IEC 60529)

Table 3-7: Comparison of backfill soil parameters

Parameter	Saha et al. (2019)	Current Study	
D_{50} (mm)	0.742	0.897	0.885
C_u	5.81	6.29	6.48
C_c	2.04	1.89	1.94
Fine Content (%)	1.3	1.32	1.47
Gravel Content (%)	0.87	0.82	2.57
USCS	SW	SW	SW
Specific Gravity	2.63		
e_{min}	0.33	0.31	
e_{max}	0.65	0.55	
$\gamma_{d,min}$ (kN/m^3)	N/A	16.58	
$\gamma_{d,max}$ (kN/m^3)	19.3	19.62	
$\gamma_{d,max,proctor}(kN/m^3)$	18.8		

Table 3-8: Full-scale test programme

Test	Pipe Diameter, D (mm)	Burial Depth, H (mm)	H/D	Pulling Rate (mm/min)	Compaction Method	Average Density (kN/m^3)
Test 1	60.3	625	10.36	0.5	Vibratory Plate Tamper	18.1
Test 2	60.3	625	10.36	2	Vibratory Plate Tamper	18.1
Test 3	60.3	625	10.36	0.25	Hand Tamper	17.5
Test 4	60.3	625	10.36	1	Hand Tamper	17.5
Test 5	60.3	625	10.36	0.5	Uncompacted	14.8
Test 6	60.3	625	10.36	2	Uncompacted	14.8
Test 7	60.3	625	10.36	0.25	Vibratory Plate Tamper	18.1
Test 8	60.3	480	7.96	0.5	Hand Tamper	17.5
Test 9	42.2	625	14.81	0.5	Vibratory Plate Tamper	18.1
Test 10	42.2	625	14.81	2	Vibratory Plate Tamper	18.1
Test 11	42.2	625	14.81	0.5	Hand Tamper	17.5
Test 12	42.2	625	14.81	2	Hand Tamper	17.5
Test 13	42.2	340	8.06	2	Hand Tamper	17.5
Test 14	42.2	600	14.22	0.5	Hand Tamper	17.5
Test 15	42.2	600	14.22	0.5	Hand Tamper	17.5

Table 3-9: Peak axial force and corresponding soil displacement for conducted tests

Test	Peak Load, P_u (kN)	Soil Displacement at P_u (mm)	Remarks
Test 1 (D = 60.3 mm, 0.5 mm /min)	6.44	34.4	Bare pipe
Test 2 (D = 60.3 mm, 2 mm /min)	6.63	44.4	Bare pipe
Test 3 (D = 60.3 mm, 0.25 mm /min)	3.56	22.4	Bare pipe
Test 4 (D = 60.3 mm, 1 mm /min)	3.68	18.8	Bare pipe
Test 5 (D = 60.3 mm, 0.5 mm /min)	1.31	5.7	Bare pipe
Test 6 (D = 60.3 mm, 2 mm /min)	1.63	6.2	Bare pipe
Test 7 (D = 60.3 mm, 0.25 mm /min)	6.20	51.6	FOS
Test 8 (D = 60.3 mm, 0.5 mm /min)	4.95	26.2	Bare pipe
Test 9 (D = 42.2 mm, 0.5 mm /min)	4.68	46.4	Bare pipe
Test 10 (D = 42.2 mm, 2 mm /min)	4.96	66.2	Bare pipe
Test 11 (D = 42.2 mm, 0.5 mm /min)	3.03	32.9	Bare pipe
Test 12 (D = 42.2 mm, 2 mm /min)	3.35	38.8	Bare pipe
Test 13 (D = 42.2 mm, 2 mm /min)	3.94	34.7	Bare pipe
Test 14 (D = 42.2 mm, 0.5 mm /min)	3.76	38.2	Bare pipe, First pull
Test 15 (D = 42.2 mm, 0.5 mm /min)	6.31	102.8	FOS, First pull

Table 3-10: Predicted K values using Meidani et al. (2018) equation with Test K values

<table>
<tr><th rowspan="2">Test</th><th rowspan="2">P_u (kN)</th><th rowspan="2">K_0 = (1 – Sinφ)</th><th rowspan="2">D (mm)</th><th rowspan="2">H (mm)</th><th rowspan="2">E_s (MPa)</th><th rowspan="2">φ</th><th rowspan="2">γ (kN/m3)</th><th rowspan="2">Compaction Method</th><th rowspan="2">Δt (mm)</th><th colspan="2">K</th></tr>
<tr><th>Test</th><th>Equation (3-4)</th></tr>
<tr><td>Test 1</td><td>6.44</td><td rowspan="2">0.305</td><td rowspan="7">60.3</td><td rowspan="6">625</td><td rowspan="2">5.08</td><td rowspan="2">44</td><td rowspan="2">18.1</td><td rowspan="2">Vibratory Plate Tamper</td><td rowspan="12">0.8</td><td>1.31</td><td>1.34</td></tr>
<tr><td>Test 2</td><td>6.63</td><td>1.38</td><td>1.34</td></tr>
<tr><td>Test 3</td><td>3.56</td><td rowspan="2">0.331</td><td rowspan="2">4.16</td><td rowspan="2">42</td><td rowspan="2">17.5</td><td rowspan="2">Hand Tamper</td><td>0.40</td><td>1.27</td></tr>
<tr><td>Test 4</td><td>3.68</td><td>0.45</td><td>1.27</td></tr>
<tr><td>Test 5</td><td>1.31</td><td rowspan="2">0.398</td><td rowspan="2">3.06</td><td rowspan="2">37</td><td rowspan="2">14.8</td><td rowspan="2">Loose Fill</td><td>0.25</td><td>-</td></tr>
<tr><td>Test 6</td><td>1.63</td><td>0.25</td><td>-</td></tr>
<tr><td>Test 8</td><td>4.95</td><td>0.331</td><td>480</td><td>3.65</td><td>42</td><td>17.5</td><td>Hand Tamper</td><td>1.54</td><td>1.35</td></tr>
<tr><td>Test 9</td><td>4.68</td><td rowspan="2">0.305</td><td rowspan="5">42.2</td><td rowspan="4">625</td><td rowspan="2">5.08</td><td rowspan="2">44</td><td rowspan="2">18.1</td><td rowspan="2">Vibratory Plate Tamper</td><td>1.40</td><td>1.56</td></tr>
<tr><td>Test 10</td><td>4.96</td><td>1.55</td><td>1.56</td></tr>
<tr><td>Test 11</td><td>3.03</td><td rowspan="3">0.331</td><td rowspan="2">4.16</td><td rowspan="3">42</td><td rowspan="3">17.5</td><td rowspan="3">Hand Tamper</td><td>0.70</td><td>1.47</td></tr>
<tr><td>Test 12</td><td>3.35</td><td>0.89</td><td>1.47</td></tr>
<tr><td>Test 13</td><td>3.94</td><td>340</td><td>3.07</td><td>3.08</td><td>1.68</td></tr>
</table>

Table 3-11: Axial pullout forces and relevant tank displacements with mobilized frictional lengths of pipe

Test	Mobilized Frictional Length (m)	Tank Displacement (mm)	Axial Pullout Force (N)	Axial Force / Mobilized Length (kN/m)
Test 7	0.5	1.4	762.9	1.53
	1	2.4	1213.6	1.21
	1.5	3.7	1673.2	1.12
	2	4.8	1982.2	0.99
	2.5	7.2	2509.9	1.00
	3	10.4	3029.2	1.01
	3.5	14.2	3515.5	1.00
Test 15	0.5	2.4	633.3	1.27
	1	6.6	2189.8	2.19
	1.5	13.8	3574.2	2.38
	2	22.6	4376.1	2.19
	2.5	34.2	5021.5	2.01
	3	45.8	5440.4	1.81
	3.5	57.6	5719.9	1.63

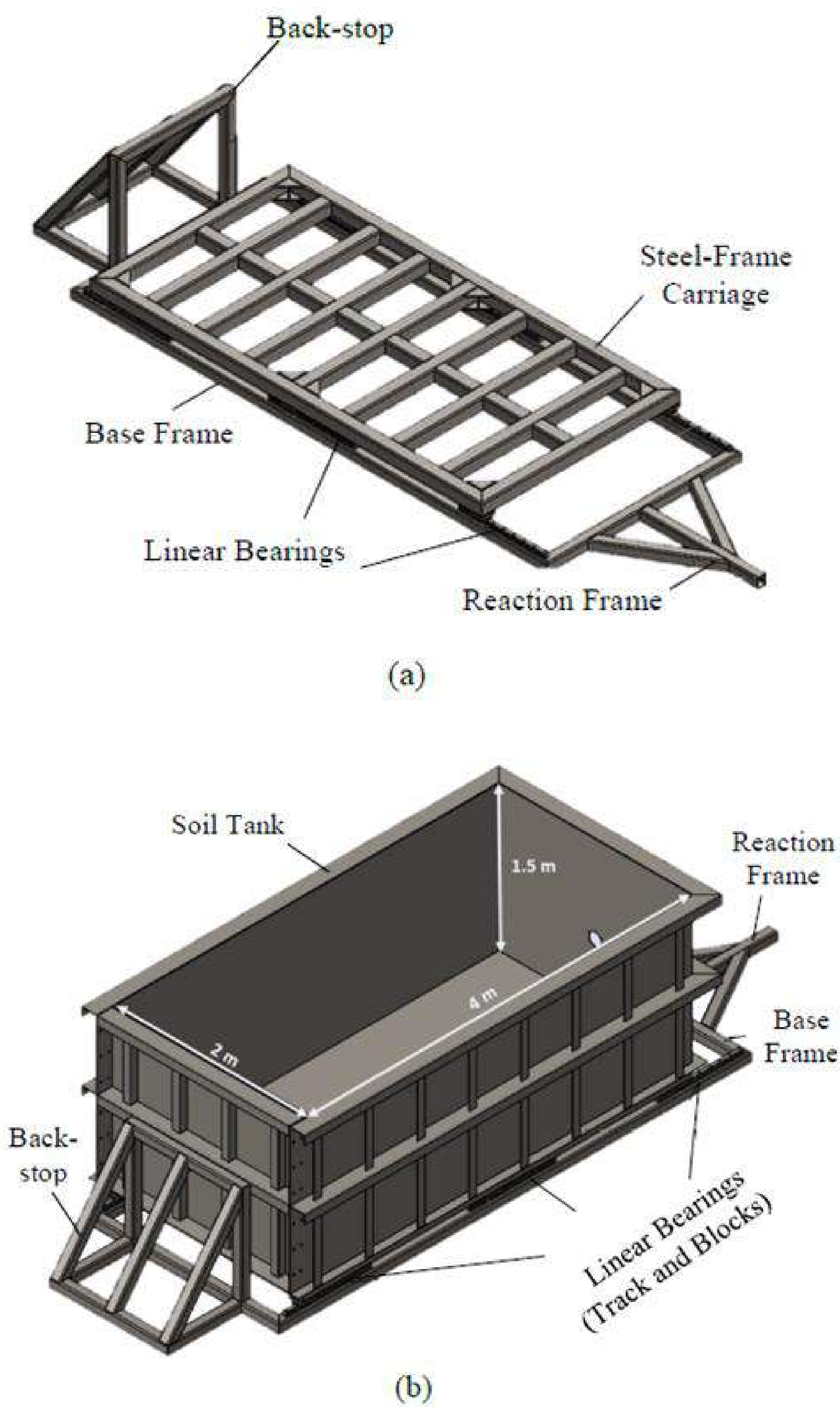

Figure 3-1: The schematic layout of the current test facility at Memorial University of Newfoundland: (a) Without soil tank (b) With soil tank (after Andersen, 2024)

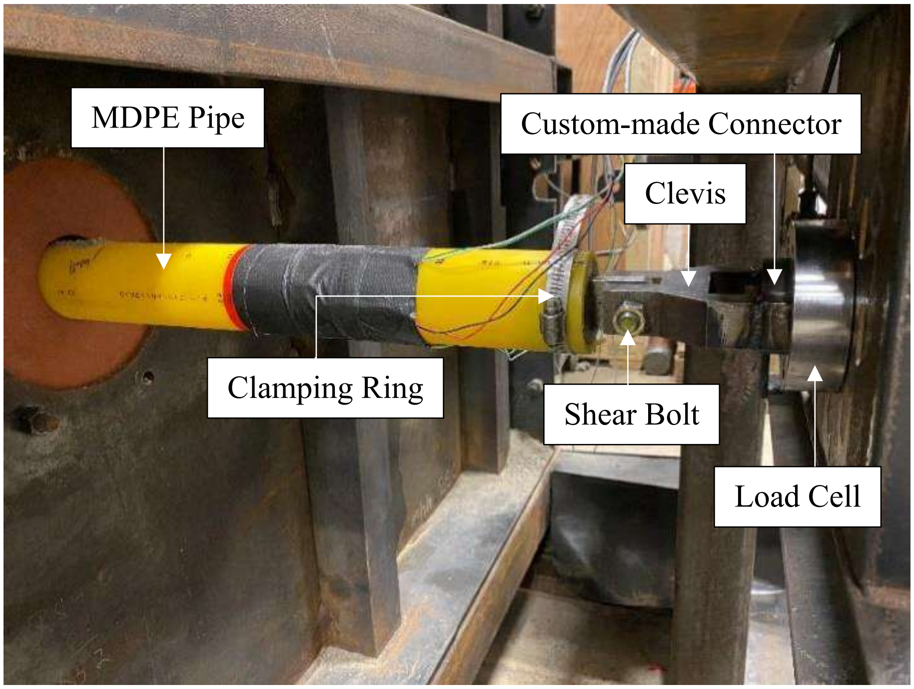

(a)

(b)

Figure 3-2: (a) The configuration of the connection between the load cell and the pipe segment (b) Steel adapters for 60.3 mm and 42.2 mm diameter pipes

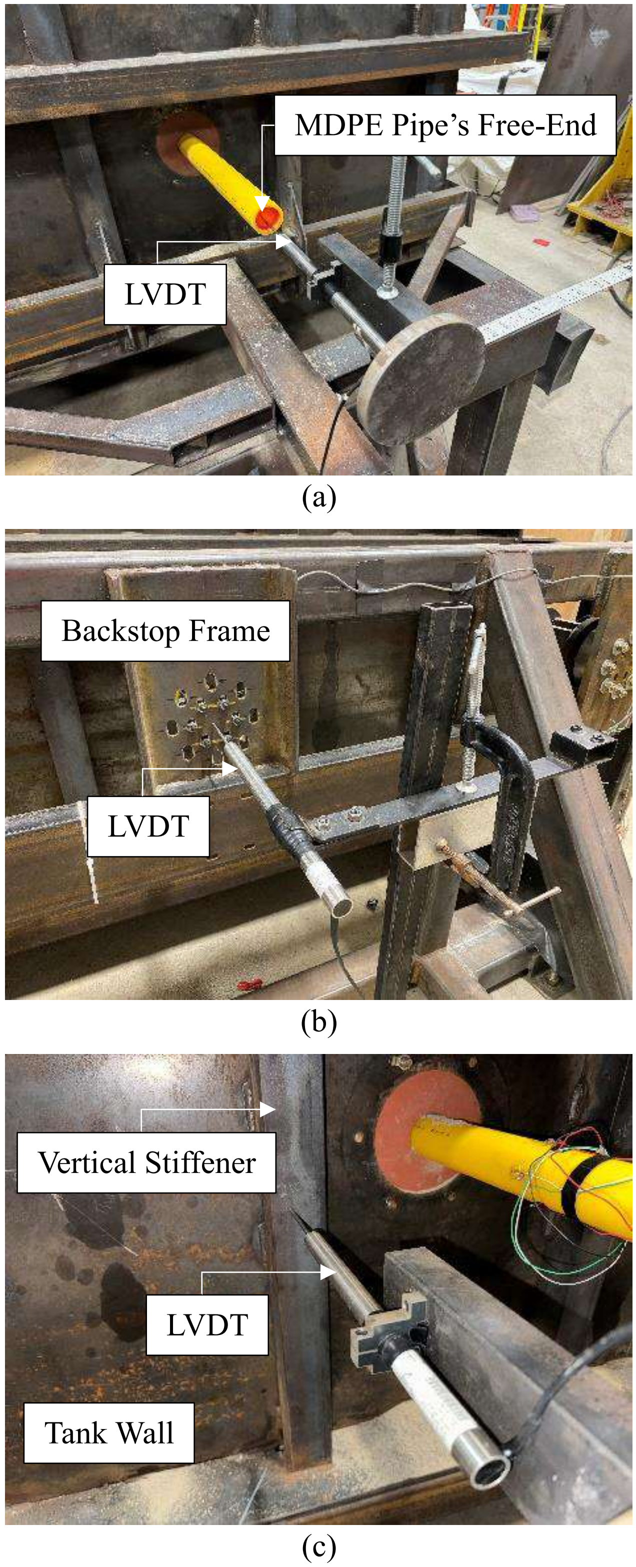

Figure 3-3: The arrangement of the LVDTs at different locations: (a) At the pipe segment's free end (b) At the backstop frame (c) At the tank wall

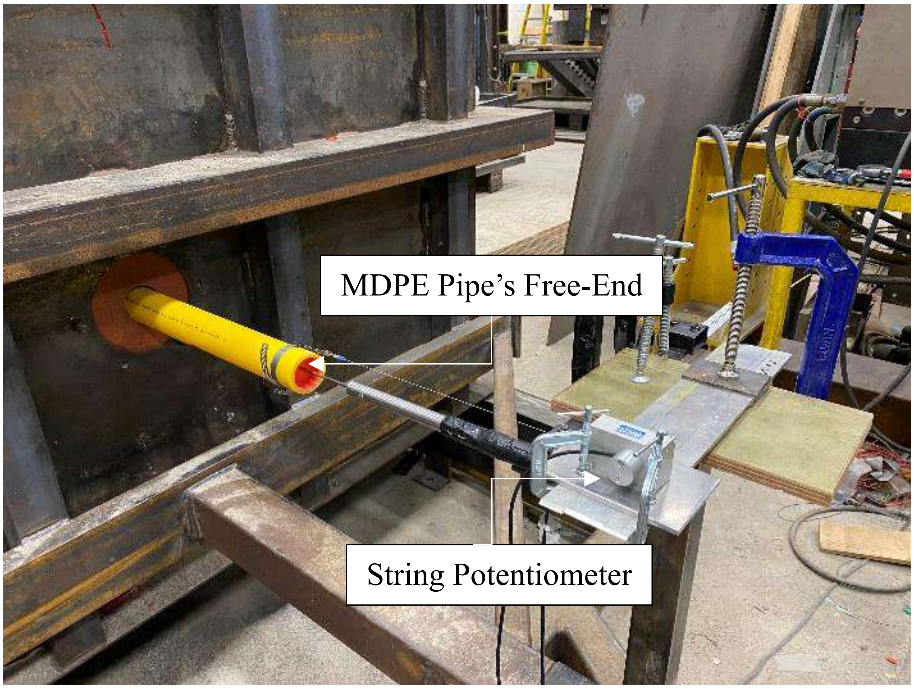

(a)

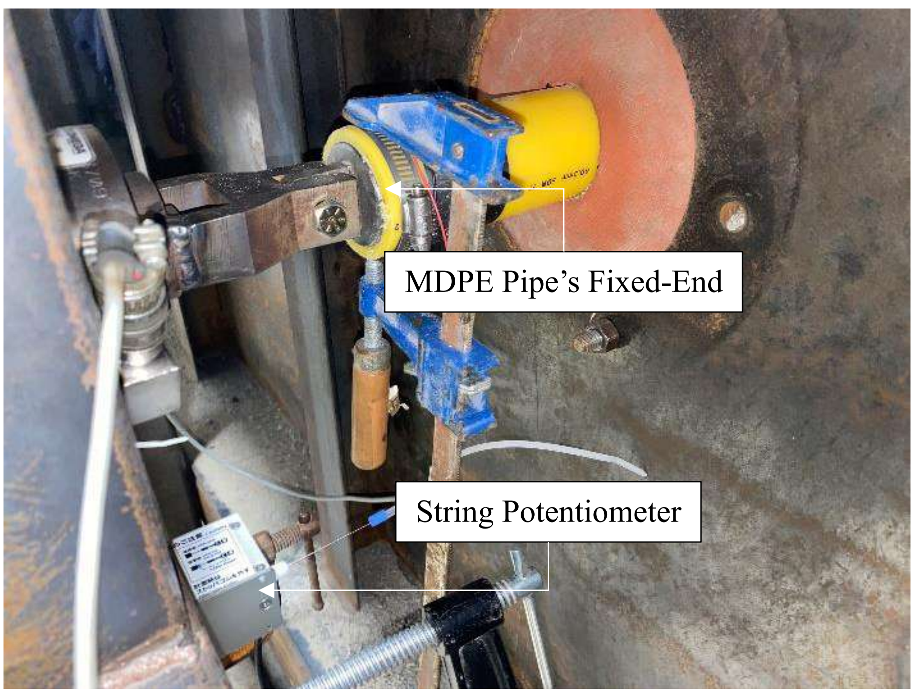

(b)

Figure 3-4: The arrangement of the potentiometers at different locations: (a) At the pipe segment's free end (b) At the pipe segment's fixed end

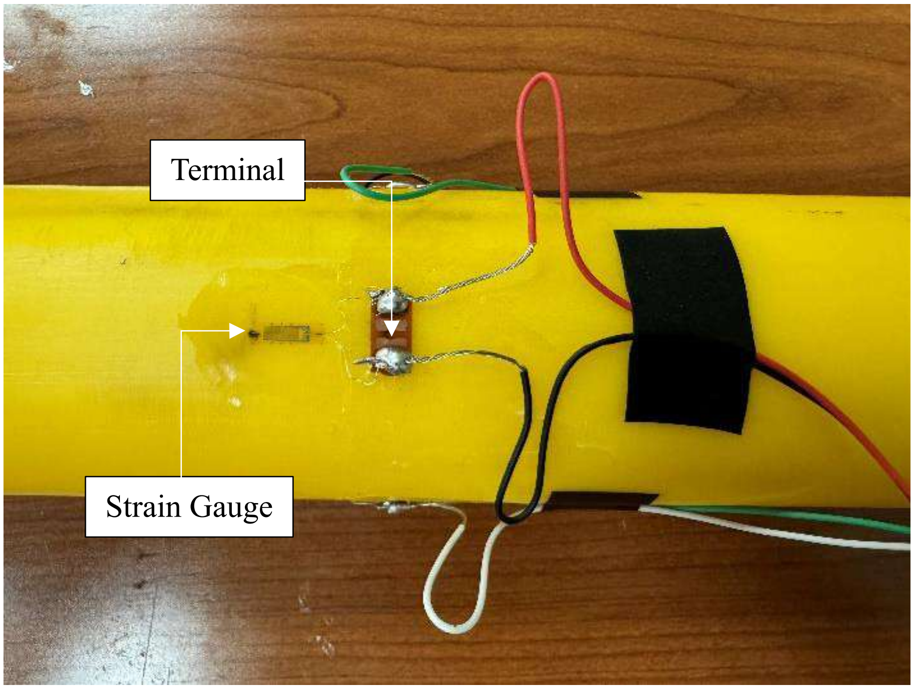

(a)

(b)

Figure 3-5: The configuration of the electrical resistivity strain gauges: (a) U-shaped loop connection (b) Wrapped with poly sheets and sheathing tape

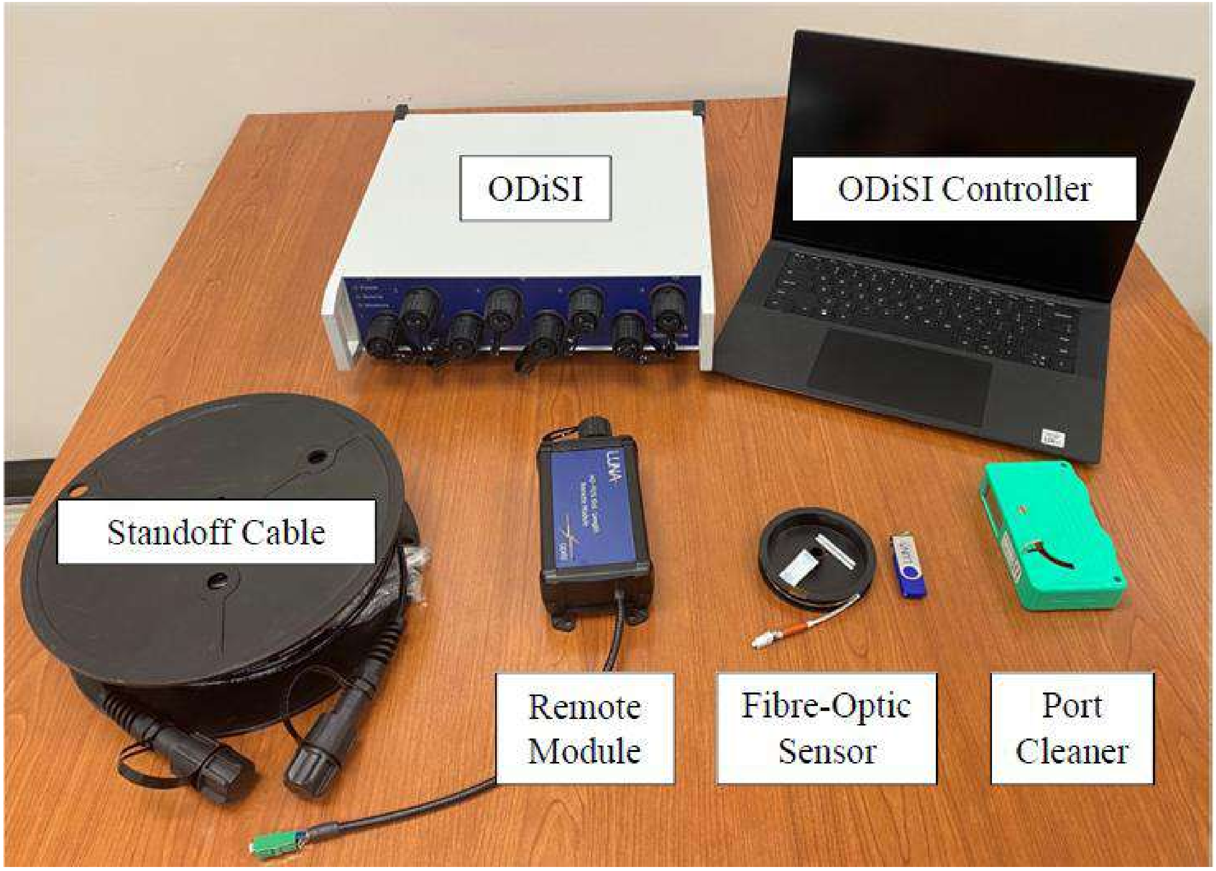

Figure 3-6: The LUNA ODiSI 6100 fiber-optic sensor system (after Andersen, 2024)

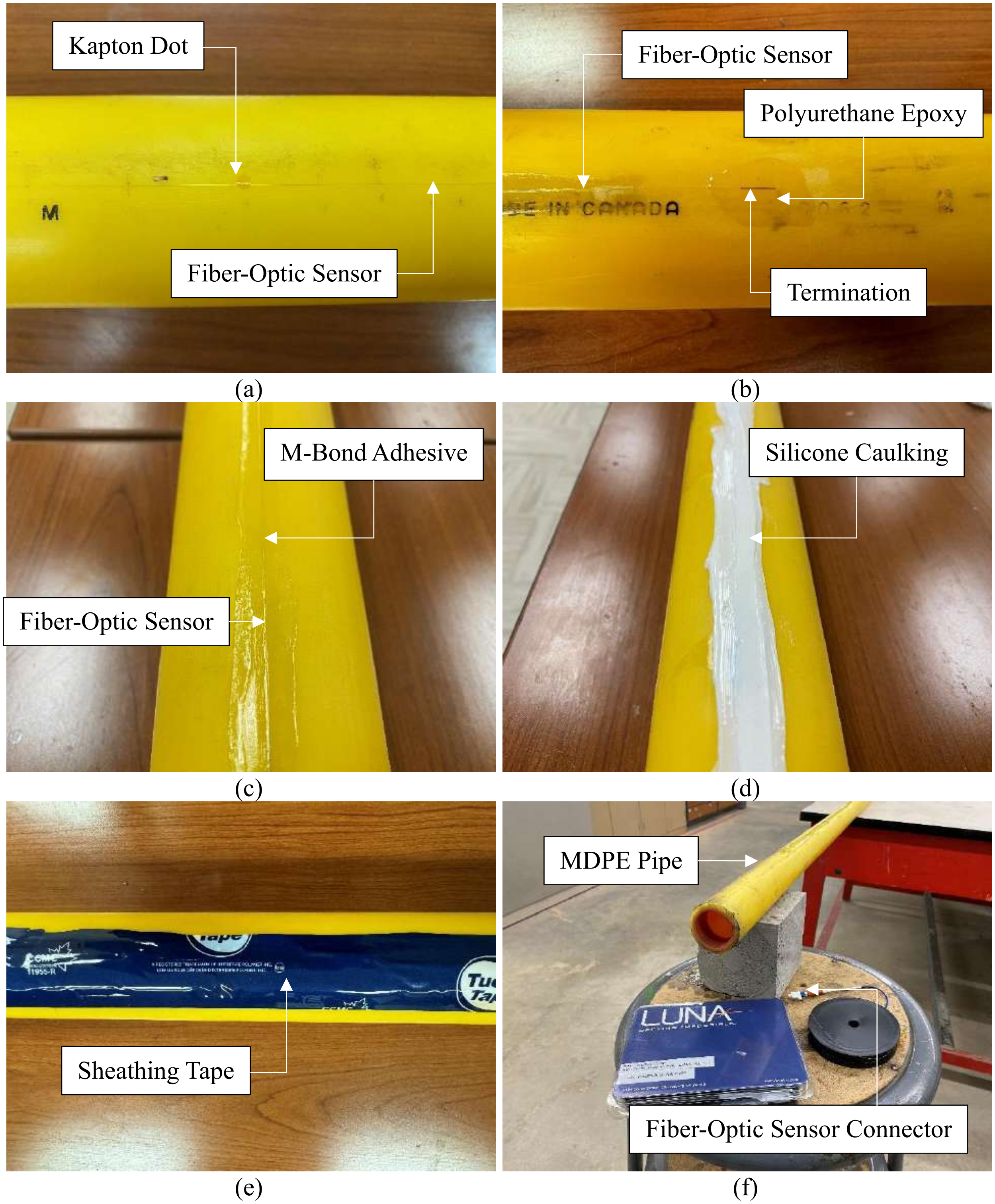

Figure 3-7: The procedures for instrumenting the fiber-optic sensors to the MDPE pipe: (a) Fiber-optic sensor aligned to the pipe's crown and temporarily held with Kapton dots (b) Polyurethane epoxy applied to both ends of the sensors (c) M-bond 200 adhesive applied to bond the sensor with pipe's surface (d) Silicone caulking applied over the bonded sensors for protection (e) Sheathing tape wrapped over the caulking layer (f) Fiber-optic sensor

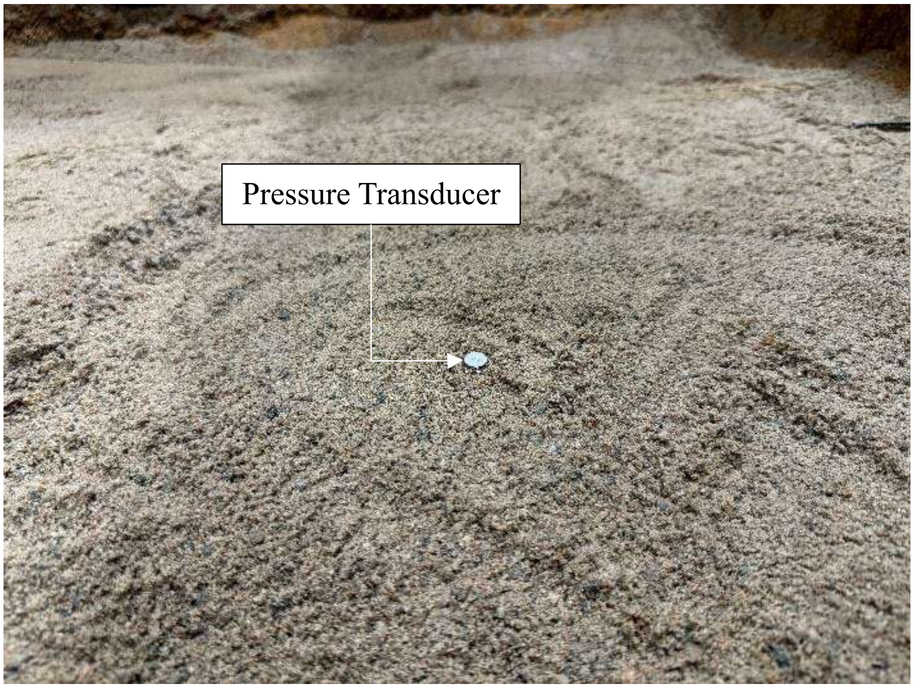

(a)

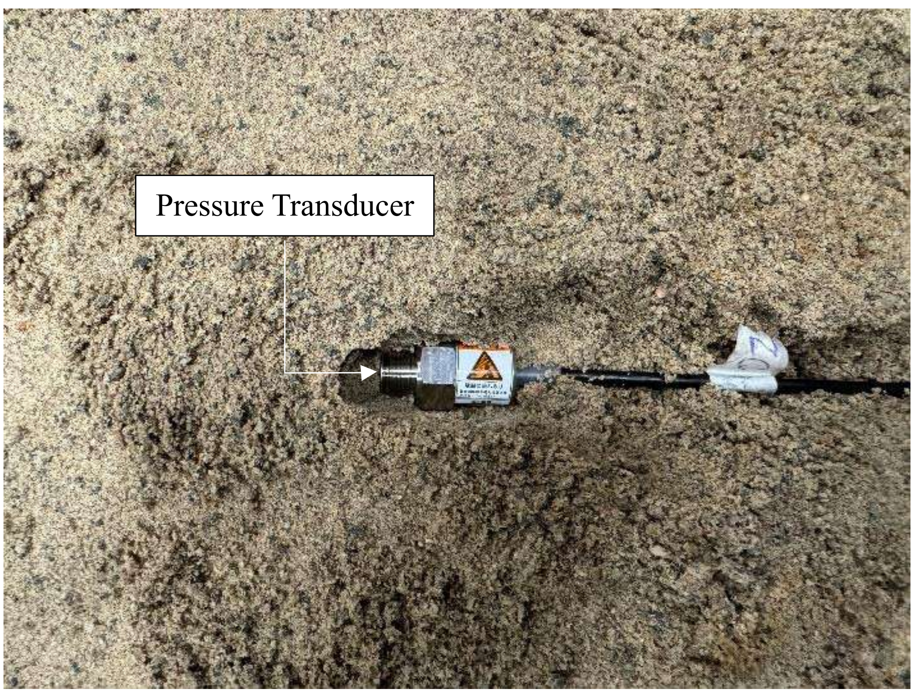

(b)

Figure 3-8: The arrangement of the pressure transducers: (a) To measure vertical soil pressure (b) To measure horizontal soil pressure

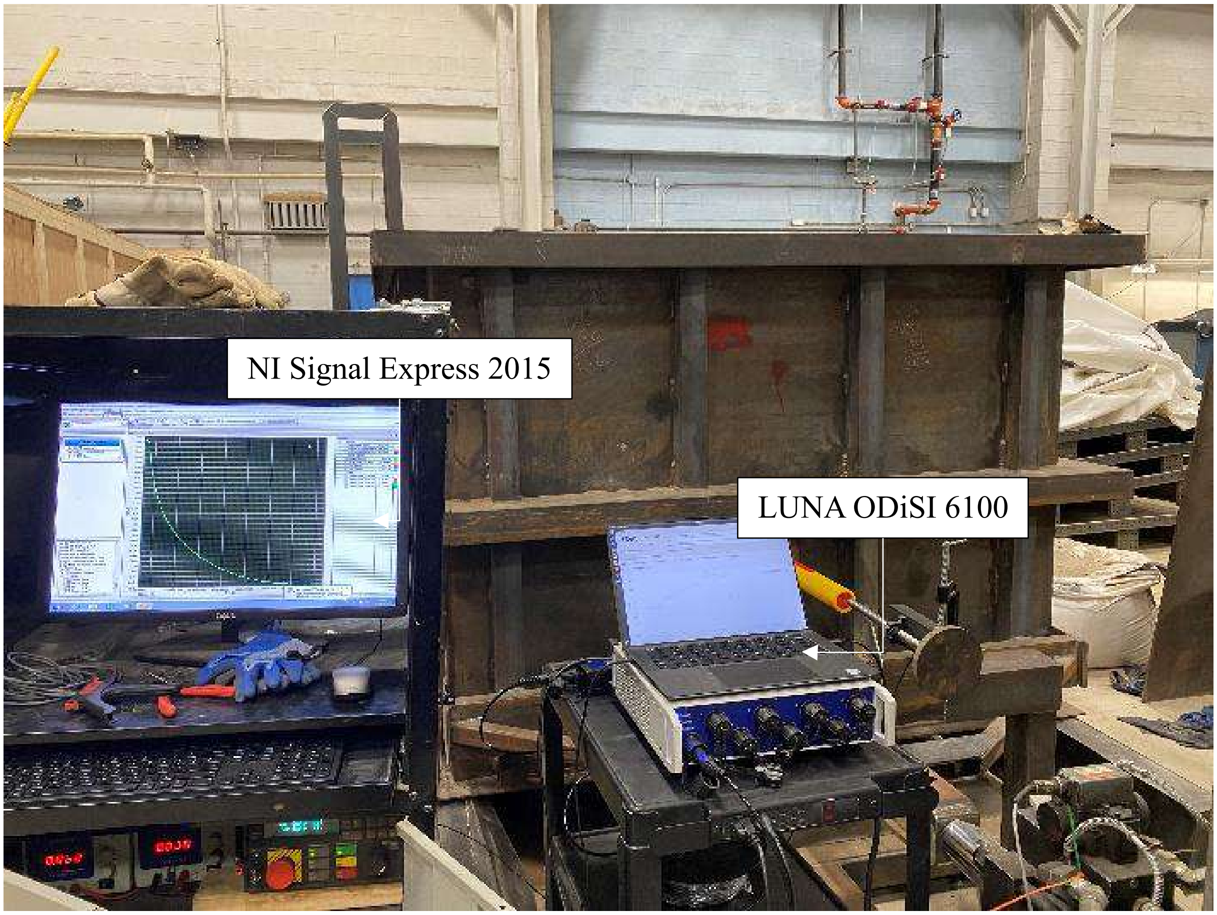

Figure 3-9: Data acquisition system

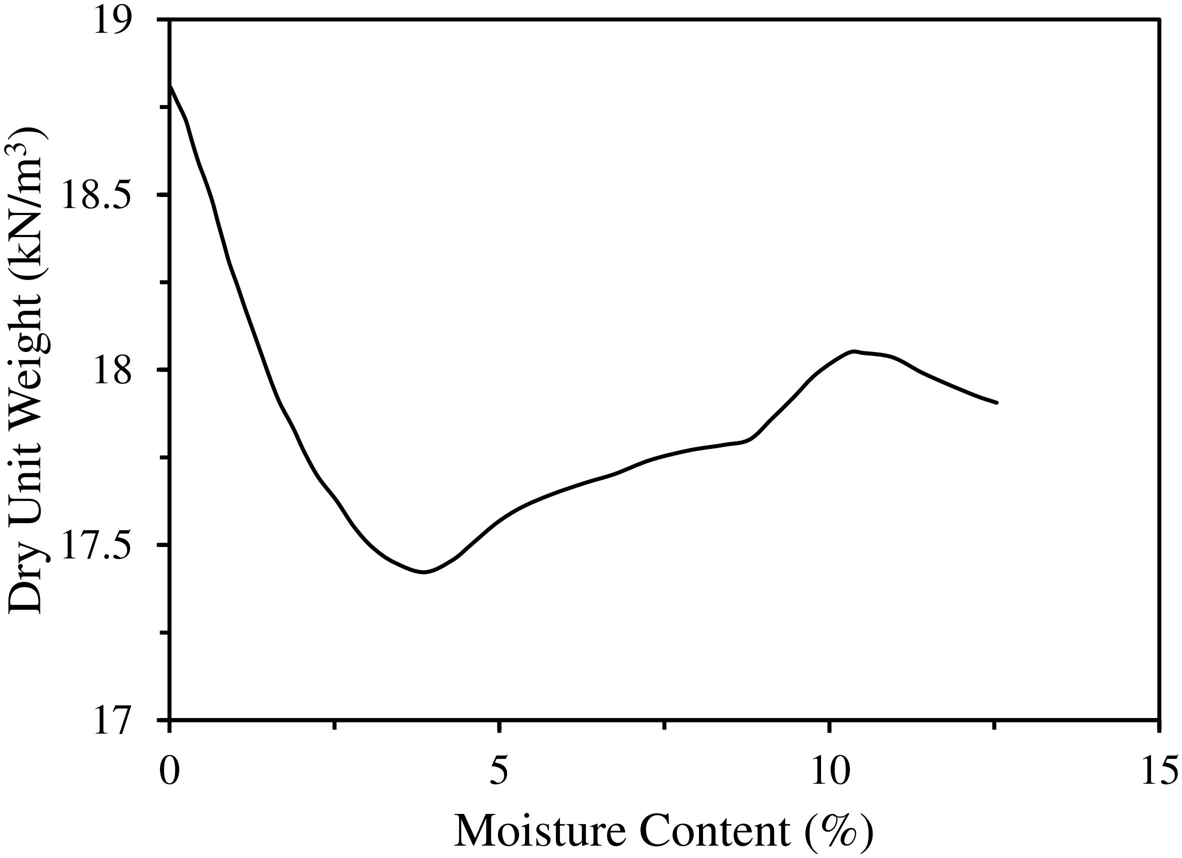

Figure 3-10: Proctor compaction test results of backfill sand (after Saha et al., 2019)

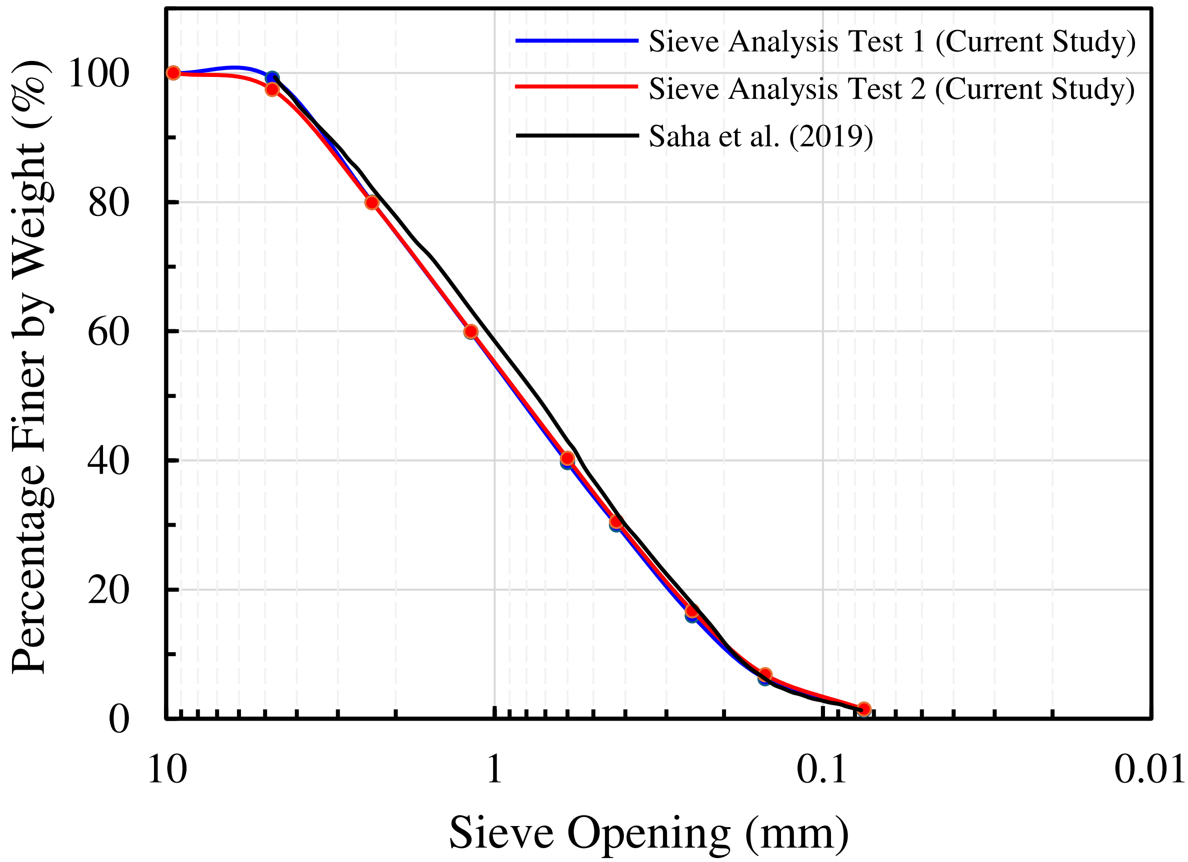

Figure 3-11: Particle size distribution of backfill sand (after Saha et al., 2019)

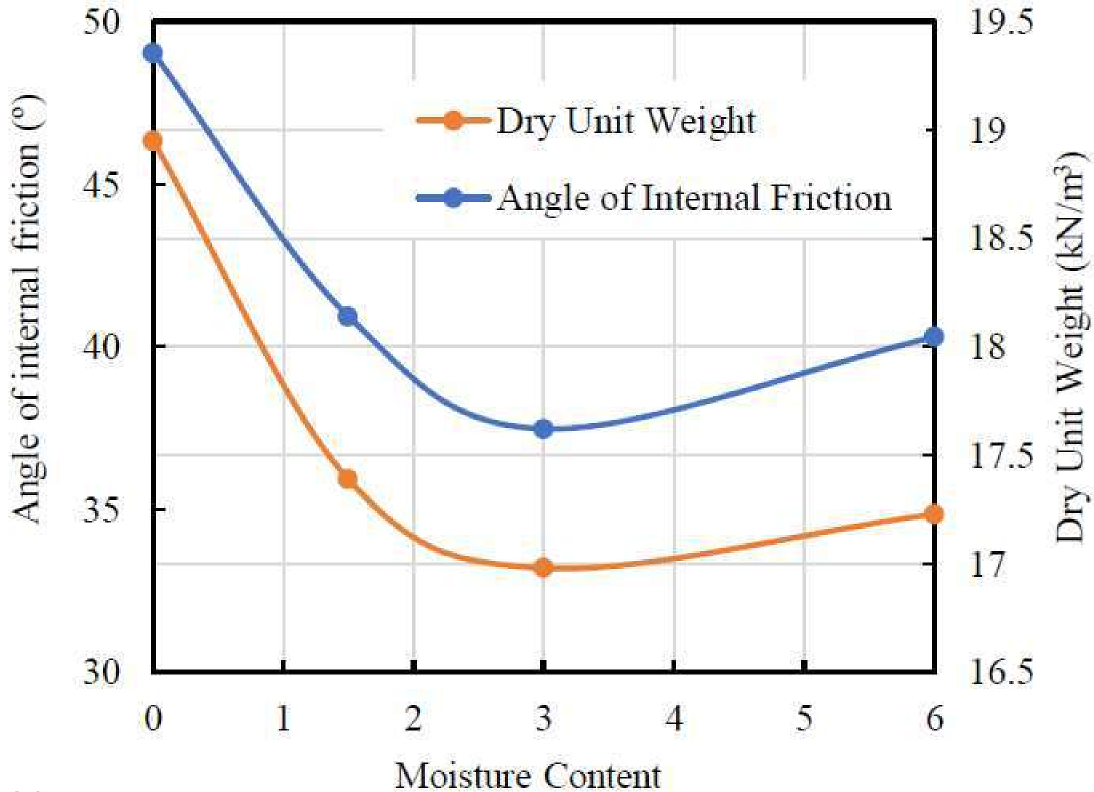

Figure 3-12: Effect of moisture content on the angle of internal friction and dry unit weight of compacted backfill sand (after Saha, 2021)

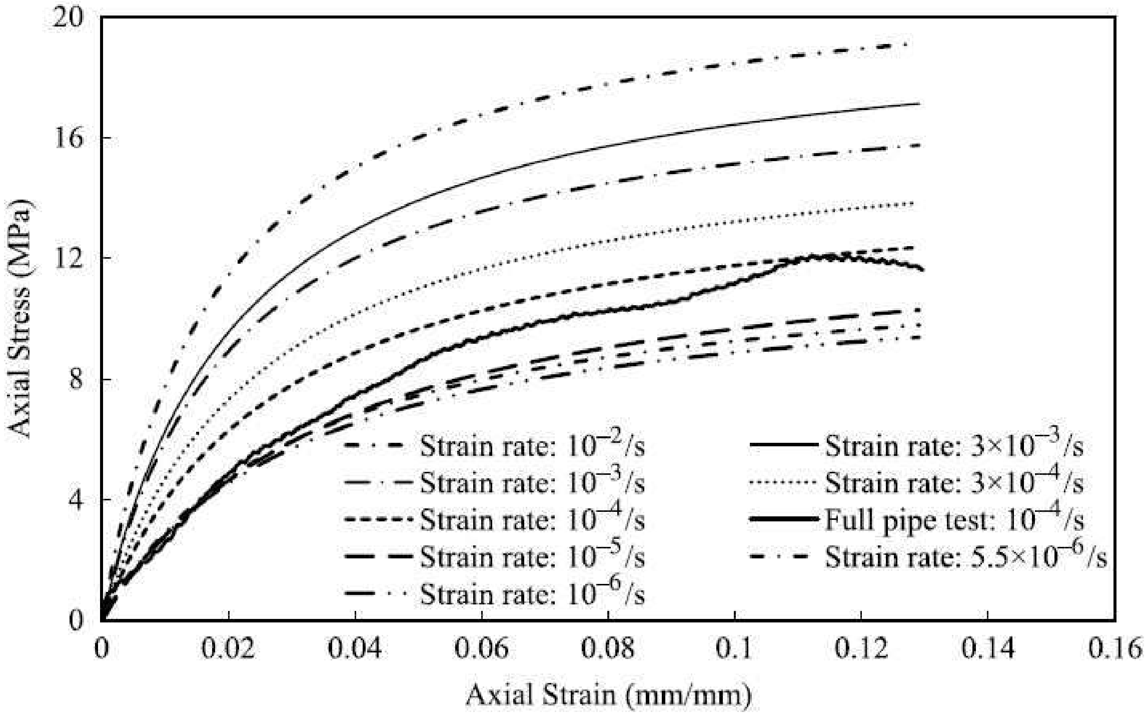

Figure 3-13: Rate-dependent stress-strain responses from constant strain-rate tests (after Das and Dhar, 2021)

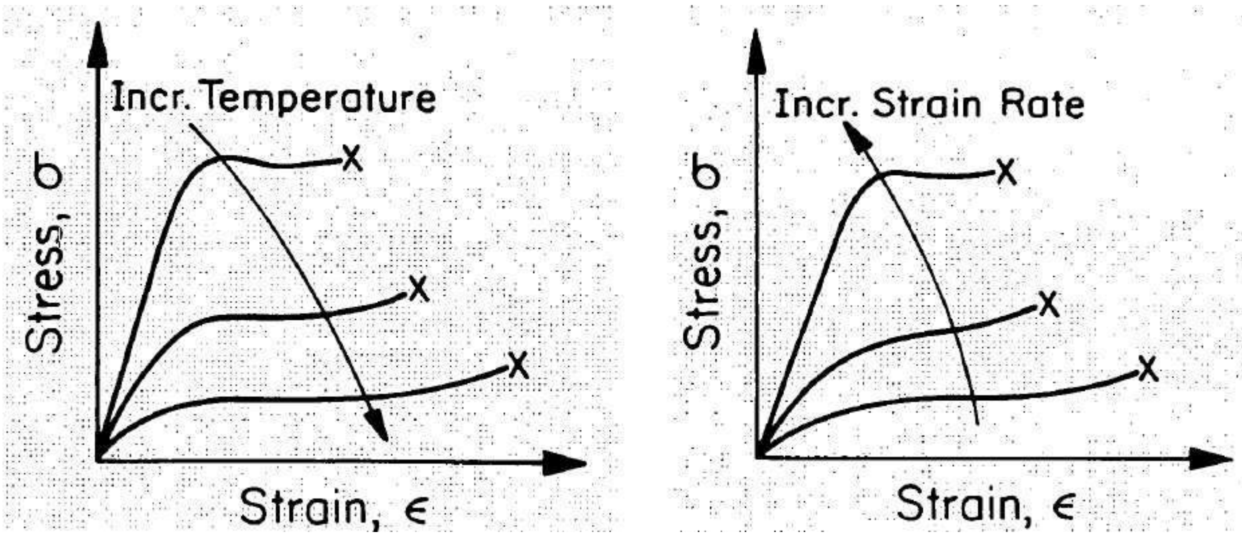

(a) (b)

Figure 3-14: Stress-strain responses of polyethylene: (a) Effect of temperature (b) Effect of strain rate (after Stewart et al., 1999)

(a)

(b)

Figure 3-15: Two different compaction methods: (a) Battery-operated vibrating plate tamper (Wacker Neuson APS1135e) (b) Manual hand tamper

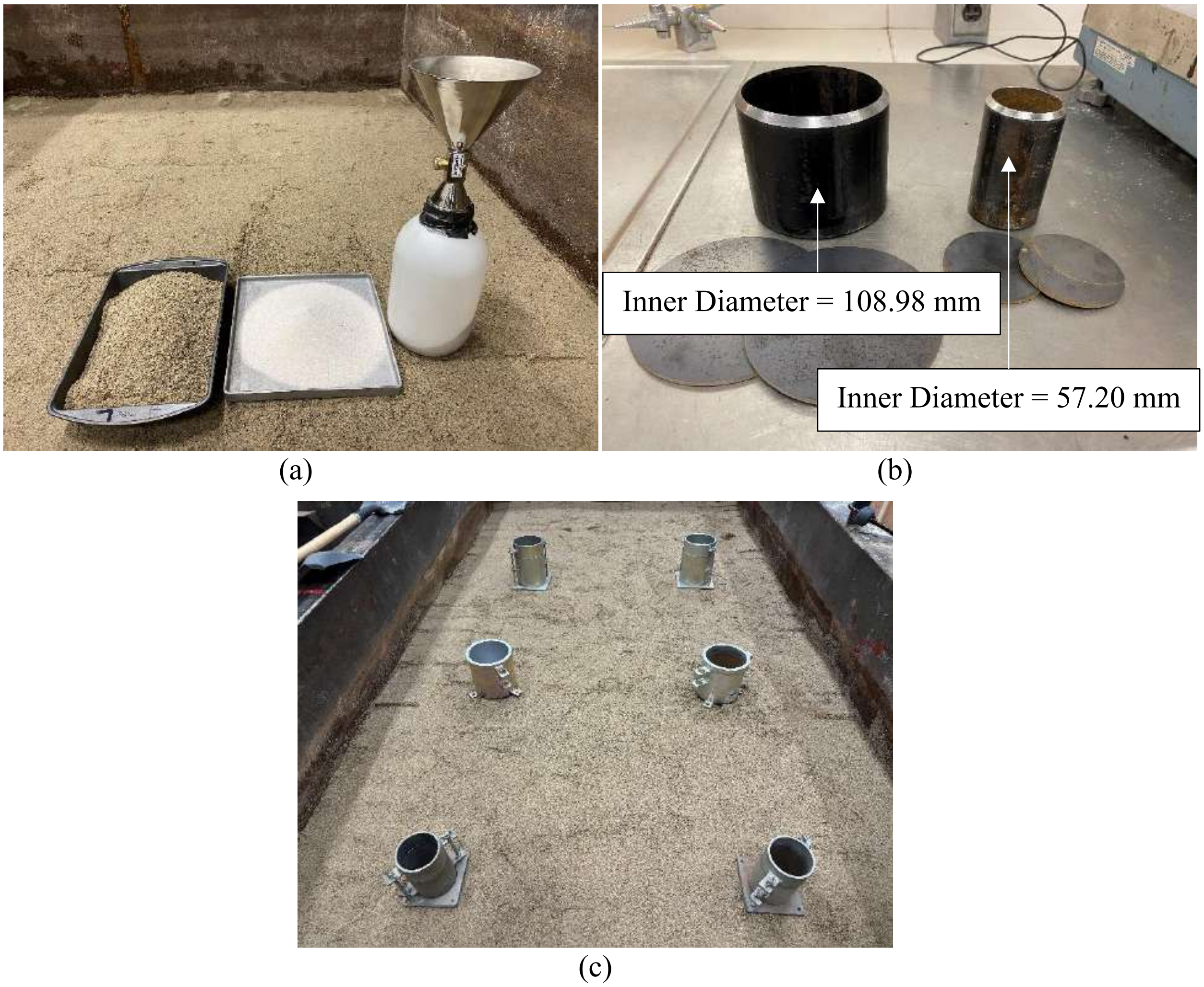

Figure 3-16: Conducted in-situ density tests: (a) Sand cone replacement test (b) In-situ density measurement cylinders (c) Proctor compaction and relative density moulds used for determining density of loose sand

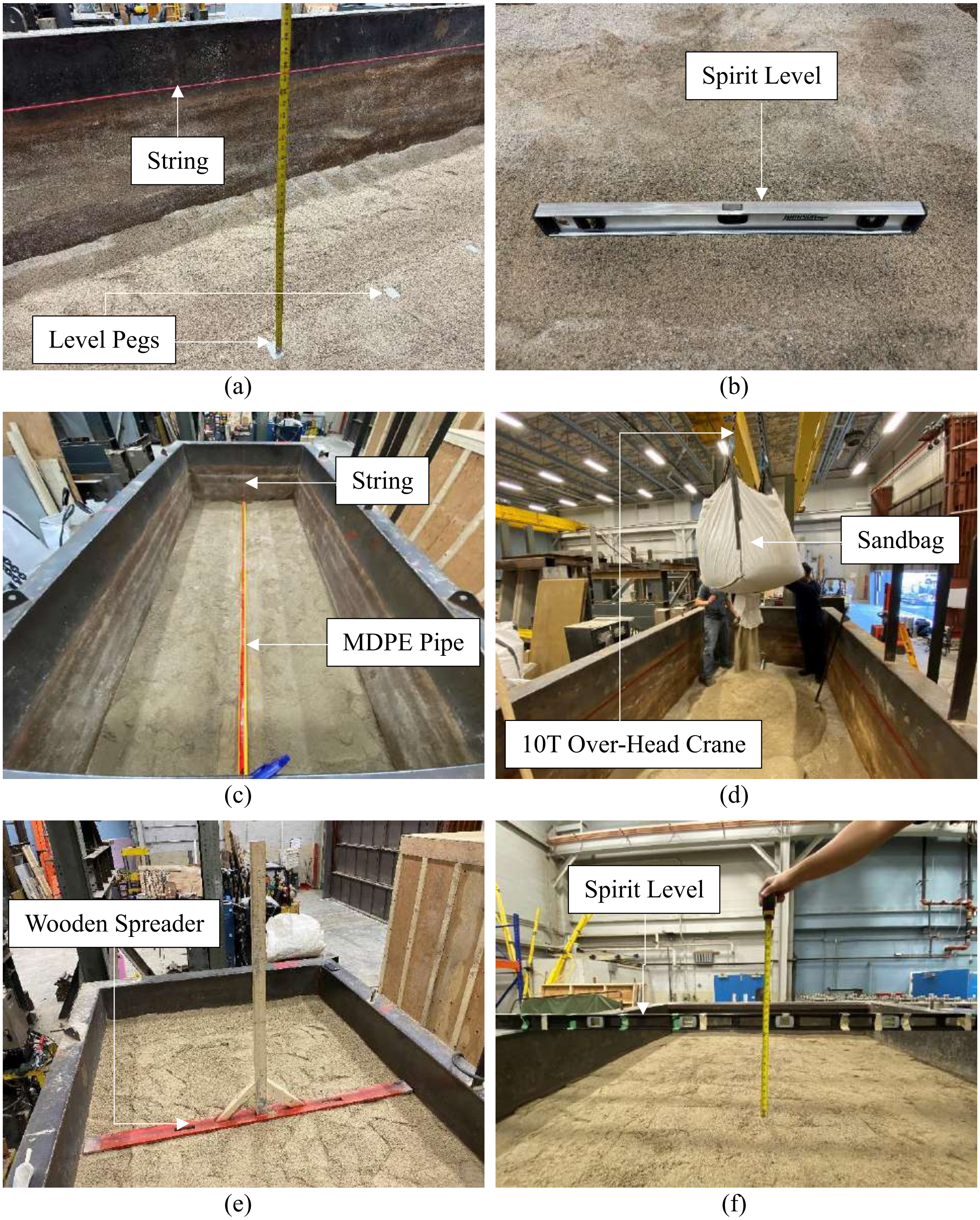

Figure 3-17: Test preparation works: (a) Establishing pipe invert level with string and level pegs (b) Checking soil bed's horizontal level using spirit level (c) Aligning pipe with the use of string (d) 10T overhead crane used to pour the soil into the tank (e) Handmade wooden spreader used for spreading and levelling the soil's top surface (f) Reconfirming burial depth

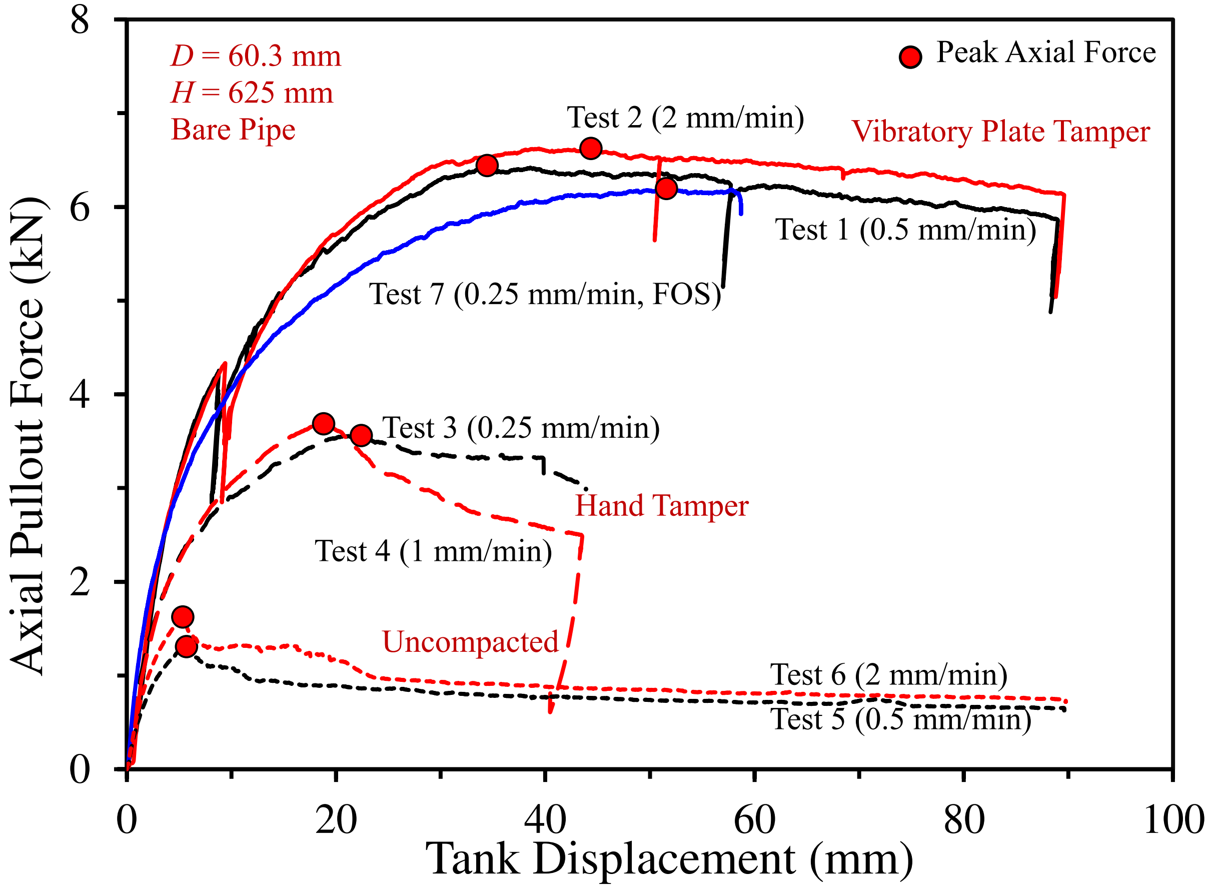

Figure 3-18: Axial force-displacement responses of 60.3 mm diameter bare MDPE pipes

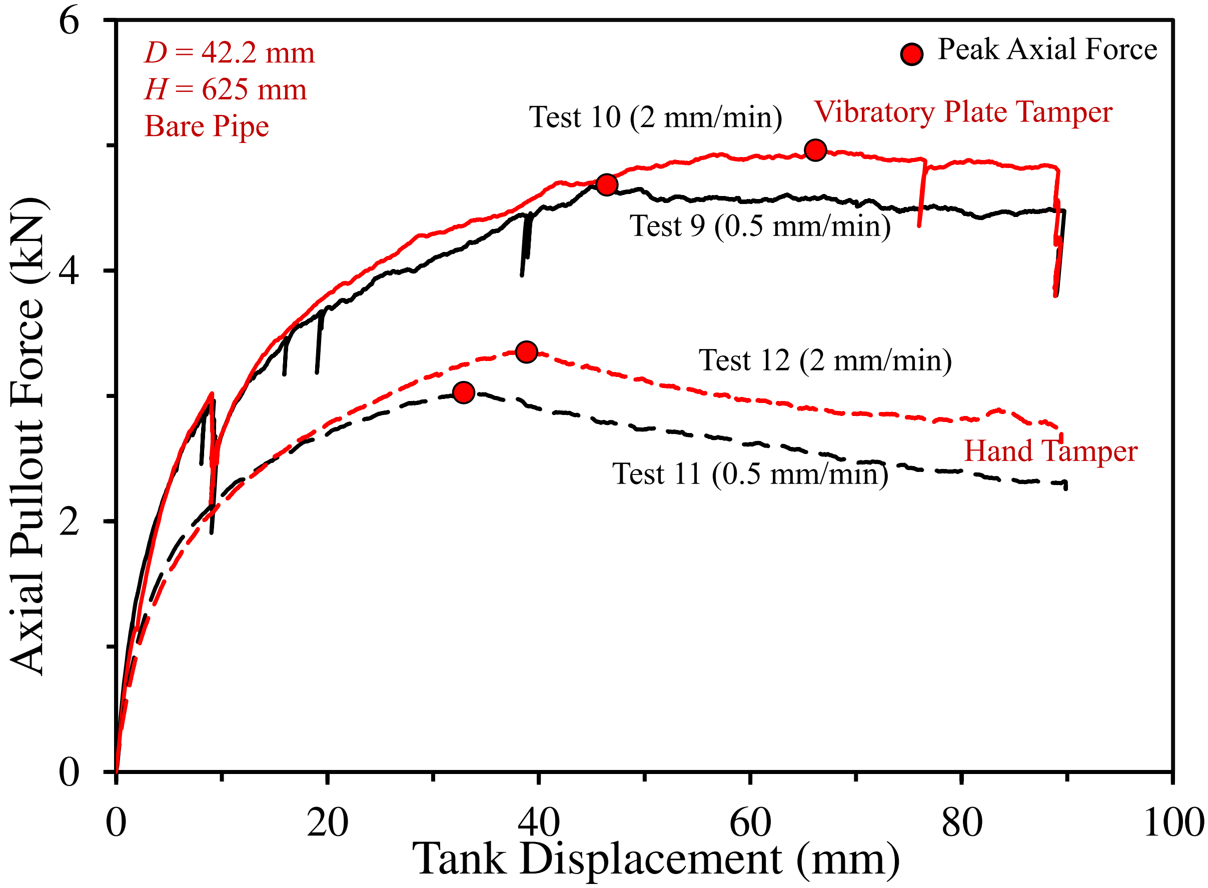

Figure 3-19: Axial force-displacement responses of 42.2 mm diameter bare MDPE pipes

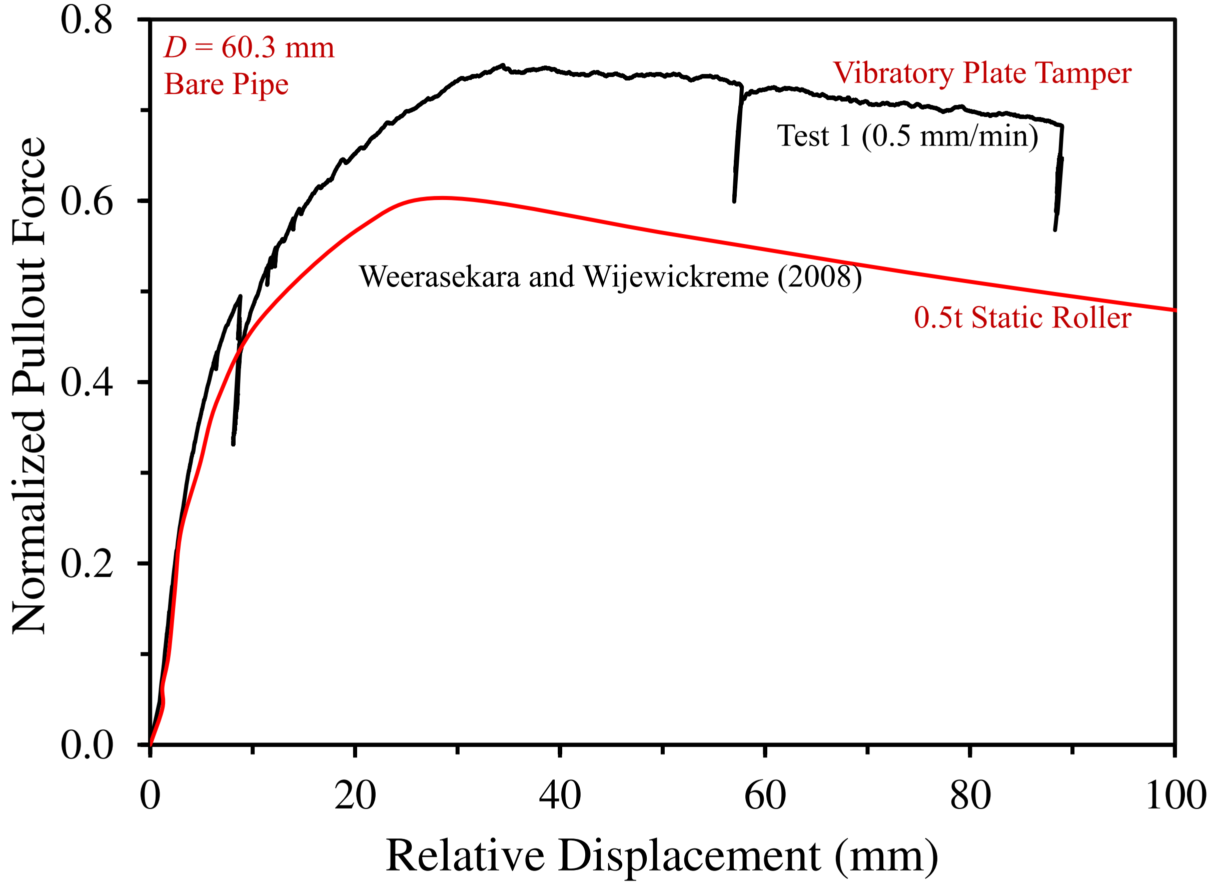

Figure 3-20: Normalized axial force versus displacement for different compaction techniques

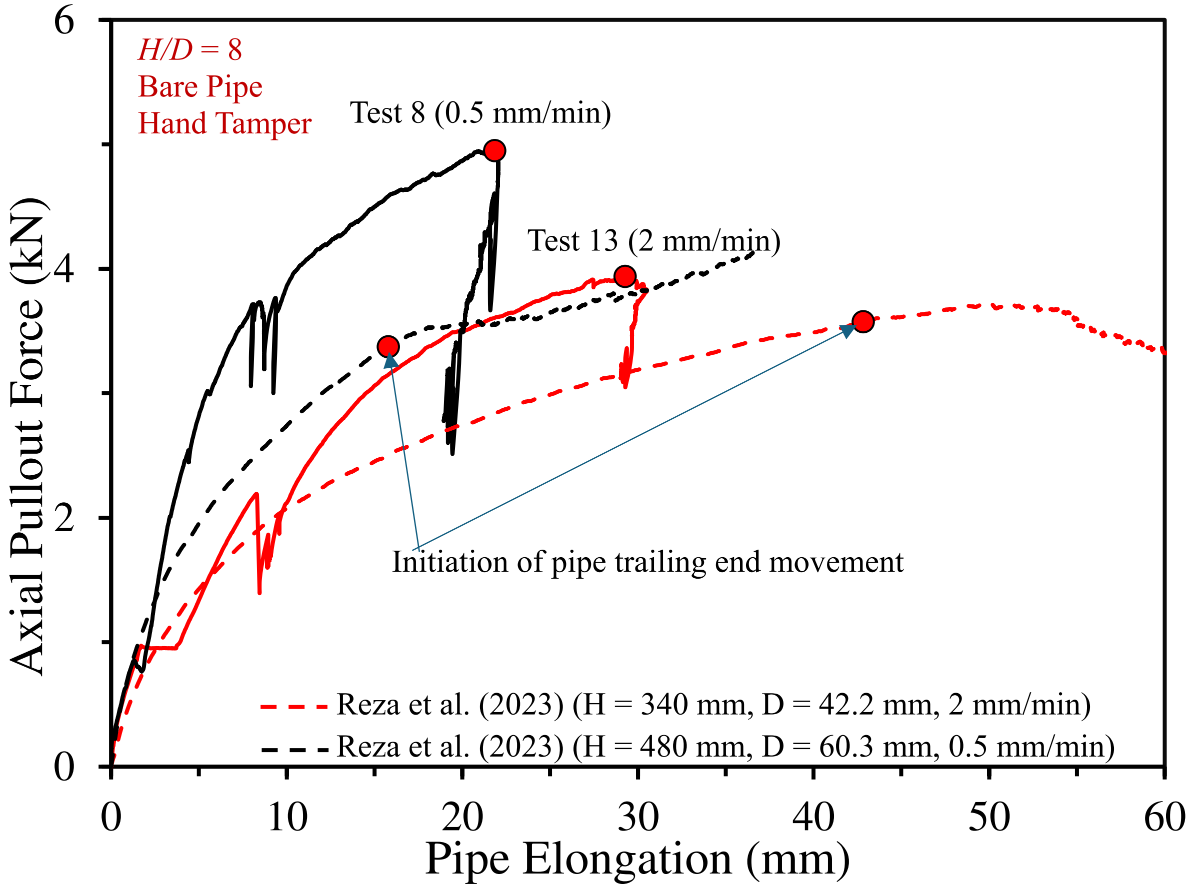

Figure 3-21: Comparison of results from pipe-pull and soil-pull tests

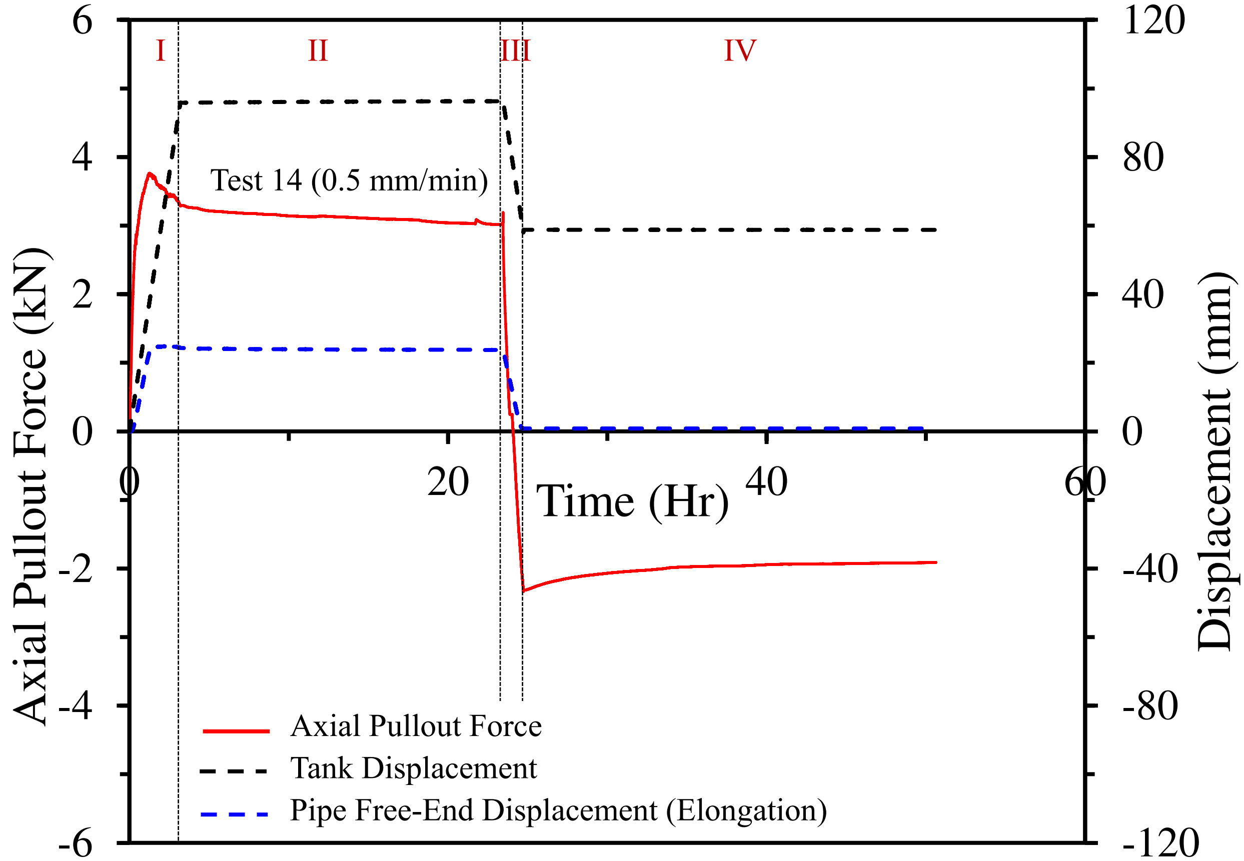

I : Pulling 1
II : Relaxation 1
III : Pushing 1
IV : Relaxation 2

Figure 3-22: Variation of axial pullout force, tank displacement and elongation with time (Test 14)

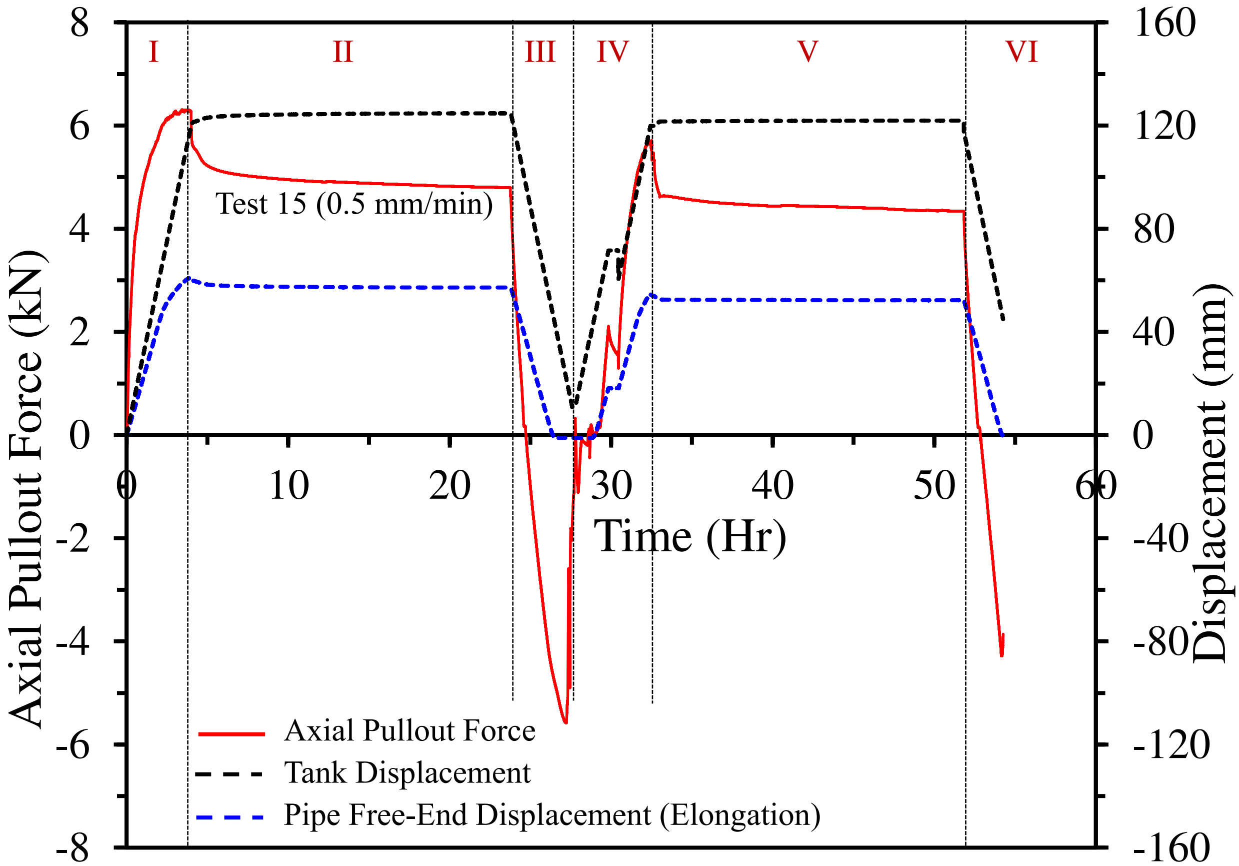

I : Pulling 1
II : Relaxation 1
III : Pushing 1
IV : Pipe Straightening and Pulling 2
V : Relaxation 2
VI : Pushing 2

Figure 3-23: Variation of axial pullout force, tank displacement and elongation with time (Test 15)

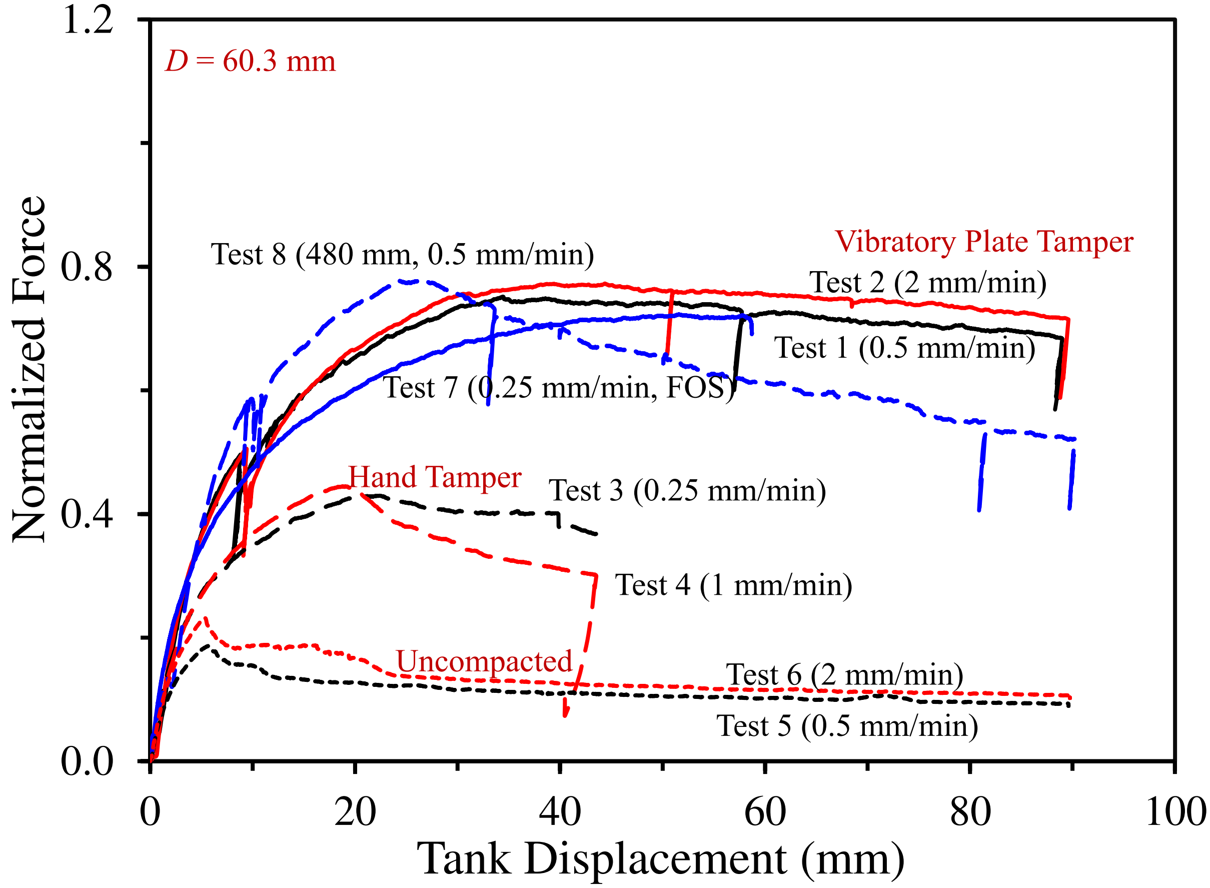

Figure 3-24: Normalized axial force versus displacement for 60.3 mm diameter bare pipes

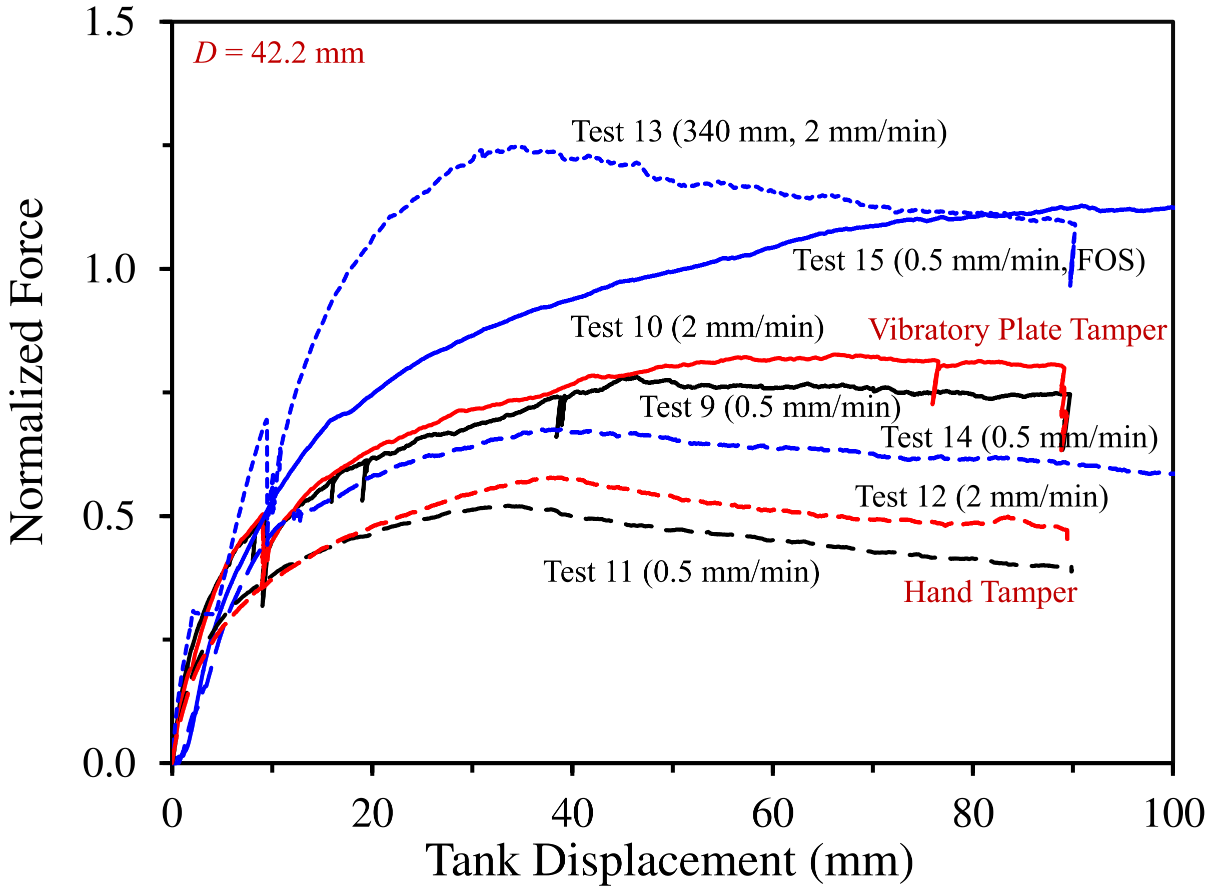

Figure 3-25: Normalized axial force versus displacement for 42.2 mm diameter bare pipes

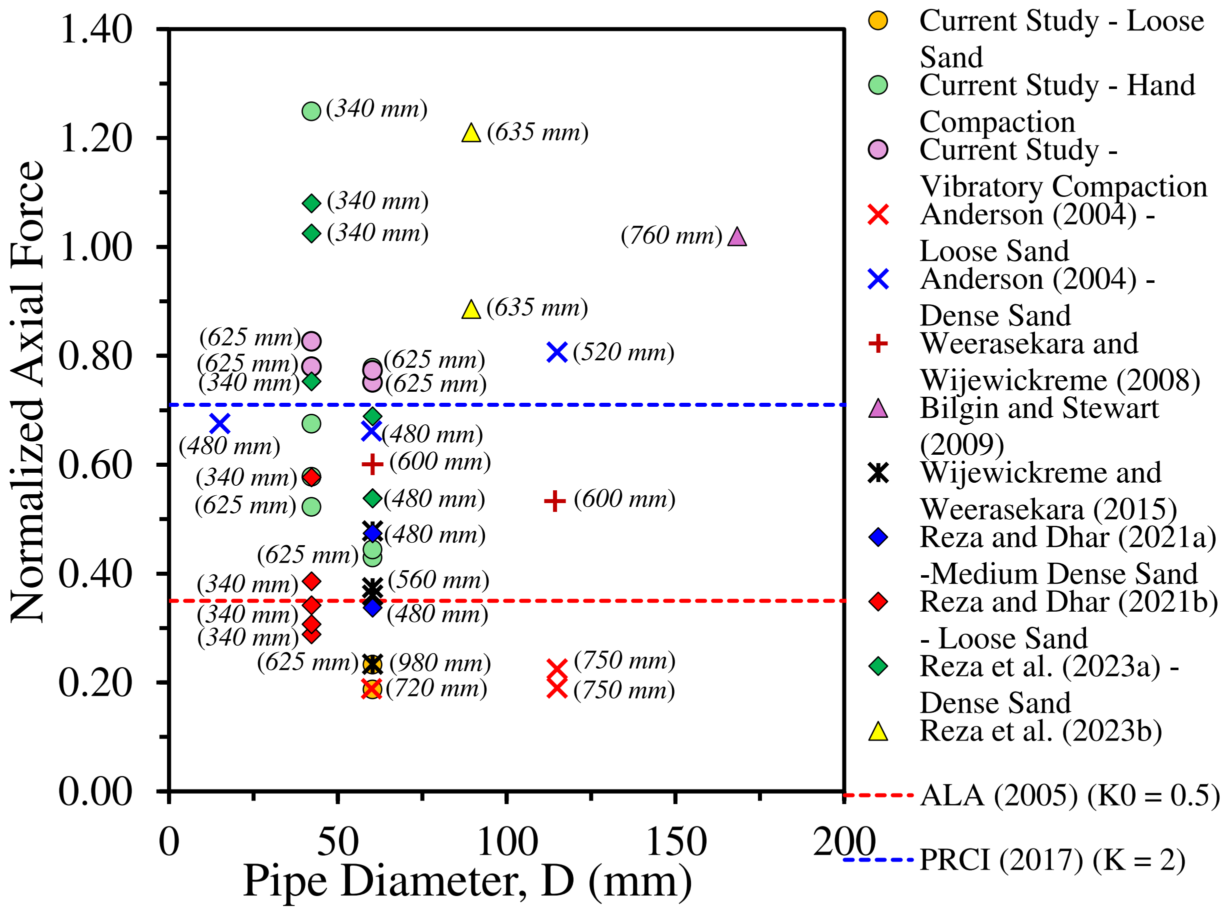

Figure 3-26: Comparison of normalized axial force against pipe diameter. (The burial depths are mentioned within the brackets)

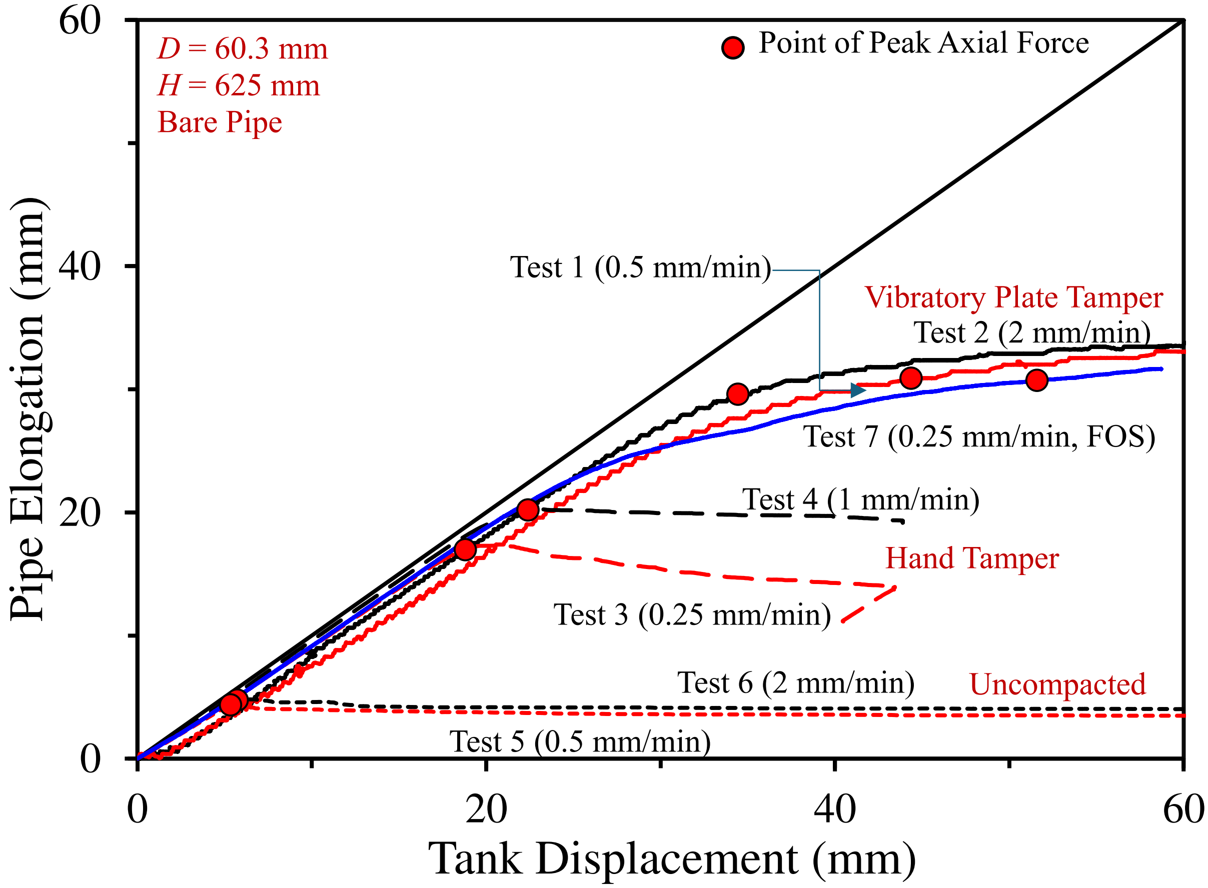

Figure 3-27: Variation of elongation with tank displacement of 60.3 mm diameter bare pipes

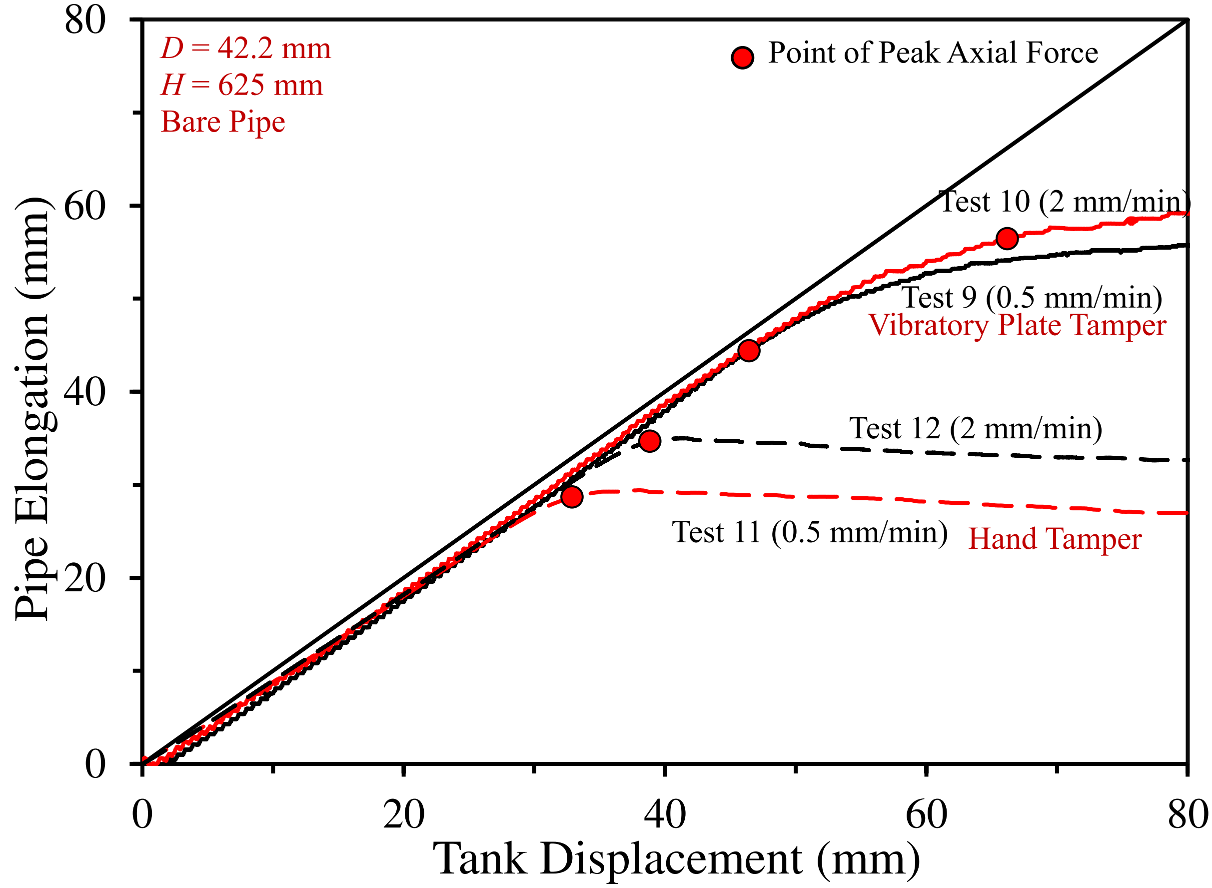

Figure 3-28: Variation of elongation with tank displacement of 42.2 mm diameter bare pipes

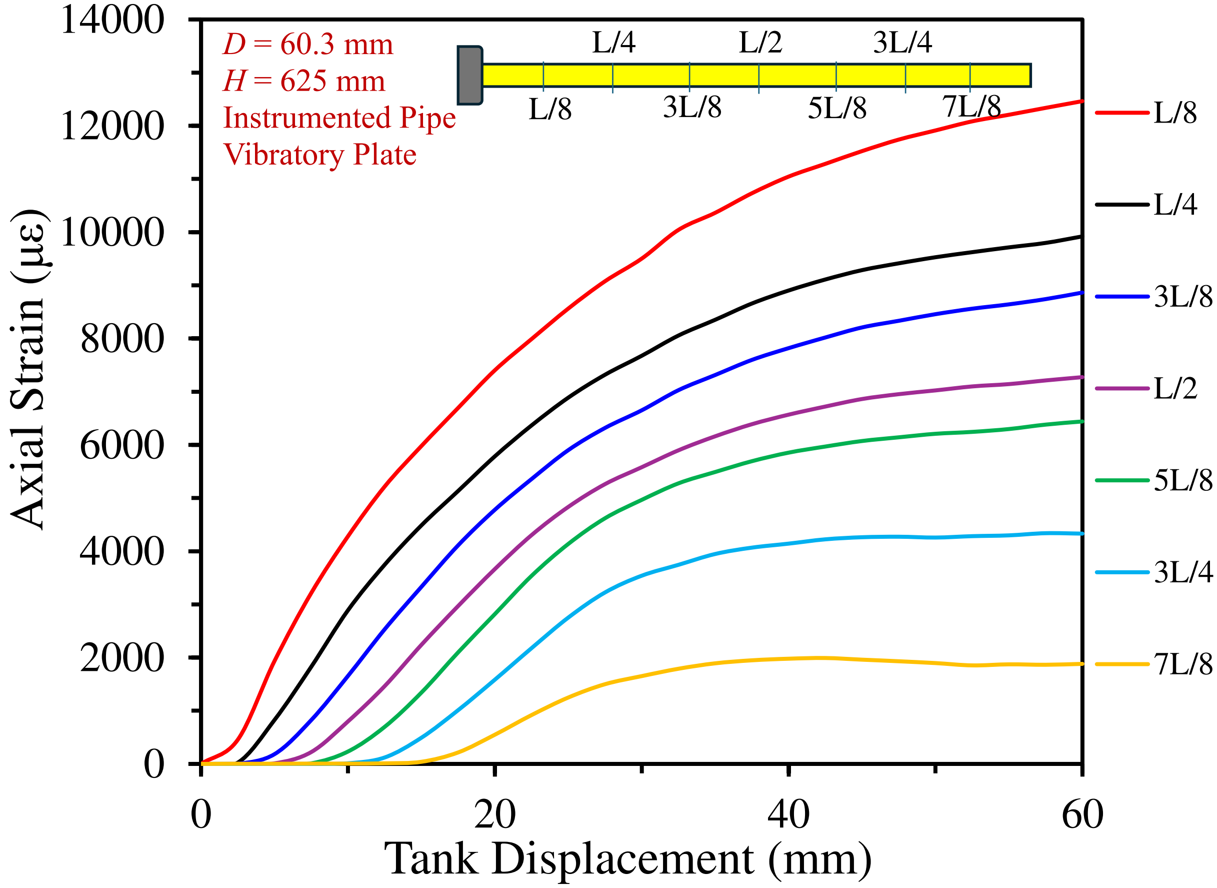

Figure 3-29: Comparison of axial strains at various pipe locations in Test 7

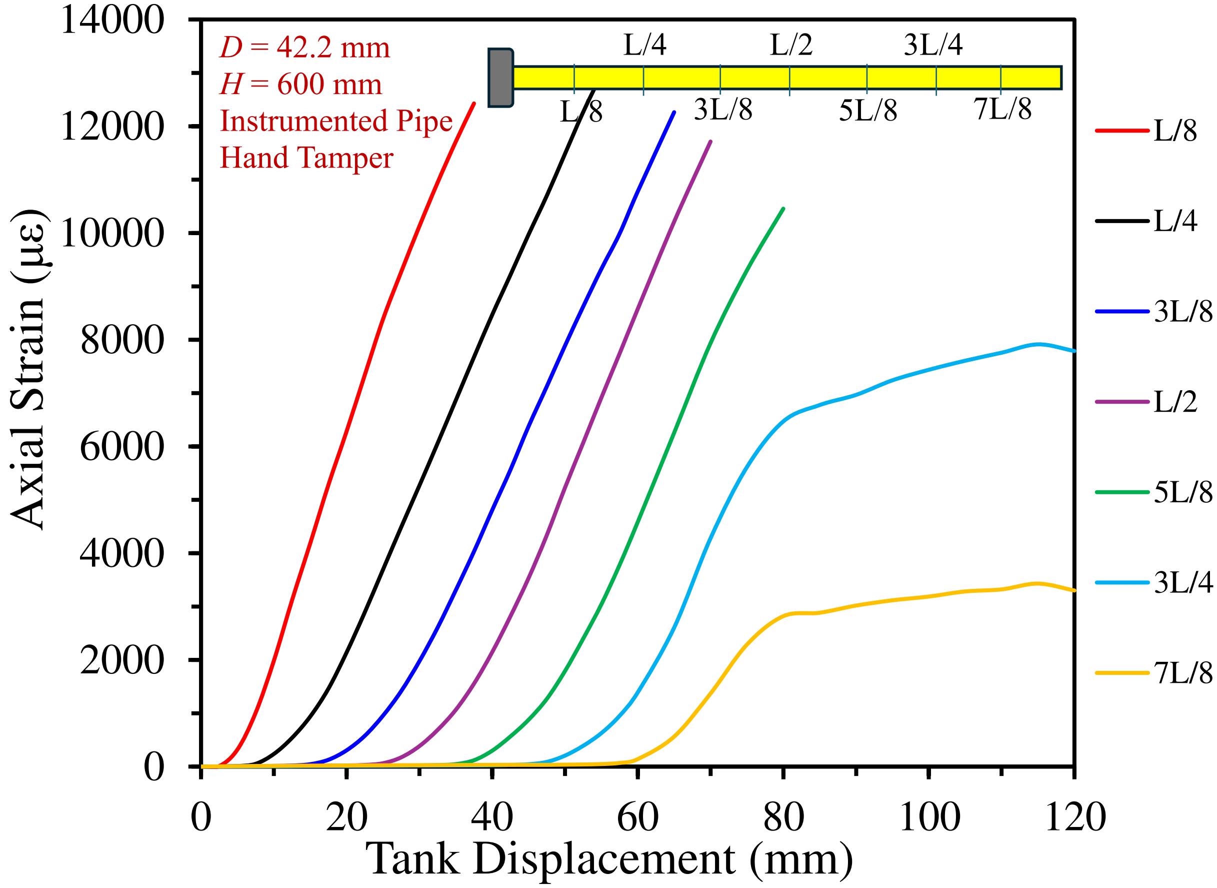

Figure 3-30: Comparison of axial strains at various pipe locations in Test 15

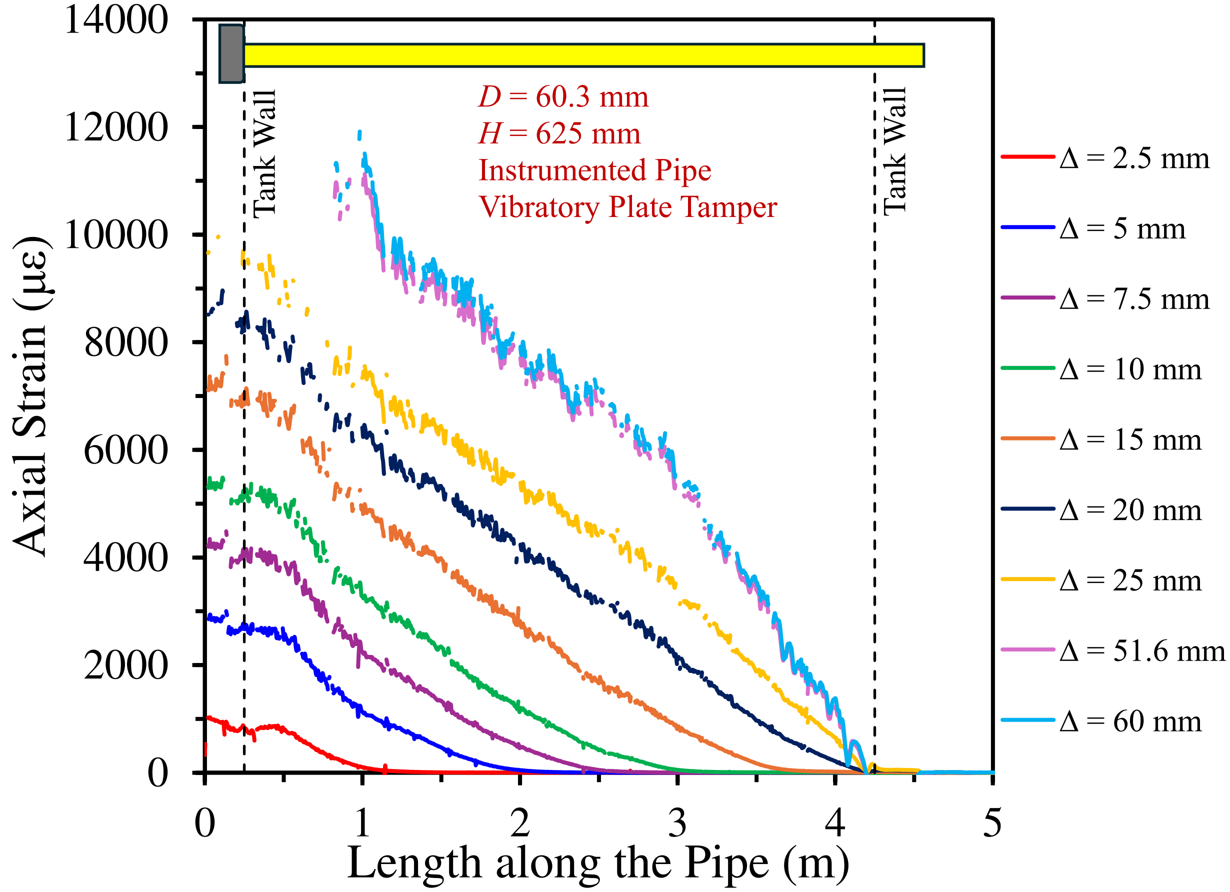

Figure 3-31: Axial strain distribution along the length of pipe of Test 7

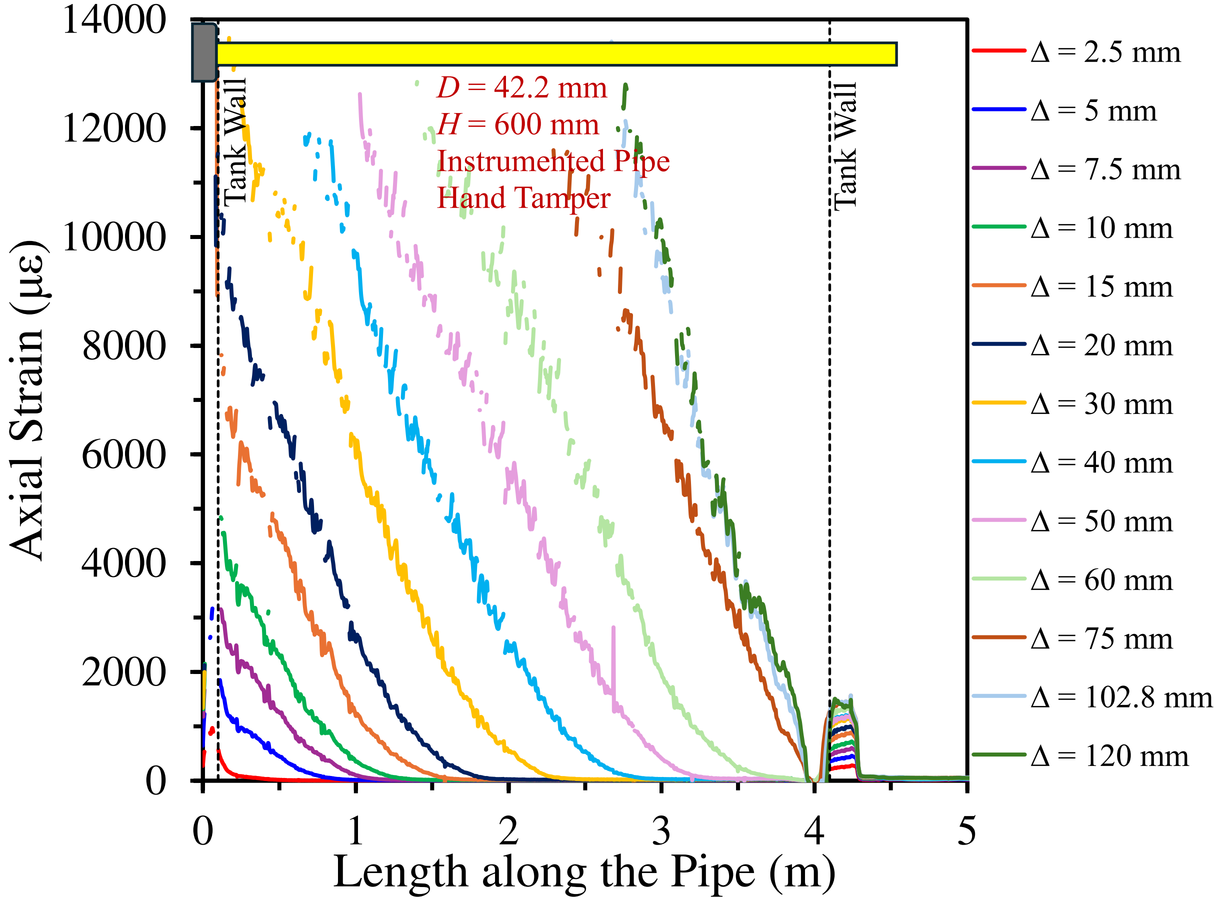

Figure 3-32: Axial strain distribution along the length of pipe of Test 15

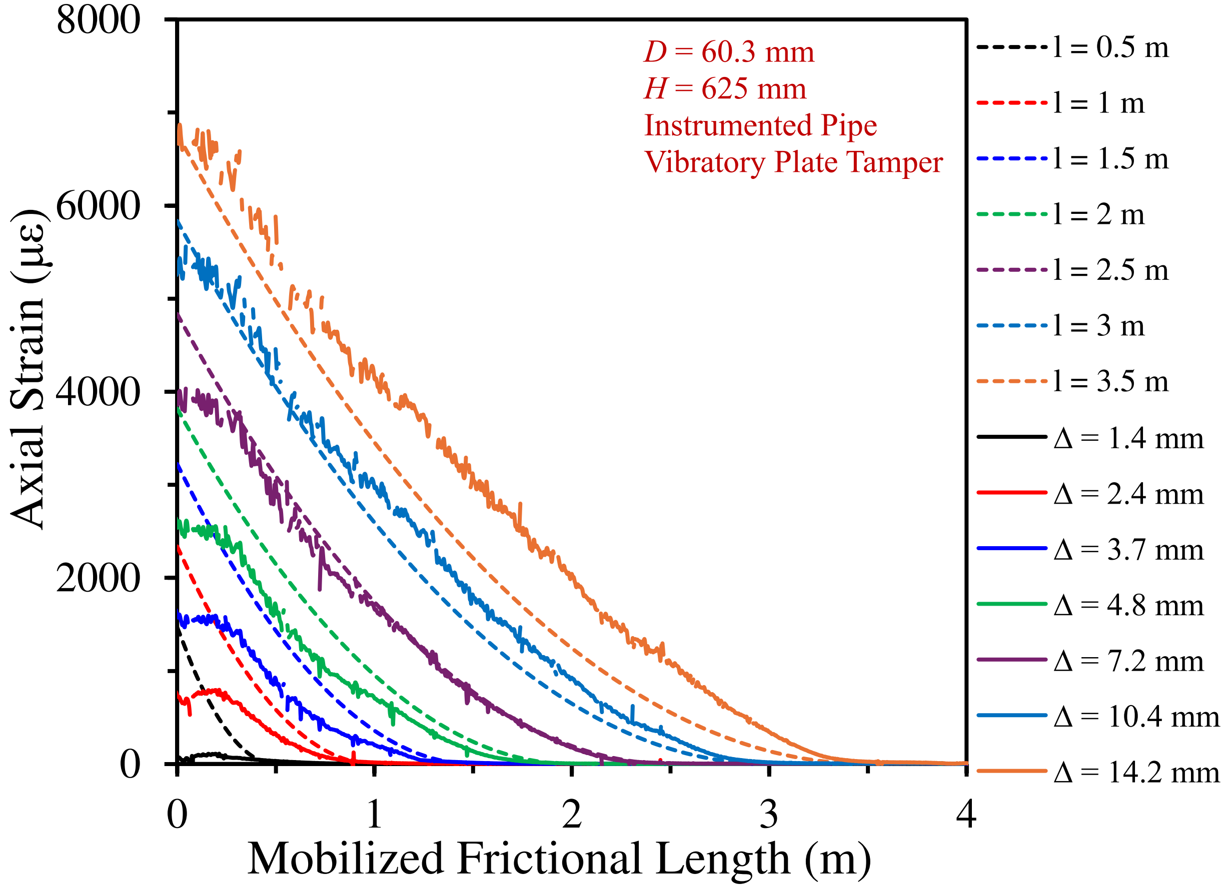

Figure 3-33: Comparison of axial strain distribution over the mobilized frictional length of pipe of Test 7

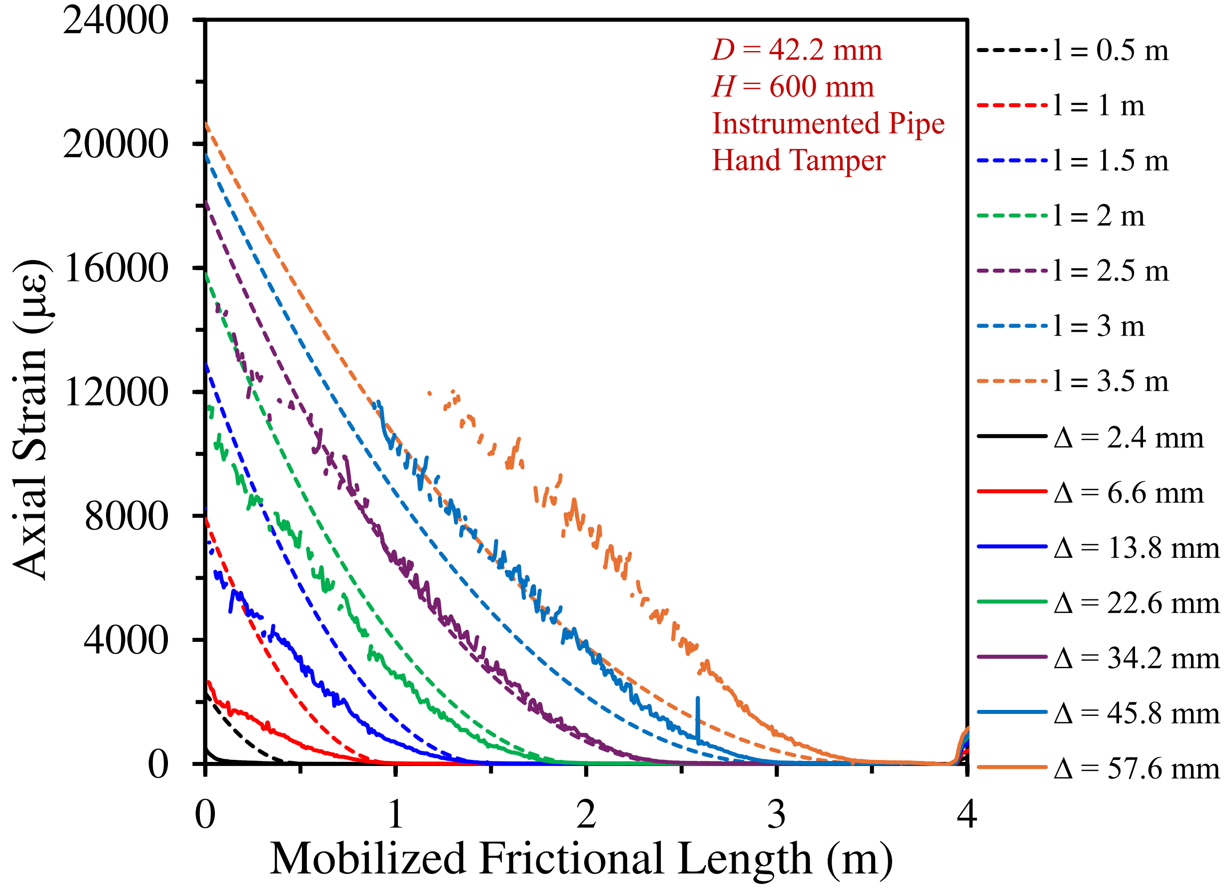

Figure 3-34: Comparison of axial strain distribution over the mobilized frictional length of pipe of Test 15

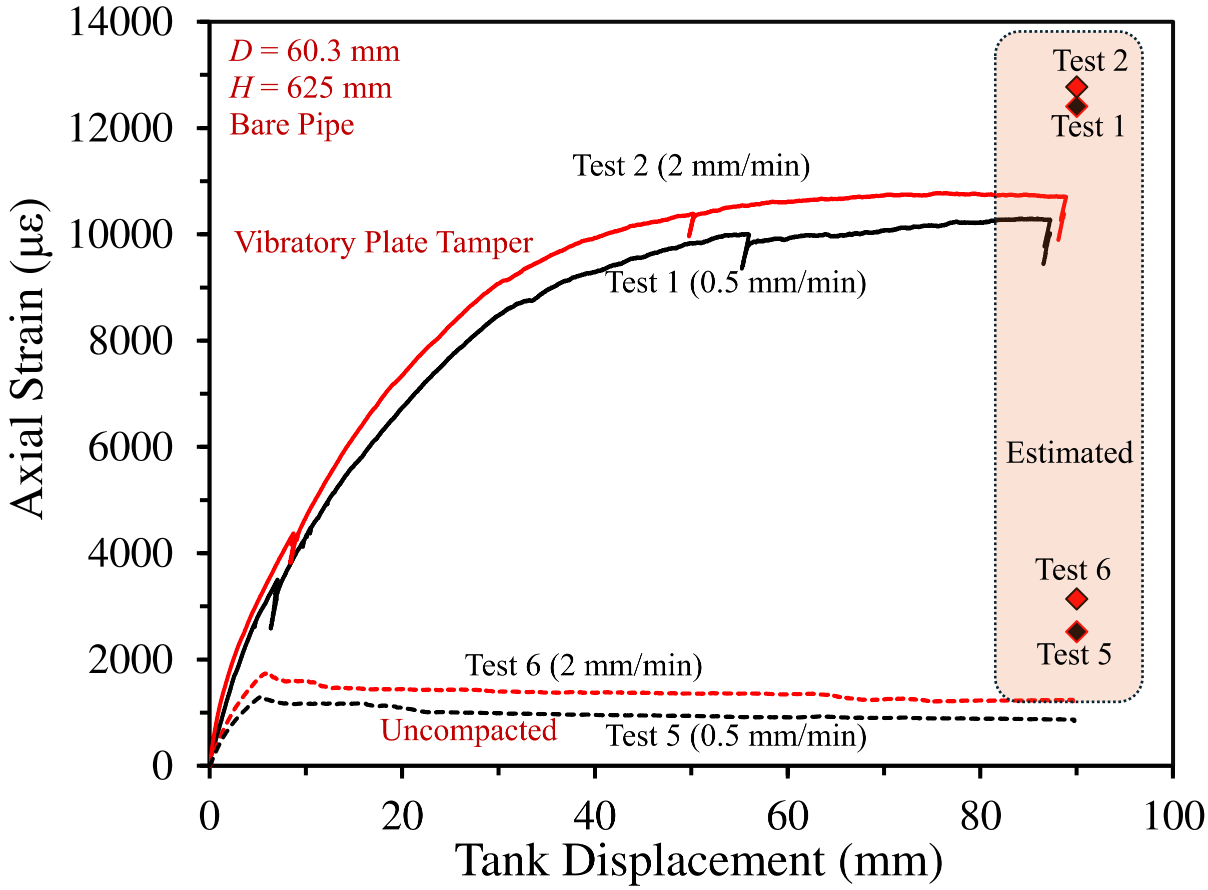

Figure 3-35: Comparison of axial strain on the pipe segment outside the soil box for 60.3 mm pipes

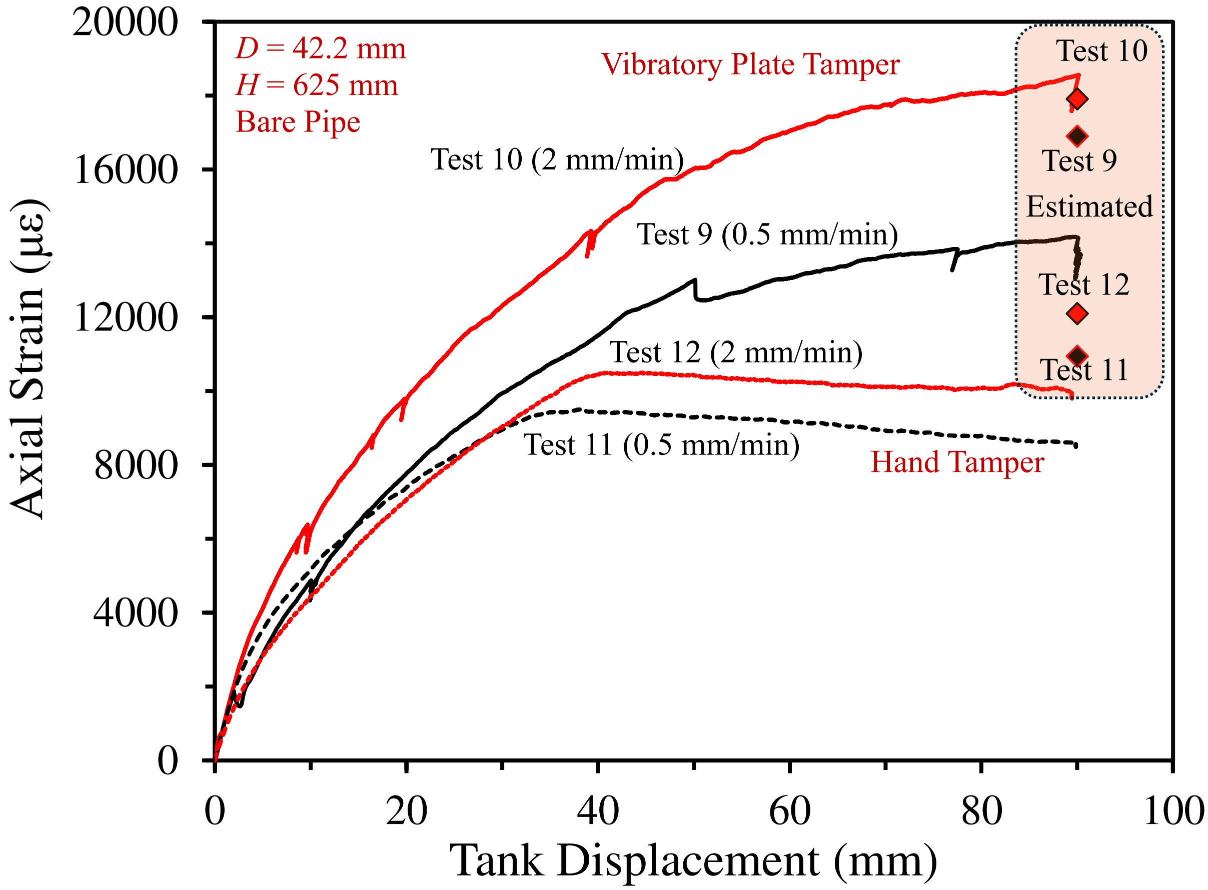

Figure 3-36: Comparison of axial strain on the pipe segment outside the soil box for 42.2 mm pipes

CHAPTER 4: Finite Element Modelling of Buried Medium-Density Polyethylene Pipes in Sand Subjected to Axial Ground Movement

4.1 Introduction

Buried pipelines are integral components of infrastructure, facilitating the transport of essential resources like water, gas, and oil across extensive distances. However, these subsurface conduits are vulnerable to a range of ground movement events, such as landslides, seismic activity, and soil subsidence (Kishawy and Gabbar, 2010; Feng et al., 2015; Lee et al., 2016; Psyrras and Sextos, 2018; Weerasekara and Rahman, 2019; Vesseghi et al., 2021). Understanding the mechanical response of buried pipelines during such events is crucial to ensuring their integrity, reliability, and safety. Ground movement events impose complex loading conditions on buried pipelines, including axial, bending, and shear stresses, which are further influenced by the mechanical properties of the surrounding soil (Weerasekara, 2011; Ni, 2016). Different types of soil, soil saturation levels, and pipeline material properties all contribute to how the soil-pipeline system responds to external stresses. When ground movements occur, they can result in deformation, displacement, or even rupture of pipelines, with potential implications for environmental safety, public health, and economic stability.

The behaviour of buried pipelines, particularly under axial loading conditions, has gathered significant attention due to its critical relevance in pipeline design and maintenance, especially in environments with shifting or uneven ground conditions. MDPE is widely favoured for buried pipelines for its flexibility, durability, and ease of installation. To better predict and manage the risks associated with buried pipelines due to ground movement, researchers employ advanced modelling techniques, including FE analysis and DEM, to simulate soil-pipeline interactions under various conditions. Understanding and predicting the axial response of MDPE pipelines buried in soils remains a complex task due to the intricate soil-pipe interaction mechanisms influenced by soil properties, loading conditions, and the material characteristics of both the pipe and the surrounding soil. Recent advances in FEA, with robust software like ABAQUS, have allowed researchers to incorporate sophisticated soil constitutive models and complex contact algorithms that simulate the soil-pipe interface behaviour with high fidelity.

However, it is important to understand the underlying mechanics of the soil, structure and their interaction for properly incorporating these during numerical modelling. Unfortunately, it is difficult or sometimes impossible to measure or observe these mechanics during full-scale testing to develop the understanding. To this end, overall responses of the pipes are often measured during full-scale tests, and then numerical modelling is performed, implementing some assumed mechanisms to reproduce the test results. Shear-induced soil dilation of the soil-pipe interface is generally assumed as predominant mechanism contributing to higher axial force on pipes in dense sand. However, considering the uncertainties involved in measuring soil stress, extensive studies are required, measuring the interface stress to confirm the mechanism. Wijewickreme et al. (2009) measured interface soil strength using pressure sensors installed on steel pipe wall. They reported higher stresses measured by these sensors during the axial pulling of pipes. No other study on the measurement of stress is available in published literature. The authors made different attempts to measure the stress using null pressure sensors, tekscan pressure sensors and low-pressure transducers, with limited conclusive data.

Nonetheless, researchers performed numerical modelling to artificially induce the effect of interface soil dilation to match with global response measured in tests. Wijewickreme et al. (2009) used 2D plane strain analysis by radial expanding the interface soil to apply the dilation effect (i.e., the expansion of volume). Muntakim and Dhar (2018) and Murugathasan et al. (2018) also expanded a thin zone around the pipe to simulate dilation effects during 3D FE analysis. Meidani et al. (2017, 2018) used DEM to draw the same conclusion as Wijewickreme et al. (2009). Reza and Dhar (2024) applied rigorous 3D continuum-based FE analysis to understand the mechanics of soil pipe interaction. To account for the effect of interface soil dilation, they applied Mohr-Coulomb plasticity with a non-associated flow rule using a constant dilation angle. Thus, they did not apply artificial volume increase to impose a dilation-induced effect. Their study with various angles of dilation revealed that the dilation effect is not very significant on the axial pulling force. They argued that the compaction-induced stress might be responsible for high axial pullout forces for pipes in dense sand. The compaction-induced stresses recommended in Duncan and Seed (1986) were successfully applied to simulate the test results with axial pullout tests. The current study focuses on applying this technique to pipes exposed to axial ground movement. In addition, higher lateral earth pressure coefficients were used in FE analysis as an alternative technique to apply the effect of compaction-induced stresses. Lateral earth pressure coefficients recommended in Meidani et al. (2018) were examined. Three different pulling mechanisms (soil tank movement, soil movement, and pipe movement) were investigated under compaction-induced stresses to analyze their impact on the axial pullout behaviour of MDPE pipes. In the soil tank movement scenario, one end of the pipe was held fixed while the entire soil tank was displaced during FE analysis. In the soil movement scenario, the soil tank was omitted, and instead, a soil block was subjected to displacement while keeping one end of the pipe fixed. Lastly, in the pipe movement scenario, similar to soil movement, the soil tank was not considered; however, in this case, the fixed end of the pipe was displaced while the surrounding soil block remained stationary.

4.2 Full-scale Testing

FE analysis performed in this study was validated with experimental results discussed in Chapter 3. As discussed in Chapter 3, fifteen axial pullout tests were conducted at the full-scale test facility available at Memorial University of Newfoundland. MDPE pipes with 42.2 mm and 60.3 mm diameters with different burial depths (340 mm, 480 mm, 600 mm, 625 mm), various pulling rates (0.25 mm/min, 0.5 mm/min, 1 mm/min, 2 mm/min), with different compaction techniques (vibratory plate tamper, hand tamper, uncompacted loose) were included in the tests. More details of tests can be found in Chapter 3.

4.3 Finite Element Modelling

To understand the various aspects of pipe-soil interaction during axial ground movements, a continuum-based FEA was performed using the commercially available software ABAQUS. The ABAQUS/Standard module was utilized, as it is well-suited for modelling non-linear problems through an implicit numerical approach (Muntakim and Dhar, 2021). The pipe responses observed in full-scale tests (Chapter 3) are simulated using the FEM. The dimensions of the idealized problem are the same as the full-scale test setup. Each component of the test setup (steel tank, soil block, and pipe) is modelled as a 3D deformable solid object. A more detailed discussion on the development of the finite element model is provided in a subsequent section.

From the outcomes of the experimental test results, it was evident that the peak axial force is higher than those given by the equations in the design guidelines. It is assumed that the compaction-induced stresses are predominantly responsible for the higher axial force (After Reza and Dhar, 2024). In the current numerical study, the compaction-induced stresses were modelled as equivalent thermal loading (Saleh et al., 2021; Reza and Dhar, 2024) and also by assigning a higher lateral earth pressure coefficient (K). A detailed explanation of the equivalent thermal loading technique, including the methodology and calculation procedures, is provided in Section 4.3.1. It is worth noting that the horizontal stresses are eventually calculated from the equivalent thermal loading or lateral earth pressure coefficient to obtain the nodal forces during the FE analysis. Hence, utilizing thermal loading or a higher lateral earth pressure coefficient is fundamentally the same for FE analysis for earth pressures at the pipe springline level. However, the latter technique is only able to apply a compaction-induced stress value throughout the depth with a constant K value. The variation of compaction-induced lateral stresses with depth can be better represented by the equivalent thermal loading technique.

4.3.1 Equivalent Temperature Loading

Duncan and Seed (1986) revealed that the compaction-induced lateral stress in the ground is higher near the ground surface and decreases with depth. Reza and Dhar (2024) argued that the compaction-induced stresses govern the axial force on shallow buried pipes. Researchers employed the equivalent thermal loading to simulate the compaction-induced stresses at any soil layer under fix-to-fix boundary conditions during the numerical analysis (Dezfooli, 2013; Saleh et al., 2021; Reza and Dhar, 2024). Equation 4-1 is used to calculate the equivalent temperature for a specific magnitude of the coefficient of thermal expansion and known compaction-induced stress. In Equation 4-1, $\Delta\sigma_{soil}$ is the compaction-induced lateral stress in the soil layer; E is the modulus of elasticity of soil; α is the coefficient of expansion for soil; ΔT is the change in soil temperature applied to the soil layer.

$$\Delta\sigma_{soil} = (E\alpha\Delta T)_{soil} \qquad \text{Equation 4-1}$$

Figure 4-1 shows the variation of compaction-induced lateral stresses with depth, reported by researchers focusing on different studies. Duncan and Seed (1986) proposed analytical procedures for the evaluation of compaction-induced lateral earth pressures. Duncan et al. (1991) developed earth pressure charts to estimate compaction-induced horizontal earth pressures for different compaction methods. Chen and Fang (2008) measured the compaction-induced lateral earth pressure due to vibratory compaction. Saleh et al. (2021) used an equation to calculate the additional lateral earth pressure due to compaction based on the theory of Boussinesq (1885) for distributed strip loads. As seen in Figure 4-1, the compaction-induced stresses from the Duncan and Seed (1986) analytical procedures were higher than those reported by other studies. The stresses from Duncan and Seed (1986) simulated reasonably the compaction-induced stresses for the compaction employed in the current study (Reza and Dhar, 2024) and, therefore, considered in this study.

Reza and Dhar (2024) developed curves (Figure 4-2) for the variation of compaction-induced stresses with depths based on the procedure described in Duncan and Seed (1986). As seen in Figure 4-2, the compaction-induced stresses were determined as the difference between the peak horizontal stresses and the respective at-rest lateral stresses. Then, the corresponding equivalent thermal loads were calculated using Equation 4-1. For example, using Figure 4-2, the compaction-induced lateral stress was calculated as 11.1 kPa at a springline depth of 625 mm. By using the same curve, Reza and Dhar (2024) reported 24.7 kPa and 16.2 kPa for the depths 340 mm and 480 mm, respectively. Using Equation 4-1, for E = 5 MPa and α = 0.00005 /°C, the equivalent thermal loading was calculated as 44.4 °C for the springline depth of 625 mm. In ABAQUS, the thermal loading can be applied to the FE model as a predefined field in the horizontal direction (perpendicular to the pipe) during the analysis. Figure 4-3 shows the applied temperature loading to the backfill soil to simulate the compaction-induced stresses.

4.3.2 Lateral Earth Pressure Coefficient

The lateral earth pressure can also be applied in ABAQUS using a higher coefficient of lateral earth pressure. Meidani et al. (2018) proposed a modified lateral earth pressure coefficient to account for the shear-induced dilation of the surrounding soil during axial pullout. The proposal by Meidani et al. (2018) was used as the basis for this technique to select the relevant lateral earth pressure coefficients. However, Reza and Dhar (2024) revealed that the effect of dilation is negligible for the axial pipe-soil interaction of MDPE pipes. As the shear-induced dilation effect is negligible, the lateral earth pressure coefficients were considered to be due to the effect of compaction-induced stresses and used to simulate the experimental results of the current study. As stated in Chapter 3, a shear zone thickness of 0.8 mm was assumed to determine the lateral earth pressure coefficient of each test condition. The higher lateral earth pressure coefficients were applied to the soil layer in the FE model as a predefined field during the analysis.

4.3.3 Contact Interaction

Contact interactions are defined in ABAQUS to simulate the interactions between different components of a model. It defines how surfaces interact with each other, accounting for friction, separation, and the transfer of forces. The technique permits separation and sliding with finite amplitude and arbitrary rotation of the contact surfaces. Two common contact formulations such as general contact and surface-to-surface contact are commonly available. The surface-to-surface contact algorithm offers detailed control over contact conditions between two defined surfaces. The general contact algorithm provides an automated, comprehensive solution for managing multiple contact interactions in complex models.

In this study, the contact interface between the pipe and soil was modelled using the surface-to-surface contact algorithm for simulating tank movement against a stable pipe, which involves both soil-pipe and soil-tank interactions. For analysis involving only soil-pipe interaction, the general contact algorithm was used.

Both tangential and normal behaviours were specified between the interacting surfaces (i.e., soil-pipe and tank-soil interactions). For normal behaviour, a hard contact condition was applied, allowing separation after contact. Tangential behaviour was defined using an isotropic penalty algorithm, with friction coefficient values derived from the tangent of the interface friction angle, δ, between the two surfaces. In pipe-soil interactions, this friction angle was calculated as $\delta = f\varphi$, where the friction factor (f) multiplies the friction angle of the soil (φ). Reza and Dhar (2021a) proposed a pulling-rate-dependent friction factor for MDPE materials, with values of 0.75 for a rate of 0.5 mm/min, 0.86 for 1 mm/min, and 0.9 for 2 mm/min. While guidelines such as those from ASCE (1984), ALA (2005), and PRCI (2017) suggest a friction factor (f) of 0.6 for polyethylene, previous research has shown that soil particle embedment into the flexible surface of the pipe increases friction at the pipe-soil interface (Scarpelli et al., 2003; Reza et al., 2023a; Guo and Zhou, 2024). Based on the full-scale axial pullout tests conducted in this study, the effect of the pulling rate was found to be negligible. However, given the scratches and soil particle embedment observed on the MDPE pipe surface, a friction factor (f) of 0.75 was used in the finite element analysis. Previous experimental and numerical studies have demonstrated the minimal impact of soil-tank friction on pipe response. Reza and Dhar (2021) stated that no sidewall treatment was applied to reduce wall friction between the cell wall and the soil. Murugathasan et al. (2018) conducted numerical simulations using interface friction angles ranging from 1° to 15° and concluded that soil-tank friction had a negligible influence on pipe response due to the sufficient width of the tank. Similarly, Wijewickreme et al. (2009) reported that the effect of sidewall friction in axial pullout tests was insignificant, supporting the assumption that soil does not slide relative to the test cell walls under axial loading. Additionally, studies by Dhar and Moore (2004) emphasized that while sidewall friction is critical under vertical loading due to the arching effect, it plays a less significant role in axial loading conditions. Considering these previous studies, for the pipe-tank interaction, a lower friction coefficient of 0.1 corresponding to the soil-tank interface friction angle of 6° was applied to the numerical modelling in the current study.

The contact algorithm in ABAQUS defines master and slave surfaces. The master surface dictates contact behaviour and generates contact forces, while the slave surface adapts to the forces imposed by the master surface (Boulbes, 2020). The stiffer surface is typically modelled as the master surface, while the less stiff surface is assigned the slave role (Dassault Systems, 2019). For the soil-pipe interaction, the outer surface of the pipe was modelled as the master surface and the interacting soil surface as the slave surface. For soil-tank interaction, the inner surface of the tank was defined as the master surface, with the interacting soil surface acting as the slave surface.

4.3.4 Mesh Sensitive Analysis

A mesh sensitivity analysis was performed to confirm that the solution is independent of the mesh size, ensuring that the results have converged. Once the results exhibit mesh independence, the optimum mesh size is identified and used in the finite element model.

In this study, the pipe, soil, and tank domains were modelled using eight-noded linear brick elements with reduced integration (C3D8R). These reduced integration elements are efficient due to fewer integration points, but they can be susceptible to hourglassing, a numerical instability where elements deform unrealistically. To address this, ABAQUS offers enhanced hourglass control, which improves element behaviour and minimizes hourglassing, particularly in cases involving nonlinear material behaviour or large deformations (Schäfer et al., 2020). Although enhanced hourglass control increases computational effort slightly, it offers better stability. All models employed structured hexahedral meshing, which typically yields more accurate and reliable convergence compared to unstructured meshes. Several researchers used C3D8R elements to successfully model the pipe-soil interaction problems (Roy et al., 2016; Almahakeri et al., 2016; Murugathasan et al., 2021; Muntakim and Dhar, 2021; Reza and Dhar, 2021a, 2021b, 2024). Researchers also used C3D20R elements, which is a twenty-noded quadratic brick element with reduced integration feature. However, Almahakeri et al. (2016) reported convergence difficulties for the analysis performed with C3D20R elements.

During the axial pipe-soil interaction analysis, significant stress nonlinearity was observed around the pipe (Muntakim and Dhar, 2018). Therefore, finer mesh was applied around the pipe to capture this stress nonlinearity effectively. As depicted in Figure 4-4, finer mesh was used within a radial distance of 2.5 times the pipe diameter (2.5D) to accurately capture the behaviour around the pipe, while a coarser mesh was applied beyond 2.5D to minimize computational cost. This approach aligns with similar studies conducted by Muntakim and Dhar (2021) and Reza and Dhar (2021a, 2021b, 2024).

The mesh sensitivity analysis involved varying the number of elements in the radial direction within the finer mesh region while keeping the coarser mesh region constant. Two key parameters, axial force and normal stress on the pipe surface, were evaluated against the number of elements. The analytical solution of Hoeg (1968) was used for comparison of the calculated normal stresses. Note that the solution of Hoeg (1968) is based on the idealization of semi-infinite media and, therefore, may not fully represent the test conditions presented in this study. Figures 4-5 and 4-6 illustrate the comparison of normal stress and axial pullout force with respect to the number of elements. As the results show, the finite element model with approximately 82,000 elements produced normal stress values within 2.8% of the analytical solution provided by Hoeg (1968), and the model with 71,000 elements yielded normal stress values within 3% of the analytical solution, and the axial pullout forces for both models were nearly identical. Considering both computational efficiency and result accuracy, the model with approximately 71,000 elements was deemed appropriate for the current study. The minimum element size used in this model was 3.47 mm.

4.3.5 Material Models

4.3.5.1 MDPE

The stress-strain responses of MDPE pipe material are highly nonlinear, strain-rate dependent and temperature dependent (Stewart et al., 1999; Sulieman and Coore, 2004; Hamouda et al., 2007; Bilgin et al., 2007; Bilgin and Stewart, 2009a; Weerasekara, 2011; Das and Dhar, 2021). Konder (1963) proposed a hyperbolic equation (Equation 4-2) to represent the nonlinear response of the MDPE pipe material, where σ is the stress; ε is the strain; E_{ini} is the initial modulus of elasticity of MDPE; η is the hyperbolic constant.

$$\sigma = E_{ini}\left(\frac{\varepsilon}{1+\eta\varepsilon}\right) \qquad \text{Equation 4-2}$$

Suleiman and Coree (2004) proposed Equation 4-3, to capture the strain-rate dependent nonlinear response of the MDPE pipe, where $\dot{\varepsilon}$ is the strain rate; and a and b are the constants obtained from uniaxial tension or compression tests.

$$E_{ini} = a(\dot{\varepsilon})^b \qquad \text{Equation 4-3}$$

The hyperbolic constant η can be found from the following Equation 4-4 (Suleiman and Coree, 2004), where c and d are constants that can be determined from uniaxial tension or compression tests.

$$\eta = \frac{a(\dot{\varepsilon})^b}{c + d\ln(\dot{\varepsilon})} \qquad \text{Equation 4-4}$$

Das and Dhar (2021) reported the constants a, b, c, and d as 2000, 0.137, 27.5 and 1.29, respectively, based on the uniaxial tension tests conducted on MDPE pipe material at an ambient temperature of 22±1°C. In the current study, axial strain measurements from full-scale tests revealed that the maximum strain rates for the 60.3 mm MDPE pipe ranged from 2.87×10^{-6}/s to 1.44×10^{-5}/s, and for the 42.2 mm MDPE pipe, the strain rates ranged from 4.89×10^{-6}/s to 1.64×10^{-5}/s, for pulling rates of 0.5 mm/min to 2 mm/min. Using the stress-strain model proposed by Das and Dhar (2021), the stress-strain responses for the above strain rates were calculated and plotted for the 60.3 mm and 42.2 mm MDPE pipe materials, as illustrated in Figure 4-7. These responses served as input for the finite element analysis. The yield stress and strain, as shown in Figure 4-7, was employed in the elastic-plastic isotropic model. The Poisson's ratio of 0.46 and the density of MDPE of 940 kg/m^3 were assumed at the nominal temperature of 22±1°C. Additionally, a constant modulus of elasticity of 550 MPa was applied to simulate the experimental results. This value has been proven effective in similar FE analyses by Reza and Dhar (2021a, 2021b). The effect of temperature on the properties of the MDPE material was not considered in this study, with the assumption that the ambient temperature remained relatively constant during the tests.

4.3.5.2 Backfill Soil

As discussed in Chapter 3, the stress-dependent modulus of elasticity of the backfill soil was determined using the power law equation of Janbu (1963). Several researchers used the equation proposed by Janbu (1963) for estimating the modulus of soil in numerical modelling for pipe-soil interaction analysis (Taleb and Moore, 1999; Yimsiri et al., 2004; Guo and Stolle, 2005; Daiyan et al., 2011; Jung et al., 2013). More recently, Reza and Dhar (2024) employed a stress-dependent modulus of elasticity based on Janbu's (1963) formulation using a user-defined subroutine. Their study indicated that there was no significant difference in the pullout forces between the stress-dependent modulus of elasticity and a constant value of 5 MPa. Janbu's (1963) stress-dependent modulus of elasticity of soil depends on the mean effective confining pressure, atmospheric pressure, material constant (k), and power law exponent (n). As described in Chapter 3, the material constant (k) of sand varies from 100 to 400 for loose sand to dense sand (Holtz et al., 2011). In the present study, k values of 100, 125, and 150 were used for loose sand, dense sand (hand compaction) and dense sand (vibratory compaction), respectively, with a power law exponent (n) value of 0.5 (Roy et al., 2016; Reza and Dhar, 2021a, 2021b, 2024; Muntakim and Dhar, 2021; Fellenius, 2023). The mean effective confining pressure is determined by the unit weight of the soil with an atmospheric pressure of 101.3 kPa. Using Janbu's (1963) equation (Chapter 3, Equation 3-3), the modulus of elasticity of soil at springline depth of 625 mm was calculated as 3 MPa for loose sand, 4 MPa (for hand compaction), and 5 MPa (for vibratory plate compaction) for dense sand. Even though the stress-dependent modulus of elasticity of soil varies with depth, to simplify the current FE analysis, a constant modulus values corresponding to the springline depth were used for respective FE simulations.

For the plastic soil behaviour, the Mohr-Coulomb (MC) model, with a constant dilation angle, is widely applied in soil-pipe interaction analysis (Yimsiri et al., 2004; Ni et al., 2018; Almahakeri et al., 2019; Katebi et al., 2021; Muntakim and Dhar, 2021; Murugathasan et al., 2021; Reza and Dhar, 2021a, 2021b, 2024; Chen et al., 2023). However, when dealing with higher plastic shear strains (>10%), a modified Mohr-Coulomb (MMC) model is preferred (Guo and Stolle, 2005; Daiyan et al., 2011; Robert and Thusyanthan, 2015; Pike, 2016; Roy et al., 2016, 2018; Robert, 2017; Robert et al., 2020). According to MC model, plastic deformation occurs when the stress state reaches the constant yield surface, and the soil dilates at a constant dilation angle. The MMC model accounts for variations in the friction and dilation angles as plastic shear strains increase. Finite element analysis using the MC model conducted by Reza and Dhar (2024) showed that plastic strains developed in a thin zone of soil around the pipe surface. Consequently, the current study adopted the MC model for the axial pipe-soil interaction analysis.

The friction angle of the backfill sand was based on the test results from Saha (2021). Their research found that the friction angle of the sand is influenced by its density, stress level and moisture content. Based on Figure 3-12 (Chapter 3), which depicts the relationship between the moisture content, angle of internal friction, and the dry unit weight of compacted sand, the internal friction angles corresponding to soil densities of 18.1 kN/m^3 and 17.5 kN/m^3 were estimated to be 44°, and 42°, respectively, depending on the compaction effort applied using a vibratory plate tamper, and hand tamper, respectively. A critical state friction angle of 35° for the backfill sand was also reported by Saha (2021). Considering the kneading effect during the backfilling and levelling of backfill sand, it was difficult to maintain the soil layers at pure loose condition. Accommodating these, a friction angle of 37° was reasonable for the uncompacted backfill with a density of 14.8 kN/m^3. Bolton (1986) provided an equation (Equation 4-5) to calculate the peak dilation angle under high confining stress. However, in the current study, the confining stress is expected to be low due to the shallow burial depth of the pipe. Therefore, the relationships proposed by Chakraborty and Salgado (2010) for determining the dilation angle under very low confining stress were deemed more appropriate and are used in this analysis (Equations 4-6, 4-7, and 4-8).

$$\psi_p = \frac{\emptyset'_p - \emptyset'_{crit}}{0.8} \qquad \text{Equation 4-5}$$

$$\psi_p = \emptyset'_p - \emptyset'_{crit} = 3.8 I_R \qquad \text{Equation 4-6}$$

$$I_R = I_D \left(Q - \ln \frac{100 \sigma'_{mp}}{P_A} \right) - R \qquad \text{Equation 4-7}$$

$$Q = 7.4 + 0.60 \ln \sigma'_c \qquad \text{Equation 4-8}$$

Here, ψ_p is the peak dilation angle of soil; $\emptyset'_p$ is the peak internal frictional angle of soil; $\emptyset'_{crit}$ is the critical state friction angle of soil; I_R is the relative dilatancy index; I_D is the relative density (ranging from 0 to 1); Q and R are fitting parameters that depend on the intrinsic sand characteristics; σ'_{mp} is the mean effective stress; σ'_c is the confining pressure; and P_A is the reference pressure (100 kPa). Based on Chakraborty and Salgado (2010), the calculated dilation angles are 15°, 12°, and 3° for the respective friction angles of 44°, 42°, and 37°. The Poisson's ratio of the loose sand and dense sand was assumed as 0.25 and 0.3, respectively (Budhu, 2011). The cohesion for sand is zero. However, for numerical stability during the finite element analysis, a value of 0.1 kPa was used.

4.3.5.3 Steel Tank

The density of 7850 kg/m^3, modulus of elasticity of 210 GPa with a Poisson's ratio of 0.265 was used as the material property for the steel tank.

4.3.6 Loading and Boundary Conditions

The finite element analysis was conducted in two primary steps. In the first step, referred to as the geostatic step, gravity load was applied to the entire model. Additionally, geostatic stresses were introduced as a predefined field to establish the initial stress and strain states of the model, accounting for the self-weight of the soil. This was followed by the pulling step, where a displacement of 90 mm was applied in the specified direction. For the geostatic step, a time period of 1 was used with an increment size of 10^{-8} (i.e., 10^{-8} times the total load was applied in each increment), while for the pulling step, a time period of 3 with an increment size of 10^{-9} was applied for numerical convergence. For the models with equivalent thermal loading, an increment size of 10^{-8} was applied with a time period of 1 during the application of thermal loading.

The pipe's fixed end was constrained (all degrees of freedom of nodes are fixed) during the gravity, application of thermal loading, application of internal pressure (if any) and pulling steps, which effectively prevented any displacement or rotation. A quasi-static analysis was performed using the dynamic implicit modelling technique, a method similarly employed by Reza and Dhar (2021a, 2021b, 2024) in their studies of axial pipe-soil interaction. The analysis used the full-Newton method for solving, incorporating nonlinear geometry to account for large deformations throughout the simulation.

For the simulation of soil tank movement, boundary conditions were applied to the steel tank. Murugathasan et al. (2018) showed that the soil tank walls can be considered rigid under axial pullout loading from the FE analysis. A zero-displacement boundary condition was enforced on the bottom and each side of the tank wall to prevent any movement in these regions. During the pulling step, the entire tank was allowed to move in the specified direction up to a displacement of 90 mm.

In the soil-pull simulation (ignoring the tank), boundary conditions were applied to the external surfaces of the soil block. Zero-displacement conditions were enforced perpendicular to the respective external surfaces, ensuring no movement in those directions. During the pulling step, the bottom and all four sides of the soil block were allowed to move in the specified direction up to a displacement of 90 mm.

For the pipe-pull simulation, the boundary conditions were similar to those in soil-pull simulation. During the pulling step, the fixed end of the pipe was pulled to a displacement of 90 mm in the specified direction, with other external surfaces constrained as necessary to simulate desired soil-pipe interaction. Figure 4-8 illustrates the idealization of these three different pulling mechanisms.

4.3.7 Energy Verification

The accuracy of the results of numerical simulation is also examined by examining the energy balance within the system. For an ideal simulation, the total energy input into the system should be consistent with the energy outputs involving deformation, frictional losses, damping, or plastic work. For a quasi-static analysis, the kinetic energy (ALLKE) should be very small, indicating that the system is not undergoing significant dynamic motion. As a general rule, the kinetic energy of the model should not exceed 5%–10% of its internal energy (ALLIE) throughout the process for a quasi-static analysis (Dassault Systems, 2019). In a well-converged analysis, the sum of internal, kinetic, and dissipated energies (ALLFD, ALLVD) should equal the external work (ALLWK) done on the system. High levels of artificial energy (ALLAE) can signal numerical problems such as excessive mesh distortion or the need for better hourglass control in reduced-integration elements. Similarly, if kinetic energy grows unexpectedly in a quasi-static simulation, it might indicate that the solution is becoming unstable or too dynamic. Artificial energy should be a small percentage of the total energy (ETOTAL), typically less than 1%. If it is too large, the mesh or hourglass control may need to be adjusted (Boulbes, 2020).

Figures 4-9 and 4-10 present the energy from the FE models with various approaches of applying compaction-induced stresses (equivalent thermal loading and using higher lateral earth pressure coefficients), respectively. These figures indicate that the kinetic energy of the system remained below 5% of its internal energy in both cases, confirming minimal inertial effects and validating the quasi-static conditions of the simulation. Additionally, the artificial strain energy was maintained below 1% of the system’s total energy, demonstrating effective control over numerical artifacts such as hourglassing and shear locking, which did not significantly impact the solution's accuracy. Thus, the model maintains a robust energy balance, essential for ensuring the stability and reliability of the simulation results.

4.4 Finite Element Results

The full-scale tests conducted in this study served as a critical benchmark for validating the developed FE models for soil-pipeline interaction analysis. Additionally, the study analyzed different pulling mechanisms, such as tank-pull, soil-pull, and pipe-pull, to assess their relative impacts on axial force-displacement behaviour.

4.4.1 Responses with Compaction-Induced Stresses as Equivalent Thermal Loading

To simulate the force-displacement behaviour observed in full-scale tests subjected to various compaction efforts, FE analysis was conducted by modelling compaction-induced lateral stresses as equivalent thermal loading. The soil tank was pulled to the desired displacement in this simulation (i.e. tank-pull). The material parameters used in these simulations are summarized in Table 4-1, while Figure 4-3 illustrates the variation of applied equivalent thermal loading with depth. Figures 4-11 and 4-12 compare the force-displacement responses obtained from the FE analysis with the corresponding global responses recorded in full-scale tests for 60.3 mm diameter pipes (Tests 1 to 4) and 42.2 mm diameter pipes (Tests 9 to 12), respectively. As shown in Figure 4-11, for the 60.3 mm pipes without compaction-induced stresses, the FE analysis predicted a peak force of 2.16 kN, which is significantly less than measured forces. When compaction-induced stresses were included, following the methodology of Reza and Dhar (2024), the peak forces increased to 3.54 kN and 3.44 kN for tests with vibratory compaction and hand compaction, respectively. Similarly, for the 42.2 mm pipes (Figure 4-12), the FE analysis yielded a peak force of 1.34 kN in the absence of compaction-induced stresses, while the inclusion of these stresses resulted in peak forces of 2.15 kN and 2.11 kN for tests with vibratory and hand compaction, respectively. Thus, the compaction-induced stresses estimated using the procedure developed by

Duncan and Seed (1986) for vibratory plate compaction significantly underestimated the peak force values compared to those recorded in full-scale experiments. Specifically, for the 60.3 mm pipes, the FE predicted peak forces were 45.1% to 46.6% lower than the actual test values, while for the 42.2 mm pipes, the predicted values were 54.1% to 56.7% lower than the measured experimental forces. On the other hand, for the hand tamper compaction of the 60.3 mm pipes, the FE model incorporating Duncan and Seed's (1986) compaction-induced stresses successfully replicated the experimental results. However, for the 42.2 mm pipes subjected to hand tamper compaction, the FE analysis again underestimated the peak forces, with values 30.4% to 37.1% lower than those observed in the experimental tests.

It is important to note that in Tests 1, 2, 9 and 10, the backfill soil was compacted using a vibratory plate tamper, whereas in the study by Reza and Dhar (2024), a manual hand tamper was employed. Duncan and Seed (1986) and Duncan et al. (1991) reported that vibratory compaction generates lateral stresses approximately two to four times greater than those induced by static compaction. This suggests that the vibratory compaction method used in Tests 1, 2, 9 and 10 likely induced significantly higher lateral stresses than those accounted for in the FE analysis. However, further investigations are required to enhance the accuracy of compaction-induced stress modelling and its integration into FE simulations.

4.4.2 Responses with Compaction-Induced Stresses using Higher Lateral Earth Pressure Coefficient

The coefficient of lateral earth pressure, K, estimated from Meidani et al. (2018) were utilized in the FE analysis to simulate the test results under various compaction conditions. The soil tank was pulled to the desired displacement in this simulation (i.e. tank-pull). For tests conducted with loose backfill (Tests 5 and 6), the at-rest earth pressure coefficient (K_0) values suggested by Jaky (1944) were employed. Table 4-2 summarizes the material parameters used for these simulations. It is important to note that, as previously discussed, this approach does not allow for variations in lateral earth pressure across the soil depth. Instead, a constant lateral earth pressure coefficient, corresponding to the lateral earth pressure at the pipe's springline, was applied throughout the depth of the backfill.

As illustrated in Figures 4-13 and 4-14, the peak forces obtained from the FE analysis using this method were significantly lower than the corresponding test results for both compaction methods. Specifically, for vibratory compaction, the FE-predicted peak forces were 54.9% to 56.3% lower than the measured peak forces for 60.3 mm pipes and 58.8% to 61.1% lower for 42.2 mm pipes. Similarly, for hand tamper compaction, the FE-predicted peak forces were 23.6% to 26.1% lower for 60.3 mm pipes and 40.3% to 45.7% lower for 42.2 mm pipes. These discrepancies indicate that the approach proposed by Meidani et al. (2018) does not provide an accurate representation of the experimental conditions in the current study. Conversely, the FE simulation of the uncompacted fill effectively captured the global response observed in the tests (Figure 4-15).

4.4.3 Comparison of Tank-pull, Soil-pull and Pipe-pull Mechanisms

Three pulling mechanisms, termed as Tank-pull, Soil-pull, and Pipe-pull, were explored through 3D FEA where compaction-induced stresses were modelled using a higher lateral earth pressure coefficient. The results of Test 1 were simulated to compare the load-displacement responses through the above-mentioned mechanisms. Tank-pull involves pulling all the tank nodes, mimicking the conditions of the experimental test setup. Soil-pull refers to pulling the soil block from the soil block's outer surface nodes without consideration of the tank. During the tank-pull and soil-pull, the pipe was fixed at one end, and the soil block was moved. Pipe-pull pertains to pulling the fixed end of the pipe while keeping the soil block stationary. Table 4-3 summarizes the soil parameters used for the simulation of Test 1. In addition, lateral earth pressure coefficient of 4.2 was used to simulate the peak axial force, to accommodate the effect of compaction-induced stress. Figure 4-16 shows the simulated finite element results for Test 1, with peak pullout forces of 6.45 kN, 6.48 kN, and 6.51 kN, respectively, for tank-pull, soil-pull, and pipe-pull mechanisms. It was found that the variation of axial pullout force between different pulling mechanisms was negligible (<1%). However, based on the comparison of the experimental results of the current study with Reza et al. (2023a), it was found that the soil-pull mechanism provides higher axial resistance than the pipe-pull mechanism. To validate the observed differences, further tests and numerical modelling are required.

The variation of average normal stress along the pipe's length in response to relative displacement (tank displacement, soil displacement, or pipe leading end displacement) is depicted in Figure 4-17. Analysis of stress distribution at specific points L/4, L/2, and 3L/4 reveals similar trends across all three pulling mechanisms (tank-pull, soil-pull, and pipe-pull), with only minor variations observed. At L/4, under low relative displacements (<5 mm), the maximum recorded average normal stress for the tank-pull mechanism reached 28.32 kPa, while slightly reduced values of 27.50 kPa and 27.31 kPa were observed for the soil-pull and pipe-pull mechanisms, respectively. In contrast, at higher relative displacements (>70 mm), the average normal stress values converged, with tank-pull, soil-pull, and pipe-pull mechanisms recording approximately 7.92 kPa, 7.83 kPa, and 8.06 kPa, respectively. For the soil-pull and pipe-pull mechanisms, the average normal stresses recorded at L/4, L/2, and 3L/4 remained nearly identical under both low and high relative displacement conditions, indicating consistent stress distribution along the pipe length. Thus, the conventional continuum-based FE analysis was unable to capture the differences in mechanism observed during the experiments. Further study is therefore required to explore the mechanism.

4.4.4 FE Responses of Tests 3 and 4 Using Equivalent Thermal Loading

As seen in Figure 4-10, the global response of Tests 3 and 4 was successfully captured by the FE analysis using equivalent thermal loading subjected to tank-pull mechanism. Hence, the FE analysis of Tests 3 and 4 was used to explore the elongation, axial strain, and interface stresses.

4.4.4.1 Pipe Elongation and Axial Strain

The results from the FE analysis were compared against the measured pipe elongations obtained from full-scale experimental tests. Figure 4-18 presents a comparison between the predicted pipe elongation from FE simulations and the experimentally measured values for 60.3 mm MDPE pipes subjected to hand tamper compaction (Tests 3 and 4). The FE analysis demonstrated a slight overestimation of pipe elongation. Specifically, in Tests 3 and 4, the FE model predicted a peak elongation of 23.9 mm, which marginally exceeded the experimentally recorded peak elongations of 17.3 mm and 20.2 mm, respectively. This discrepancy can be attributed to variations in the peak axial forces obtained from the FE simulations and those measured during the full-scale tests.

Figure 4-19 plots the contour of pipe elongation and axial strain along the length of the pipe. As depicted in Figure 4-19, the axial strains are higher near the fixed end of the pipe and progressively decrease towards the free end, where the axial strain approaches zero. This observed non-uniformity in axial strain distribution along the MDPE pipe is supported by fiber optic sensor measurements recorded in Tests 7 and 15 (refer to Chapter 3, Figures 3-29 and 3-30). Furthermore, the observed axial strain mobilization pattern aligns with findings from previous studies conducted by Weerasekara and Wijewickreme (2008), Wijewickreme and Weerasekara (2015), Reza and Dhar (2021a, 2021b), and Reza et al. (2023a). These studies reported similar axial strain mobilization behaviour in scenarios where a pipe was subjected to pullout through static soil, wherein strain initiation occurred near the leading end and subsequently propagated along the pipe as displacement increased.

As observed from the axial strain measurements outside the soil tank in full-scale tests, it was evident that during pulling, the pipe element near the fixed end of the pipe starts to elongate first, which leads to the immediate responses of strain gauges attached near to the fixed end of the pipe. Given that one end of the pipe remains fixed, the cumulative elongation of pipe segments along its length, from the fixed end to the free end, results in an overall displacement of the pipe toward the free end. This is attributed to the observed variation of pipe elongation, as seen in Figure 4-19. It is worth noting that the pipe elongation is considered as the displacement of the pipe's free end relative to its initial position prior to the pulling, as the displacement at the pipe's fixed end is zero.

4.4.4.2 Interface Stresses

The interaction between pipelines and surrounding soil is governed by the forces transmitted through the pipe-soil interface, which play a critical role in defining the structural response of buried pipelines subjected to ground movement. However, direct measurement of interface stresses during experimental tests presents significant challenges, and in some cases, it is impractical. To this end, previous studies by Wijewickreme et al. (2009) and Guo and Zhou (2024) have employed pressure sensors and force sensing resistors (FSRs), respectively, to quantify interface stresses on steel pipe walls. Since the FE analysis reasonably simulated the global response of Tests 3 and 4, the interface stresses from the FE analysis were explored. Figure 4-20 presents the distribution of normal interface stresses around the pipe circumference under three different conditions: (a) gravitational loading only, (b) gravitational and compaction-induced loading, and (c) post-ground displacement of 90 mm. Under gravitational loading alone (Figure 4-20a), the stress distribution aligns well with calculated geostatic stresses, with higher stress concentrations observed at the crown and invert of the pipe compared to the springline. However, when compaction-induced stresses are introduced (Figure 4-20b), the lateral stresses around the pipe increase, resulting in higher stresses at the springline and lower stresses at the crown and invert. During the pulling, the axial load causes elongation of the pipe, as previously discussed. The axial strain is more pronounced near the fixed end, leading to a higher elongation of pipe elements in that region. This elongation, in turn, induces a reduction in pipe diameter, which decreases the contact pressure between the pipe and the surrounding soil (Figure 4-20c). The magnitude of this diametric reduction is greatest near the fixed end (i.e. L/4), resulting in lower contact pressures in this region compared to the far end (i.e. 3L/4).

The variation of normal stresses at three specific locations along the pipe (i.e. L/4, L/2, and 3L/4 from the fixed end) was analyzed at different circumferential points (crown, invert, and springlines), as plotted in Figure 4-21 against the soil tank displacement. The results reveal that contact stresses were highest at the pipe's springlines compared to the crown and invert. However, beyond a certain displacement threshold, the normal stresses decreased with increasing tank displacement, a phenomenon attributed to the reduction in pipe diameter caused by axial loading during pulling. Furthermore, Figure 4-21 highlights a variation in contact stresses along the pipe length: stresses were lower near the fixed end (L/4) compared to the far end (3L/4). This trend is consistent with the higher diametric reduction occurring near the fixed end. Beyond the tank displacement corresponding to the peak pullout force, the contact stresses remain constant as the shear strength is fully mobilized along the entire pipe length (i.e. 4m). A key observation from Figure 4-21 is that the normal stresses at different points along the pipe (i.e. L/4, L/2, and 3L/4 from fixed end of pipe) do not change simultaneously but instead exhibit to change at different tank displacements due to the gradual mobilization of the axial forces with increasing tank displacement. This finding aligns with the numerical results reported by Reza and Dhar (2024). Additionally, the mobilization of interface shear strength was consistent with the changes in the normal stresses, as depicted in Figure 4-22.

The variation of circumferentially averaged shear stresses with relative displacement (pipe elongation) was examined at three key locations along the pipe (L/4, L/2, and 3L/4 from the fixed end), as illustrated in Figure 4-22. The peak shear strength was attained at an approximate elongation of 0.5 mm for the 60 mm diameter pipe. The results indicate that shear stress at any given location increased once elongation was initiated, reaching peak shear strength before gradually decreasing as normal stresses reduced. However, it is important to note that pipelines in operational conditions typically may experience high internal pressures. The presence of such internal pressure may mitigate the reduction in pipe diameter and associated changes in normal stresses under axial loading conditions. Consequently, the effects observed in these experimental and numerical simulations may be less pronounced in pressurized pipelines, warranting further investigation to accurately model real-world pipeline behaviour.

4.5 Conclusions

This chapter evaluates the 3D continuum FEA to explore the axial pipe-soil interaction mechanisms of buried MDPE pipes. Full-scale tests conducted in the current study were simulated using FEA. The main conclusions reached from the analysis are presented below.

- Application of compaction-induced stress is required to simulate the peak axial force observed during the tests. The compaction-induced stresses could be applied using equivalent thermal loads or a higher coefficient of lateral earth pressures during analysis.
- The compaction-induced stresses estimated using the procedure developed by Duncan and Seed (1986) for vibratory plate compaction significantly underestimated the peak axial forces compared to the experimental results.
- Application of compaction-induced stresses from Duncan and Seed (1986) and lateral earth pressure coefficients from Meidani et al. (2018) underestimated the peak axial forces.
- FE simulations of the tank-pull, soil-pull, and pipe-pull approaches provided similar results, while full-scale pipe-pull and soil-pull tests exhibited differences. The soil-pulling

provided higher axial forces than pipe-pulling, that was not successfully simulated by the conventional FE analysis.

- Results of FE analysis revealed the gradual mobilization of axial force from the fixed end toward the free end of the pipe, which is similar to the mechanism observed during pipe-pulling tests.
- Interface shear force at any location along the pipe length increases gradually with the soil movement reaching the peak value at certain displacement at this location (i.e., 0.5 mm for the 60 mm diameter pipe) and then decreases due to the reduction in the normal stress.
- The normal stress on the pipe reduced due to the reduction of pipe diameter during ground movements.
- No increase of normal stress on the pipe surface was observed during axial movement, indicating no effect of interface soil dilation on the axial force.

4.6 Acknowledgments

The authors extend their sincere gratitude to the National Science and Engineering Research Council of Canada's Alliance Grants program, as well as FortisBC Energy Inc., SaskEnergy Canada Inc., and WSP Canada Inc., for their invaluable financial and in-kind support, which made this research possible.

Table 4-1: Summary of parameters used for FE simulation using equivalent thermal loading

Test	E_s (MPa)	v	γ (kN/m^3)	φ	ψ	f	Compaction-Induced Stress (kPa) at Springline
Test 1	5	0.3	18.1	44	15	0.75	11.1
Test 2	5	0.3	18.1	44	15	0.75	11.1
Test 3	4	0.3	17.5	42	12	0.75	11.1
Test 4	4	0.3	17.5	42	12	0.75	11.1
Test 9	5	0.3	18.1	44	15	0.75	11.1
Test 10	5	0.3	18.1	44	15	0.75	11.1
Test 11	4	0.3	17.5	42	12	0.75	11.1
Test 12	4	0.3	17.5	42	12	0.75	11.1

Table 4-2: Summary of parameters used for FE simulation using lateral earth pressure coefficient

Test	E_s (MPa)	v	γ (kN/m^3)	φ	ψ	f	K
Test 1	5	0.3	18.1	44	15	0.75	1.34
Test 2	5	0.3	18.1	44	15	0.75	1.34
Test 3	4	0.3	17.5	42	12	0.75	1.27
Test 4	4	0.3	17.5	42	12	0.75	1.27
Test 5	3	0.25	14.8	37	3	0.60	0.398
Test 6	3	0.25	14.8	37	3	0.60	0.398
Test 9	5	0.3	18.1	44	15	0.75	1.56
Test 10	5	0.3	18.1	44	15	0.75	1.56
Test 11	4	0.3	17.5	42	12	0.75	1.47
Test 12	4	0.3	17.5	42	12	0.75	1.47

Table 4-3: Soil parameters for the finite element analysis of Test 01

Parameters	Value
Modulus of elasticity of soil, E_s (MPa)	5
Poisson's ratio, v	0.3
Unit weight, γ (kN/m^3)	18.1
Internal friction angle, φ	44º
Dilation angle, ψ	15º
Cohesion, c (kPa)	0.1

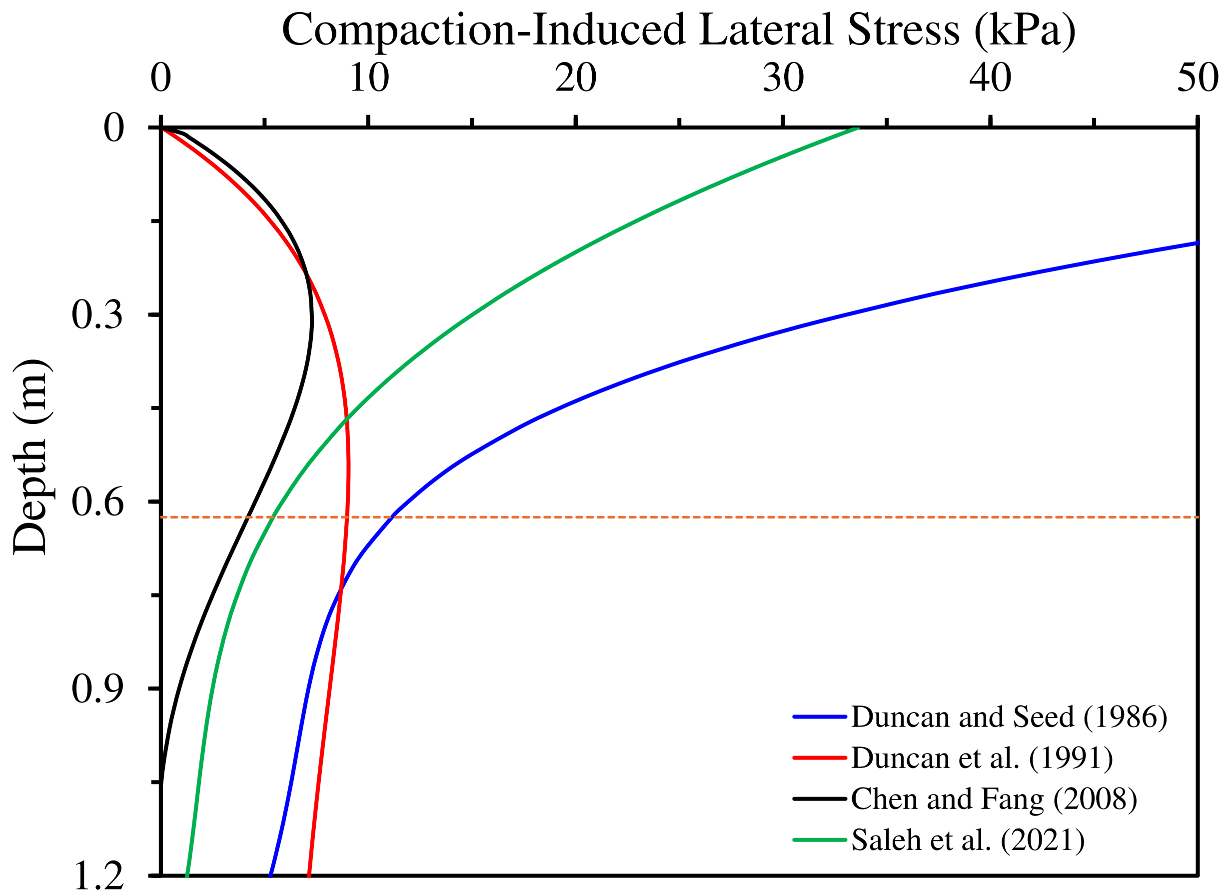

Figure 4-1: Variation of compaction-induced lateral stresses with depth (after Duncan and Seed, 1986; Duncan et al., 1991; Chen and Fang, 2008; Saleh et al., 2021)

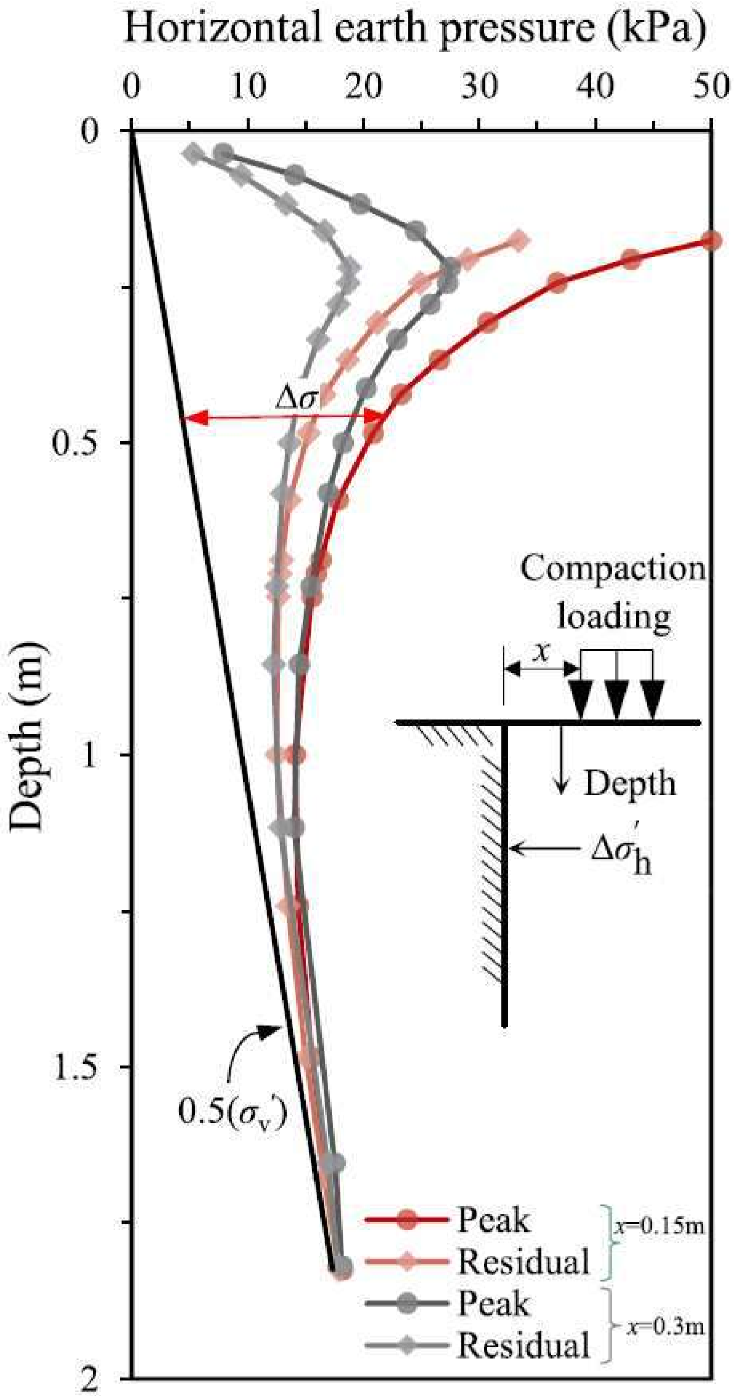

Figure 4-2: Calculated compaction-induced lateral earth pressure, after Duncan and Seed (1986) and Reza and Dhar (2024)

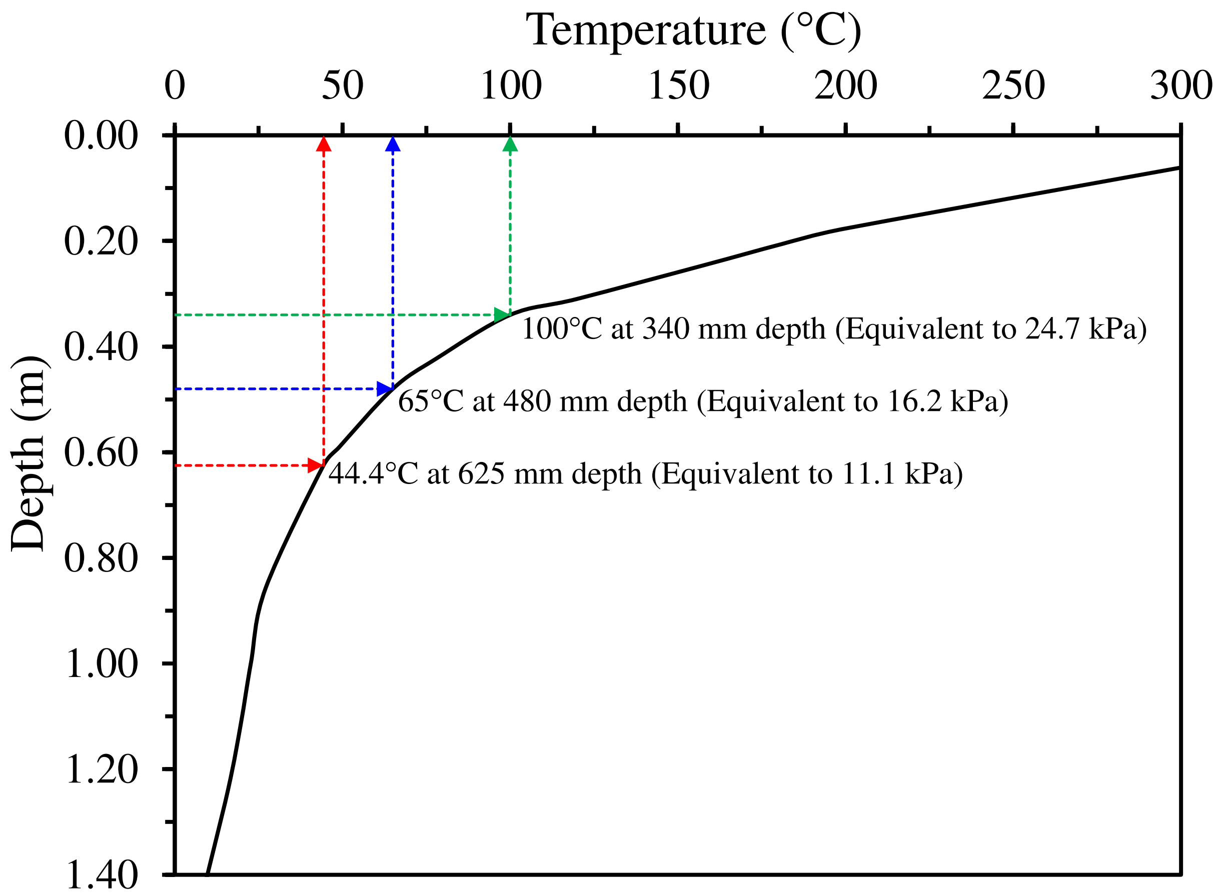

Figure 4-3: Variation of equivalent temperature with depth

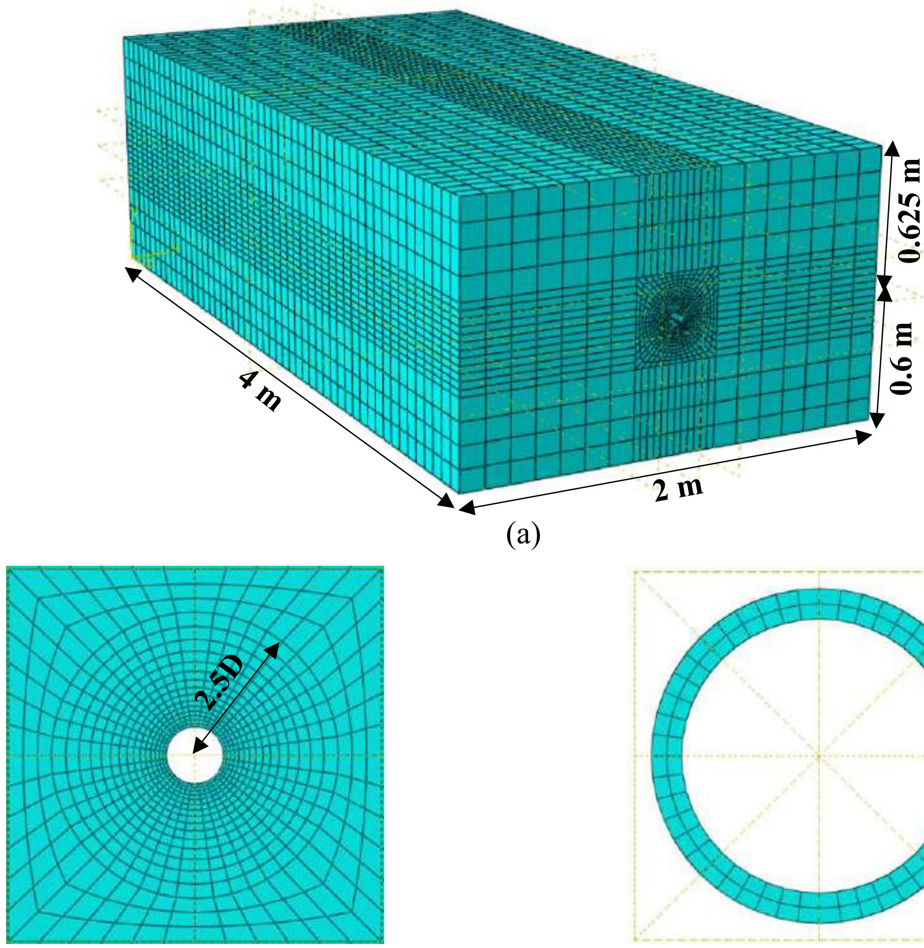

(a)

(b) (c)

Figure 4-4: Typical finite element model: (a) 3D finite element mesh (b) cross-section near the pipe (c) cross-section of the pipe

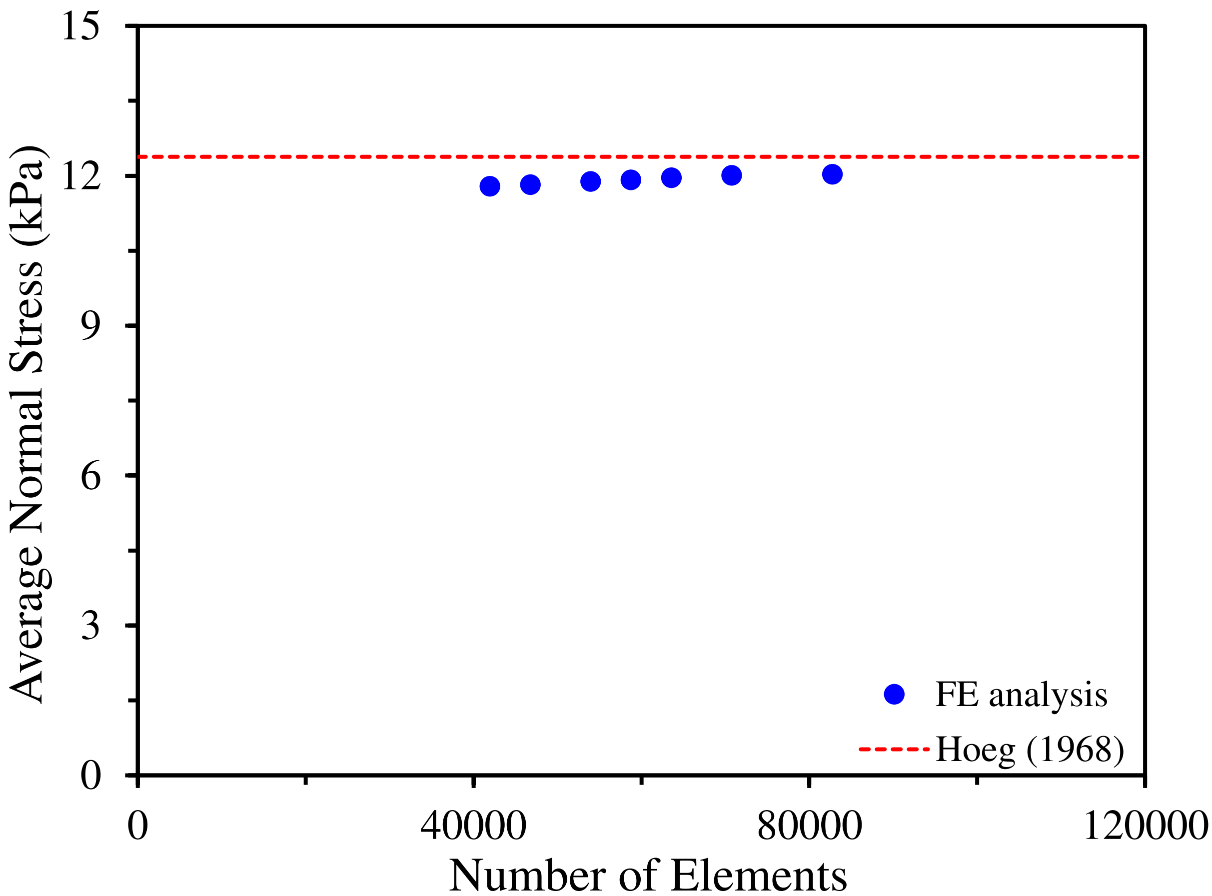

Figure 4-5: Mesh sensitivity analysis with average normal stress around the pipe

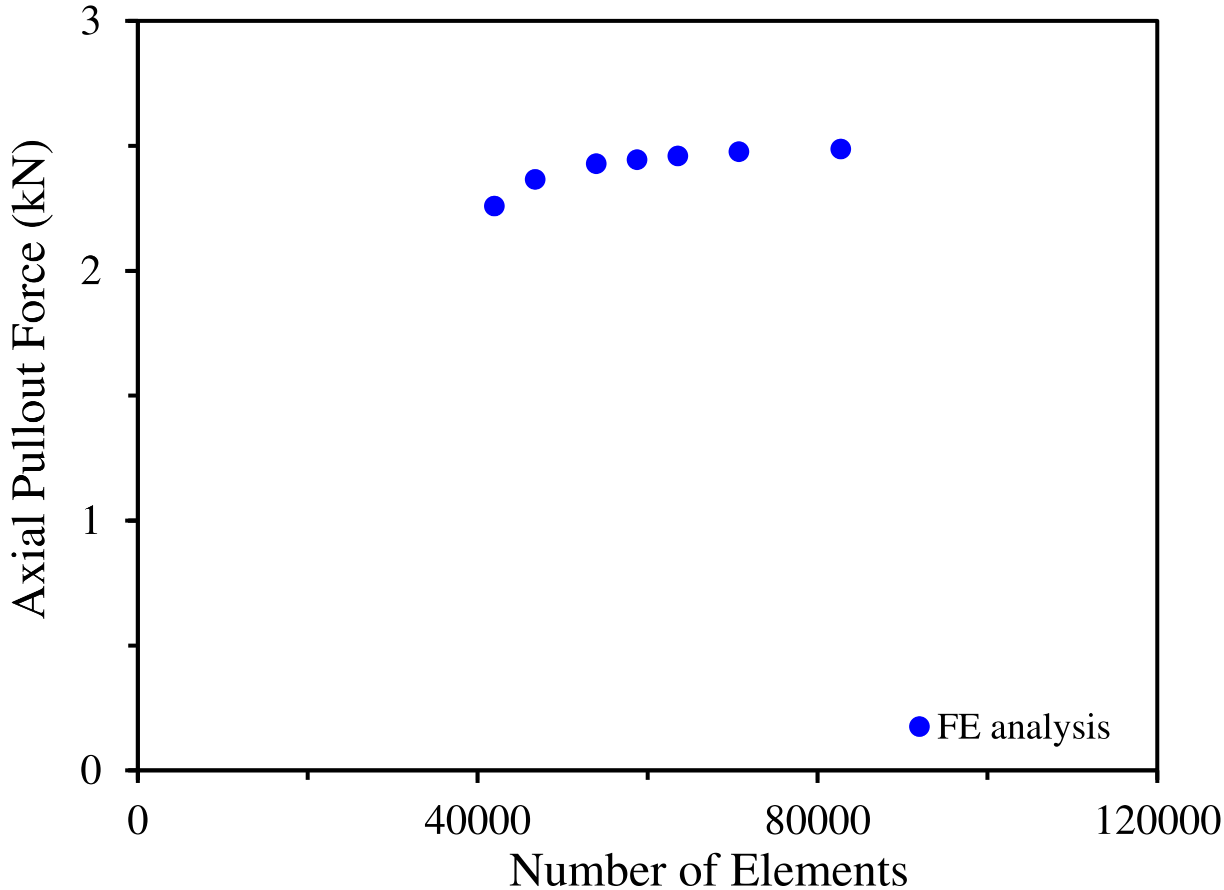

Figure 4-6: Mesh sensitivity analysis with axial pullout force

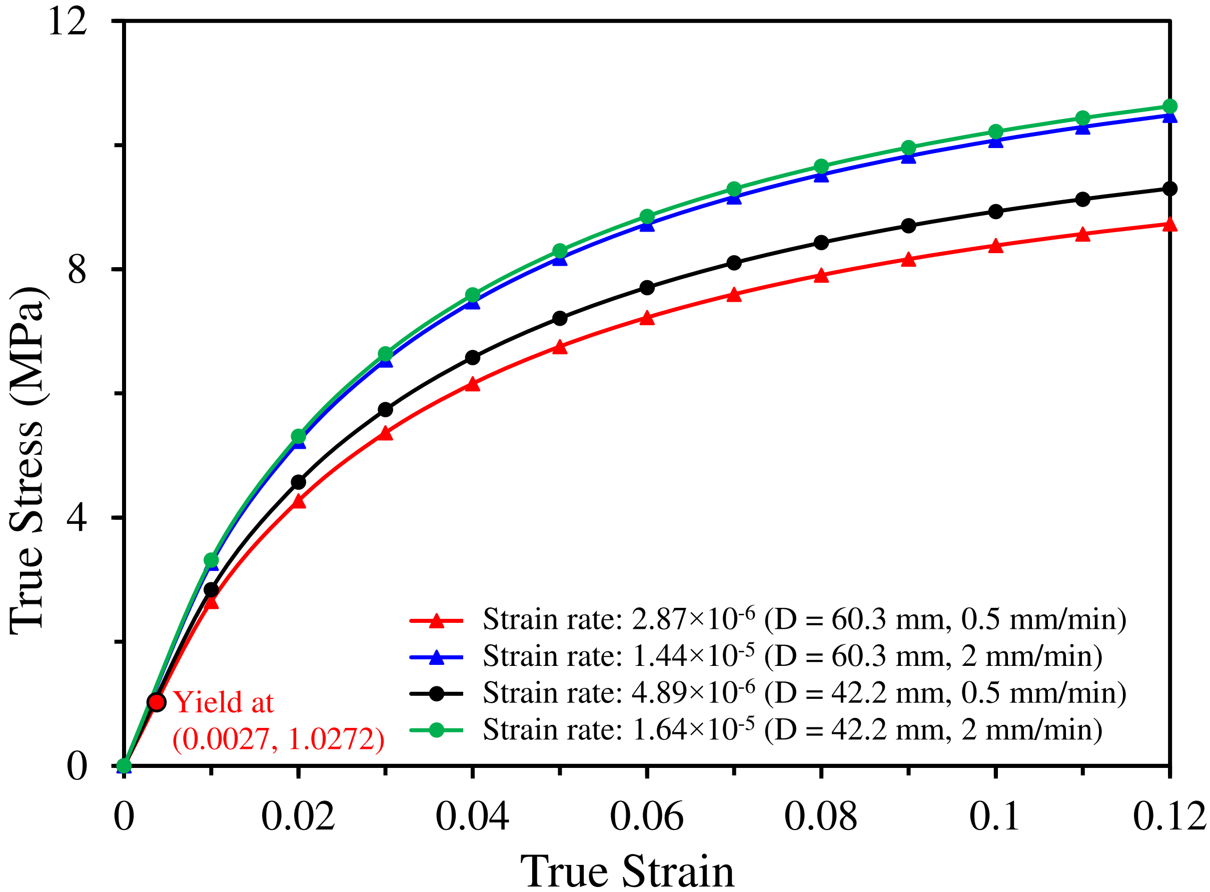

Figure 4-7: True stress-strain responses for MDPE pipes, based on the model of Das and Dhar (2021)

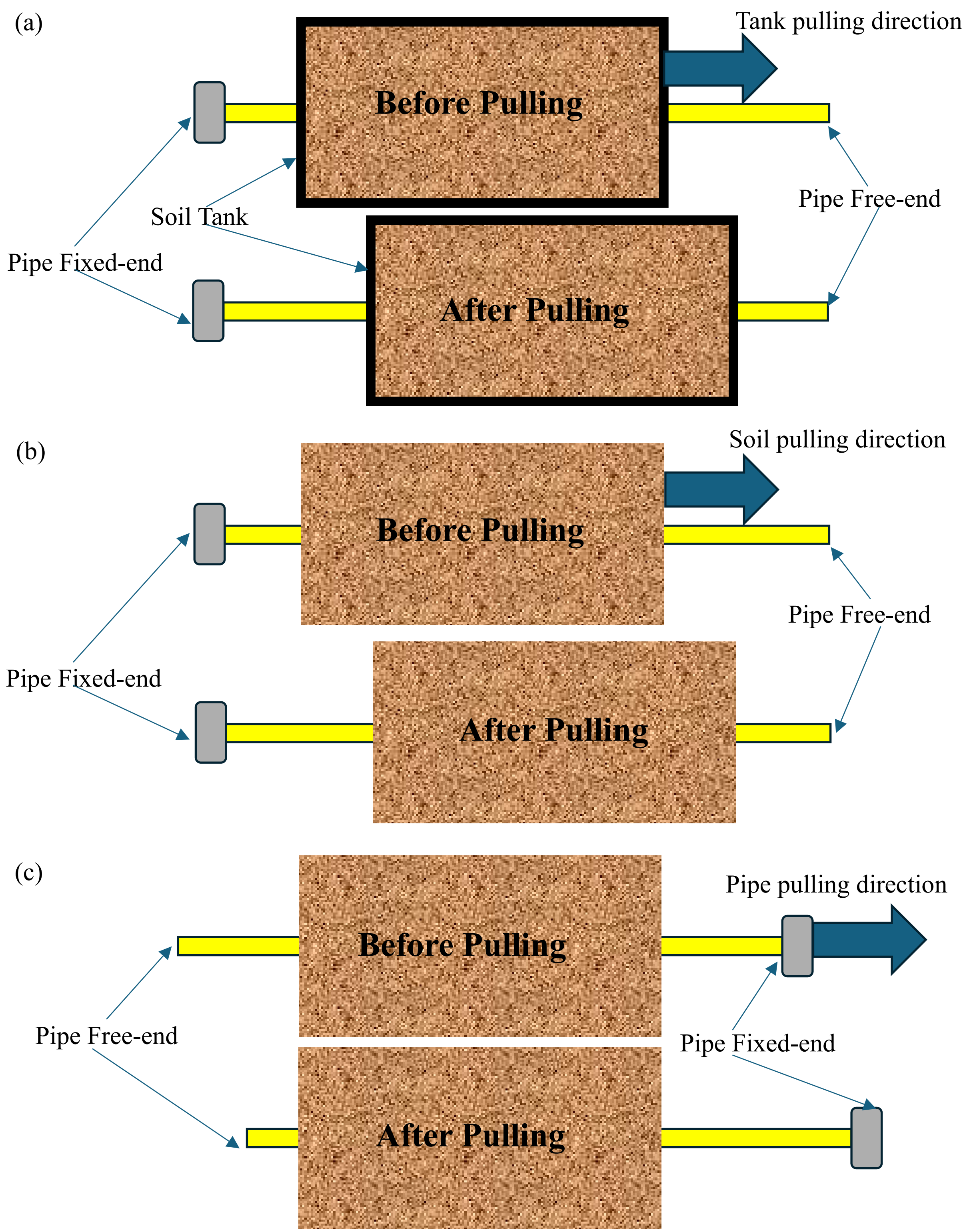

Figure 4-8: Idealization of three different pulling mechanisms: (a) Soil tank movement (b) Soil block movement (c) Pipe movement

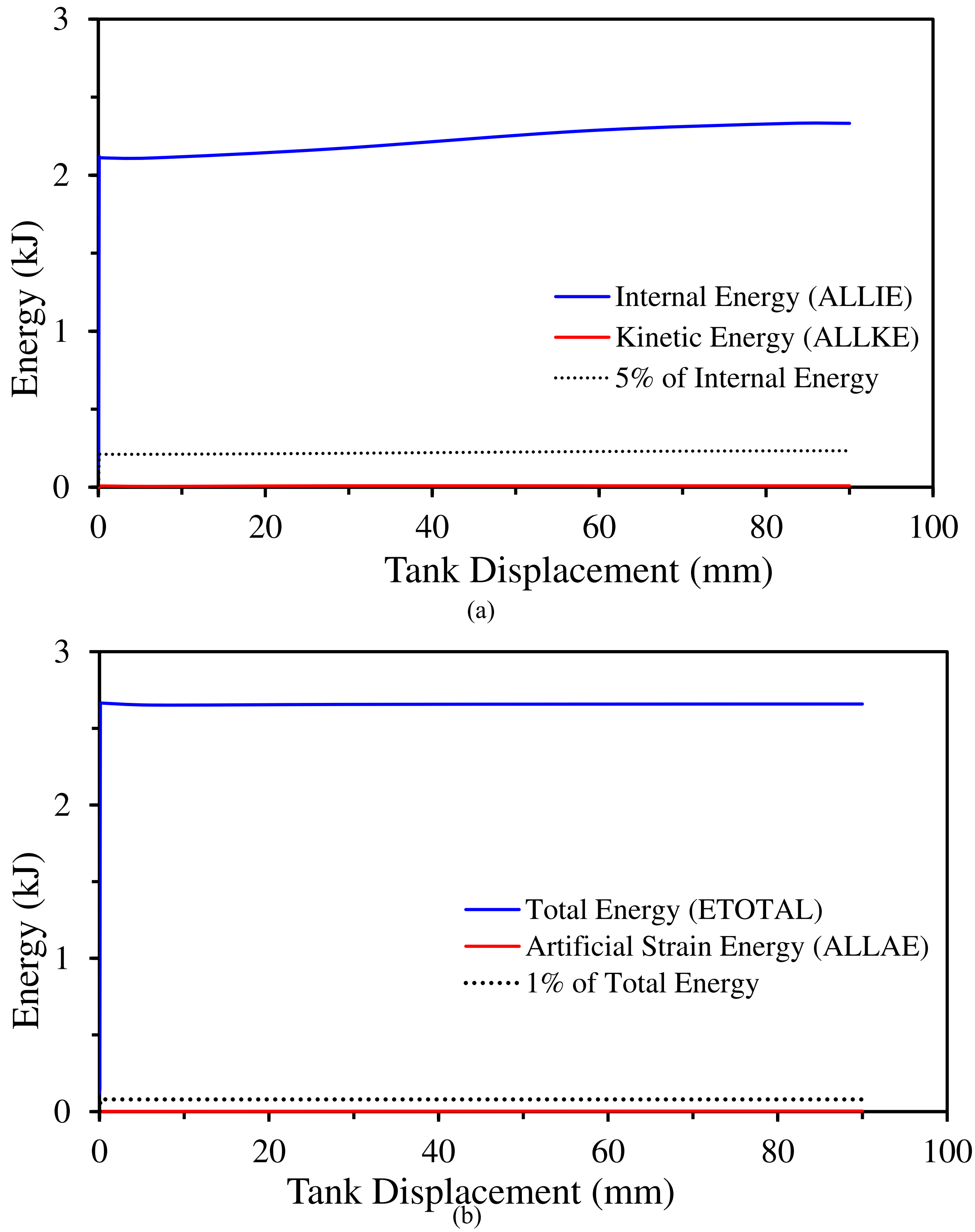

Figure 4-9: Energy verification for FE models with equivalent thermal loading: (a) Kinetic energy and internal energy variation with tank displacement (b) Total energy and artificial strain energy variation with tank displacement

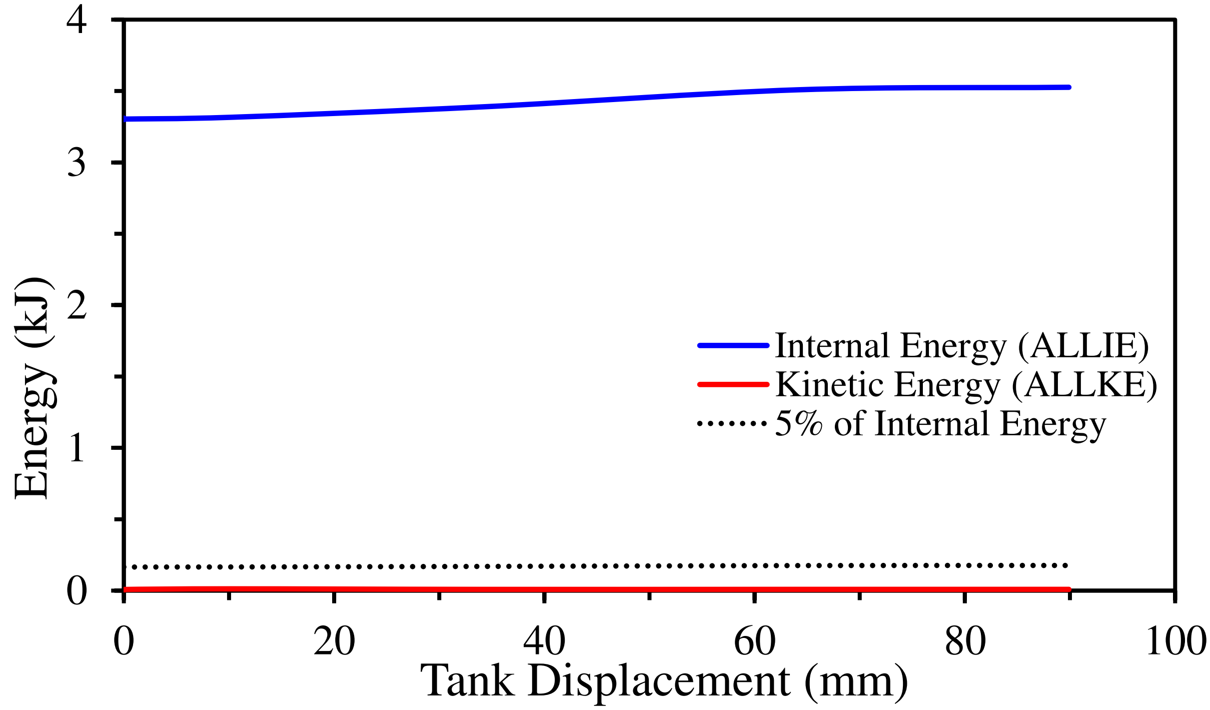

(a)

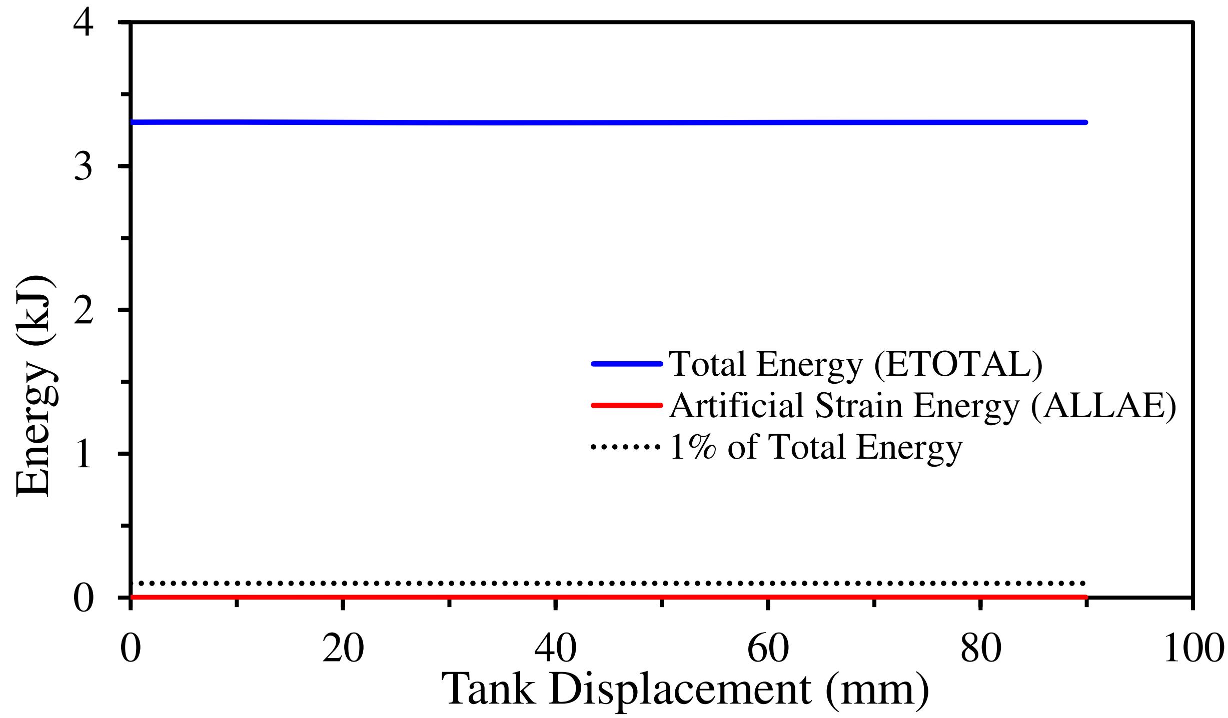

(b)

Figure 4-10: Energy verification for FE models with higher lateral earth pressure coefficients: (a) Kinetic energy and internal energy variation with tank displacement (b) Total energy and artificial strain energy variation with tank displacement

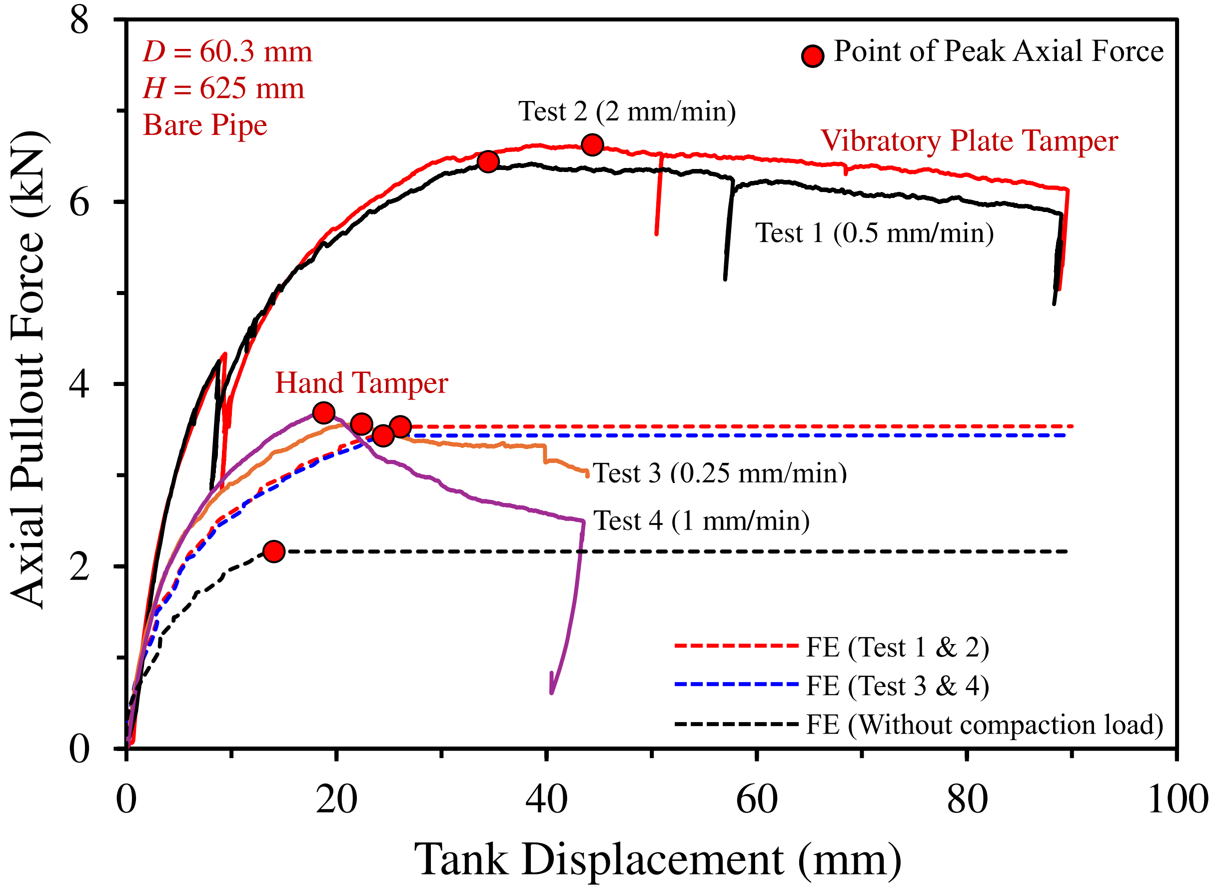

Figure 4-11: Comparison of axial pullout forces of full-scale tests of 60.3 mm diameter pipes with FE analysis subjected to compaction-induced stresses as equivalent thermal loading

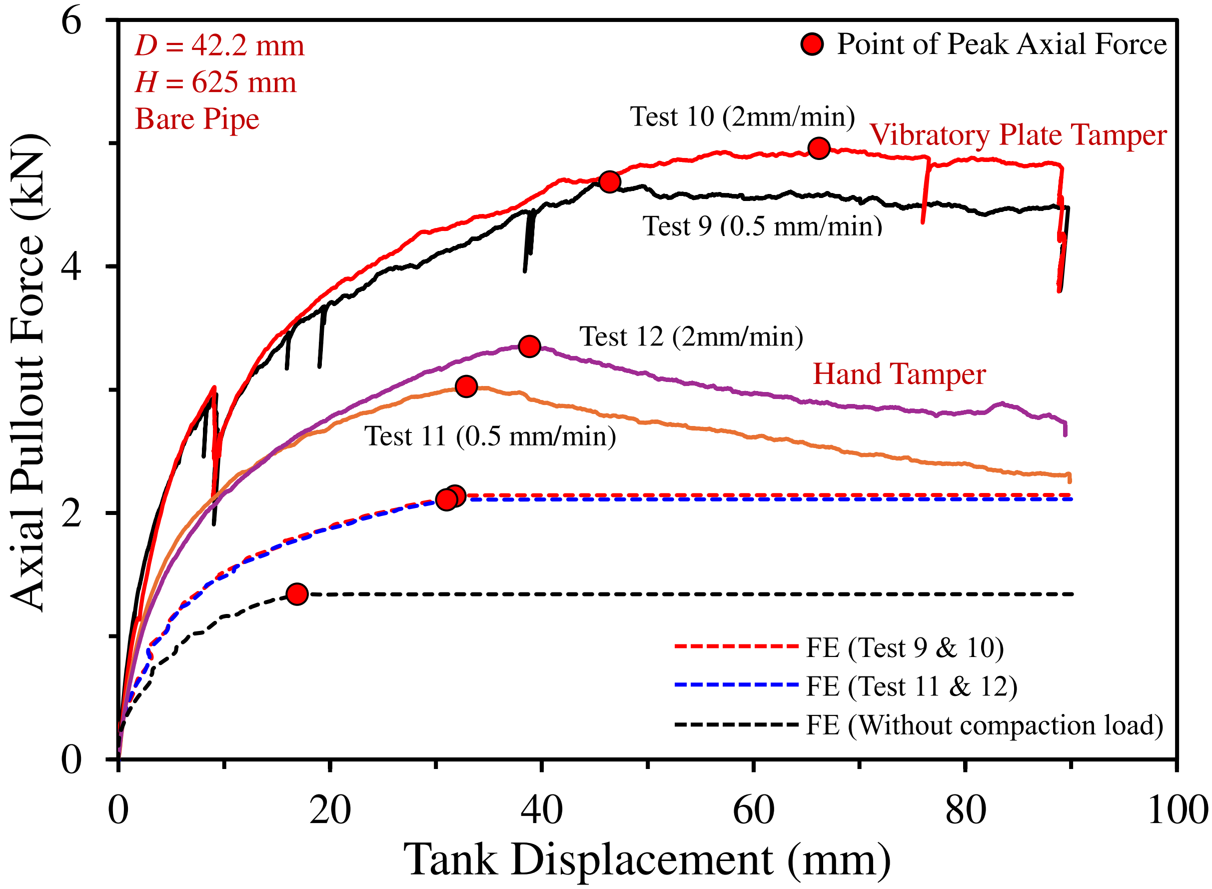

Figure 4-12: Comparison of axial pullout forces of full-scale tests of 42.2 mm diameter pipes with FE analysis subjected to compaction-induced stresses as equivalent thermal loading

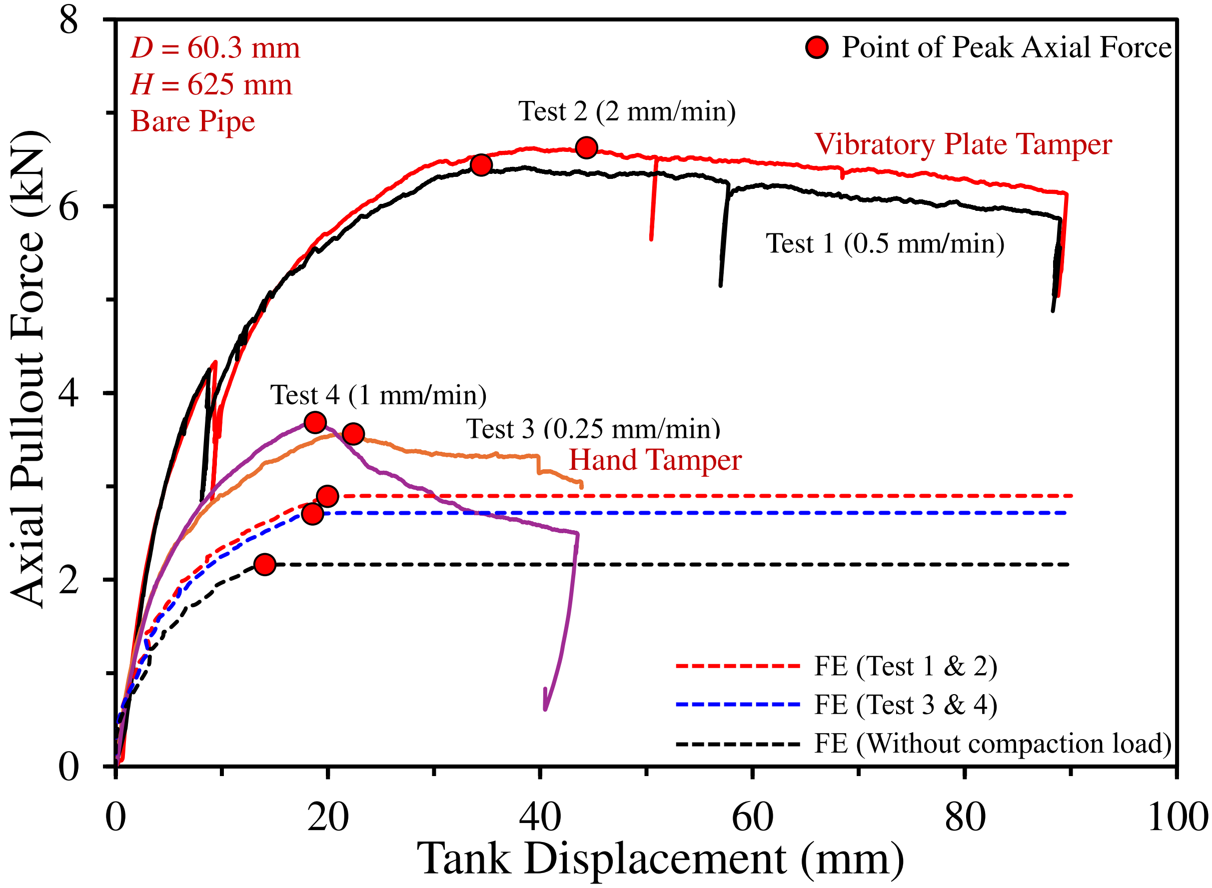

Figure 4-13: Comparison of axial pullout forces of full-scale tests of 60.3 mm diameter pipes with FE analysis subjected to compaction-induced stresses using K

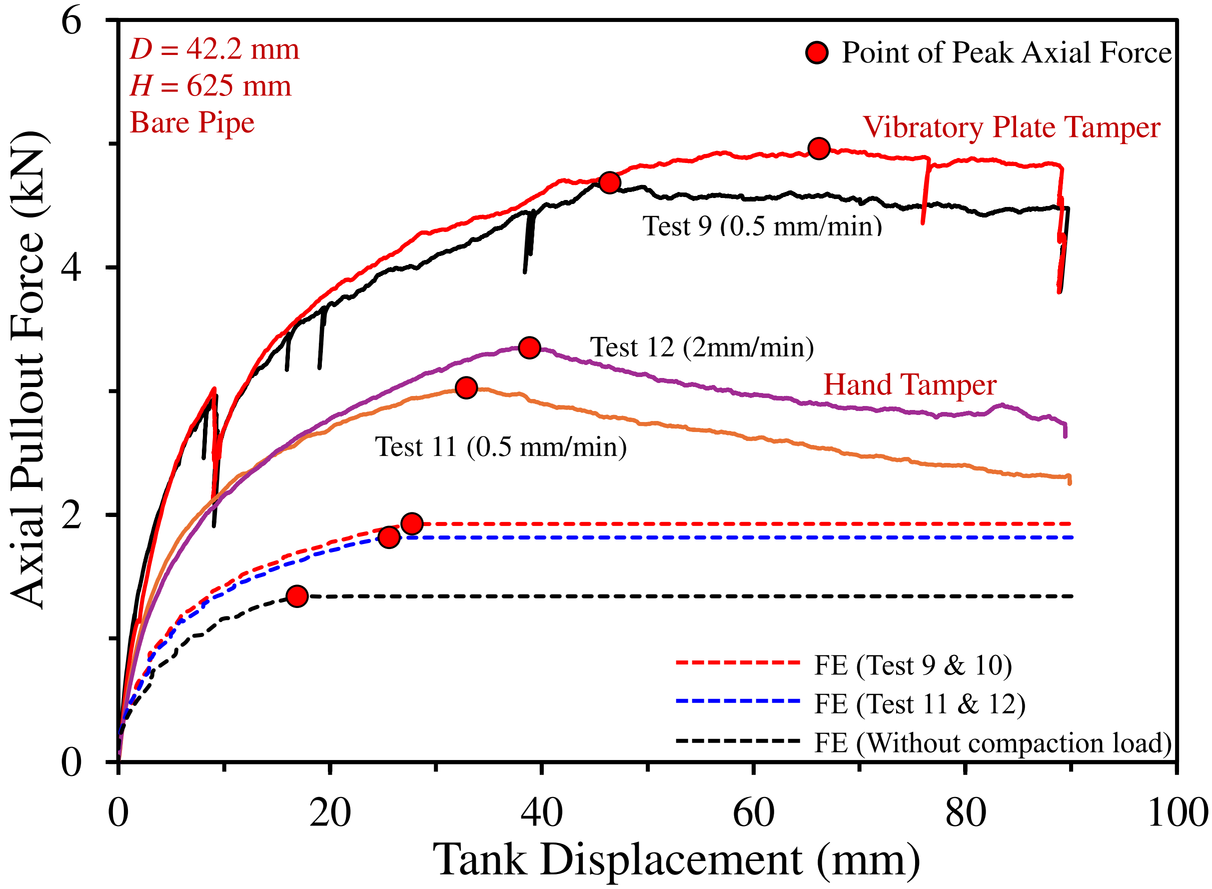

Figure 4-14: Comparison of axial pullout forces of full-scale tests of 42.2 mm diameter pipes with FE analysis subjected to compaction-induced stresses using K

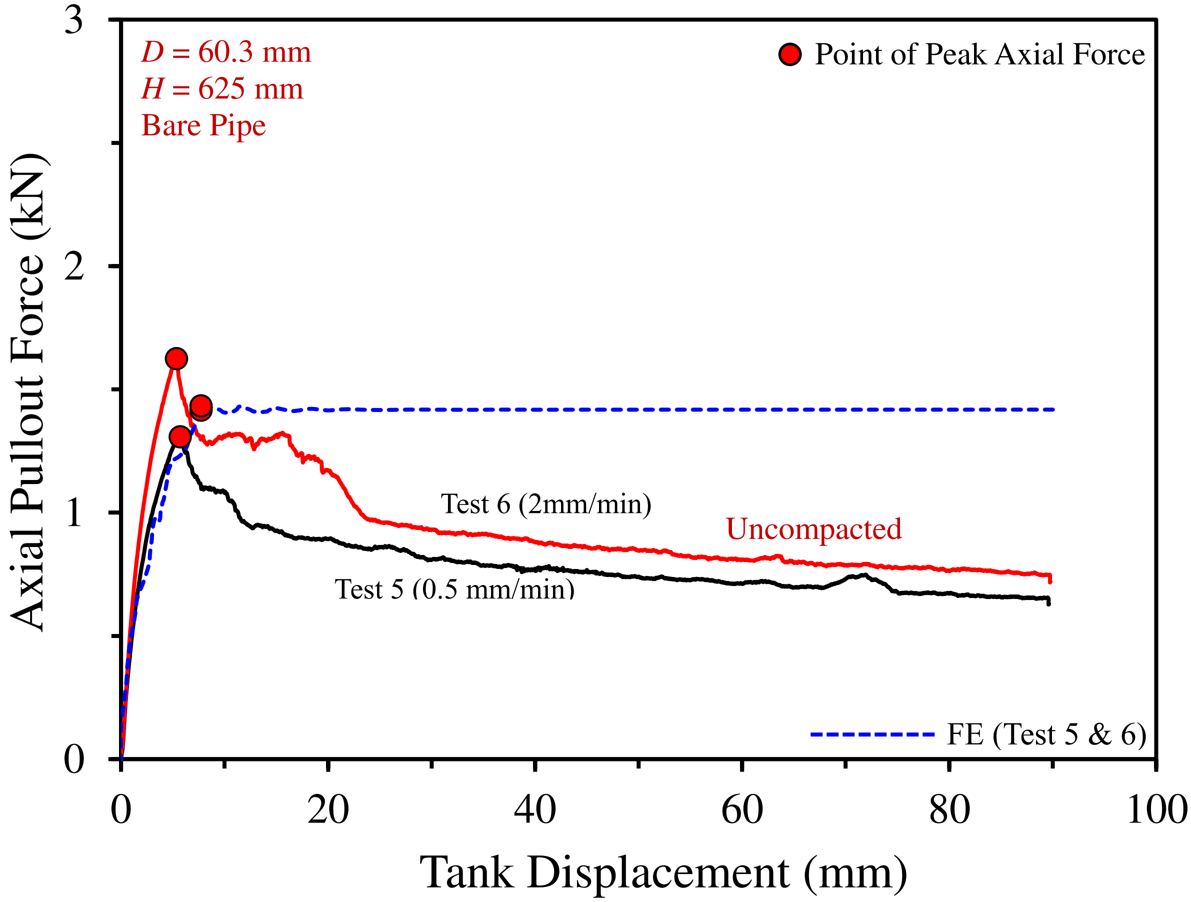

Figure 4-15: Comparison of axial pullout forces of full-scale tests of 42.2 mm diameter pipes with FE analysis subjected to compaction-induced stresses using K

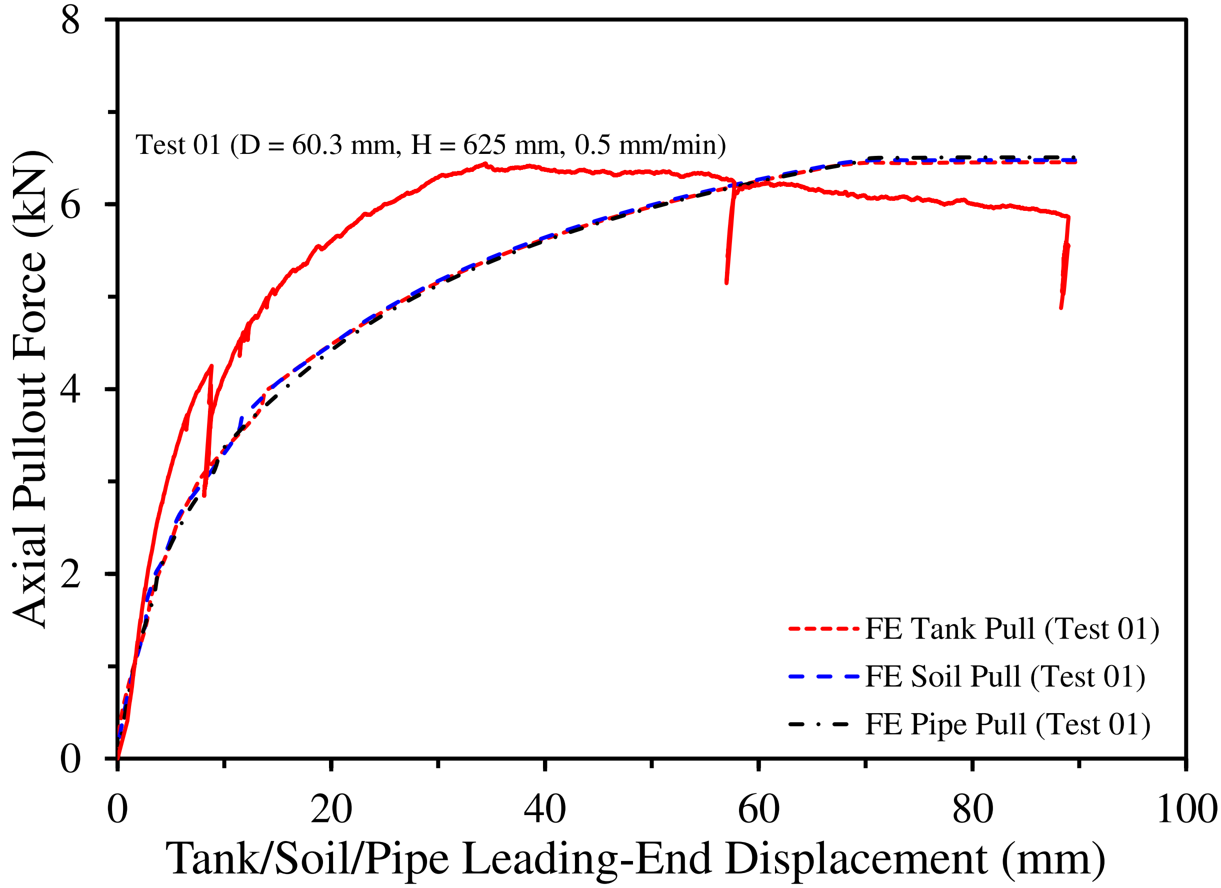

Figure 4-16: Comparison of axial pullout forces of Test 01 through different pulling mechanisms

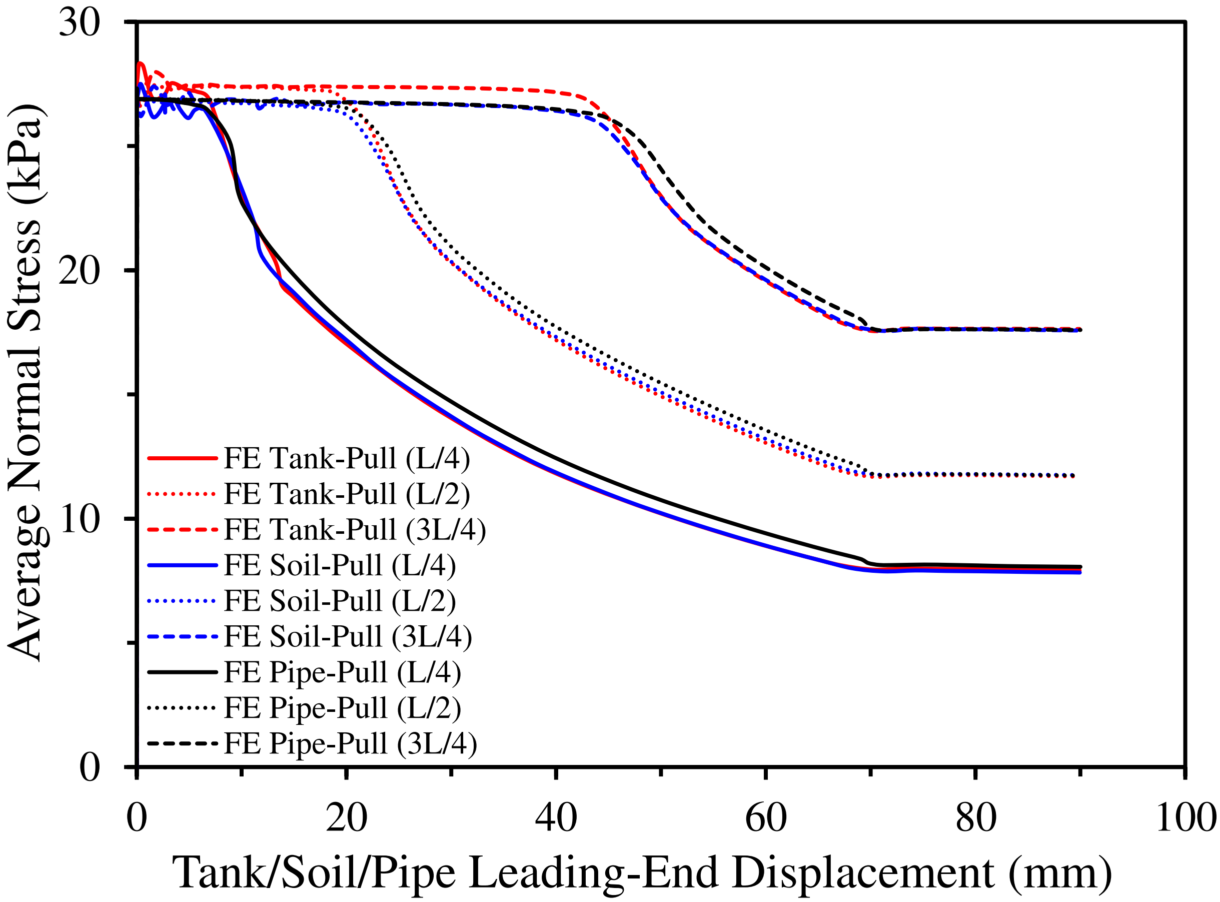

Figure 4-17: Variation of average normal stress around the pipe of Test 01 through different pulling mechanisms

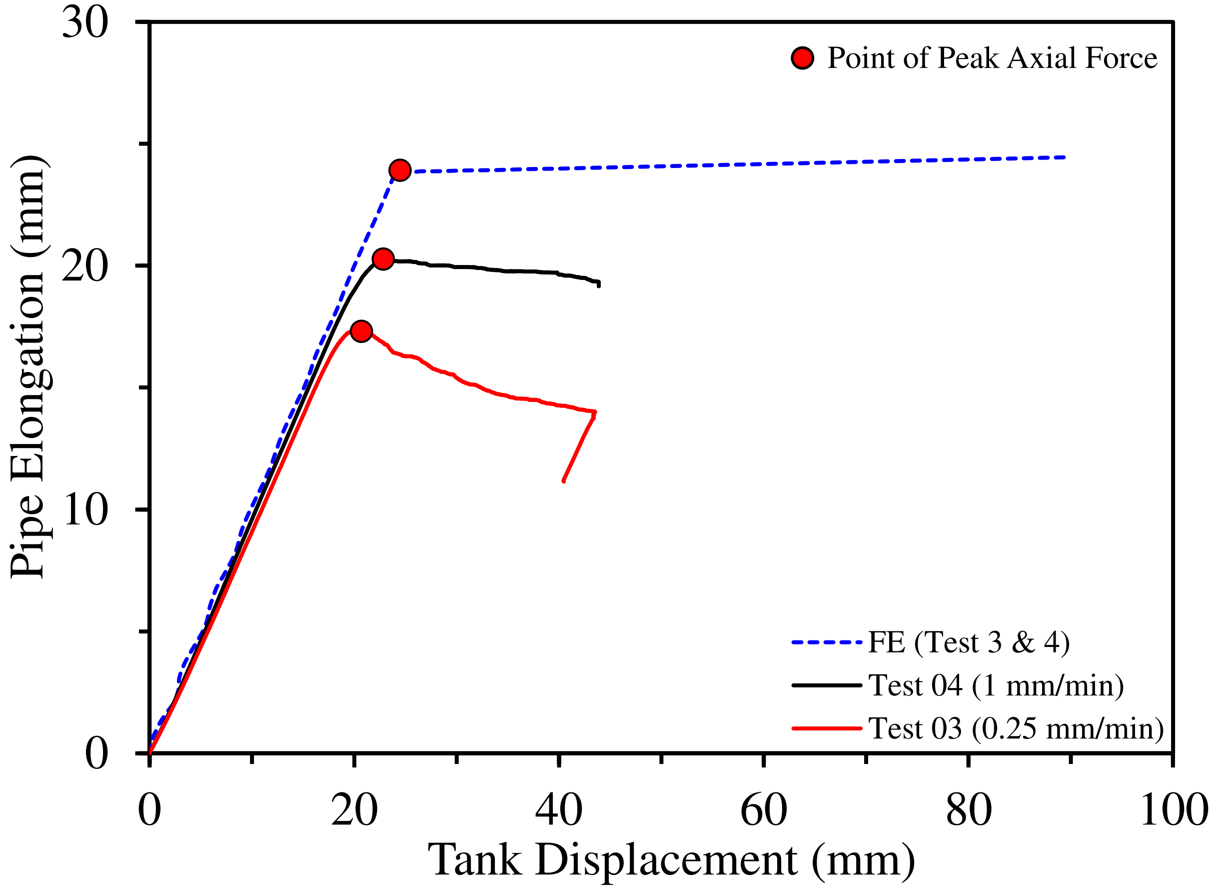

Figure 4-18: Comparison of pipe elongation measured in Tests 3 and 4 with FE simulation results

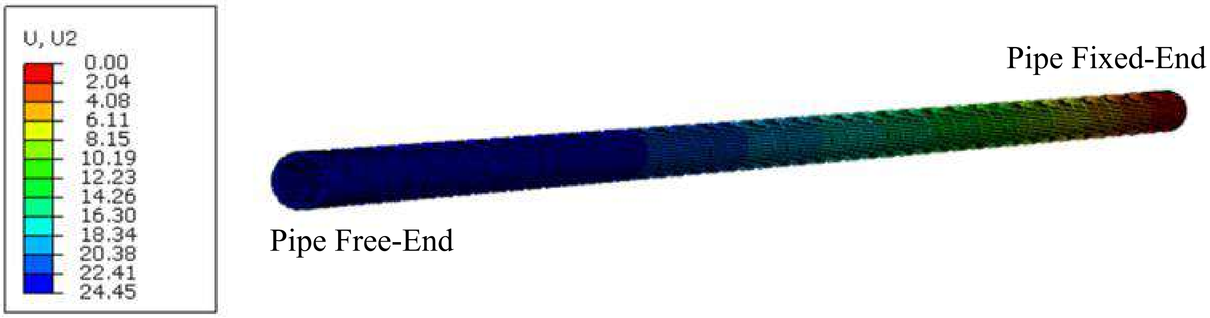

(a)

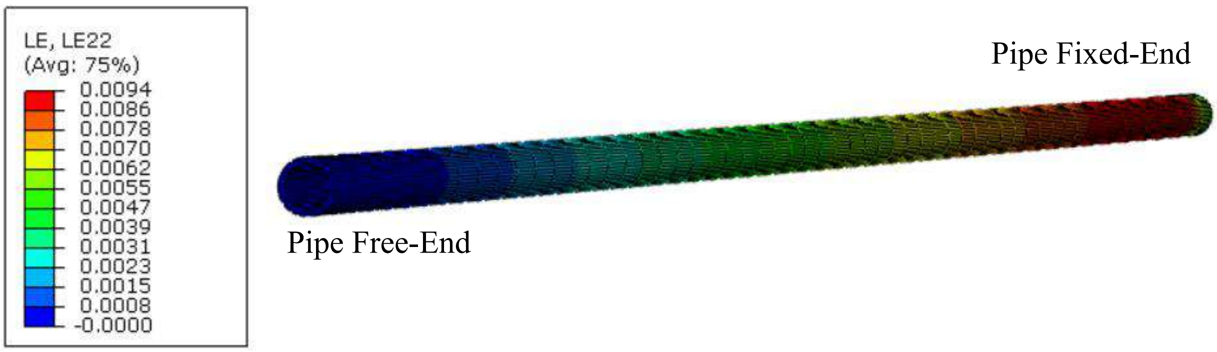

(b)

Figure 4-19: Contour of (a) pipe elongation and (b) axial strains along the pipe length from FE simulation of Tests 3 and 4

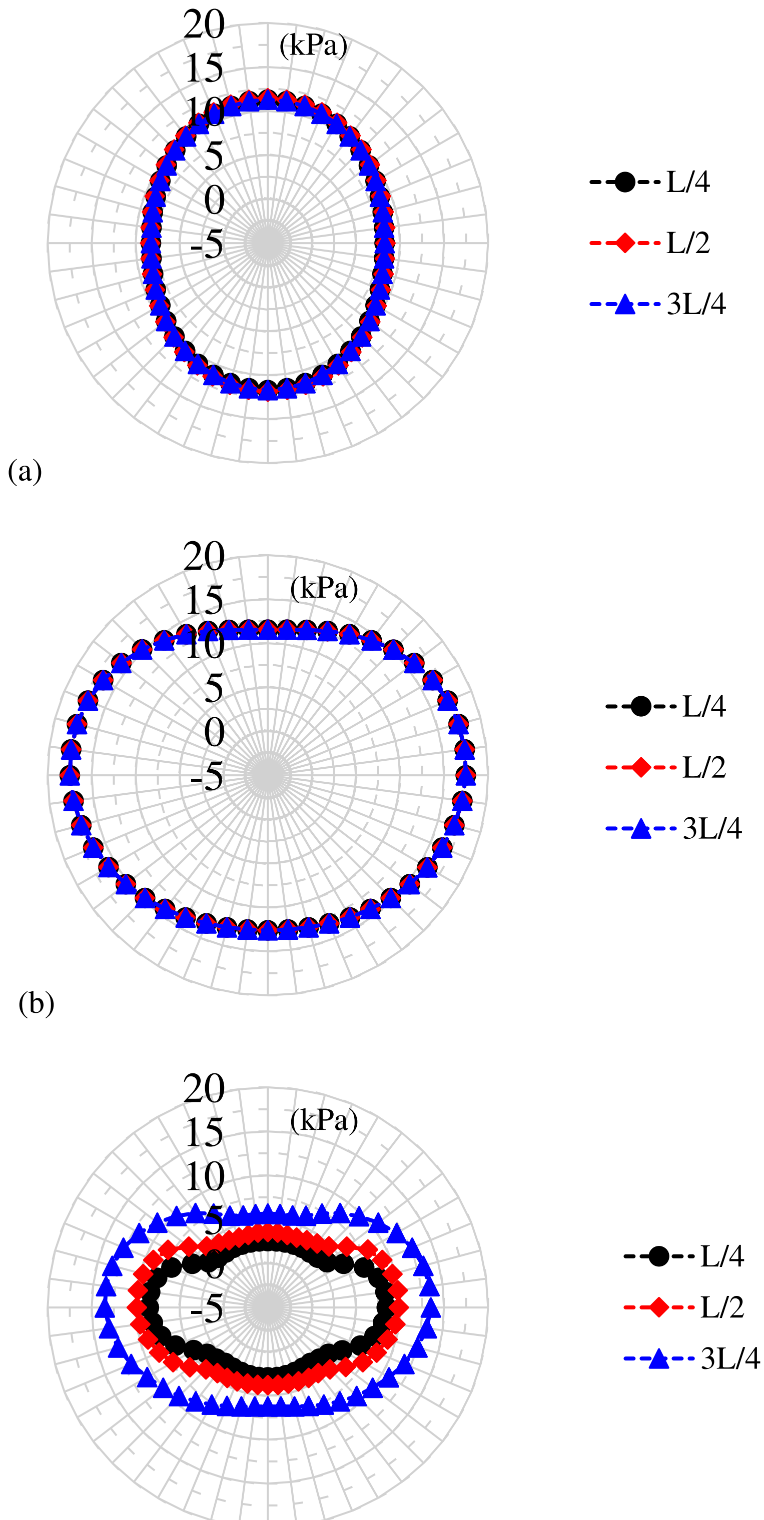

Figure 4-20: Interface normal stresses around the pipe circumference: (a) without compaction-induced stresses; (b) with compaction-induced stresses; (c) at the end of desired ground movement of 90 mm, from FE simulation of Tests 3 and 4

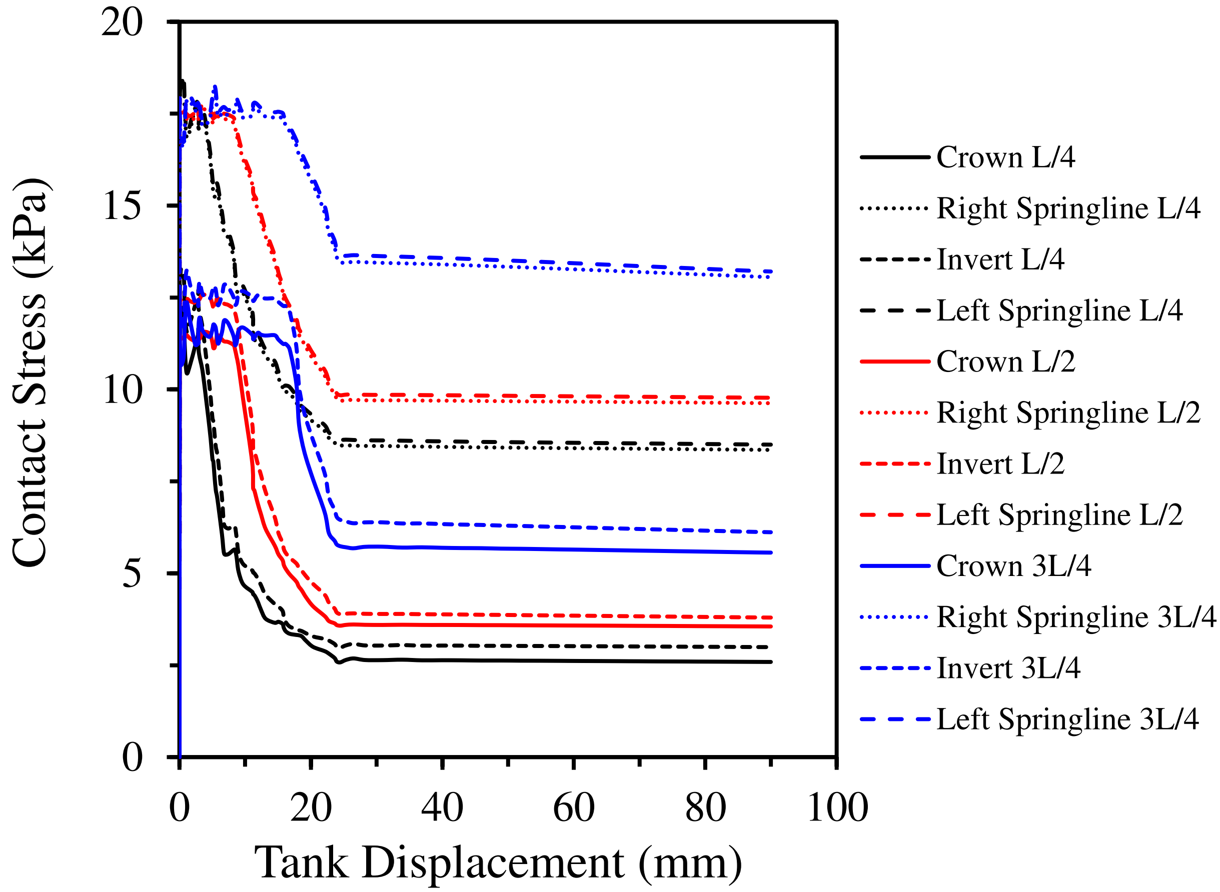

Figure 4-21: Changes in contact normal stresses at pipe crown, springlines and invert at L/4, L/2, and 3L/4 from fixed-end of pipe, from FE simulation of Tests 3 and 4

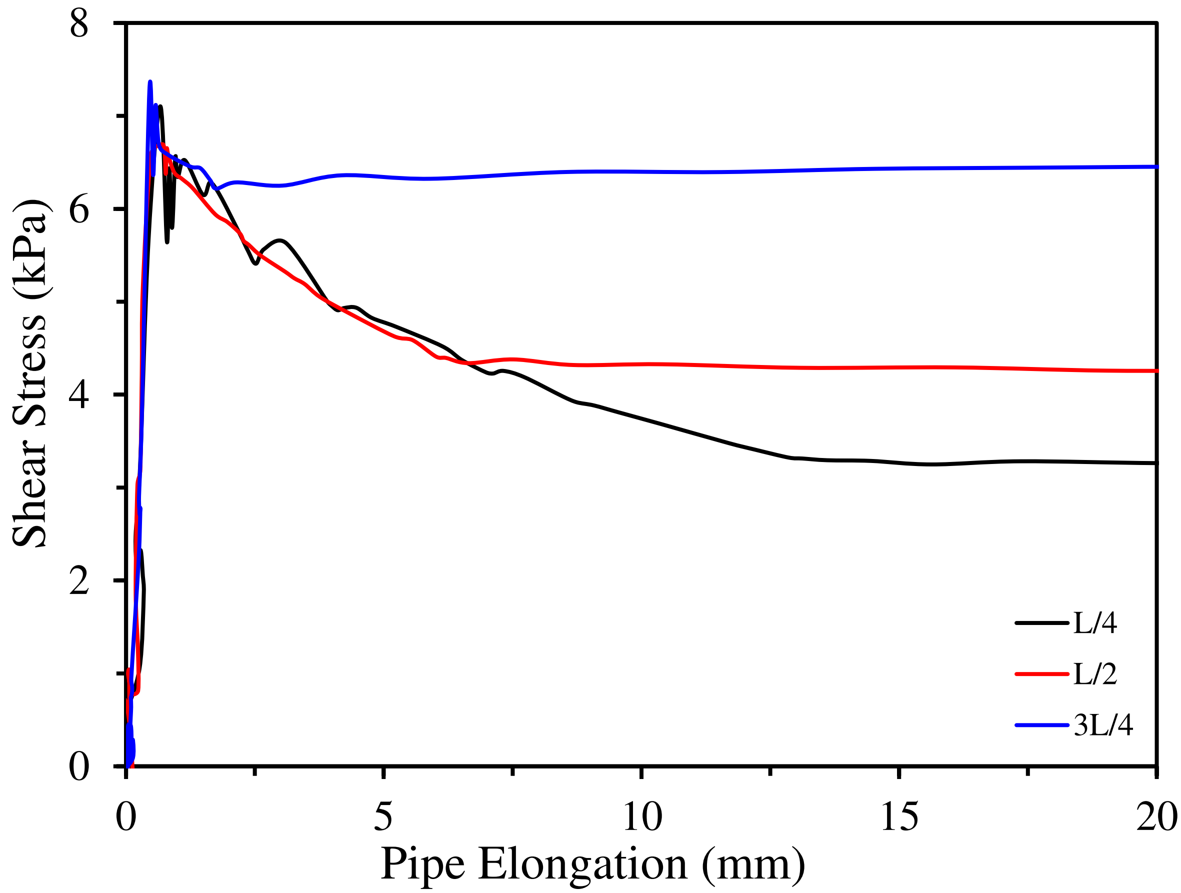

Figure 4-22: Variation of shear stresses with displacements of pipe points, from FE simulation of Tests 3 and 4

CHAPTER 5: Conclusions and Recommendations for Future Research

5.1 Conclusions

Pipelines, particularly those made of MDPE, serve a critical role in modern society, transporting essential resources across varying terrains and environments. This thesis investigates the axial pullout behaviour of small-diameter MDPE pipes buried at various depths under axial loading scenarios subjected to different backfill compaction efforts. The findings, based on full-scale testing and FEM, shed light on the complex pipe-soil interaction mechanisms, influenced by factors such as soil compaction, pipe diameter, and movement rates. Through extensive experimental work, it was observed that the axial force development in buried pipes is nonlinear, with force transfer progressing along the pipe length from the fixed end to the free end. Both experimental and simulation findings underscore the significant role of backfill compaction on pipe-soil interaction, with compacted soils exhibiting notably higher resistance. In this chapter, the overall findings from the full-scale experimental tests and simulation through 3D continuum FEM are discussed. The specific conclusions relevant to the Chapters are presented in Chapters 3 and 4.

5.2 Major Findings from the Full-scale Tests

During the full-scale tests, the behaviour of pipes subjected to axial ground movements was examined when a soil mass was moved against a static pipe. Most previous studies investigated the axial pullout behaviour of a pipe by pulling a pipe through a static soil mass.

- Axial force in MDPE pipes increased nonlinearly with tank displacement, peaking as interface shear strength was mobilized. The axial force was observed to decrease slightly upon load transfer to the surrounding soil, marking a redistribution of forces along the pipe length.

- Peak axial force was notably higher in pipes buried in compacted backfill as opposed to loose backfill. For 60.3 mm diameter pipes, axial resistance was 147% higher with hand-compacted backfill compared to loose backfill, highlighting the influence of compaction-induced stresses. The normalized forces were higher for smaller-diameter pipes than the larger ones at the same burial depths.
- Varying the tank displacement rates from 0.25 mm/min to 2 mm/min had minimal effect on the axial force, suggesting that displacement rates play a secondary role compared to factors like compaction and pipe diameter for soil-pull mechanism. However, in pipe pulling tests reported in the previous studies indicated the effect of pulling rate on the axial forces.
- The soil movement against a fixed pipe resulted in greater axial force than a pipe pulled through a static soil mass (i.e. pipe-pull). This effect was more pronounced in larger-diameter pipes.
- Soil resistance was reduced by approximately 10% during repeated loading cycles, indicating a degradation in resistance over successive cycles.
- Axial strain mobilization is initiated at the fixed end, progressing towards the free end. A nonlinear distribution of axial strains was observed initially and was linear after mobilization of shearing resistance over full pipe length.

5.3 Major Findings from the Finite Element Analysis

The conventional continuum-based finite element modelling was evaluated with the test results of the pipes subjected to the axial ground movement. Some of the mechanisms, such as pipe-soil interface shearing and compaction-induced stresses, were incorporated in FE modelling. To capture the effect of dilation during interface shearing, Mohr-Coulomb criteria with non-associated flow rule was applied. The compaction-induced stresses recommended in Duncan and Seed (1986) were implemented using an equivalent temperature load. The use of a higher lateral earth pressure coefficient was also examined.

- The compaction-induced stresses recommended in Duncan and Seed (1986) for vibratory plate compaction significantly underestimated the peak axial forces compared to corresponding test results. However, these reasonably simulated the peak axial forces for the pipe in the backfill compacted using hand temper compaction method.
- The lateral earth pressure coefficient recommended in Meidani et al. (2018) was not successful in simulating the test results.
- Simulations using the tank-pull, soil-pull, and pipe-pull approaches provided similar results, while full-scale pipe-pull and soil-pull tests exhibited differences. Thus, the conventional FE analysis did not successfully simulated the differences in the mechanism during pipe-pull and soil-pull.
- The results of analysis revealed that the effect of interface soil dilation was negligible for the pipe subjected to axial ground movement. The normal stress on the interface reduced due to the reduction of pipe diameter during axial pullout.

While discrepancies were observed between the FE predictions and the experimental results—particularly in relation to the pipe-pull versus soil-pull mechanisms, compaction-induced stress simulation methods, and pulling rate effects—the FE analysis still provides valuable practical insights. The FE models allowed for a systematic evaluation of different stress application techniques (equivalent thermal loading versus modified lateral earth pressure coefficient) and helped visualize the general trends in soil-pipe interaction under varying conditions. Although the absolute magnitudes of the axial forces did not always match the physical test outcomes, the numerical simulations confirm that accounting for compaction-induced stresses significantly increases soil restraint, and that modelling methods capturing depth-dependent stress variations (e.g., equivalent thermal loading) yield results more consistent with observed behaviour. Thus, the FE analysis serves as a complementary tool to better understand the mechanisms identified in experimental work, rather than as a direct predictive model for exact axial force magnitudes.

5.4 Recommendations for Future Research

To expand upon the findings of this study and address the limitations encountered, the following recommendations are proposed for future research:

- In the current study, accounting for the compaction-induced stress provided a better estimation of the maximum axial force measured during the tests. The compaction-induced stress, however, reduces with burial depth and become negligible after a certain depth. Therefore, it is recommended to investigate the behaviour of pipes with different burial depths to confirm the hypothesis of compaction-induced stresses.
- The axial forces on the pipe were found to be different for soil-pull and pipe-pull tests. However, no difference was observed from FE analysis. Additional tests with soil-pulling and pipe-pulling under similar pipe burial conditions should be conducted to validate the findings.

- Extensive cyclic loading tests can be conducted to better understand the degradation in soil resistance and its impact on axial resistance over multiple load cycles. This is particularly relevant for pipelines in seismically active areas or regions prone to frequent ground movements.
- Investigate the influence of varying temperatures and environmental factors (e.g., moisture content changes) on MDPE pipe performance, as these factors can significantly affect material properties and interface friction.
- Perform tests on larger-diameter pipes and alternative pipe materials (e.g., HDPE and PVC) to generalize the findings and provide a comprehensive understanding of pipe-soil interactions across various pipe types and applications.
- Utilize more sophisticated soil models in finite element analysis to account for the mechanisms during soil-pulling and pipe-pulling and the effects of interface soil dilation.
- Expand research to explore the effects of lateral and oblique loading, simulating scenarios where pipelines may be subjected to multi-directional ground movements, such as landslides or tectonic shifts.

5.5 References (General)

Abuel-Naga, H. M., Shaia, H. A., & Bouazza, A. (2018). Effect of surface roughness and hardness of continuum materials on interface shear strength of granular materials. *Journal of Testing and Evaluation, 46*(2), 826-831.

ALA (American Lifelines Alliance). (2005). *Guidelines for the design of buried steel pipe*. Federal Emergency Management Agency (FEMA), Washington, DC, USA, and American Society of Civil Engineers (ASCE), Reston, VA, USA.

Almahakeri, M., Moore, I., & Fam, A. (2016). Numerical study of longitudinal bending in buried GFRP pipes subjected to lateral earth movements. *Journal of Pipeline Systems Engineering and Practice, 8*(1), 702–710.

Almahakeri, M., Moore, I. D., & Fam, A. (2019). Numerical techniques for design calculations of longitudinal bending in buried steel pipes subjected to lateral Earth movements. *Royal Society Open Science, 6*(7), 181550.

Al-Khazaali, M., & Vanapalli, S. K. (2019). Axial force–displacement behaviour of a buried pipeline in saturated and unsaturated sand. *Géotechnique, 69*(11), 986-1003.

Al-Khazaali, M., Vanapalli, S. K., & Oh, W. T. (2019). Numerical investigation of soil–pipeline system behavior nearby unsupported excavation in saturated and unsaturated glacial till. *Canadian Geotechnical Journal, 56*(1), 69-88.

Allegro Energy Consulting. (2005). *Safety incidents on natural gas distribution systems: Understanding the hazards: A report prepared for the Office of Pipeline Safety U.S. Department of Transportation.*

American Gas Association. (2022). *ANSI/GPTC Z380.1, Guide for Gas Transmission, Distribution, and Gathering Piping Systems, 2022 Edition*. American Gas Association (AGA), United States.

Andersen, D., & Dhar, A. S. (2023). Investigation of small-diameter steel pipes subjected to axial ground movement. In *Annual Conference of Canadian Geotechnical Society, GeoSaskatoon 2023*, Saskatchewan, Canada.

Andersen, D. (2024). *Behaviour of small-diameter buried steel pipes subjected to axial ground movement* (Master's thesis, Memorial University of Newfoundland).

Anderson, C. D. (2004). *Response of buried polyethylene natural gas pipelines subjected to lateral ground displacement* (Doctoral dissertation, University of British Columbia).

ASCE (American Society of Civil Engineers). (1984). *Guidelines for the seismic design of oil and gas pipeline systems*. Committee on Gas and Liquid Fuel Lifelines, American Society of Civil Engineers, New York, NY, USA.

ASTM (2016). *Standard Test Methods for Minimum Index Density and Unit Weight of Soils and Calculation of Relative Density*. D4254-16. American Society for Testing and Materials, West Conshohocken, PA, USA.

ASTM (2016). *Standard Test Method for Density and Unit Weight of Soil in Place by Sand-Cone Method*. D1556/D1556M-15. American Society for Testing and Materials, West Conshohocken, PA, USA.

ASTM (2019). *Standard Test Methods for Maximum Index Density and Unit Weight of Soils Using a Vibratory Table*. D4253-16e1. American Society for Testing and Materials, West Conshohocken, PA, USA.

ASTM (2021). *Standard Test Methods for Particle-Size Distribution (Gradation) of Soils Using Sieve Analysis*. D6913/D6913M-17. American Society for Testing and Materials, West Conshohocken, PA, USA.

Bilgin, Ö., & Stewart, H. E. (2009a). Design guidelines for polyethylene pipe interface shear resistance. *Journal of Geotechnical and Geoenvironmental Engineering, 135*(6), 809-818.

Bilgin, Ö., & Stewart, H. E. (2009b). Pullout resistance characteristics of cast iron pipe. *Journal of Transportation Engineering, 135*(10), 730–735.

Bilgin, Ö., Stewart, H. E., & O'Rourke, T. D. (2007). Thermal and mechanical properties of polyethylene pipes. *Journal of Materials in Civil Engineering, 19*(12), 1043-1052.

Blaker, Ø., Lunne, T., Vestgården, T., Krogh, L., Thomsen, N. V., Powell, J. J. M., & Wallace, C. F. (2015). Method dependency for determining maximum and minimum dry unit weights of sands. In *Proceedings of the 3rd International Symposium on Frontiers in Offshore Geotechnics (ISFOG)* (pp. 1159-1166). Taylor & Francis Group, Oslo.

Bolton, M. D. (1986). The strength and dilatancy of sands. *Géotechnique, 36*(1), 65-78.

Bonasera, M., Taboni, B., Caselle, C., Acquaotta, F., Fubelli, G., Masciocco, L., Bonetto, S. M. R., Ferrero, A. M., & Umili, G. (2024). Instrumental monitoring of a slow-moving landslide in Piedmont (Northwest Italy) for the definition of rainfall thresholds. *Sensors, 24*(11), 3327.

Boulbes, R. J. (2020). *Troubleshooting Finite-Element Modeling with Abaqus*. Fransa.

Boulon, M., & Foray, P. (1986). Physical and numerical simulation of lateral shaft friction along offshore piles in sand. In *Proceedings of the 3rd International Conference on Numerical Methods in Offshore Piling* (pp. 127-147), Nantes, France.

Boussinesq, J. (1885). Sur la distribution des pressions dans un massif élastique. *Comptes rendus de l'Académie des Sciences, 100,* 935–938.

Brachman, R. W. I. (1999). *Structural performance of leachate collection pipes* (Ph.D. thesis, Department of Civil and Environmental Engineering, University of Western Ontario).

Bridgewater, J. (1980). On the width of failure zones. *Géotechnique, 30*(4), 533–536.

Bruschi, R., Tomassini, D., Cuscana, S., & Venzi, S. (1995). Failure modes for pipelines in landslide areas. In *Proceedings of the 14th International Conference on Offshore Mechanics and Arctic Engineering* (pp. 65–78). American Society of Mechanical Engineers.

Bruschi, R., Glavina, S., Spinazze, M., Tomassini, D., Bonanni, S., & Cuscuna, S. (1996). Pipelines subjected to slow landslide movements: Structural modeling vs. field measurement. In *Proceedings of the 15th International Conference on Offshore Mechanics and Arctic Engineering* (pp. 343–353). American Society of Mechanical Engineers.

Budhu, M. (2011). *Soil Mechanics and Foundations* (3rd ed.). John Wiley & Sons, Inc.

Bughi, S., Aleotti, P., Bruschi, R., Andrei, G., Milani, G., & Scarpelli, G. (1996). Slow movements of slopes interfering with pipelines: Modeling and monitoring. In *Proceedings of the 15th International Conference on Offshore Mechanics and Arctic Engineering* (pp. 363–372). American Society of Mechanical Engineers.

Byrne, P. M., Cheung, H., & Yan, L. (1987). Soil parameters for deformation analysis of sand masses. *Canadian Geotechnical Journal, 24*(3), 366-376.

Carder, D. R., Pocock, R. G., & Murray, R. T. (1977). *Experimental retaining wall facility-Lateral stress measurements with sand backfill* (No. TRRL Lab Report 766). Transport and Road Research Laboratory, Crowthorne, Berkshire, United Kingdom.

Carder, D. R., Murray, R. T., & Krawczyk, J. V. (1980). *Earth pressures against an experimental retaining wall backfilled with silty clay* (No. LR 946 Monograph). Transport and Road Research Laboratory, Crowthorne, Berkshire, United Kingdom.

Carey, T. J., Stone, N., & Kutter, B. L. (2020). Grain size analysis and maximum and minimum dry density testing of Ottawa F-65 sand for LEAP-UCD-2017. In Kutter, B., Manzari, M., & Zeghal, M. (Eds.), *Model tests and numerical simulations of liquefaction and lateral spreading* (pp. 263-278). Springer, Cham.

CEPA (Canadian Energy Pipeline Association). (2016). *Pipeline industry performance report*. Retrieved from https://www.aboutpipelines.com/en/pipeline-101/pipeline-history/

CER (Canada Energy Regulator). (2021). *Canada's pipeline system 2021: Economics of CER-regulated infrastructure*. Government of Canada. https://www.cer-rec.gc.ca/en/data-analysis/facilities-we-regulate/canadas-pipeline-system/2021/index.html

CGA (Canadian Gas Association). (2021). When was Canada's natural gas distribution system built, and what is it made of. *Energy Magazine, Issue 1*.

Chakraborty, S. (2022). *Behavior of branched buried MDPE gas distribution pipes under relative axial ground movements* (Master's thesis, Memorial University of Newfoundland).

Chakraborty, S., Anjum, S., Dhar, A. S., & Rahman, M. (2023). Loading-unloading-reloading responses of MDPE pipes in sand subjected to axial ground movement. In *Annual Conference of Canadian Geotechnical Society, GeoSaskatoon*.

Chakraborty, T., & Salgado, R. (2010). Dilatancy and shear strength of sand at low confining pressures. *Journal of Geotechnical and Geoenvironmental Engineering, 136*(3), 527-532.

Cheaib, A., Lacroix, P., Zerathe, S., Jongmans, D., Ajorlou, N., Doin, M. P., & Abdallah, C. (2022). Landslides induced by the 2017 Mw7.3 Sarpol Zahab earthquake (Iran). *Landslides, 19*(3), 603-619.

Chen, T. J., & Fang, Y. S. (2008). Earth pressure due to vibratory compaction. *Journal of Geotechnical and Geoenvironmental Engineering, 134*(4), 437-444.

Chen, Q., Ni, P., & Qin, X. (2023). Numerical investigation on failure modes of bell-spigot jointed ductile iron pipelines subjected to dip-slip faults with different dip angles. *Tunnelling and Underground Space Technology, 133*, 104982.

Cheng, Z., Gong, W., Tang, H., Juang, C. H., Deng, Q., Chen, J., & Ye, X. (2021). UAV photogrammetry-based remote sensing and preliminary assessment of the behavior of a landslide in Guizhou, China. *Engineering Geology, 289*, 106172.

Clayton, C. R. I., Symons, I. F., & Heidra-Coho, J. C. (1991). The pressure of clay backfill against retaining structures. *Canadian Geotechnical Journal, 28*(2), 309-315.

Clayton, C. R. I., & Symons, I. F. (1992). The pressure of compacted fill on retaining walls. *Géotechnique, 42*(1), 127-130.

Cruden, D. M., & Varnes, D. J. (1996). Landslides: Investigation and mitigation. Chapter 3—Landslide types and processes. *Transportation Research Board Special Report, 247*.

Daiyan, N., Kenny, S., Phillips, R., & Popescu, R. (2011). Investigating pipeline–soil interaction under axial–lateral relative movements in sand. *Canadian Geotechnical Journal, 48*(11), 1683–1695.

Danish submarine pipeline guidelines. (1985). Danish submarine pipeline guidelines. First draft.

Das, S., & Dhar, A. S. (2021). Nonlinear time-dependent mechanical behaviour of medium-density polyethylene pipe material. *Journal of Materials in Civil Engineering, 33*(5), 04021068.

Dassault Systems. (2019). *ABAQUS/CAE user's guide*. Providence, RI: Dassault Systems.

Dezfooli, M. S., Abolmaali, A., & Razavi, M. (2015). Coupled nonlinear finite-element analysis of soil–steel pipe structure interaction. *International Journal of Geomechanics, 15*(1), 04014032.

Dhar, A. S., & Moore, I. D. (2001). Liner buckling in profiled polyethylene pipes. *Geosynthetics International, 8*(4), 303–326.

Dhar, A. S., Moore, I. D., & McGrath, T. J. (2004). Two-dimensional analysis of thermoplastic culvert deformations and strains. *Journal of Geotechnical and Geoenvironmental Engineering, 130*(2), 199-208.

Dove, J. E., & Frost, J. D. (1999). Peak friction behavior of smooth geomembrane-particle interfaces. *Journal of Geotechnical and Geoenvironmental Engineering, 125*(7), 544-555.

Dove, J. E., & Jarrett, J. B. (2002). Behavior of dilative sand interface in a geotribology framework. *Journal of Geotechnical and Geoenvironmental Engineering, 128*(1), 25–37.

Duncan, J. M., & Seed, R. B. (1986). Compaction-induced earth pressures under K_0-conditions. *Journal of Geotechnical Engineering, 112*(1), 1-22.

Duncan, J. M., & Chang, C. Y. (1970). Nonlinear analysis of stress and strain in soils. *Journal of the Soil Mechanics and Foundations Division, ASCE, 96*(5), 1629-1653.

Duncan, J. M., Williams, G. W., Sehn, A. L., & Seed, R. B. (1991). Estimation of earth pressures due to compaction. *Journal of Geotechnical Engineering, 117*(12), 1833-1847.

Elshimi, T. M., & Moore, I. D. (2013). Modeling the effects of backfilling and soil compaction beside shallow buried pipes. *Journal of Pipeline Systems Engineering and Practice, 4*(4), 04013004.

Ezzeldin, I., & El Naggar, H. (2021). Three-dimensional finite element modeling of corrugated metal pipes. *Transportation Geotechnics, 27*, 100467.

Ezzeldin, I., & El Naggar, H. (2022). Numerical modelling of induced stresses in buried corrugated metal structures due to compaction efforts. *Transportation Geotechnics, 32*, 100706.

Ezzeldin, I., El Naggar, H., & Newhook, J. (2022). 3D numerical modelling of earth pressures on a non-yielding rigid wall due to compaction efforts. In *Annual Conference of Canadian Geotechnical Society, GeoCalgary2022*, Alberta, Canada.

Farhadi, B., & Lashkari, A. (2017). Influence of soil inherent anisotropy on behavior of crushed sand-steel interfaces. *Soils and Foundations, 57*(1), 111-125.

Fellenius, B. H. (2023). *Basics of foundation design*. Electronic Edition. Retrieved from www.Fellenius.net

Feng, W., Huang, R., Liu, J., Xu, X., & Luo, M. (2015). Large-scale field trial to explore landslide and pipeline interaction. *Soils and Foundations, 55*(6), 1466–1473.

Ferreira, N. J., & Blatz, J. A. (2021). Measured pipe stresses on gas pipelines in landslide areas. *Canadian Geotechnical Journal, 99*(999), 1855–1869.

Ghanadizadeh, A., Tabatabaie Shourijeh, P., & Lashkari, A. (2022). Laboratory investigation and constitutive modeling of the mechanical behavior of sand–GRP interfaces. *Acta Geotechnica, 17*(1), 1-23.

Groves, J., & Wijewickreme, D. (2013). Field monitoring of buried polyethylene natural gas pipelines subjected to ground movement. In *Proceedings of GéoMontréal 2013*, Montreal, Canada.

Gui, M., Phan, T., & Pham, T. (2020). Impacts of compaction load and procedure on stress-deformation behaviors of a soil geosynthetic composite (SGC) mass—A case study. *Applied Sciences, 10*(18), 6339.

Guo, P., & Stolle, D. (2005). Lateral pipe-soil interaction in sand with reference to scale effect. *Journal of Geotechnical and Geoenvironmental Engineering, 131*(3), 338–349.

Guo, C., & Zhou, C. (2024). Axial behaviour of steel pipelines buried in sand: Effects of surface roughness and hardness. *Géotechnique*, 1-37.

Hamouda, H. B. H., Laiarinandrasana, L., & Piques, R. (2007). Viscoplastic behaviour of a medium density polyethylene (MDPE): Constitutive equations based on double nonlinear deformation model. *International Journal of Plasticity, 23*(8), 1307-1327.

Han, F., Ganju, E., Salgado, R., et al. (2018). Effects of interface roughness, particle geometry, and gradation on the sand–steel interface friction angle. *Journal of Geotechnical and Geoenvironmental Engineering, 144*(12), 04018096.

Hoeg, K. (1968). Stresses against underground structural cylinders. *Journal of Soil Mechanics and Foundations Division, 94*(4), 833-858.

Holtz, R. D., Kovacs, W. D., & Sheahan, T. C. (2011). *An introduction to geotechnical engineering* (2nd ed.). Pearson.

Holtz, R. D., Kovacs, W. D., & Sheahan, T. C. (2022). *An introduction to geotechnical engineering* (3rd ed.). Pearson.

Honeywell. (2024). *Model JEC-AG series: Long stroke LVDTs*. Honeywell. Retrieved August 19, 2024, from https://sps.honeywell.com/ca/en/products/sensing-solutions/industrial-sensing/industrial-test-and-measurement/lvdts/long-stroke-lvdts/model-jec-ag-series

Jaky, Z. (1944). The coefficient of earth pressure at rest. *Journal of the Soil Mechanics and Foundations Division, Proceedings of the American Society of Civil Engineers, 70,* 1231–1239.

Janbu, N. (1963). Soil compressibility as determined by oedometer and triaxial tests. In *Vol. 1 of Proceedings of the European Conference on Soil Mechanics and Foundation Engineering* (pp. 19–25). Essen, Germany: German Society for Earthworks and Foundations.

Johnston, I. W., Lam, T. S. K., & Williams, A. F. (1987). Constant normal stiffness direct shear testing for socketed pile design in weak rock. *Géotechnique, 37*(1), 83–89.

Jung, J., O'Rourke, T., & Olson, N. (2013). Uplift soil–pipe interaction in granular soil. *Canadian Geotechnical Journal, 50*(7), 744–753.

Kalaugher, P. G., Hodgson, R. L. P., & Grainger, P. (2000). Pre-failure strains as precursors of sliding in a coastal mudslide. *Journal of Engineering Geology and Hydrogeology, 33*, 325-334.

Karimian, S. A. (2006). *Response of buried steel pipelines subjected to longitudinal and transverse ground movement* (Doctoral dissertation, University of British Columbia).

Katebi, M., Wijewickreme, D., Maghoul, P., & Roy, K. (2021). Lateral force–displacement response of buried pipes in slopes. *Géotechnique, 73*(5), 375–387.

Katona, M. G., Smith, J. M., Odello, R. S., & Allgood, J. R. (1976). *CANDE–A modern approach for the structural design and analysis of buried culverts*. Final Report No. FHWA-RD-77-5.

Keefer, D. K., & Johnson, A. M. (1983). Earth flows: Morphology, mobilization, and movement. *Professional Paper*.

Kennedy, R. P., Chow, A. W., & Williamson, R. A. (1977). Fault movement effects on buried oil pipeline. *Transportation Engineering Journal, ASCE, 103*, 617-633.

Kishawy, H. A., & Gabbar, H. A. (2010). Review of pipeline integrity management practices. *International Journal of Pressure Vessels and Piping, 87*(7), 373–380.

Kondner, R. L. (1963). Hyperbolic stress-strain response: cohesive soils. *Journal of the Soil Mechanics and Foundations Division, 89*(1), 115–143.

Kyowa Electronic Instruments Co., Ltd. (2024a). *Type DTPA-A displacement transducers*. Kyowa Electronic Instruments. Retrieved August 19, 2024, from https://product.kyowa-ei.com/en/products/displacement-transducers/type-dtpa-a

Kyowa Electronic Instruments Co., Ltd. (2024b). *Type KFEL strain gages*. Kyowa Electronic Instruments. Retrieved August 19, 2024, from https://product.kyowa-ei.com/en/products/strain-gages/type-kfel

Kyowa Electronic Instruments Co., Ltd. (2024c). *Type PGM-G pressure transducers*. Kyowa Electronic Instruments. Retrieved August 19, 2024, from https://product.kyowa-ei.com/en/products/pressure-transducers/type-pgm-g

Lee, E. M., Audibert, J. M. E., Hengesh, J. V., & Nyman, D. J. (2009). Landslide-related ruptures of the Camisea pipeline system, Peru. *Quarterly Journal of Engineering Geology and Hydrogeology, 42*(2), 251-259.

Lee, E. M., Fookes, P. G., & Hart, A. B. (2016). Landslide issues associated with oil and gas pipelines in mountainous terrain. *Quarterly Journal of Engineering Geology and Hydrogeology, 49*(2), 125-131.

Li, H. J., Zhu, H. H., Zhang, C. X., & Zhang, W. (2022). Modelling and analysing failure modes of buried pipelines perpendicularly crossing landslide boundaries. *Soil Dynamics and Earthquake Engineering, 162*, 107447.

Lings, M. L., & Dietz, M. S. (2005). The peak strength of sand-steel interfaces and the role of dilation. *Soils and Foundations, 45*(6), 1-14.

Liu, H., Polak, M. A., & Penlidis, A. (2008). A practical approach to modeling time-dependent nonlinear creep behavior of polyethylene for structural applications. *Polymer Engineering & Science, 48*(1), 159-167.

Los Angeles Daily News. (2024). *Images from the Northridge earthquake on Jan. 17, 1994*. Retrieved from https://www.dailynews.com/2024/01/17/los-angeles-daily-news-images-from-the-northridge-earthquake-on-jan-17-1994/

Luna Innovations Inc. (2020). *User's guide ODiSI 6*. Luna Innovations Inc., Blacksburg, VA, USA.

Luna Innovations Inc. (2017). *ODiSI fiber optic sensor installation guide*. Luna Innovations Inc., Blacksburg, VA, USA.

Lunne, T., Knudsen, S., Blaker, Ø., Vestgården, T., Powell, J. J. M., Wallace, C. F., ... & Ghanekar, R. K. (2019). Methods used to determine maximum and minimum dry unit weights of sand: Is there a need for a new standard? *Canadian Geotechnical Journal, 56*(4), 536-553.

Macciotta, R., & Hendry, M. T. (2021). Remote sensing applications for landslide monitoring and investigation in western Canada. *Remote Sensing, 13*(3), 366.

Marinos, V., Stoumpos, G., & Papazachos, C. (2019). Landslide hazard and risk assessment for a natural gas pipeline project: The case of the Trans Adriatic Pipeline, Albania Section. *Geosciences, 9*(2), 61.

Marino, G., & Osouli, A. (2020). Slip resistance behaviour of coal tar–coated steel pipelines buried in clayey and sandy backfills from ground movement. *Journal of Pipeline Systems Engineering and Practice, 11*(3), 05020001.

Masada, T., & Sargand, S. M. (2007). Peaking deflections of flexible pipe during initial backfilling process. *Journal of Transportation Engineering, 133*(2), 105–111.

Massarsch, K. R., & Fellenius, B. H. (2002). Vibratory compaction of coarse-grained soils. *Canadian Geotechnical Journal, 39*(3), 695-709.

Matymish, J., Moore, I. D., Woods, J. E., & Hoult, N. A. (2023). Axial pullout behaviour of fusible PVC pipes and fusion weld joints assessed using distributed fibre optic sensors. *Canadian Geotechnical Journal, (ja).*

McAllister, E. W. (2001). *Pipeline Rules of Thumb Handbook*. Gulf Professional Publishing, 648 p. Houston, Tex..

McGrath, T. J. (1998). Replacing E' with the constrained modulus in flexible pipe design. In *Proceedings of the Pipeline Division Conference* (Castronovo, J. P. & Clark, J. A., Eds.), ASCE, San Diego, CA, USA, pp. 28–40.

McGrath, T. J., Selig, E. T., Webb, M. C., & Zoladz, G. V. (1999). *Pipe Interaction with the Backfill Envelope, FHWA-RD-98-191*. National Science Foundation, Washington, DC, USA.

Meidani, M., Meguid, M. A., & Chouinard, L. E. (2017). Evaluation of soil–pipe interaction under relative axial ground movement. *Journal of Pipeline Systems Engineering and Practice, 8*(4), 04017009.

Meidani, M., Meguid, M. A., & Chouinard, L. E. (2018). Estimating earth loads on buried pipes under axial loading condition: Insights from 3D discrete element analysis. *International Journal of Geo-Engineering, 9*(1), 1-20.

Meidani, M., Meguid, M. A., & Chouinard, L. E. (2020). A finite-discrete element approach for modelling polyethylene pipes subjected to axial ground movement. *International Journal of Geotechnical Engineering*.

Merry, S. M., & Bray, J. D. (1996). Geomembrane response in the wide strip tension test. *Geosynthetics International, 3*(4), 517-536.

Mines, A. E., Beckstrand, D. L., & Bunn, M. D. (2022). *Landslide monitoring methods: Application of existing technologies to long-term and real-time monitoring of slope movements* (No. cmr 23-002). Missouri Department of Transportation, Construction and Materials Division.

Muntakim, A. H., & Dhar, A. S. (2018). Investigating axial pullout behavior of buried polyethylene pipelines. *Newsletter of the International Association for Computer Methods and Advances in Geomechanics, 23*, 10–21.

Muntakim, A. H., & Dhar, A. S. (2021). Assessment of axial pullout force for buried medium-density polyethylene pipelines. *Journal of Pipeline Systems Engineering and Practice, 12*(2), 04020074.

Murugathasan, P. (2019). *Experimental and numerical investigations of axial pullout behavior of buried ductile iron pipe* (Master's thesis, Memorial University of Newfoundland).

Murugathasan, P., Dhar, A. S., & Hawlader, B. C. (2018). A laboratory facility for studying pullout behaviour of buried pipelines. In *Annual Conference of Canadian Geotechnical Society, GeoEdmonton 2018*, Alberta, Canada.

Murugathasan, P., Dhar, A. S., & Hawlader, B. C. (2021). An experimental and numerical investigation of pullout behaviour of ductile iron water pipes buried in sand. *Canadian Journal of Civil Engineering, 48*(2), 134–143.

Natural Resources Canada. (2020). *Pipelines across Canada*. Government of Canada. Retrieved from https://natural-resources.canada.ca/our-natural-resources/energy-sources-distribution/fossil-fuels/pipelines/pipelines-across-canada/18856

NBC News. (2014). Looking back at the '89 Loma Prieta quake, planning for the next one. *NBC News*. Retrieved from https://www.nbcnews.com/nightly-news/looking-back-89-loma-prieta-quake-planning-next-one-n228616

Newmark, N. M., & Hall, W. J. (1975). Pipeline design to resist large fault displacement. In *Proceedings of U.S. National Conference on Earthquake Engineering* (pp. 416-425), Ann Arbor, Michigan.

Ni, P. (2016). *Nonlinear soil-structure interaction for buried pressure pipes under differential ground motion* (Doctoral dissertation, Department of Civil Engineering, Queen's University, Kingston, ON, Canada).

Ni, P., Moore, I. D., & Take, W. A. (2018). Numerical modeling of normal fault-pipeline interaction and comparison with centrifuge tests. *Soil Dynamics and Earthquake Engineering, 105*, 127–138.

Ni, Q. (2003). Effects of particle properties and boundary conditions on soil shear behaviour: 3-D numerical simulations (Doctoral dissertation, University of Southampton).

Omega Engineering. (2024). *LCHD series: Pancake-style load cells*. Omega Engineering. Retrieved August 19, 2024, from https://www.omega.ca/en/force-and-strain-measurement/load-cells/p/LCHD

O'Rourke, T. D. (1996). Lessons learned for lifeline engineering from major urban earthquakes. In *Proceedings of the 11th World Conference on Earthquake Engineering*.

O'Rourke, M. J., Liu, X., & Flores-Berrones, R. (1995). Steel pipe wrinkling due to longitudinal permanent ground deformation. *Journal of Transportation Engineering, 121*(5), 443–451.

O'Rourke, T. D., Druschel, S. J., & Netravali, A. N. (1990). Shear strength characteristics of sand-polymer interfaces. *Journal of Geotechnical Engineering, 116*(3), 451-469.

Ozanne, H. S. (2011). Chapter 6—Overview of pipeline materials. In *Pipeline Planning and Construction Field Manual* (pp. 93-103), Menon, E. S. (Ed.).

Park, S. S. (2010). Evaluation of the sand-cone method for determination of the in-situ density of soil. *Géotechnique, 60*(9), 701–707.

Paulin, M. J., Phillips, R., Clark, J. I., Trigg, A., & Konuk, I. (1998). A full-scale investigation into pipeline/soil interaction. In *Proceedings of International Pipeline Conference, ASME* (pp. 779-788), Calgary, AB.PHMSA (Pipeline and Hazardous Materials Safety Administration). (2018). *Pipeline Safety: Safety of Gas Distribution Pipelines and Other Pipeline Safety*

Initiatives. Department of Transportation (DOT), 49 CFR Parts 191, 192, and 198 [Docket No. PHMSA–2018–0046] RIN 2137–AF53.

PHMSA (Pipeline and Hazardous Materials Safety Administration). (2018). *Pipeline Safety: Safety of Gas Distribution Pipelines and Other Pipeline Safety Initiatives*. Department of Transportation (DOT), 49 CFR Parts 191, 192, and 198 [Docket No. PHMSA–2018–0046] RIN 2137–AF53.

PHMSA (Pipeline and Hazardous Materials Safety Administration). (2024). *Distribution, transmission, gathering, LNG, and liquid accident and incident data*. U.S. Department of Transportation. Retrieved from https://www.phmsa.dot.gov/data-and-statistics/pipeline/distribution-transmission-gathering-lng-and-liquid-accident-and-incident-data

Pike, K. P. (2016). *Physical and numerical modelling of pipe/soil interaction events for large deformation geohazards* (Doctoral dissertation, Memorial University of Newfoundland).

PRCI (Pipeline Research Council International). (2009). *Guidelines for constructing natural gas and liquid hydrocarbon pipelines through areas prone to landslides and subsidence hazards*. Prepared by D.G. Honegger Consulting and D.SSD Inc. Project ENV-1, 219 pages.

PRCI (Pipeline Research Council International). (2017). *Pipeline seismic design and assessment guideline*. Catalogue No: PR-268-134501-R01. Chantilly, VA, USA: PRCI.

Psyrras, N. K., & Sextos, A. G. (2018). Safety of buried steel natural gas pipelines under earthquake-induced ground shaking: A review. *Soil Dynamics and Earthquake Engineering, 106*, 254-277.

Rajani, B. B., Robertson, P. K., & Morgenstern, N. R. (1995). Simplified design methods for pipelines subject to transverse and longitudinal soil movements. *Canadian Geotechnical Journal, 32*(2), 309-323.

Rehnman, S. E., & Broms, B. B. (1972). Lateral pressures on basement wall: Results from full-scale tests. In *Proceedings of the Fifth European Conference on Soil Mechanics and Foundation Engineering*.

Reza, A., & Dhar, A. S. (2021a). Axial pullout behavior of buried medium-density polyethylene gas distribution pipes. *International Journal of Geomechanics, 21*(7), 04021120.

Reza, A., & Dhar, A. S. (2021b). Effects of axial relative ground movement on small diameter polyethylene piping in loose sand. *Infrastructures, 6*(12), 168.

Reza, A., Dhar, A. S., & Rahman, M. (2023a). Strain assessment of polyethylene pipes in dense sand subjected to axial displacement. *Geosynthetics International*, 1-18.

Reza, A., Kuwata, Y., & Dhar, A. S. (2023b). Investigation of buried pipes under axial tension and compression loadings. In *Annual Conference of Canadian Geotechnical Society, GeoSaskatoon*.

Reza, A., & Dhar, A. S. (2024). Finite-element modelling of axial movements of polyethylene pipes in dense sand. *Transportation Geotechnics*, 101366.

Reza, A. (2024). *Investigation of axial pullout behaviour of small diameter medium-density polyethylene pipes in sand* (Doctoral dissertation, Memorial University of Newfoundland).

Rizkalla, M., Turner, R. D., & Colquhoun, I. R. (1993). State of development of a fibre optic technology-based pipeline structural integrity monitoring system. In *Proceedings of the 12th Offshore Mechanics and Arctic Engineering Symposium* (Vol. V, pp. 295-302).

Robert, D. J. (2017). A modified Mohr-Coulomb model to simulate the behavior of pipelines in unsaturated soils. *Computers and Geotechnics, 91*, 146–160.

Robert, D. J., & Thusyanthan, N. I. (2015). Numerical and experimental study of uplift mobilization of buried pipelines in sands. *Journal of Pipeline Systems Engineering and Practice, 6*(1), 04014009.

Robert, D. J., Britto, A., & Setunge, S. (2020). Efficient approach to simulate soil–pipeline interaction. *Journal of Pipeline Systems Engineering and Practice, 11*(1), 04019046.

Roscoe, K. H. (1970). 10th Rankine lecture: The influence of strains in soil mechanics. *Géotechnique, 20*(2), 129–170.

Rostami, H., Osouli, A., & Kumar, S. (2023). Experimental modeling of far-field effects in buried pipelines subjected to reverse faulting. *Soil Dynamics and Earthquake Engineering, 164*, 107561.

Roy, K., Hawlader, B., Kenny, S., & Moore, I. (2016). Finite element modeling of lateral pipeline–soil interactions in dense sand. *Canadian Geotechnical Journal, 53*(3), 490–504.

Roy, K., Hawlader, B., Kenny, S., & Moore, I. (2018). Upward pipe–soil interaction for shallowly buried pipelines in dense sand. *Journal of Geotechnical and Geoenvironmental Engineering, 144*(11), 04018078.

Saberi, M., Annan, C.-D., Konrad, J.-M., & Lashkari, A. (2016). A critical state two-surface plasticity model for gravelly soil-structure interfaces under monotonic and cyclic loading. *Computers and Geotechnics, 80*, 71–82.

Saberi, M., Annan, C. D., & Sheil, B. B. (2022). An efficient numerical approach for simulating soil-pipe interaction behaviour under cyclic loading. *Computers and Geotechnics, 146*, 104666.

Saha, R. C., Dhar, A. S., & Hawlader, B. C. (2019). Shear strength assessment of a well-graded clean sand. In *Annual Conference of Canadian Geotechnical Society, GeoSt. John's*.

Saha, R. C. (2021). *Shear strength assessment of a manufactured well-graded sand* (Master's thesis, Memorial University of Newfoundland).

Saiyar, M., Ni, P., Take, W. A., & Moore, I. D. (2016). Response of pipelines of differing flexural stiffness to normal faulting. *Géotechnique, 66*(4), 275-286.

Saleh, A. E., Jalali, H. H., Pokharel, A., & Abolmaali, A. (2021). Deformation of buried large diameter steel pipes during staged construction and compaction: Case study and finite element analysis. *Transportation Geotechnics, 31*, 100649.

Sargand, S. M., Hazen, G. A., & Masada, T. (2002). *Field Verification of Structural Performance of Thermoplastic Pipe under Deep Backfill Conditions*, FHWA/OH-2002/023, Final Report. Ohio Department of Transportation, Cincinnati, OH, USA.

Sarvanis, G. C., Karamanos, S. A., Vazouras, P., Mecozzi, E., Lucci, A., & Dakoulas, P. (2017). Permanent earthquake-induced actions in buried pipelines: Numerical modeling and experimental verification. *Earthquake Engineering & Structural Dynamics, 47*(4), 966–987.

Scarpelli, G., Sakellariadi, E., & Furlani, G. (2003). Evaluation of soil–pipeline longitudinal interaction forces. *Rivista Italiana di Geotecnica, 4*(3), 24-41.

Scarpelli, G., Aleotti, P., Baldelli, P., Milani, G., & Brambati, E. (1995). Field experience of pipelines in geologically unstable areas. In *Proceedings of the 14th International Conference on Offshore Mechanics and Arctic Engineering* (pp. 65-78), Copenhagen, Denmark. American Society of Mechanical Engineers, New York, NY.

Schäfer, B., Dörr, D., & Kärger, L. (2020). Reduced-integrated 8-node hexahedral solid-shell element for the macroscopic forming simulation of continuous fibre-reinforced polymers. *Procedia Manufacturing, 47*, 134–139.

Schell, C. A., Lever, E., & Groth, K. M. (2023). Strain-based design and assessment for pipeline integrity management: A review of applications and gaps. *International Journal of Pressure Vessels and Piping, 204*, 104973.

Sheil, B. B., Martin, C. M., Byrne, B. W., Plant, M., Williams, K., & Coyne, D. (2018). Full-scale laboratory testing of a buried pipeline in sand subjected to cyclic axial displacements. *Géotechnique, 68*(8), 684–694.

Sheil, B. B., Martin, C. M., & Byrne, B. W. (2021). Simulation of overburden pressure during laboratory investigations of axial pipe–soil interaction. *Géotechnique, 71*(3), 272–278.

Spangler, M. G. (1941). *The Structural Design of Flexible Pipe Culverts*. Iowa State College Engineering Experimental Station, Ames, IA, USA.

Stewart, H. E., Bilgin, Ö., O'Rourke, T. D., & Keeney, T. M.-J. (1999). Technical reference for improved design and construction practices to account for thermal loads in plastic gas pipelines. *Final Report No. GRI-99/0192*, Gas Research Institute, Chicago.

Suleiman, M. T., & Coree, B. J. (2004). Constitutive model for high density polyethylene material: Systematic approach. *Journal of Materials in Civil Engineering, 16*(6), 511-515.

Taleb, B., & Moore, I. D. (1999). Metal culvert response to earth loading: Performance of two-dimensional analysis. *Transportation Research Record, 1656*(1), 25-36.

Terzaghi, K., Peck, R. B., & Mesri, G. (1996). *Soil mechanics in engineering practice* (3rd ed.). John Wiley & Sons.

Tokyo Weekender. (2023). *On this day in Japan: The 1995 Great Hanshin earthquake*. Retrieved from https://www.tokyoweekender.com/art_and_culture/japanese-culture/on-this-day-in-japan-the-1995-great-hanshin-earthquake/

Vanapalli, S. K., & Oh, W. T. (2010). A model for predicting the modulus of elasticity of unsaturated soils using the soil-water characteristic curve. *International Journal of Geotechnical Engineering, 4*(4), 425-433.

Vanapalli, S. K., Fredlund, D. G., Pufahl, D. E., & Clifton, A. W. (1996). Model for the prediction of shear strength with respect to soil suction. *Canadian Geotechnical Journal, 33*(3), 379-392.

Vasseghi, A., Haghshenas, E., Soroushian, A., & Rakhshandeh, M. (2021). Failure analysis of a natural gas pipeline subjected to landslide. *Engineering Failure Analysis, 119*, 105009.

Vilca, N. S., Gómez-Amador, A. M., & Jiménez de Cisneros Fonfría, J. J. (2024). Soil–structure interaction analysis using the finite element method in thin-walled steel pipes buried under haul roads. *Applied Sciences, 14*(1), 167.

Watkins, R. K., & Spangler, M. G. (1958). Some characteristics of the modulus of passive resistance of soil: a study in similitude. *Highway Research Board Proceedings*, Highway Research Board, Washington, DC, USA, 37, 576–583.

Weerasekara, L. (2007). *Response of buried natural gas pipelines subjected to ground movement* (Master's thesis, University of British Columbia).

Weerasekara, L., & Wijewickreme, D. (2008). Mobilization of soil loads on buried polyethylene natural gas pipelines subject to relative axial displacements. *Canadian Geotechnical Journal, 45*(9), 1237-1249.

Weerasekara, L. (2011). *Pipe-soil interaction aspects in buried extensible pipes* (Doctoral dissertation, University of British Columbia).

Weerasekara, L., & Rahman, M. (2019). Framework for assessing integrity of natural gas distribution pipes in landslide areas. In *Proceedings of GeoSt. John's, 72nd Canadian Geotechnical Conference*, Newfoundland and Labrador, Canada.

Weerasekara, L., Wijewickreme, D., & Rahman, M. (2023). Performance of buried natural gas distribution pipes in a landslide area: Observations from nine years of pipe strain monitoring. In *Proceedings of the 76th Canadian Geotechnical Conference, GeoSaskatoon* (pp. 1–4).

Weidlich, I., & Achmus, M. (2008). Measurement of normal pressures and friction forces acting on buried pipes subjected to cyclic axial displacements in laboratory experiments. *Geotechnical Testing Journal, 31*(4), 334–343.

Wijewickreme, D., Karimian, H., & Honegger, D. (2009). Response of buried steel pipelines subjected to relative axial soil movement. *Canadian Geotechnical Journal, 46*(7), 735-752.

Wijewickreme, D., & Weerasekara, L. (2015). Analytical modeling of field axial pullout tests performed on buried extensible pipes. *International Journal of Geomechanics, 15*(2), 04014044.

Williams, D. A., & Glasmeier, A. K. (2023). Evaluation of error across natural gas pipeline incidents. *Risk Analysis, 43*(6), 1079–1091.

Wong, C. K., Wan, R. G., & Wong, R. C. (2021). Performance of buried pipes in moving slopes under axial loading–evaluation tools. *Journal of Pipeline Science and Engineering, 1*(2), 167-175.

Wood Environment & Infrastructure Solutions. (2021). *Monitoring report 2020: West Quesnel Land Stability Program, Quesnel, BC: A report for City of Quesnel.*

Xie, X., Symans, M. D., O'Rourke, M. J., Abdoun, T. H., O'Rourke, T. D., Palmer, M. C., & Stewart, H. E. (2013). Numerical modeling of buried HDPE pipelines subjected to normal faulting: A case study. *Earthquake Spectra, 29*(2), 609-632.

Yang, Z. X., Jardine, R. J., Zhu, B. T., Foray, P., & Tsuha, C. D. H. C. (2010). Sand grain crushing and interface shearing during displacement pile installation in sand. *Géotechnique, 60*(6), 469-482.

Yimsiri, S., Soga, K., Yoshizaki, K., Dasari, G. R., & O'Rourke, T. D. (2004). Lateral and upward soil–pipeline interactions in sand for deep embedment conditions. *Journal of Geotechnical and Geoenvironmental Engineering, 130*(8), 830-842.

Yu, D., Wang, Y. Y., Liu, B., & Chen, X. (2020). A review of pipe-soil interaction models for strain demand estimation. In *International Pipeline Conference* (Vol. 84454, p. V002T06A016). American Society of Mechanical Engineers.

Zhang, G., Wang, L., & Zhang, J. M. (2011). Dilatancy of the interface between a structure and gravelly soil. *Géotechnique, 61*(1), 75-84.

Zhou, M., Wang, F., Du, Y. J., & Liu, M. D. (2017). Performance of buried HDPE pipes–Part II: total deflection of the pipe. *Geosynthetics International, 24*(4), 396–407.

APPENDIX A: Effects of Backfill Compaction Method on the Axial Pipe-Soil Interaction for Buried Small-Diameter MDPE Pipes

Effects of backfill compaction method on the axial pipe-soil interaction for buried small-diameter MDPE pipes

Thirojan Jayabalasingham[1], Auchib Reza[1], Ashutosh Sutra Dhar[1] and Mujib Rahman[2]
[1]*Department of Civil Engineering, Memorial University of Newfoundland, St. John's, NL, Canada*
[2] *ForisBC Energy Inc.*

ABSTRACT
Polyethylene pipes, widely used in natural gas distribution in North America and worldwide, are prone to damage from ground deformations. They are often subjected to axial ground movements when soil mass moves parallel to the pipe axis. All the previous studies on the axial loading of pipelines were conducted by pulling a pipe through a static soil mass. However, axial force on static pipe against moving soil was not examined. Besides, the backfill soils near existing structures are often compacted using different methods, yet the influence of these compaction techniques on pipe response remains unstudied. This paper presents the results of seven full-scale tests conducted on 42.2 mm and 60.3 mm diameter medium-density polyethylene (MDPE) at Memorial University of Newfoundland. The backfills in the tests were compacted using either a vibratory plate compactor or a hand tamper to investigate the effects of the compaction method on the measured responses. Tests were conducted at two different displacement rates of the soil box (0.5 mm/min and 2 mm/min) to understand the effects of the rate of ground movements on the behaviour of the pipes. During testing, the frictional force, axial strain at the fixed end of the pipe (outside of the box), and pipe elongation were monitored. Results indicated that vibratory compaction provided higher soil resistance, especially in shallow burial depths, despite the relative compaction of the soil is similar. The test results also showed insignificant differences in the pipe axial forces for the displacement rates selected.

RÉSUMÉ
Les tuyaux en polyéthylène, largement utilisés pour la distribution du gaz naturel en Amérique du Nord et dans le monde entier, sont susceptibles d'être endommagés par les déformations du sol. Elles sont souvent soumises à des mouvements axiaux du sol lorsque la masse du sol se déplace parallèlement à l'axe de la conduite. Toutes les études précédentes sur la charge axiale des pipelines ont été menées en tirant un tuyau à travers une masse de sol statique. Cependant, la force axiale sur une conduite statique contre un sol en mouvement n'a pas été examinée. En outre, les sols de remblai à proximité des structures existantes sont souvent compactés à l'aide de différentes méthodes, mais l'influence de ces techniques de compactage sur la réponse des canalisations n'a pas encore été étudiée. Cet article présente les résultats de sept essais en vraie grandeur menés sur du polyéthylène de densité moyenne (MDPE) de 42,2 mm et 60,3 mm de diamètre à l'Université Memorial de Terre-Neuve. Les remblais des essais ont été compactés à l'aide d'un compacteur à plaque vibrante ou d'une dameuse manuelle afin d'étudier les effets de la méthode de compactage sur les réponses mesurées. Les essais ont été menés à deux vitesses de déplacement différentes de la boîte de sol (0,5 mm/min et 2 mm/min) pour comprendre les effets de la vitesse des mouvements du sol sur le comportement des tuyaux. Pendant les essais, la force de frottement, la déformation axiale à l'extrémité fixe du tuyau (à l'extérieur de la boîte) et l'allongement du tuyau ont été contrôlés. Les résultats ont indiqué que le compactage vibratoire offrait une plus grande résistance du sol, en particulier à des profondeurs d'enfouissement peu importantes, bien que le compactage relatif du sol soit similaire. Les résultats du test ont également montré une différence insignifiante dans les forces axiales du tuyau pour les taux de déplacement sélectionnés.

1 INTRODUCTION

Natural gas pipelines are generally divided into two primary categories: distribution and transmission. Both pipelines play an integral role in North America's energy infrastructure. According to PHMSA (2018), there are ~2.54 million miles of natural gas pipelines in the United States, of which distribution lines account for ~87% and transmission lines account for ~12% of total pipe. Distribution pipelines are typically smaller diameter lines with lower pressures that deliver natural gas directly to local homes and businesses. At present, plastic pipes are the most common type of pipe used in the gas distribution network. Among them, medium-density polyethylene (MDPE) pipes are widely used in distribution networks due to their favourable properties, such as flexibility, durability, lightweight, and resistance to corrosion and aging (PHMSA, 2018). Over two decades, from 1999 to 2019, there were 1,438 reported incidents related to natural gas distribution pipelines (Williams and Glasmeier, 2023), including corrosion, material fatigue, and external damage from activities like accidental digging and ground movements. Ground deformation hazards such as landslides, soil liquefaction, uplift, subsidence, and tectonic fault movements often threaten the structural integrity of the pipelines and the safety of the surrounding geoenvironments. (Psyrras and Sextos, 2018).

For pipeline integrity assessments, slope inclinometers and vibrating wire piezometers are often utilized to monitor ground movements and pore water pressures in landslide-prone locations. Survey-based technologies such as GPS units and survey prism (Groves and Wijewickreme, 2013; Ferreira and Blatz, 2021) and remote sensing technology such as LiDAR, InSAR, UAV photogrammetry and laser scanning also accompanied the monitoring of ground movements. However, estimating the pipe conditions using the measured ground movements is still very challenging. Pipe responses (e.g., pipe wall strain) to ground movements are generally calculated using beam-on-spring analysis for a known (measured) ground displacement (ALA, 2005; PRCI, 2017). The design guidelines proposed elastic-perfectly plastic parameters for axial, lateral, and vertical springs. These springs are developed based on small-scale laboratory tests of rigid pipes. The applicability of spring parameters developed based on rigid pipes for flexible pipes was not well-validated.

Although some experimental studies have been conducted to investigate the response of flexible (HDPE and MDPE) pipes under axial loading (Weerasekara and Wijewickreme, 2008; Bilgin and Stewart, 2009; Wijewickreme and Weerasekara, 2015; Reza and Dhar, 2021a, 2021b; Reza et al., 2023), more field and laboratory testing data for flexible pipes are required for pipe burial conditions and ground movement scenarios expected in the field. Bilgin and Stewart (2009) measured the effects of reductions in pipe diameter on the interface shearing resistance between the pipe and soil. Weerasekara and Wijewickreme (2008) and Reza et al. (2023) reported force-displacement relations from axial pullout tests of MDPE pipes in dense sand. They found that the axial forces increase with displacements until reaching peak values and then decrease. Wijewickreme and Weerasekara (2015) developed analytical formulations, assuming that individual pipe sections would be subjected to different levels of interface shear displacements, to simulate the test results of pipe strains. Reza and Dhar (2021a and 2021b) conducted axial pullout tests with different rates of pulling and proposed pulling rate–dependent interface friction coefficients to account for the rate effects.

In all the above studies, tests were conducted by pulling a pipe through a static soil mass, referred to as "Pipe-Pull". However, axial force on static pipes against moving soil, referred to as "Soil-Pull", was not extensively examined. It generally assumed that pipe-pull and soil-pull would have the equal effects on the pipes. The assumption of equality implies that the soil's shear resistance encountered by the moving pipe is equivalent to the shearing force due to the soil movement. While this assumption of equal forces might be useful for conceptual analysis, real-world conditions (where soil moves against fixed pipes) may involve complexities, leading to differences in the measured forces. For instance, as soil displaces, finer particles could occupy the spaces between larger particles, thereby increasing the contact area with the interface structure (Yang et al., 2010). Particles near the interface may also exhibit rolling and overriding of neighbouring particles during shearing, which could result in non–uniform particle displacement around the pipe. On the other hand, soil particles at the interface may not move at all during pipe-pull, particularly for a smooth pipe like MDPE. Therefore, the contact pressure between the soil and the pipe could differ significantly in each scenario (pipe pullout and soil box displacement). In order to examine the possible distinctions between the two methods, the current study compares the behaviour of MDPE pipes subjected to pipe pullout and soil box displacement obtained using the testing facility at Memorial University of Newfoundland.

2 MOTIVATION

2.1 Compaction-Induced Stresses on Buried Pipes

Gas distribution pipelines are usually buried below the ground surface at depths of less than one meter (Ferreira and Blatz, 2021). The backfills are sometimes compacted when these pipelines are located near existing structures or below the road embankments. Compacting the backfill soil adjacent to the structure can be substantial for pipes and culverts buried shallowly (Taleb and Moore, 1999; Elshimi and Moore, 2013). During compaction, the vertical and horizontal earth pressures increase in soil mass due to force or energy transferred by compaction equipment. After compaction, as the compaction equipment moves away, both pressures undergo a reduction; however, these remained noticeably higher than the precompaction values in the horizontal direction, and the vertical value was reduced to the overburden pressure value (Duncan and Seed 1986; Chen and Fang, 2008). Near the surface, depending on the compaction loads, the residual lateral pressures can be as high as the passive earth pressure values. At greater depths, the horizontal earth pressure converged with the earth pressure at rest.

Different compaction methods are generally used in practice during the placement of pipes in the field. The stresses induced due to compaction also depend on the equipment used for compaction, e.g. manual compaction with tampers, static rollers, vibrating plate tampers and rammers (Duncan et al., 1991). Several authors explored the compaction-induced lateral pressures experimentally (Rehman and Broms, 1972; Carder et al., 1977; Carder et al., 1980; Duncan et al., 1991; Clayton et al., 1991; Clayton and Symons, 1992; Massarsch and Fellenius, 2002; Gui et al., 2020; Ezzeldin et al., 2022) and through finite element analysis (Katona et al., 1976; Taleb and Moore, 1999; Elshimi and Moore, 2013; Dezfooli et al., 2015; Ezzeldin and El Naggar, 2021; Saleh et al., 2021; Ezzeldin and El Naggar, 2022; Vilca et al., 2024). Table 1 summarizes the resulting horizontal stresses on the buried structure caused by backfill compaction. More recently, Reza and Dhar (2024) employed compaction-induced lateral earth pressure in the three-dimensional finite-element (FE) analysis that successfully simulated the measured pipe response obtained during the axial movements of pipes in dense sand. However, the current design guidelines (ALA, 2005; PRCI, 2017) do not account for the effect of backfill compaction to estimate the maximum axial soil resistance of pipes subjected to axial ground movement.

2.2 Ground Movement Rate and Relaxation Behaviour of MDPE Pipes

Landslides are inherently complex geological processes that can vary widely in their characteristics, including speed, volume, and type of movement (Cheaib et al., 2022). The effects of the rate of ground movements and the pipe–soil relaxation mechanisms are the two crucial factors for understanding the interaction between soil and buried pipelines, especially for MDPE pipes, as they show nonlinear time–dependent stress–strain behaviour (Bilgin et al., 2007; Das and Dhar 2021). Ferreira and Blatz (2021) measured an average downslope ground movement of 25 to 40 mm/year at active landslide areas in western Manitoba. Groves and Wijewickreme (2013) recorded an even slower-moving landslide, a total ground movement of 450 mm over seven years, with an average rate of 5 mm/month in a subdivision in British Columbia. These landslides are considered very slow-moving landslides according to the classification system in Cruden and Varnes (1996). However, slow-moving landslides may become very rapid-moving landslides due to earthquakes, as reported in Cheaib et al. (2022). The rate of ground movement fluctuates with the seasons, increasing during periods of high precipitation or snow melting and decreasing in drier periods (Keefer and Johnson, 1983). Furthermore, ground movement occurs intermittently, with periods of inactivity followed by reactivation of slow-moving landslides, often triggered by heavy rainfall or ice and snow melting (Wood Environment & Infrastructure Solutions, 2021). The relaxation during the inactive period of a landslide may help to reduce the imposed stresses due to the forces from the moving ground (Bruschi et al., 1995; Scarpelli et al., 1995). The ground movement rate can differ from place to place and even within the same area, with stress relaxation at the pipe–soil interaction. Hence, the effect of ground movement rates and relaxation behaviour on the axial response of buried MDPE pipelines should be examined thoroughly.

Reza and Dhar (2021a and 2021b) and Reza et al. (2023) experimentally investigated the pulling rate effects (0.5 mm/min to 2 mm/min) on the axial pullout behaviour of MDPE pipes, revealing the rate-dependency of the interface frictional behaviour. Weerasekara (2011) and Reza (2024) investigated the impact of stress relaxation in MDPE pipes by stopping the pipe pulling for 9–10 days, during axial pullout tests. It was found that the measured pullout resistance dropped significantly, and the pipe wall strains were redistributed along the pipe length during the relaxation period (over 9–10 days).

To this end, the current study aimed to examine the effect of backfill compaction methods on the axial pullout response of the buried MDPE pipes. Full-scale laboratory tests were conducted with different diameter pipes, pulling rates, compaction techniques, and burial depths. Furthermore, successive soil pulls were performed with relaxation periods between them to observe pipe behaviour during simulated consecutive ground movement events. The mobilization of axial soil resistance, elongation of the pipe, and strains at the pipe's restrained end outside the soil box were monitored during the tests.

Table 1. Summary of compaction-induced horizontal stresses on the buried structures

Source	Compaction Method	Soil Type	Maximum Induced-Stress (kPa)	Depth (m)	Remarks
Rehman and Broms (1972)	Loose	Gravelly Sand	21	0.75	Due to the wheel loads of 7.5 tons
	Vibratory Plate	Gravelly Sand	7.6	0.75	
	Loose	Silty Fine Sand	12.8	0.75	
	Vibratory Plate	Silty Fine Sand	6	0.75	
Carder et al. (1977)	Twin–roll Vibratory Roller	Clean Medium Sand	11.3	0.83	
Carder et al. (1980)	Static Roller	Silty Clay	14.5	0.83	
Duncan and Seed (1986)	Single Drum Roller	Sand	25.7	0.22	Roller 0.3 m away from wall
		Sand	54.6	0.17	Roller 0.15 m away from wall
Clayton et al. (1991)		Medium to high plasticity clay	0.2 to 0.4 times C_u		
Clayton and Symons (1992)		Clay	0.8 times C_u		
Chen and Fang (2008)	Vibratory Plate	Air-dry Ottawa Sand	7.6	0.25	
Gui et al. (2020)	Vibratory Plate		28.6		
	Vibratory Roller		30.6		
Ezzeldin et al. (2022)	Vibratory Plate	Air-dry Ottawa Sand	5.9	0.45	
Katona et al. (1976)			34.5		Applied vertical pressure to simulate compaction
Taleb and Moore (1999)		Granular	Rankine Passive Earth Pressure		Upper limit for induced-stress

Elshimi and Moore (2013)			Kneading coefficient times Rankine Passive Earth Pressure	Upper limit for induced stress
Dezfooli et al. (2015)		Cohesive Soil	0.5 times C_u	
Ezzeldin and El Naggar (2021)			15 to 30	Applied surface loading to simulate compaction
Ezzeldin and El Naggar (2022)			10 to 40	Applied surface loading to simulate compaction
Vilca et al. (2024)		Cohesive Soil	0.8 times C_u	
Saleh et al. (2021)	Jumper Jack		Distributed strip load	
	Embedment Wheel		Distributed line load	

3 AXIAL PULLOUT TEST

3.1 Test Facility

Test facility developed at the Memorial University of Newfoundland was used to conduct the full-scale axial soil–pipe interaction tests. The facility allows a soil block to move against a pipe fixed at one end (Andersen and Dhar, 2023), thus simulating conditions anticipated during actual ground movement. Using the test facility, the axial pipe–soil interaction behaviour was investigated for small-diameter MDPE pipes buried in sand. The test facility includes a steel tank with internal dimensions of 4 m x 2 m x 1.5 m (Length x Width x Height), which can accommodate various burial depths for the pipes. A hydraulic actuator system pulls the soil tank at different rates, simulating the different rates of ground movements. The moving mechanism features a carriage frame sliding on linear bearings between a base frame, providing movement with a travel limit of 300 mm. Instrumentation included load cell, LVDT, and electrical strain gauges. All instruments were connected to a data acquisition system with a personal computer for simultaneous data recording. The soil box's width is sufficiently large to reduce boundary effects during the axial pullout tests (Reza and Dhar, 2021a). More detailed information on the current test facility can be found in Andersen and Dhar (2023).

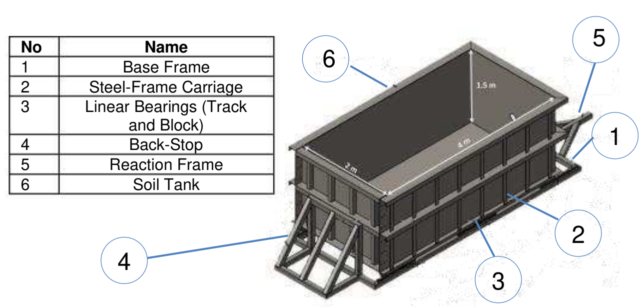

Figure 1. Schematic diagram of the test facility (after Andersen and Dhar, 2023)

During tests, the soil box was pulled at either 0.5 mm/min or 2 mm/min by a hydraulic ram with a maximum displacement of 90 mm in one direction. A 22.5 kN capacity pancake load cell was positioned between the pipe's fixed end and the backstop frame of the test facility. This load cell measured the axial forces developed during the movement of the box. LVDTs (capacity of 110 mm) and String Potentiometers (capacity of 500 mm) were attached to the pipe's free and fixed ends to measure pipe elongation. An electrical resistivity strain gauge was also attached on the pipe's crown (outside the soil box) near the fixed end to monitor the pipe's axial strain during testing. However, results of the strain gauges are not reported here due to brevity. Figure 1 presents the schematic layout of the current test facility.

3.2 Sand Backfill

Locally available well-graded sand was used as the backfill material for the experiments. This sand is manufactured through mechanically crushing rocks (Saha, 2021). This material comprises about 1.3% fines and 98.7% sand particles. The maximum dry density is estimated as 18.8 kN/m^3, using standard Proctor compaction tests (ASTM D698, ASTM 2003; Saha et al. 2019). The sand has an average particle size of 0.742 mm and a coefficient of uniformity of 5.81. The authors determined the minimum and maximum dry density as 16.6 kN/m^3 and 19.6 kN/m^3, respectively, according to ASTM D4254-16 and ASTM D4253-16e1, which implies the corresponding maximum and minimum void ratios of 0.55 and 0.31, respectively. Particle size analysis tests were also performed in accordance with ASTM D6913-17 to examine if the repeated use of the sand changes its grain size distribution. The resulting grain size distribution curve, shown in Figure 2, closely matched those reported by Saha et al. (2019). This consistency confirms that the soil particles remain intact, not fragmenting into smaller particles, despite repeated use for full-scale tests involving different levels of compaction.

During backfilling, the soil is placed in layers of approximately 100 mm to 150 mm thickness to achieve the desired burial depth. The soil was compacted using either a battery-operated vibrating plate tamper (Wacker Neuson APS1135e) or a hand tamper to achieve the required density (Figure 3). Before starting the test, the in-situ sandcone density tests (in accordance with ASTM D1556-2016) were performed at the top layer of soil to measure the soil densities. The average calculated soil density for the test compacted with a vibrating plate tamper was 18.1 kN/m^3 (96% relative compaction), whereas, for compaction with a hand tamper was 17.5 kN/m^3 (93% relative compaction). The moisture content was measured between 1% and 1.5% for all the tests reported in this paper.

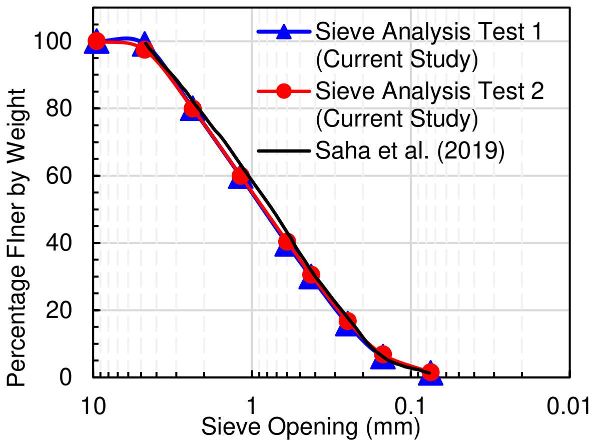

Figure 2. Particle size distribution of backfill sand (after Saha et al., 2019)

(a) (b)

Figure 3. Two different compaction methods: (a) Battery operated vibrating plate tamper (Wacker Neusor APS1135e) and (b) Manual hand tamper

3.3 Pipe Material

The current study used CSA B137.4 certified MDPE pipes with 42.2 mm and 60.3 mm outer diameters with wall thicknesses of 4.22 mm and 5.48 mm, respectively. These dimensions correspond to standard dimension ratios (SDR) of 10 and 11 for 42.2 mm and 60.3 mm diameter pipes, respectively. The stress–strain responses of MDPE pipe material are highly nonlinear and strain rate–dependent (Das and Dhar, 2021b). Das and Dhar (2021b) reported that the effect of strain rate on the stress–strain responses become negligible at rates below 10^{-6}/s. The frictional interface between the outer surface of the pipe and sand depends on the roughness of the pipe and the sand property. Considering the smooth polymer surface, the interface friction angle is recommended to be 60% of the peak friction angle of soil (ϕ′) (ALA, 2005; PRCI, 2017). However, Reza and Dhar (2021a) reported that the interface friction angle for MDPE pipe materials in sand depends on the pipe pulling rates. They found the interface friction angles as 75%ϕ′, 86%ϕ′, and 90%ϕ′, corresponding to the pulling rates of 0.5, 1, and 2 mm/min, respectively. All the tests conducted for the current study were carried out at an ambient temperature of around 20 °C

3.4 Test Program

A total of seven axial pullout tests were performed for the current study. Five tests (Test 1–5) were conducted at a burial depth of 625 mm (measured from the pipe springline to the top surface). Two additional tests were conducted with burial depths of 340 mm (Test 6) and 480 mm (Test 7) for 42.2 mm and 60.3 mm diameter pipes, respectively. The later two tests were performed to directly compare with the pipe pull tests previously done using the same testing facility and backfill materials (Reza et al., 2023). In Tests 1 to 4, compaction of the backfill was achieved using a vibratory plate tamper, whereas in Tests 5 to 7, a manual hand tamper was utilized for the compaction process.

4 TEST RESULTS AND DISCUSSION

4.1 Force–Displacement Responses

Figure 4 plots the load–displacement responses for Tests 1–4 conducted with two different pipe sizes with two different displacement rates. Note that the load was applied to the pipe by the moving soil and measured by the load cell at the fixed end (i.e., reaction force). Once the tank moved 10 mm (as planned), it was kept in the same place for 20 minutes, giving the pipe and system a relaxation period. After that, soil tank pulling resumed until 90 mm of tank movement was reached. As seen in the figure, the load (i.e., axial soil force) increases nonlinearly with the tank displacements. The nonlinearity is associated with the progressive mobilization of interface shearing resistance, starting from the fixed end towards the free end. This mechanism was explored earlier by Chakraborty et al. (2023) using the fibre optic sensors on the pipes.

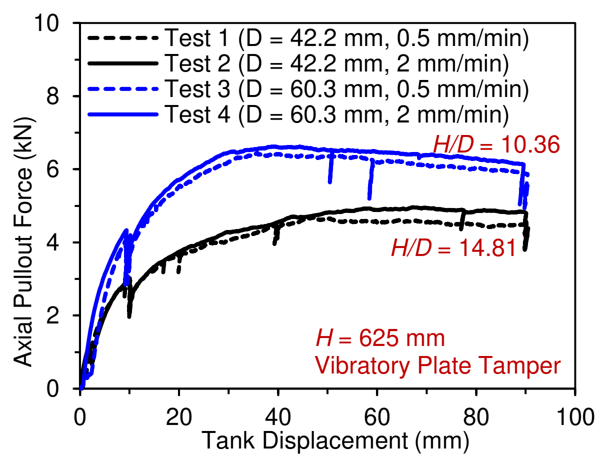

Figure 4. Axial pullout force–displacement responses

The effects of successive pulling on axial resistance are also evident in Figure 4. Once the tank's movement stops at 10 mm, the axial force decreases immediately by about 1–1.5 kN and remains steady for the rest of the time. Although there is an immediate reduction of the axial force, no reduction of axial force was observed during relaxation period (20 mins). However, the force may continue to decrease with a longer relaxation time due to time–dependent property of the pipe material. The immediate drop of axial force is associated with redistribution of stresses due to stopping of the tank movement, which can depend on the condition on the hydraulic system (hold the tank in position or shut down hydraulic system to release the tank) (Anderson, 2024). In the current study, the hydraulic system was kept running to keep the soil tank in position. During reloading, the axial force increased following the unloading path and continued further until the pipe–soil interface shear strength was fully mobilized throughout the pipe length. After full mobilization (when shear strength mobilized up to the free end), the pulling forces are slightly reduced, demonstrating a little release of the load from the pipe to the surrounding soil.

4.2 Effects of Pulling Rate

Figure 4 also illustrates the effect of soil displacement rates on the pipe's axial resistance to movement. Negligible differences in the resistances were observed for both pipes for increasing the pulling rates from 0.5 mm/min to 2 mm/min. However, Wijewickreme and Weerasekara (2015), Reza and Dhar (2021a), and Reza et al. (2023) reported that the pipe pulling rate significantly affects the pullout force of the buried MDPE pipes pulled against static soil. The higher the pulling rate, the higher the peak pullout force. The rate effect was believed to be due to the nonlinear time-dependent properties of the pipe material, which is more significant when the pipe is pulled against static soil.

4.3 Effects of Backfill Compaction Methods

Figure 5 shows the comparison of axial soil resistances for 42.2 mm diameter pipes with different compaction efforts (vibratory plate tamper in Test 1 and hand tamper in Test 5). Other conditions were the same for Tests 1 and 5. The results show that the compaction with the vibratory plate tamper provided higher axial resistance (nearly 25% higher) than the hand tamper. This could be attributed to the additional soil stresses as "locked-in" compaction-induced stresses on the pipe surface. Previously, measurements of compaction-induced earth pressure on the nondeflecting soil–structure interfaces indicate that the residual horizontal earth pressure of compacted backfill depends on the types of the compactor (such as rollers, vibratory, and rammer plates) (Duncan and Seed 1986; Duncan et al. 1991). Thus, in Tests 1 and 5, the different ways of compacting the backfill soil may influence the normal stresses on the pipes, which can essentially differ the shear resistance of the pipe during soil displacement.

The effects of compactor on the soil resistances are also shown in Figure 6. In Figure 6, the results of Test 3, compacted using vibratory plate tamper, is compared with the test results reported in Weerasekara and Wijewickreme (2008), compacted using 0.5t static roller. Both the tests were performed on 60.3 mm diameter MDPE pipes, buried at almost similar depths, and pulled at nearly a similar displacement rate. Buried pipe length was 4 m in Test 3 and 3.8 m in Weerasekara and Wijewickreme (2008). Despite the similarities in the test conditions, the results are normalized by the pipe diameter, length, buried depth, and sand density in Figure 6. It shows that the normalized axial pullout forces from the test with vibratory plate tamper are higher than forces from tests with 0.5t static roller compaction. The difference in the compaction-induced lateral stresses on the pipes between the two methods of compaction might be attributable to the above observation. It should be mentioned here that the test reported in Weerasekara and Wijewickreme (2008) was performed by pulling the pipe, whereas the soil mass was displaced in Test 3. The comparison between the results of the pipe-pull and soil-pull is discussed in detail in the next section.

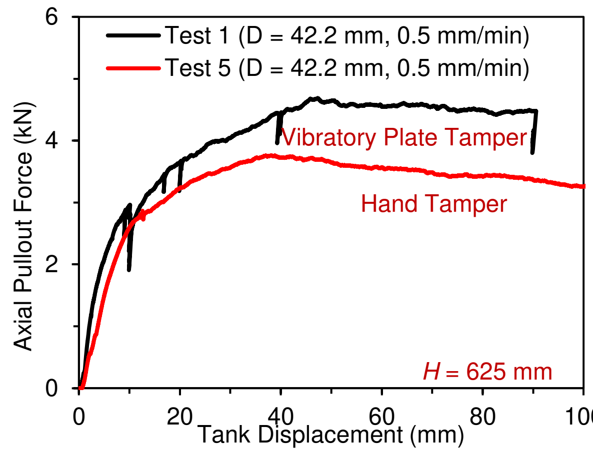

Figure 5. Axial pullout force–displacement responses for different compaction techniques

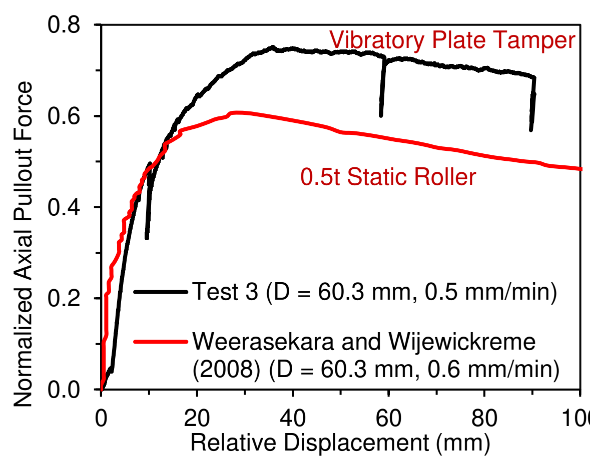

Figure 6. Normalized axial pullout force–displacement responses for different compaction techniques

4.4 Pipe-pull versus Soil-pull

Axial pullout forces obtained from soil-pull and pipe pull (Reza and Dhar 2023) tests are compared in Figure 7. In the pipe pullout test, the pipe's leading end is pulled, which is equal to the elongation of the pipe (until the trailing end of the pipe moves). However, in the soil pull test, the pipe elongation is estimated based on the difference between the two LVDT readings, one placed at the pipe fixed end and the other at the free end. Therefore, axial forces are plotted against the pipe elongation in Figure 7 for comparison. For all the tests, the H/D ratio was 8, with burial depths of 340 mm and 480 mm for the pipe diameter of 42.2 mm and 60.3 mm, respectively. Similar compaction efforts with hand tamper were employed for the tests. The pipe pullout rate and soil box displacement rate were also kept the same for the tests.

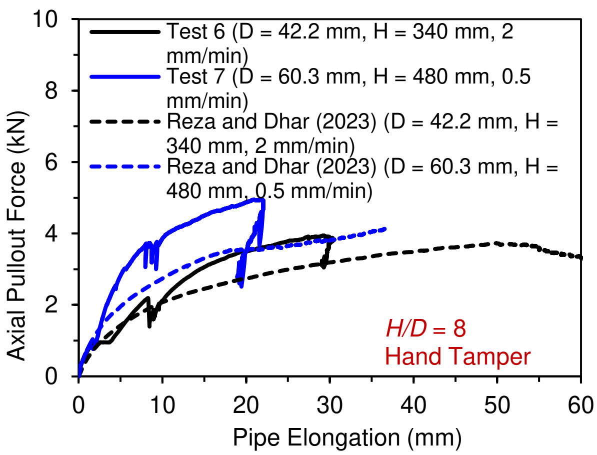

Figure 7. Pipe-pull comparison with soil-pull

As seen in Figure 7, the axial resistances were higher for the soil box displacements compared to the pipe pullout tests. The differences in peak force between the two mechanisms are higher for the 60.3 mm-diameter pipes. During the whole soil mass displacement, finer soil particles have the potential to settle into the voids among the larger soil particles, leading to an increased contact area at the pipe–soil interface. Consequently, the shear forces might be higher for the soil pullout, causing the higher pulling forces.

5 CONCLUSIONS

The following conclusions are drawn from this study:

- The axial force of pipe nonlinearly increased with tank displacement until the pipe–soil interface shear strength was fully mobilized over the pipe length, starting from the fixed end to free end of the pipe. When the interface shear stresses reach the free end, the pipe resistances are slightly reduced due to a release of the load from the pipe to the surrounding soil.
- The effect of tank displacement rates on the axial resistance of MDPE pipes is less significant compared to the pipe pullout rates previously reported for the similar pipes.
- The peak pipe axial resistance is nearly 25% higher for the backfill compaction with vibratory plate tampers compared to the hand tampers, regardless of the similar relative compaction values of the backfill soil.
- The actual mechanism of the pipe pullout tests and soil pullout tests is different, resulting in higher resistances during the tank displacement tests. The difference between the two testing setup is significant for the larger (i.e., 60.3 mm) diameter pipes.

6 ACKNOWLEDGEMENTS

This research study received funding from the Alliance Grants program of the National Science and Engineering Research Council of Canada. Financial and in-kind support from FortisBC Energy Inc. and SaskEnergy Canada Inc., and in-kind support from WSP Canada Inc. are gratefully acknowledged. The authors would like to express their gratitude for the valuable technical and laboratory assistance provided by the research group and laboratory technicians.

7 REFERENCES

ALA (American Lifelines Alliance). (2005). *Guidelines for the design of buried steel pipe.* Federal Emergency Management Agency (FEMA), Washington, DC, USA and American Society of Civil Engineers (ASCE), Reston, VA, USA.

Andersen, D., & Dhar, A. S., (2023). Investigation of small-diameter steel pipes subjected to axial ground movement. *In Annual conference of Canadian Geotechnical Society, GeoSaskatoon2023, Saskatchewan, Canada.*

Anderson, C. D. (2004). *Response of buried polyethylene natural gas pipelines subjected to lateral ground displacement* (Doctoral thesis, University of British Columbia).

Bilgin, Ö., Stewart, H. E., & O'Rourke, T. D. (2007). Thermal and mechanical properties of polyethylene pipes. *Journal of Materials in Civil Engineering,* 19(12), 1043-1052.

Bilgin, Ö., & Stewart, H. E. (2009). Design guidelines for polyethylene pipe interface shear resistance. *Journal of geotechnical and geoenvironmental engineering*, 135(6), 809-818.

Bruschi, R., Tomassini, D., Cuscana, S., and Venzi, S. 1995. Failure modes for pipelines in landslide areas. *In Proceedings of the 14th International Conference on Offshore Mechanics and Arctic Engineering, Copenhagen, Denmark.* American Society of Mechanical Engineers, New York, NY. pp. 65–78.

Carder, D. R., Pocock, R. G., & Murray, R. T. (1977). *Experimental retaining wall facility-Lateral stress measurements with sand backfill* (No. TRRL Lab Report 766). Transport and Road Research Laboratory,

Crowthorne, Berkshire, United Kingdom.
Carder, D. R., Murray, R. T., & Krawczyk, J. V. (1980). *Earth pressures against an experimental retaining wall backfilled with silty clay* (No. LR 946 Monograph). Transport and Road Research Laboratory, Crowthorne, Berkshire, United Kingdom.
Chakraborty, S., Anjum, S., Dhar, A.S., and Rahman, M., (2023). Loading-unloading-reloading responses of MDPE pipes in sand subjected to axial ground movement *In Annual conference of Canadian Geotechnical Society, GeoSaskatoon.*
Cheaib, A., Lacroix, P., Zerathe, S., Jongmans, D., Ajorlou, N., Doin, M. P., ... & Abdallah, C. (2022). Landslides induced by the 2017 Mw7. 3 Sarpol Zahab earthquake (Iran). *Landslides,* 19(3), 603-619.
Chen, T. J., & Fang, Y. S. (2008). Earth pressure due to vibratory compaction. *Journal of Geotechnical and Geoenvironmental Engineering,* 134(4), 437-444.
Clayton CRI, Symons IF and Heidra-Coho JC (1991). 'The pressure of clay backfill against retaining structures'. *Canadian Geotechnical Journal*, 28, 2, 309-315.
Clayton, C. R. I., & Symons, I. F. (1992). The pressure of compacted fill on retaining walls. *Géotechnique,* 42(1), 127-130.
Cruden, D. M., & Varnes, D. J. (1996). *Landslides: Investigation and Mitigation. Chapter 3—Landslides Types and Processes.* Transportation research board special report, 247.
Das, S., & Dhar, A. S. (2021). Nonlinear time-dependent mechanical behaviour of medium-density polyethylene pipe material. *Journal of Materials in Civil Engineering*, *33*(5), 04021068.
Dezfooli, M. S., Abolmaali, A., & Razavi, M. (2015). Coupled nonlinear finite-element analysis of soil–steel pipe structure interaction. *International Journal of Geomechanics*, 15(1), 04014032.
Duncan, J. M., & Seed, R. B. (1986). Compaction-induced earth pressures under K0-conditions. *Journal of Geotechnical Engineering*, 112(1), 1-22.
Duncan, J. M., Williams, G. W., Sehn, A. L., & Seed, R. B. (1991). Estimation earth pressures due to compaction. *Journal of geotechnical engineering*, *117*(12), 1833-1847.
Elshimi, T. M., & Moore, I. D. (2013). Modeling the effects of backfilling and soil compaction beside shallow buried pipes. *Journal of Pipeline Systems Engineering and Practice*, *4*(4), 04013004.
Ezzeldin, I., & El Naggar, H. (2021). Three-dimensional finite element modeling of corrugated metal pipes. *Transportation Geotechnics*, *27*, 100467.
Ezzeldin, I., & El Naggar, H. (2022). Numerical Modelling of Induced Stresses in Buried Corrugated Metal Structures due to Compaction Efforts. *Transportation Geotechnics*, *32*, 100706.
Ezzeldin, I., El Naggar, H., & Newhook, J. (2022). 3D numerical modelling of earth pressures on a non-yielding rigid wall due to compaction efforts. *In Annual conference of Canadian Geotechnical Society, GeoCalgary2022, Alberta, Canada.*
Ferreira, N. J., & Blatz, J. A. (2021). Measured pipe stresses on gas pipelines in landslide areas. *Canadian Geotechnical Journal*, *99*(999), 1855-1869.
Groves, J., & Wijewickreme, D. (2013). Field monitoring of buried polyethylene natural gas pipelines subjected to ground movement. *Proc., GéoMontréal*, *7*.
Gui, M., Phan, T., & Pham, T. (2020). Impacts of Compaction Load and Procedure on Stress-Deformation Behaviors of a Soil Geosynthetic Composite (SGC) Mass—A Case Study. *Applied Sciences*, *10*(18), 6339.
Katona, M. G., Smith, J. M., Odello, R. S., and Allgood, J. R. (1976)."*CANDE–A modern approach for the structural design and analysis of buried culverts*." Final Rep. No. FHWA-RD-77-5.
Keefer, D. K., & Johnson, A. M. (1983). *Earth flows: morphology, mobilization, and movement.* Professional Paper.
Massarsch, K. R., & Fellenius, B. H. (2002). Vibratory compaction of coarse-grained soils. *Canadian Geotechnical Journal*, *39*(3), 695-709.
PHMSA (Pipeline and Hazardous Materials Safety Administration). (2018). *Pipeline Safety: Safety of Gas Distribution Pipelines and Other Pipeline Safety Initiatives.* Department of Transportation. (DOT). 49 CFR Parts 191, 192, and 198 [Docket No. PHMSA–2018–0046] RIN 2137–AF53.
PRCI (Pipeline Research Council International). (2017). *Pipeline seismic design and assessment guideline*. Catalogue No: PR-268-134501-R01. Chantilly, VA, USA: PRCI.
Psyrras, N. K., & Sextos, A. G. (2018). Safety of buried steel natural gas pipelines under earthquake-induced ground shaking: A review. *Soil Dynamics and Earthquake Engineering*, *106*, 254-277.
Rehnman, S. E., & Broms, B. B. (1972). Lateral pressures on basement wall. Results from full-scale tests. In *Fifth Eur Conf On Soil Proc*.
Reza, A., & Dhar, A. S. (2021). Axial Pullout Behavior of Buried Medium-Density Polyethylene Gas Distribution Pipes. *International Journal of Geomechanics*, *21*(7), 04021120.
Reza, A., & Dhar, A. S. (2021). Effects of Axial Relative Ground Movement on Small Diameter Polyethylene Piping in Loose Sand. *Infrastructures*, *6*(12), 168.
Reza, A., Dhar, A. S., & Rahman, M. (2023). Strain assessment of polyethylene pipes in dense sand subjected to axial displacement. *Geosynthetics International*, 1-18.
Reza, A. (2023*). Investigation of axial pullout behaviour of small diameter medium-density polyethylene pipes in sand.* Doctoral (PhD) thesis, Memorial University of Newfoundland.
Reza, A. and Dhar, A.S. (2024). Finite-element modelling of axial movements of polyethylene pipes in dense sand. (under review)
Saha, R. C., Dhar, A. S., & Hawlader, B. C. (2019). Shear strength assessment of a well-graded clean sand. In *Annual conference of Canadian Geotechnical Society, GeoSt. John's*.
Saha, R.C. (2021) *Shear strength assessment of a manufactured well-graded sand.* Masters thesis, Memorial University of Newfoundland.
Saleh, A. E., Jalali, H. H., Pokharel, A., & Abolmaali, A. (2021). Deformation of buried large diameter steel pipes during staged construction and compaction-case study

and finite element analysis. *Transportation Geotechnics*, *31*, 100649.

Scarpelli, G., Aleotti, P., Baldelli, P., Milani, G., and Brambati, E. 1995. Field experience of pipelines in geologically unstable areas. *In Proceedings of the 14th International Conference on Offshore Mechanics and Arctic Engineering, Copenhagen, Denmark*. American Society of Mechanical Engineers, New York, NY. pp. 65–78.

Taleb, B., & Moore, I. D. (1999). Metal culvert response to earth loading: performance of two-dimensional analysis. *Transportation Research Record*, *1656*(1), 25-36.

Vilca, N. S., Gómez-Amador, A. M., & Jiménez de Cisneros Fonfría, J. J. (2023). Soil–Structure Interaction Analysis Using the Finite Element Method in Thin-Walled Steel Pipes Buried under Haul Roads. *Applied Sciences*, *14*(1), 167.

Weerasekara, L., & Wijewickreme, D. (2008). Mobilization of soil loads on buried, polyethylene natural gas pipelines subject to relative axial displacements. *Canadian Geotechnical Journal*, *45*(9), 1237-1249.

Weerasekara, L. (2011). *Pipe-soil interaction aspects in buried extensible pipes* (Doctoral dissertation, University of British Columbia).

Wijewickreme, D., Karimian, H., & Honegger, D. (2009). Response of buried steel pipelines subjected to relative axial soil movement. *Canadian Geotechnical Journal*, *46*(7), 735-752.

Wijewickreme, D., & Weerasekara, L. (2015). Analytical modeling of field axial pullout tests performed on buried extensible pipes. *International Journal of Geomechanics*, *15*(2), 04014044.

Williams, D. A., & Glasmeier, A. K. (2023). Evaluation of error across natural gas pipeline incidents. *Risk Analysis*, 43, 1079-1091.

Wood Environment & Infrastructure Solutions. (2021). *Monitoring Report 2020: West Quesnel Land Stability Program, Quesnel, BC:* a report for City of Quesnel

Yang, Z. X., Jardine, R. J., Zhu, B. T., Foray, P., & Tsuha, C. D. H. C. (2010). Sand grain crushing and interface shearing during displacement pile installation in sand. *Géotechnique*, *60*(6), 469-482.

APPENDIX B: Earth Pressure Measurements with Low-Pressure Transducers

B.1 Introduction

In geotechnical and pipeline engineering, accurate measurement of earth pressures around buried pipes is crucial for understanding the pipe-soil interaction mechanisms, especially under conditions like backfilling and compaction. Several researchers explored the compaction-induced lateral pressures experimentally (Rehman and Broms, 1972; Carder et al., 1977; Carder et al., 1980; Duncan and Seed, 1986; Duncan et al., 1991; Clayton et al., 1991; Clayton and Symons, 1992; Massarsch and Fellenius, 2002; Chen and Fang, 2008; Gui et al., 2020; Ezzeldin et al., 2022). As part of the full-scale axial pullout tests conducted on buried MDPE pipes, a dedicated test was designed to measure the lateral earth pressures induced during backfilling and compaction. This appendix details the experimental procedures, equipment, and observations related to the lateral earth pressure measurements, with a focus on capturing compaction-induced stresses using low-pressure transducers.

B.2 Objective

This test aims to quantify the lateral earth pressures exerted by soil during backfilling and compaction, serving as a baseline for understanding the earth pressures likely to develop in the soil surrounding buried MDPE pipes. Without the influence of a pipe's geometry or material properties, this test provides insight into pure soil behaviour under compaction-induced stress conditions. The data are intended to support the main full-scale axial pullout tests by clarifying how soil pressures evolve during compaction.

B.3 Experimental Setup

The test setup used for the full-scale axial pullout tests was utilized for the dedicated earth pressure measurement test. The backfill sand properties were described in Chapter 3 of this thesis. The moisture content of the backfill sand was maintained below 2%, similar to that in full-scale axial pullout tests. The three low-pressure transducers (refer to section 3.2.2.6 for details) were used to capture the lateral pressure variation during the backfilling and compaction stages. These pressure sensors, previously validated by Chen and Fang (2008), effectively captured vertical and horizontal earth pressure fluctuations in air-dried Ottawa sand during similar compaction processes.

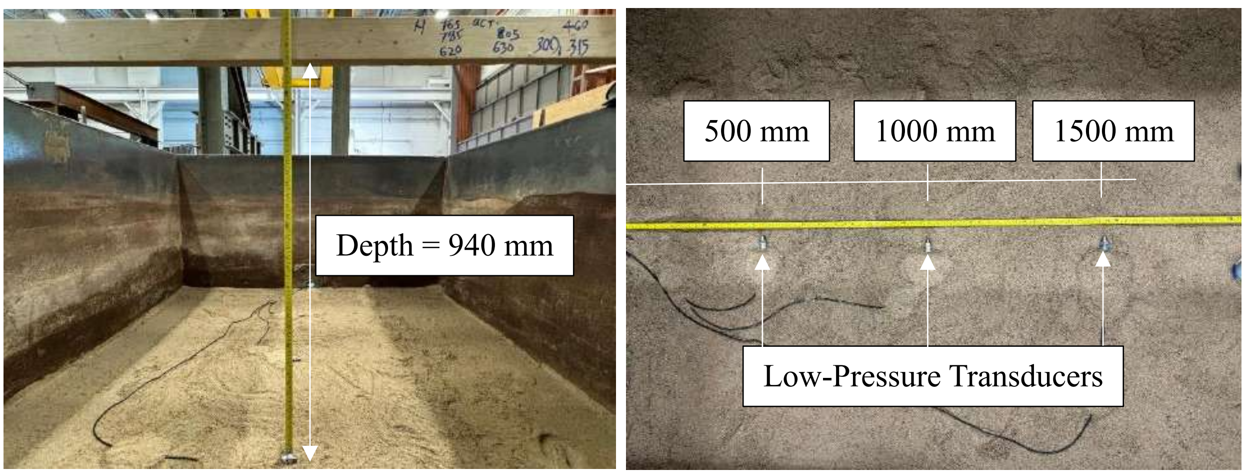

(a) (b)

Figure B-1: Arrangement of low-pressure transducers: (a) At a depth of 940 mm from top of the tank. (b) Along the pipe centerline 500 mm, 1000 mm, and 1500 mm away from the tank wall.

For the current study, as illustrated in Figure B-1, the low-pressure transducers were positioned along the pipe springline, 940 mm from the top of the test tank, and were aligned along the pipe centerline at the mid-width of the steel tank with a spacing of 500 mm between each. The backfill was done in four successive layers, with uncompacted thicknesses ranging from 140 mm to 165 mm and compacted thicknesses from 115 mm to 140 mm. Each soil layer was compacted with three passes of vibratory plate tamper.

B.4 Calibration of Low-Pressure Transducers

Calibrating the pressure transducers posed several challenges that required a systematic approach for resolution. For perfect accuracy of calibration, the transducers were pressurized by exact weights of 50 grams as per the force needed to give excited voltage, and the voltages were simultaneously recorded during each application of weight, as shown in Figure B-2.

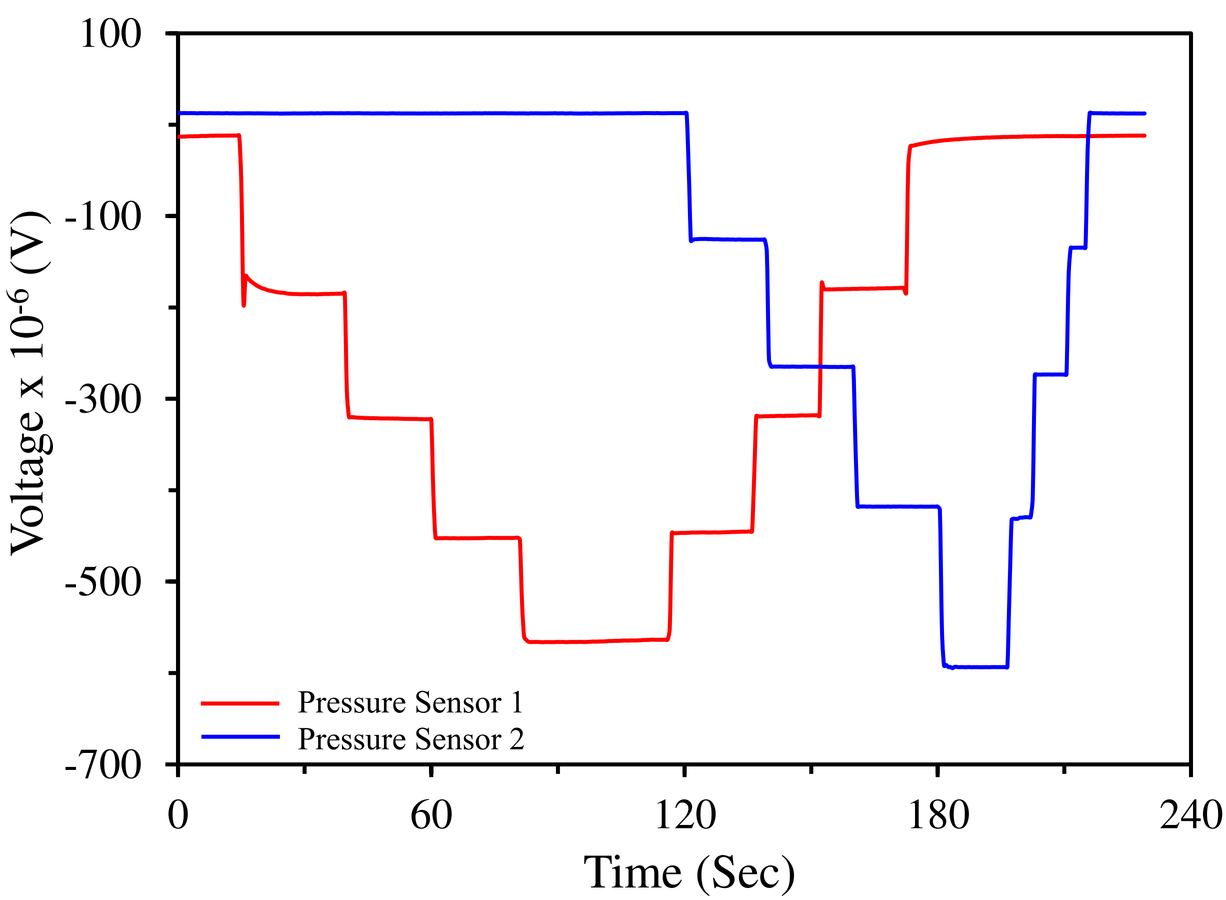

Figure B-2: Excited voltages due to known applied pressure during calibration

This process was sensitively done for some repetitions until a repeatable trend was observed out of the consecutive readings. This made it possible to develop a linear correlation between the excited voltage and the applied pressure with respect to each transducer.

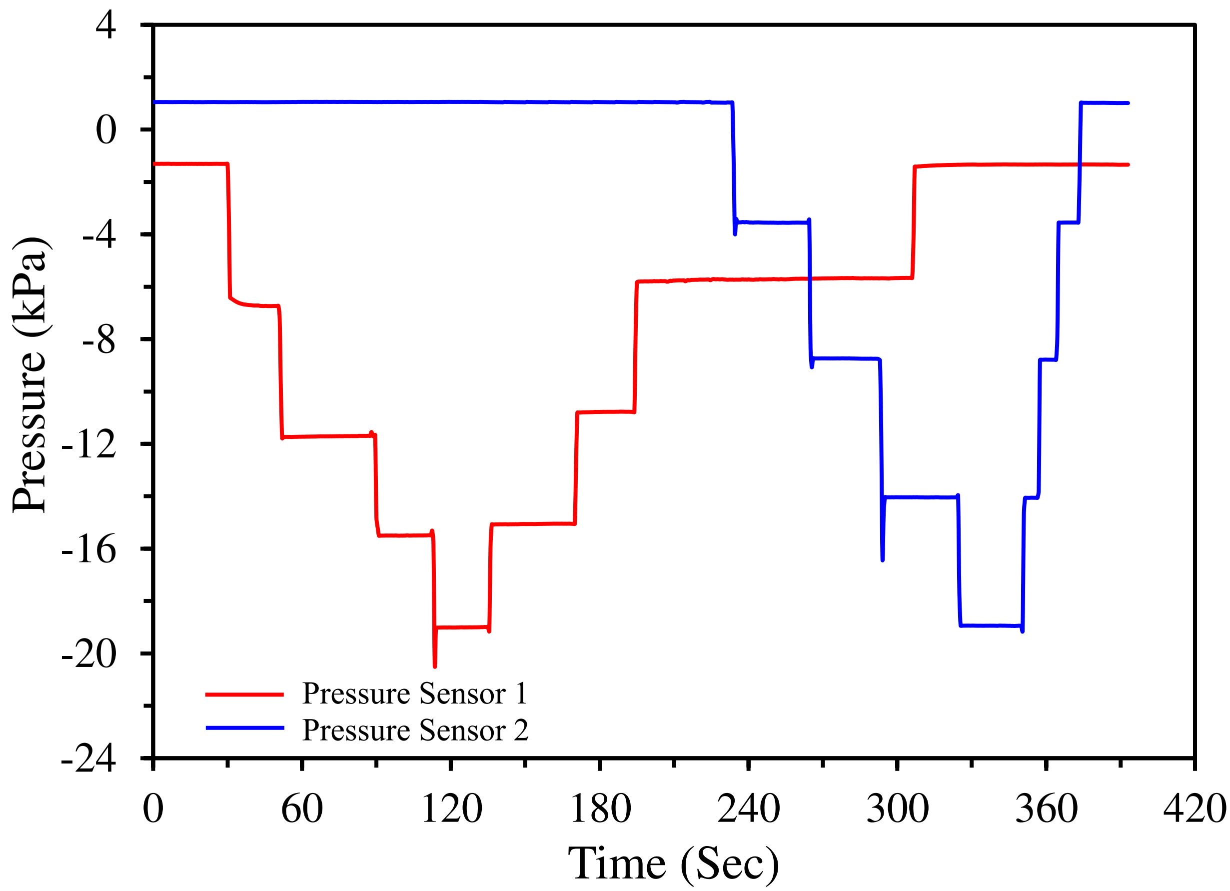

Figure B-3: Pressure measurements for the known applied pressures during verification

The developed correlation was integrated into NI Signal Express 2015 for easy data collection and recording from the pressure transducers. Following calibration, the same procedure was employed to ensure precise pressure measurements: known pressures were applied, and measurements were taken using NI Signal Express 2015. This had to be repeated a few times in order to assure that the measurements were correct and reproducible. The pressure measurements, illustrated in Figure B-3, demonstrated excellent agreement with the applied pressures, validating the calibration process.

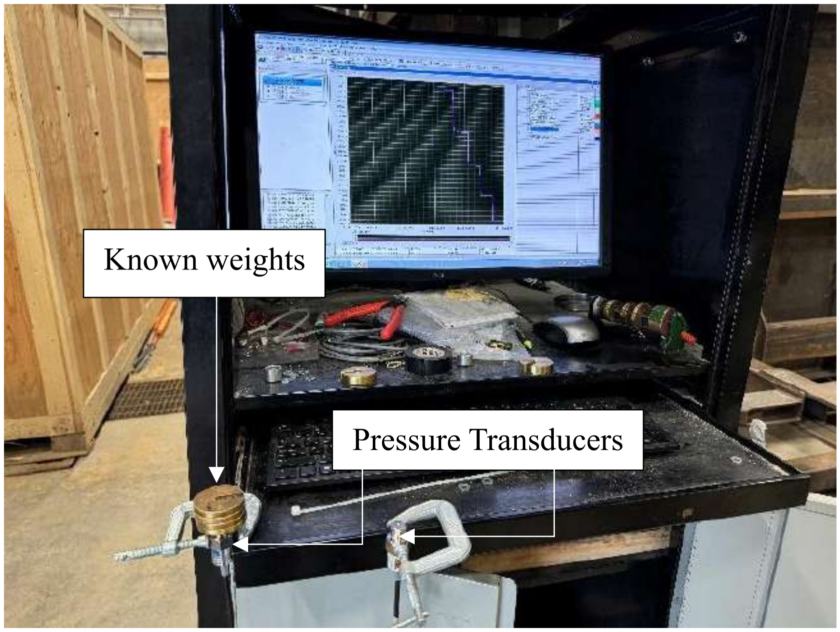

Figure B-4: Pressure transducers calibration process

The comprehensive calibration process is illustrated in Figure B-4. It is important to emphasize that the calibration of each transducer must be performed before every use to ensure accurate measurements of vertical and horizontal pressures during backfilling and compaction. This recurring calibration is essential to maintain the reliability and precision of the pressure measurements throughout the experimental process.

B.5 Test Results and Discussion

The lateral earth pressure readings obtained from the three pressure sensors are presented in Figure B-5. As depicted in this figure, all sensors exhibited a consistent pattern in lateral pressure variation. Notably, a marked increase in lateral earth pressure was recorded for the first backfill layer, in contrast to the subsequent layers, a trend similarly observed by Duncan and Seed (1986), Duncan et al. (1991), and Chen and Fang (2008). Furthermore, during the relaxation phase, lateral pressure values remained stable with no substantial fluctuations.

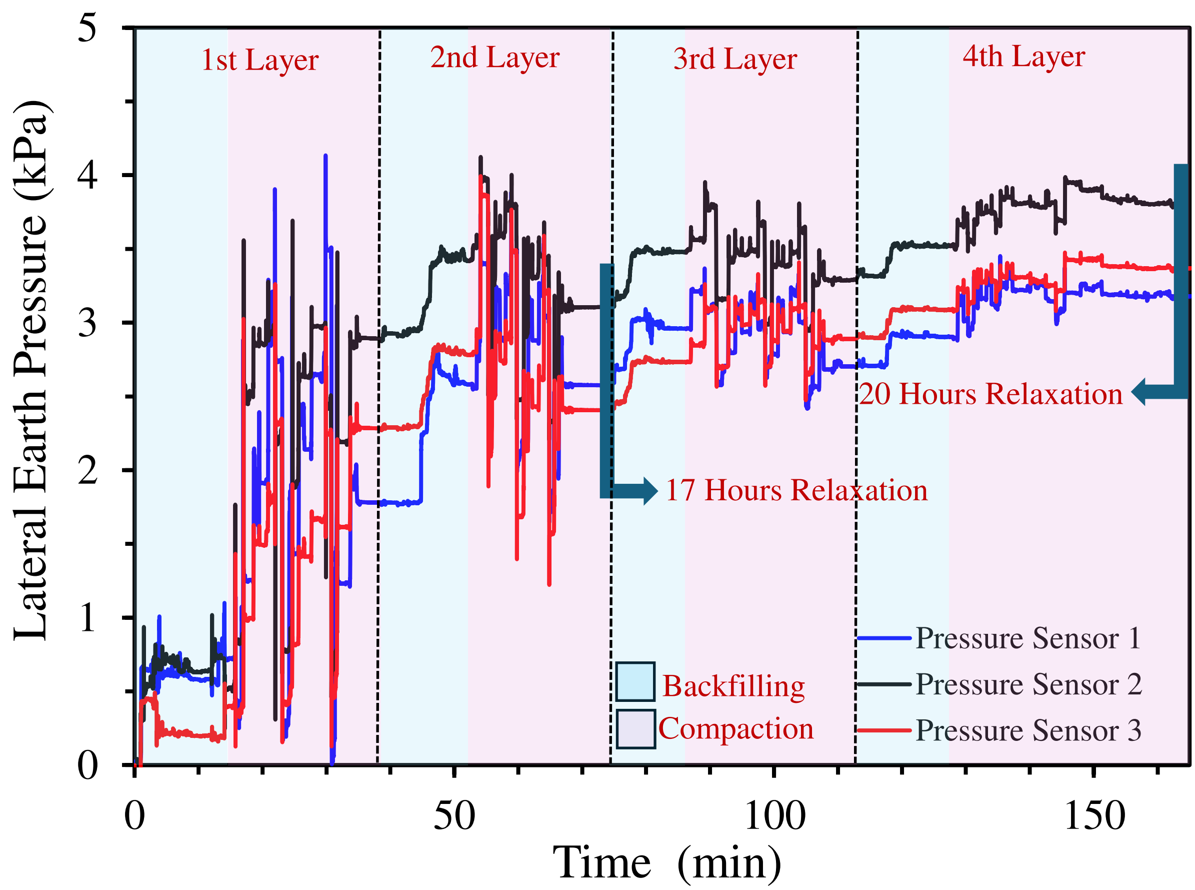

Figure B-5: Measured lateral earth pressures during backfilling and compaction

Figures B-6, B-7, B-8, and B-9 display the lateral pressure measurements from sensor 3 across the 1st, 2nd, 3rd, and 4th backfill layers during the backfilling and compaction stages. In Figure B-6, the lateral stress at the completion of the first compaction pass registered at 2.37 kPa, while the corresponding calculated vertical pressure was 2.13 kPa. This yields a lateral-to-vertical pressure ratio of 1.11, indicating an influence of compaction-induced stresses on lateral pressures, with values exceeding typical at-rest conditions. Upon initiating the second compaction pass, the lateral pressure sharply declined to 0.15 kPa, consistent with the pressure observed during the levelling phase of the first layer. By the end of this pass, lateral pressure increased again to 2.26 kPa. This fluctuation recurred during the third compaction pass, where lateral pressure dropped to 0.13 kPa before rising to 2.3 kPa upon completion. For the first layer, the loose thickness was 142 mm, compacted to a final thickness of 115 mm.

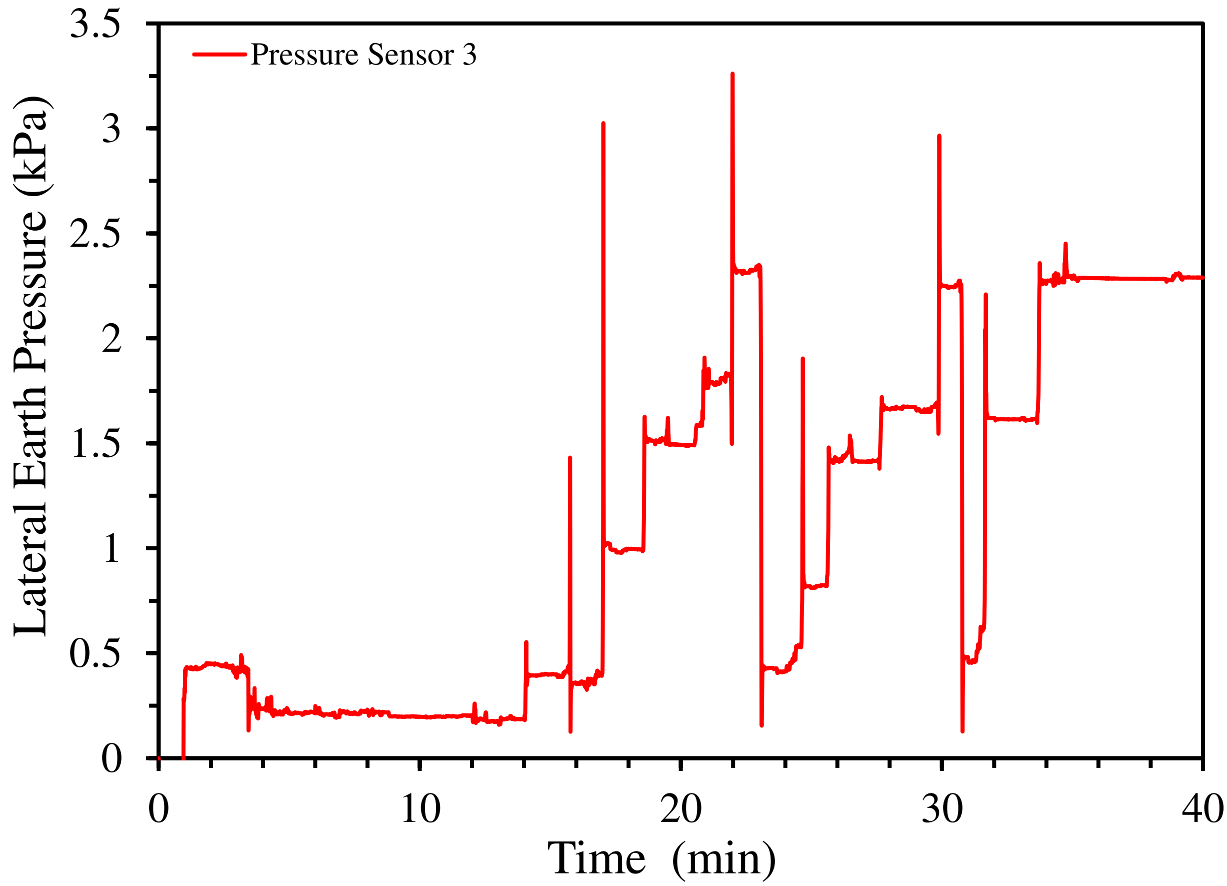

Figure B-6: Measured lateral pressure from pressure sensor 3 for 1st layer during backfilling and compaction

The observed drop in lateral pressure during each compaction pass can be attributed to minor displacements of the earth pressure sensors. As the tank side walls are rigid, when starting the compaction of the 1st strip, the soil tends to move laterally towards the direction of the pressure sensors and due to this, the earth pressure sensors moved and measured a lesser value of lateral stress. Such fluctuations would likely be mitigated if the sensors were rigidly fixed, preventing movement and providing more stable lateral stress measurements.

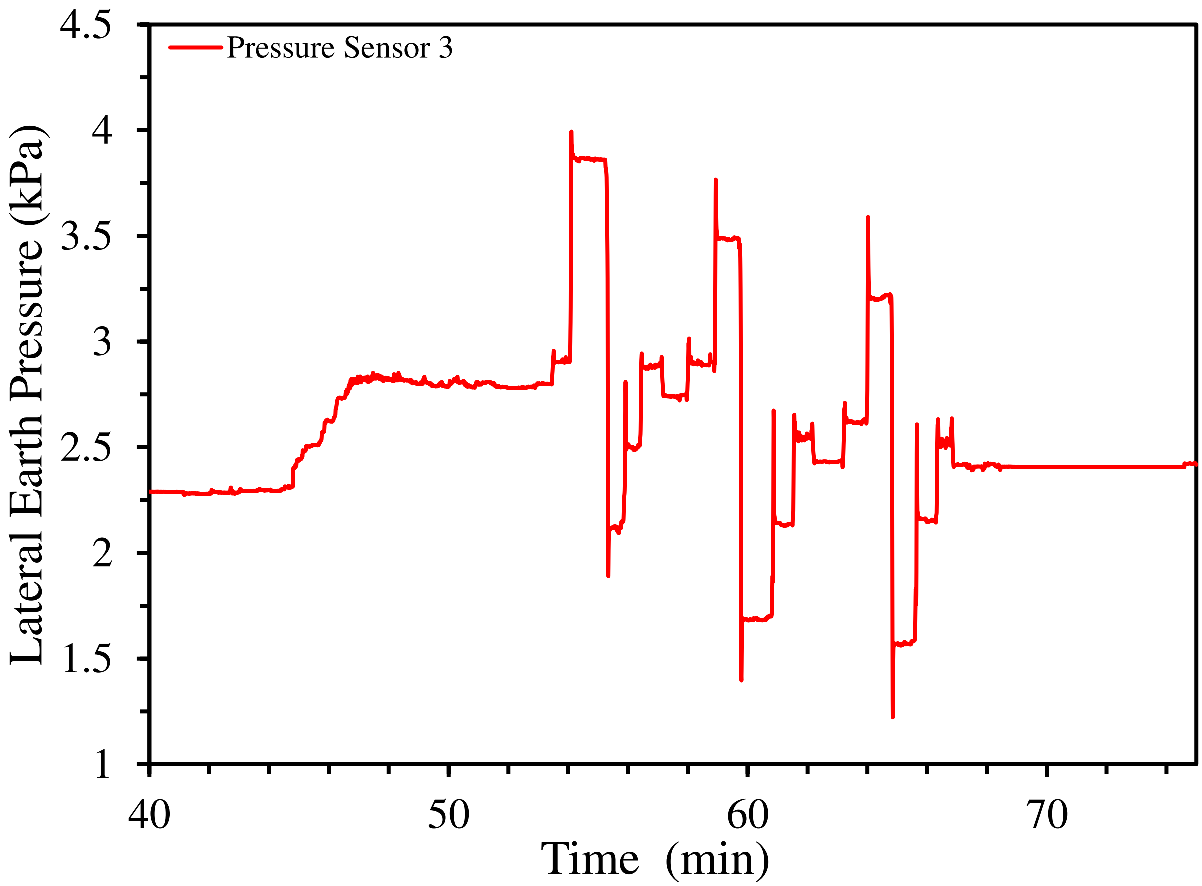

Figure B-7: Measured lateral pressure from pressure sensor 3 for 2nd layer during backfilling and compaction

Figure B-7 illustrates the lateral pressure behaviour in the second layer during backfilling and compaction stages. Initially, lateral pressure rose to 2.85 kPa during backfilling and levelling, subsequently increasing further to 3.86 kPa with compaction. During the compaction of the second strip, lateral pressure reduced to 2.09 kPa but incrementally increased with the compaction of the third through sixth strips, reaching 2.89 kPa. Upon initiating the second pass, lateral pressure again spiked to 3.48 kPa, followed by a similar reduction trend as observed in the first pass, with a drop to 1.68 kPa during the compaction of the second strip. Subsequent compaction of additional strips resulted in an increase to 2.61 kPa.

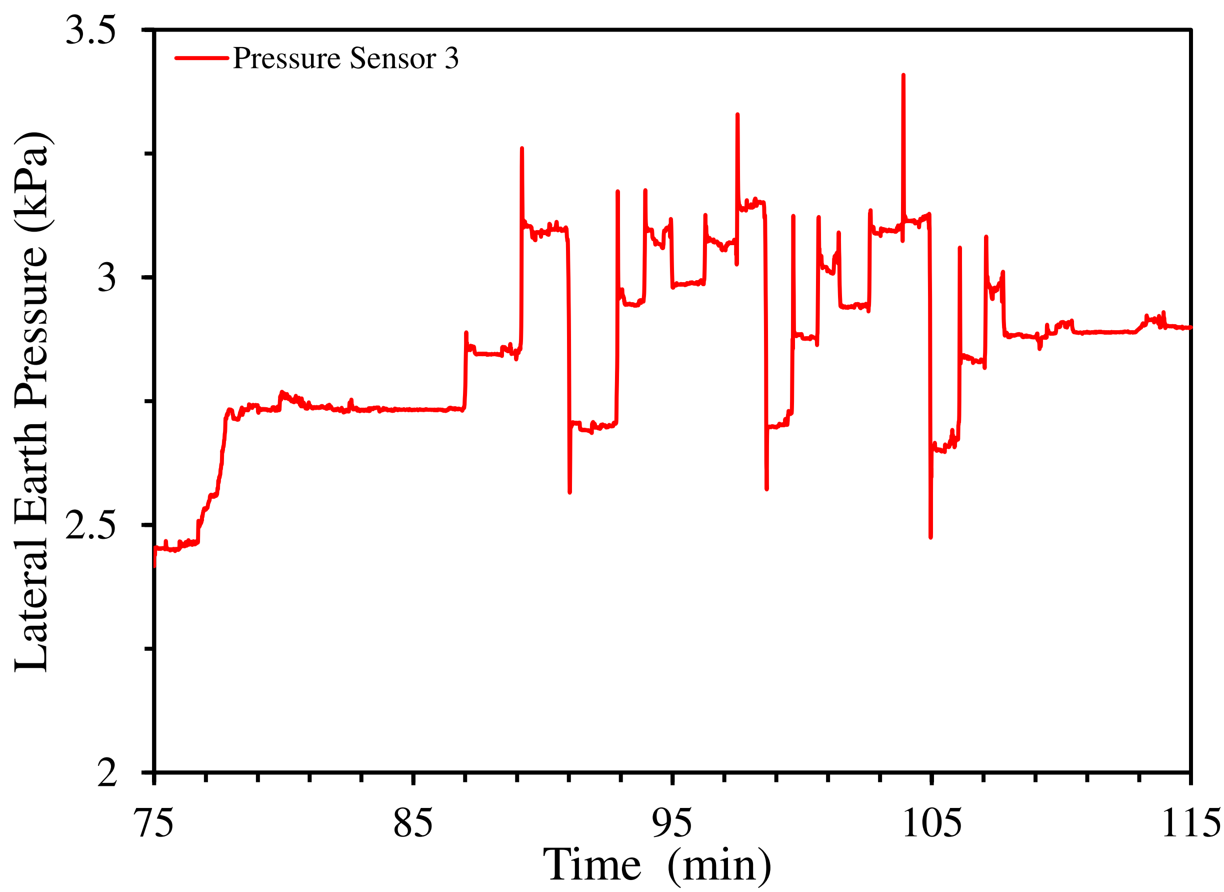

Figure B-8: Measured lateral pressure from pressure sensor 3 for 3rd layer during backfilling and compaction

A comparable pattern occurred during the third pass: lateral pressure initially increased to 3.2 kPa in the first strip, dropped to 1.57 kPa in the second strip, and then rose to 2.48 kPa in subsequent strips. Upon completion of the second layer, the calculated vertical pressure was 4.72 kPa. The uncompacted thickness of this layer was 165 mm, reducing to 140 mm after compaction.

The observed reductions in lateral pressure during compaction of the second layer are likely due to slight movements of the pressure sensors caused by the vibratory effects of compaction on the surrounding soil. This soil movement around the sensors appears to alter their positioning momentarily, resulting in periodic reductions in recorded lateral pressures.

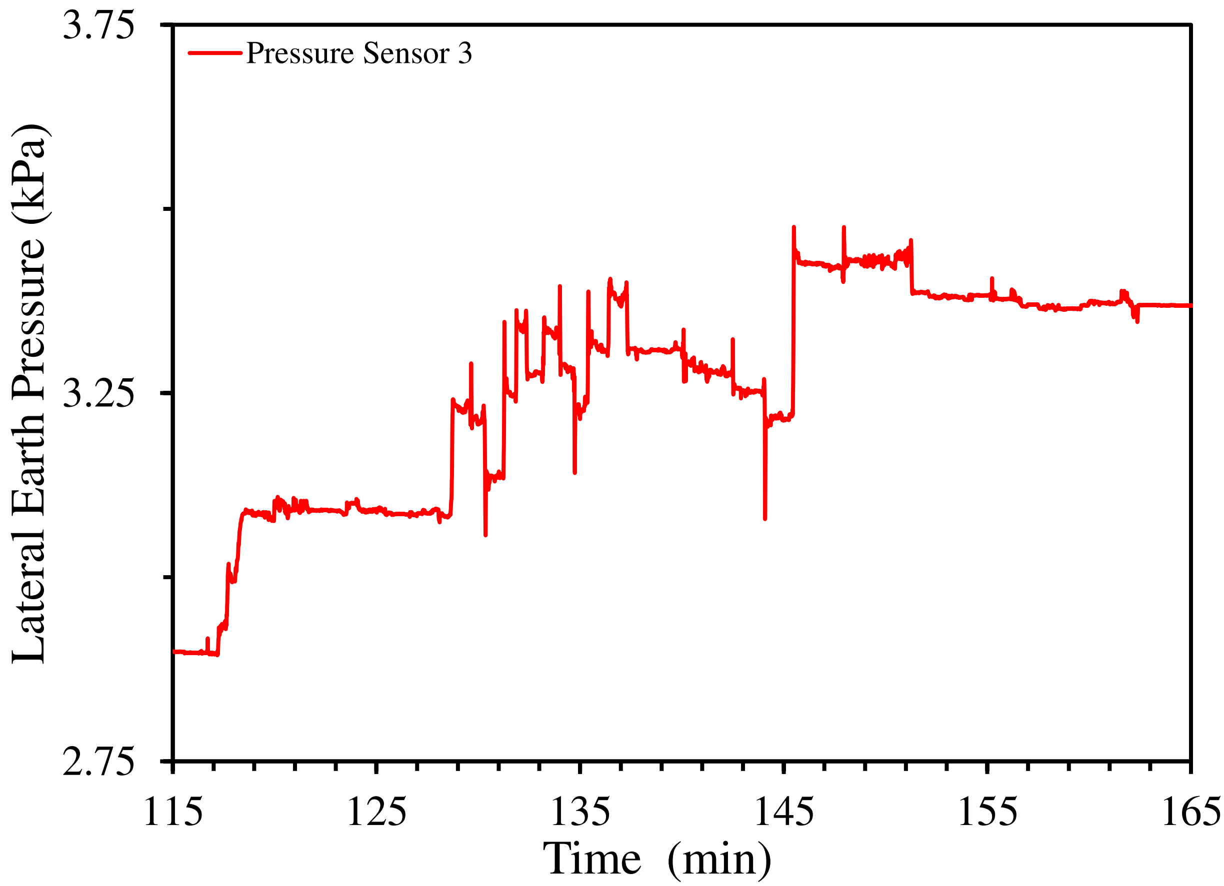

Figure B-9: Measured lateral pressure from pressure sensor 3 for 4th layer during backfilling and compaction

Figure B-8 demonstrates a similar reduction pattern in lateral pressure during the compaction of the third layer, attributed to potential movement of the pressure sensors. Notably, this reduction was approximately 0.4 kPa for the third layer, significantly less than the 1.8 kPa reduction observed in the second layer. During the backfilling and levelling process for the third layer, lateral pressure initially rose to 2.75 kPa, and by the end of compaction, it increased further to 2.91 kPa. Following the completion of the third layer, the calculated vertical pressure stood at 7.22 kPa. The third layer had an uncompacted thickness of 155 mm, which was reduced to a compacted thickness of 135 mm. These measurements indicate that the vibratory effects of compaction, while still influencing lateral pressure recordings, had a reduced impact in terms of sensor movement in the third layer compared to the second layer.

Figure B-9 shows the lateral pressure development in the fourth layer during backfilling and levelling, where pressure increased to 3.09 kPa. This pressure further rose to 3.39 kPa at the end of the compaction phase for this layer. The fourth layer had an uncompacted thickness of 150 mm, which reduced to 130 mm after compaction. Upon completing the fourth layer, the calculated vertical pressure was 9.62 kPa. The reduction in lateral pressure observed during compaction, likely due to minor sensor movement, was approximately 0.3 kPa. This drop is minimal compared to reductions noted in previous layers, suggesting that sensor stability may have improved or that soil movements induced by compaction were less impactful in this layer.

The variation of the lateral earth pressure coefficient (K) with soil depth, as illustrated in Figure B-10, reveals a distinct trend. At a shallow depth of 0.115 m, the lateral earth pressure coefficient was observed to be 1.11. With increasing depth, this coefficient exhibited a progressive reduction, decreasing to 0.82 at 0.255 m, 0.40 at 0.39 m, and ultimately stabilizing at approximately 0.35 at 0.52 m. From Chapter 3, the friction angle of the soil subjected to vibratory compaction was determined to be 44°, which, according to Jaky's empirical relationship (Jaky, 1944), corresponds to an at-rest lateral earth pressure coefficient (K_0) of 0.305.

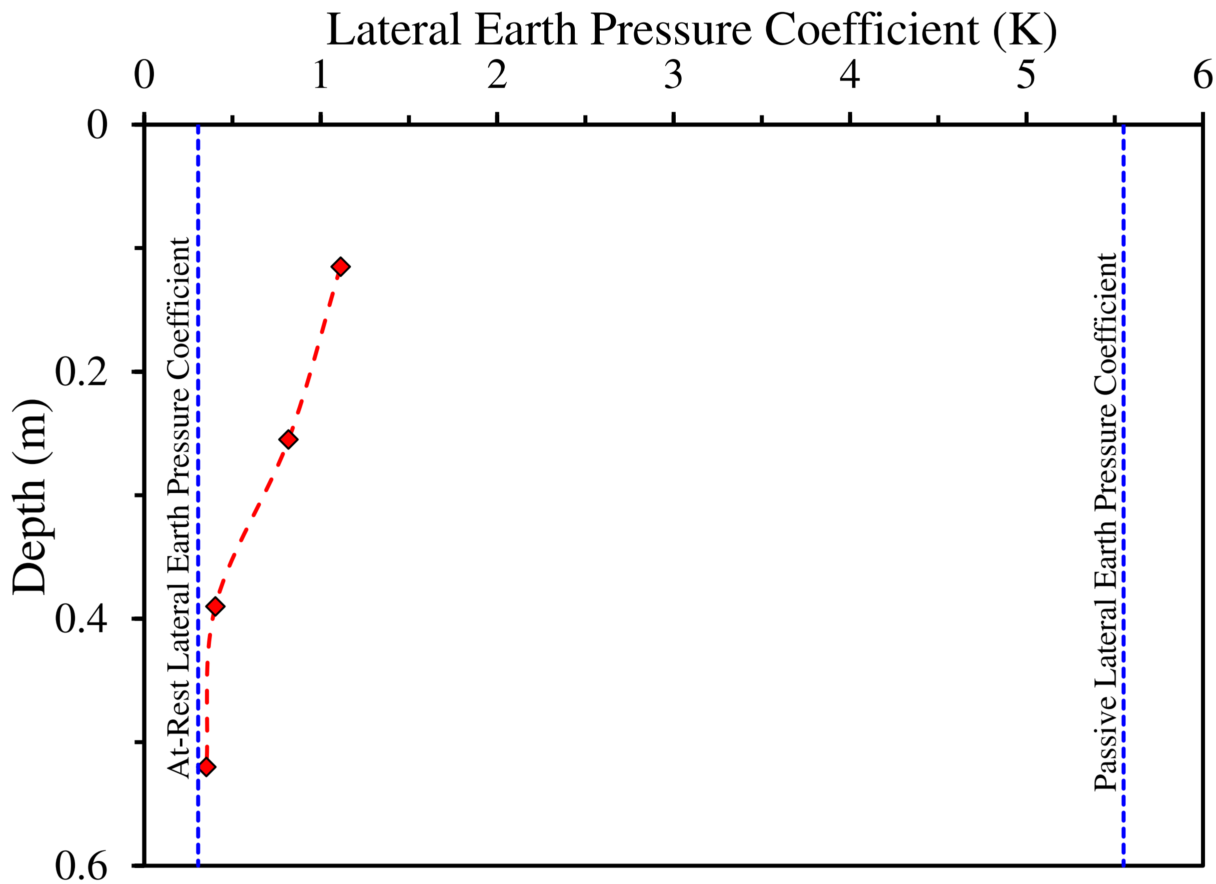

Figure B-10: Variation of lateral earth pressure coefficient with depth

The observed trend in Figure B-10 indicates that while the lateral earth pressure coefficient near the surface does not align with the theoretical passive earth pressure coefficient (K_p), a notable convergence towards the at-rest lateral earth pressure coefficient is evident with increasing depth. This suggests that vibratory compaction primarily influences the upper soil layers, inducing compaction-induced lateral stress states that deviate from at-rest conditions but gradually transition towards equilibrium as depth increases. These findings are consistent with the observations of Duncan and Seed (1986), Duncan et al. (1991), and Chen and Fang (2008), who reported similar trends in lateral earth pressure variations due to compaction effects. Their studies demonstrated that compaction-induced lateral stresses tend to be approximately equal to the passive earth pressure values near the surface, but with increasing depth, the influence of external compaction diminishes, allowing the soil to transition towards a stress state governed by fundamental soil mechanics principles.

B.6 Recommendations

In the present study, observations for a specific soil layer indicated an initial increase in lateral stresses during the first pass of compaction. However, at the onset of the second pass, lateral stresses abruptly decreased to levels comparable to those observed before the first compaction pass. This pattern was similarly noted at the beginning of the third pass. Such fluctuations in stress measurements may stem from potential movement of the pressure sensors during the compaction process, as these sensors were not rigidly affixed. To enhance the reliability of lateral earth pressure measurements during backfilling and compaction, it is recommended to secure the pressure sensors rigidly to the soil tank wall.

Additionally, force-sensing resistor (FSR) pressure sensors, as proposed by Guo and Zhou (2024), could be strategically positioned along the pipe's surface at key locations (i.e., crown, shoulder, springline, haunch, and invert) to capture normal stresses more accurately during backfilling and compaction. This approach would facilitate more precise measurements of earth pressures acting on the pipe surface, enabling the determination of accurate average normal stresses around the pipes. These refined stress values could then be compared against the axial pullout resistance of MDPE pipes, offering a robust basis for evaluating pipe-soil interaction dynamics during compaction.

B.7 References

Carder, D. R., Pocock, R. G., & Murray, R. T. (1977). *Experimental retaining wall facility - Lateral stress measurements with sand backfill* (No. TRRL Lab Report 766). Transport and Road Research Laboratory, Crowthorne, Berkshire, United Kingdom.

Carder, D. R., Murray, R. T., & Krawczyk, J. V. (1980). *Earth pressures against an experimental retaining wall backfilled with silty clay* (No. LR 946 Monograph). Transport and Road Research Laboratory, Crowthorne, Berkshire, United Kingdom.

Chen, T. J., & Fang, Y. S. (2008). Earth pressure due to vibratory compaction. *Journal of Geotechnical and Geoenvironmental Engineering, 134*(4), 437-444.

Clayton, C. R. I., Symons, I. F., & Heidra-Coho, J. C. (1991). The pressure of clay backfill against retaining structures. *Canadian Geotechnical Journal, 28*(2), 309-315.

Clayton, C. R. I., & Symons, I. F. (1992). The pressure of compacted fill on retaining walls. *Géotechnique, 42*(1), 127-130.

Duncan, J. M., & Seed, R. B. (1986). Compaction-induced earth pressures under K_0-conditions. *Journal of Geotechnical Engineering, 112*(1), 1-22.

Duncan, J. M., Williams, G. W., Sehn, A. L., & Seed, R. B. (1991). Estimation of earth pressures due to compaction. *Journal of Geotechnical Engineering, 117*(12), 1833-1847.

Ezzeldin, I., El Naggar, H., & Newhook, J. (2022). 3D numerical modelling of earth pressures on a non-yielding rigid wall due to compaction efforts. In *Annual conference of Canadian Geotechnical Society, GeoCalgary2022*, Alberta, Canada.

Gui, M., Phan, T., & Pham, T. (2020). Impacts of compaction load and procedure on stress-deformation behaviors of a soil geosynthetic composite (SGC) mass—A case study. *Applied Sciences, 10*(18), 6339.

Guo, C., & Zhou, C. (2024). Axial behaviour of steel pipelines buried in sand: Effects of surface roughness and hardness. *Géotechnique*, 1-37.

Massarsch, K. R., & Fellenius, B. H. (2002). Vibratory compaction of coarse-grained soils. *Canadian Geotechnical Journal, 39*(3), 695-709.

Rehnman, S. E., & Broms, B. B. (1972). Lateral pressures on basement wall: Results from full-scale tests. In *Proceedings of the Fifth European Conference on Soil Mechanics and Foundation Engineering*.

APPENDIX C: Soil Tests on Backfill Sand and Ottawa Sand

C.1 Introduction

In this study, a series of soil tests were conducted to verify and calibrate key soil properties. The tests performed included particle size distribution analysis, as well as minimum and maximum dry density determinations. The particle size distribution tests were carried out on the backfill sand to monitor variations in particle size, particularly since the sand was repeatedly used in full-scale pipe-soil interaction experiments. These experiments involved compaction using both a vibratory plate tamper and a manual hand tamper. The compaction process may have caused larger soil particles to break down into smaller particles. Additionally, tests to determine the minimum and maximum dry densities were conducted on both Ottawa sand and backfill sand. These measurements are crucial for calculating the relative density of sand. Various filling methods were employed during the minimum and maximum dry density tests, which will be described in subsequent sections. Further, these tests were conducted on dried soil samples. However, the moisture content of the sand during the full-scale tests was maintained below 2%.

C.2 Test Program

The test program included two particle size distribution tests on the backfill sand, conducted according to ASTM D6913-17 standards. In addition, twelve tests were performed for the minimum dry density (ASTM D4254-16) and maximum dry density (ASTM D4253-16e1) of the backfill sand, while another twelve tests were carried out for the Ottawa sand. Figure C-1 illustrates the procedures followed for these minimum and maximum dry density and grain size distribution tests. It is worth nothing that the tests were conducted on dried soil samples

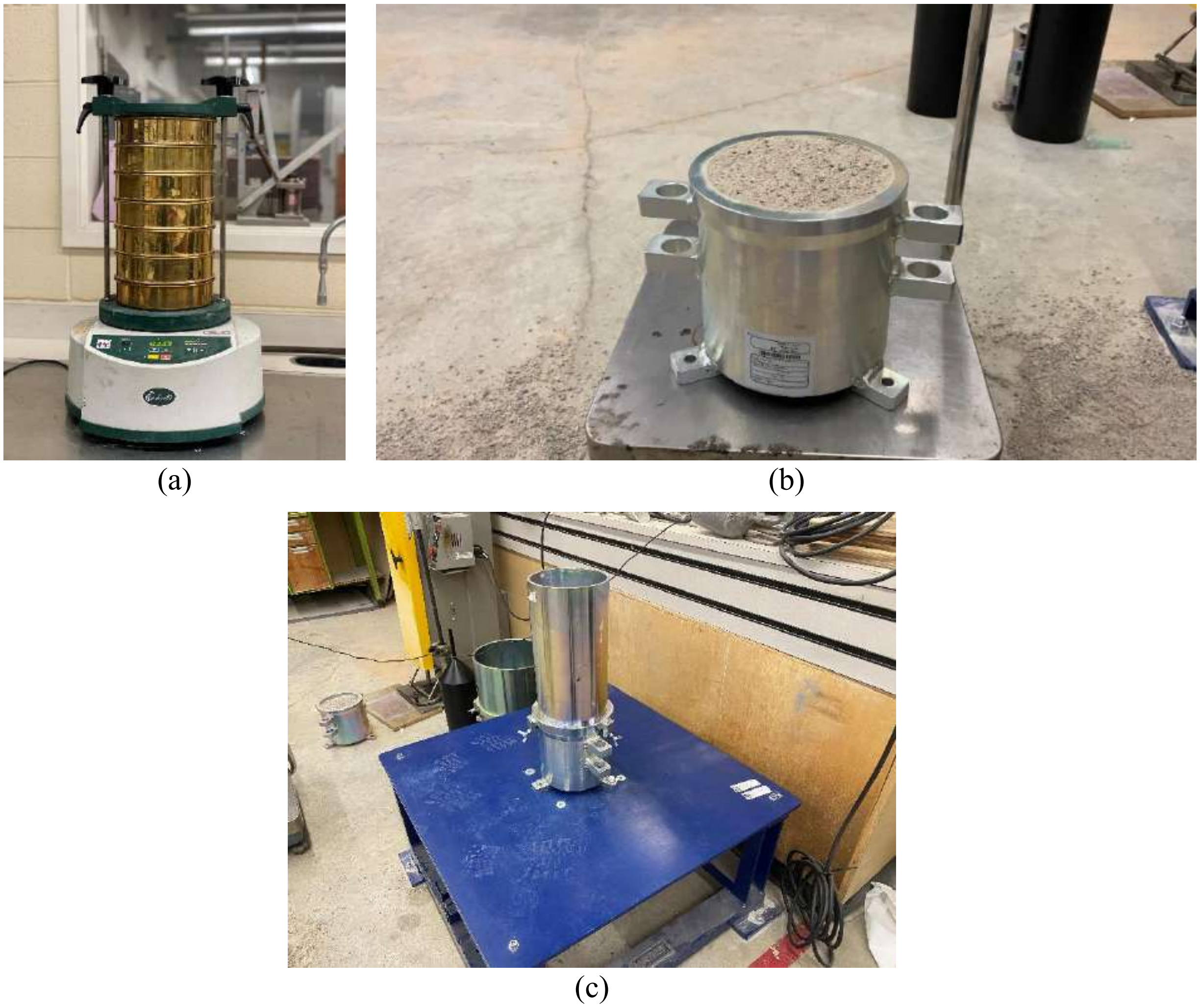

Figure C-1: Conducted soil tests: (a) Particle size distribution test (b) Minimum dry density test (c) Maximum dry density test

Figure C-2 shows the various filling techniques used to determine the minimum dry density of the sands. In methods A and B, the sand was deposited in a conical form due to the funnel's stationary position at the center of the mould. By contrast, in methods C and D, the sand was filled in a cylindrical manner by rotating the funnel's tip along a circular path from the perimeter towards the center.

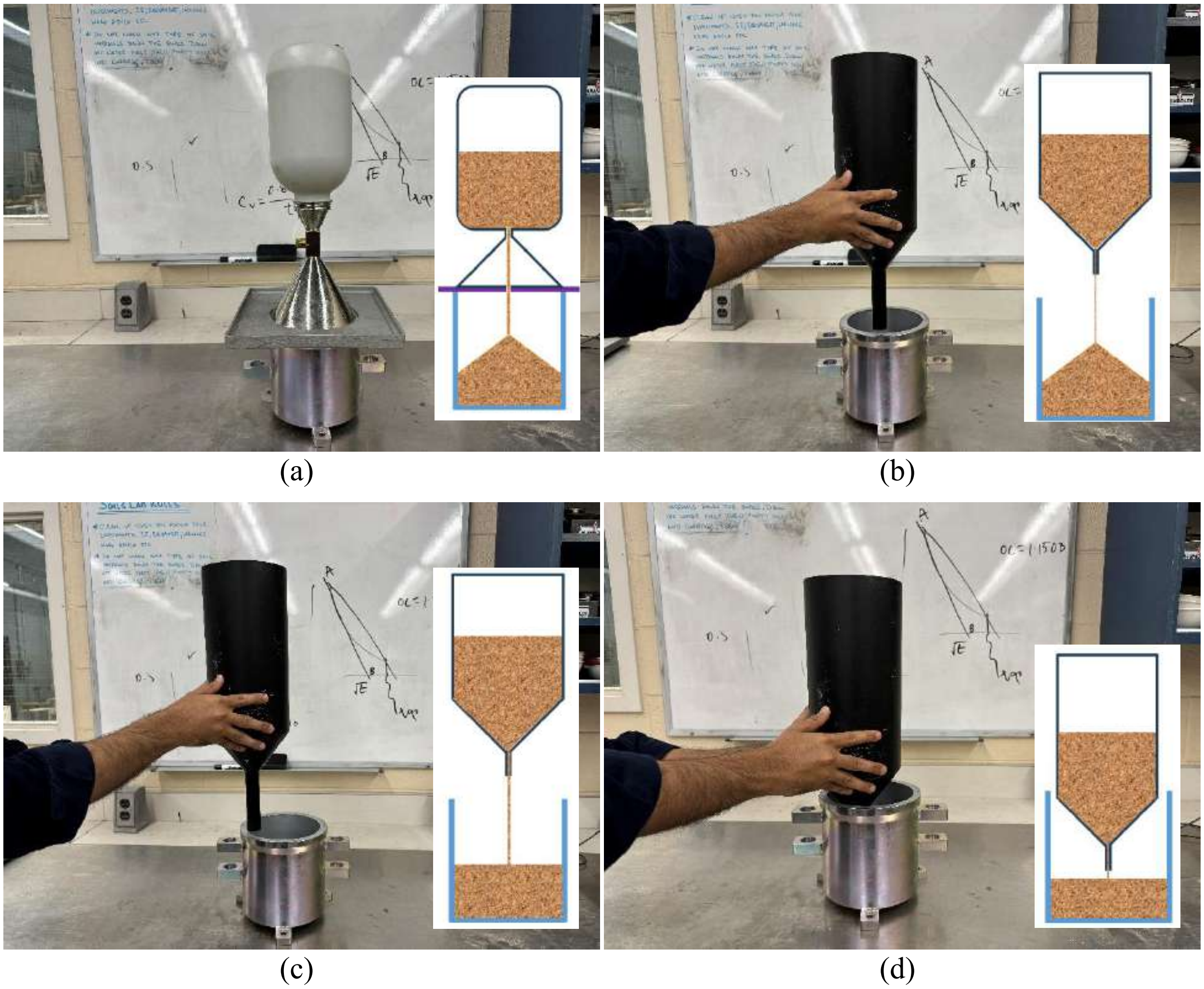

(a) (b) (c) (d)

Figure C-2: Different filling methods used to find the minimum dry density of sand: (a) Method A: By using sand cone apparatus (maximum free fall height of 12.5 inches) (b) Method B: By using a funnel with tip fixed at the center (maximum free fall height of 6.5 inches) (c) Method C: By using a funnel with a rotating tip (maximum free fall height of 6.5 inches) (d) Method D: By using a funnel with a rotating tip (maximum free fall height of 0.5 inches)

C.3 Test Results and Discussion

Table C-1 presents the average minimum and maximum dry densities of the backfill sand and Ottawa sand, based on the different filling methods used. The values are the result of three identical tests for each method. The conical filling approach (methods A and B) likely caused greater void formation around the edges of the mould, leading to lower minimum dry density values for both types of sand. On the other hand, methods C and D, which achieved a more uniform spread across the circular cross-section, produced more consistent thickness and reduced the likelihood of voids, resulting in higher minimum dry density values. It should also be noted that the maximum and minimum dry density values for any given sand can vary significantly depending on the testing standards used to determine them (Blaker et al., 2015; Lunne et al., 2019). This variability highlights the importance of establishing a globally standardized methodology for determining the minimum and maximum dry densities of sands, as emphasized by Blaker et al. (2015) and Lunne et al. (2019).

Table C-1: Average minimum and maximum dry densities of Ottawa sand and backfill sand, using different filling methods

Soil	Filling Method	Minimum Dry Density (kN/m^3)	Maximum Dry Density (kN/m^3)
Ottawa Sand	Method A	14.87	17.06
	Method B	14.90	17.10
	Method C	15.22	17.04
	Method D	15.24	17.16
Backfill Sand	Method A	15.67	19.55
	Method B	15.55	19.57
	Method C	16.62	19.60
	Method D	16.58	19.62

The grain size distribution curve obtained, illustrated in Figure C-3, closely aligned with the results reported by Saha et al. (2019). This consistency indicates that the sand particles remained intact, with no significant fragmentation into smaller particles, despite the repeated usage of the sand in full-scale tests involving compaction using both a vibratory plate tamper and a manual hand tamper.

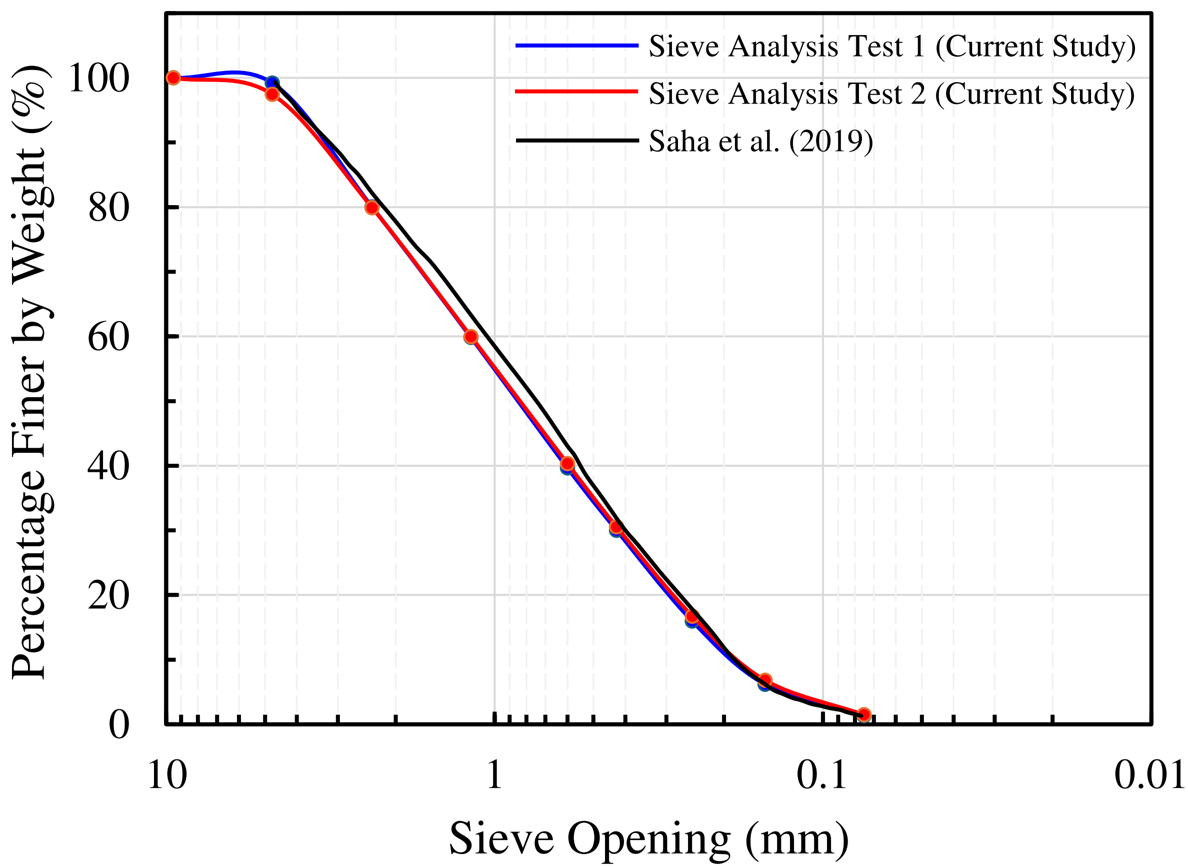

Figure C-3: Particle size distribution of backfill sand (after Saha et al., 2019)

C.3 Recommendations

The effect of moisture content on the minimum and maximum dry density of the backfill sand can be studied. Minimum and maximum dry density of the sand using different standards other than ASTM can be explored.

C.4 References

ASTM. (2016). *Standard test methods for minimum index density and unit weight of soils and calculation of relative density* (D4254-16). American Society for Testing and Materials, West Conshohocken, PA, USA.

ASTM. (2019). *Standard test methods for maximum index density and unit weight of soils using a vibratory table* (D4253-16e1). American Society for Testing and Materials, West Conshohocken, PA, USA.

ASTM. (2021). *Standard test methods for particle-size distribution (gradation) of soils using sieve analysis* (D6913/D6913M-17). American Society for Testing and Materials, West Conshohocken, PA, USA.

Blaker, Ø., Lunne, T., Vestgården, T., Krogh, L., Thomsen, N. V., Powell, J. J. M., & Wallace, C. F. (2015). Method dependency for determining maximum and minimum dry unit weights of sands. In *Proceedings of the 3rd International Symposium on Frontiers in Offshore Geotechnics (ISFOG)* (pp. 1159-1166). Taylor & Francis Group.

Lunne, T., Knudsen, S., Blaker, Ø., Vestgården, T., Powell, J. J. M., Wallace, C. F., & Ghanekar, R. K. (2019). Methods used to determine maximum and minimum dry unit weights of sand: Is there a need for a new standard? *Canadian Geotechnical Journal, 56*(4), 536-553.

Saha, R. C., Dhar, A. S., & Hawlader, B. C. (2019). Shear strength assessment of a well-graded clean sand. In *Annual Conference of Canadian Geotechnical Society, GeoSt. John's*.